SCHUSTER, Reinhold Michael, 1939-
STRENGTH AND BEHAVIOR OF COLD-ROLLED
STEEL-DECK-REINFORCED CONCRETE FLOOR
SLABS.

Iowa State University, Ph.D., 1970
Engineering, civil

University Microfilms, Inc., Ann Arbor, Michigan

STRENGTH AND BEHAVIOR OF COLD-ROLLED STEEL-DECK-REINFORCED CONCRETE FLOOR SLABS

by

Reinhold Michael Schuster

A Dissertation Submitted to the
Graduate Faculty in Partial Fulfillment of
The Requirements for the Degree of
DOCTOR OF PHILOSOPHY

Major Subject: Structural Engineering

Approved:

Signature was redacted for privacy.
In Charge of Major Work

Signature was redacted for privacy.
Head of Major Department

Signature was redacted for privacy.
Dean of Graduate College

Iowa State University
Of Science and Technology
Ames, Iowa

1970

TABLE OF CONTENTS

NOTATION

A_s	Cross-sectional area of steel deck per foot of width
a	$A_s F_y / 0.85 f'_c b$
b	Width of slab, normally 12 inches
b_d	Width of steel deck and composite test beam
c	Distance from extreme compression fiber to composite neutral axis at ultimate strength
C_m	Moment coefficient - depends on whether the system is simply supported or continuous
D	Depth of slab (out-to-out depth from lowest point of steel deck to top of slab)
d	Effective slab depth (distance from extreme concrete compression fiber to centroidal axis of steel deck)
d_d	Depth of steel deck profile
E_c	Modulus of elasticity of concrete
E_s	Modulus of elasticity of steel deck
ϵ_{es}	Experimental unit strain in steel deck
ϵ_{sb}	Experimental unit strain at bottom fiber of steel deck
ϵ_{sc}	Experimental unit strain at center of gravity of steel deck
ϵ_{st}	Experimental unit strain at top fiber of steel deck
ϵ_u	Maximum concrete compression strain at ultimate strength
ϵ_y	Unit strain in steel deck at time of yielding
f'_c	28-day compressive test cylinder strength
f_{cs}	Calculated stress in steel deck
f_{es}	Experimental stress in steel deck
F_s	Steel stress at center of gravity of steel deck

f'_t	Tensile strength of concrete
F_y	Yield stress of steel deck
g	Pitch of shear transfer devices
I_{sf}	Moment of inertia of steel deck per foot of width based on full cross-sectional deck area
I_{sn}	Moment of inertia of steel deck per foot of width based on reduced cross-sectional deck area for negative bending regions
I_{sp}	Moment of inertia of steel deck per foot of width based on reduced cross-sectional deck area for positive bending regions
k_1	Ratio of average to maximum concrete stress
k_2	Ratio of depth to resultant of compressive force, to depth to composite neutral axis
k_3	Ratio of maximum stress to 6 x 12 in. cylinder strength, f'_c
K_5, K_6 K_9, K_{10}	Regression constants - CATEGORY I
K_7, K_8	Regression constants - CATEGORY II
k_u	$\sqrt{pm + \frac{(pm)^2}{2}} - \frac{pm}{2}$
L	Length of span
L'	Length of shear span
L''_n	Equivalent simple span length in a continuous slab subjected only to positive bending
L'_y	Calculated shear span length for equal shear-bond and flexure-yielding capacity
L'_c	Calculated shear span length for equal shear-bond and flexure-crushing capacity
m	$E_s \epsilon_u / 0.85 k_1 f'_c$

M_c	Moment carried by concrete at ultimate load of shear-bond failure
m_u	Ultimate load per shear transfer device
M_{uc}	Ultimate calculated moment per foot of width based on crushing of concrete
M_{ue}	Ultimate experimental moment per foot of width
M_{uy}	Ultimate calculated moment per foot of width based on yielding of steel deck
μ	Microinches per inch
n	Es/Ec
p	A_s/bd
p_b	Balanced reinforcement ratio
P_e	Experimental applied load
P_{ue}	Ultimate experimental beam load, including tare weight
s	Center-to-center spacing of welded shear transfer devices
σ_{max}	Maximum concrete tensile stress
σ_{ct}	Concrete tensile bending stress acting between flexural cracks
t_c	Coated steel deck thickness
V_c	Transverse shear carried by concrete at ultimate load of shear-bond failure
v_c	Shear stress carried by concrete at ultimate load of shear-bond failure
V_d	Transverse shear carried by steel deck at ultimate load of shear-bond failure
V_{de}	Transverse calculated design shear per foot of width based on shear-bond failure
V_{uc}	Transverse ultimate calculated shear per foot of width based on shear-bond failure
v_{uc}	Ultimate calculated shear-bond stress

v_{ue}	Ultimate experimental shear-bond stress
V_{ue}	Ultimate experimental transverse shear per foot of width based on shear-bond failure
W_C	Construction live load
W_D	Steel deck dead load
W_L	Allowable superimposed live load
W_u	Ultimate calculated uniformly distributed load
W_W	Concrete dead load
W_1	$(W_D + W_W)$
W_2	$(W_D + W_W + W_C)$
W_3	Dead load applied to slab, exclusive of W_1
$\emptyset$	Safety reduction factor (ACI Building Code, Sect. 1504)
y_{sb}	Distance from centroidal axis of steel deck to bottom of steel deck

INTRODUCTION

General Remarks

In recent years much attention has been focused, by building and general construction industries, on the use of light gage-cold-formed steel members and decks as load carrying structural components. In particular, these general remarks are centered on the use of such decks in concrete floor construction for buildings. This combination of compositely integrating the structural properties of concrete and steel may be termed "composite steel-deck-reinforced concrete slab construction" or may also be defined as floor slabs comprised of conventional or light-weight concrete placed permanently over light gage-cold-formed steel decks. The steel deck performs the dual role of functioning as a form for the concrete at the construction stage and as positive reinforcement for the slab under service conditions.

Steel decks for composite deck-reinforced floor construction are commercially available in a variety of shapes and sizes. They normally consist of cold-formed corrugated sheets or ribbed panels to provide adequate strength during the construction stage. A typical steel deck unit might be approximately 24 in. wide, up to 40 ft. in length, from 0.020 to 0.070 inches in thickness, and between 2 and 8 psf in unit weight. Typically, each steel deck has some type of surface finish or coating for corrosion resistance purposes. These surface coatings vary in degree of application from galvanizing to phosphate-treating and, to some degree, provide a fraction of the bond contribution between the concrete and steel deck.

There are many advantages in using floor systems that employ cold-formed steel decks to act in composite fashion with concrete. The economical and cost saving advantages might very well be considered as the major reason for the increased use of these unique slab systems; this is particularly true since the on-site construction labor cost of cast-in-place conventional reinforced concrete is continually increasing. Obviously, eliminating the necessity of installing and removing temporary form falsework can be cost-saving, especially in cases where the contractor cannot take advantage of form reuse. Secondly, the light gage steel deck material is easily handled and placed, hence, rapid construction is possible with a minimum of on-site labor. After the steel panels have been placed, a safe working platform for workmen, their tools, materials and equipment is provided. Construction fires are a rarity since almost all incombustibles are removed from the job. The outer job site is cleaner and more accessible to workmen, material deliveries and storage. During the past few years various steel deck manufacturers have also developed pre-engineered raceways for electrification, communication, and air distribution which can often be most economically blended with their respective composite deck systems.

Recently, composite steel-deck-reinforced construction has also been extended and designed to act compositely with supporting beams and girders. In this case, shear transfer between supporting member and ribbed or cellular slab is secured by the usual devices, e.g., by welded steel studs or special connectors.

Object

The primary objective of this investigation was to develop strength design information for one-way simply supported composite steel-deck-reinforced concrete slab systems. Using ultimate strength procedures, this task was divided into (1) experimental beam testing and (2) analytical strength analysis. Experimental beam tests were designed in an effort to provide the necessary data for determining the ultimate strength and behavior of steel-deck-reinforced concrete slab systems. Based on the developed ultimate strength expressions, design relationships were established in accordance with load factors and capacity-reduction factors generally employed with ultimate strength procedures. Second, it was the intent to provide the steel deck manufacturer with a standard performance-test program so that he may evaluate his product on an equal and competitive basis. Resulting from the experimental beam test program, a standard performance test program was outlined for use by each steel deck manufacturer when evaluating his product.

Scope

A laboratory test program, consisting of typical simple beam elements of steel-deck-reinforced concrete slabs was planned in accordance with the continuing research at Iowa State University. Since an ultimate strength approach was adopted, it was concluded that a test program involving the loading to failure of numerous representative slab elements would be most feasible.

Four different steel deck profiles were tested; however, the majority of beam tests were conducted using one particular deck profile, namely that of company I.[a] This was done in an effort to obtain a large number of test results, embodying the most logical parametric variations. Using the results of these tests, ultimate strength expressions for predicting the load-carrying capacity were formulated. To further verify these ultimate strength expressions, a representative number of beam tests were conducted on composite units constructed with steel decks E, O and G.

Specimen behavior was observed by noting the crack patterns, load at first visible end-slip, identification of mode of failure and through load-deflection measurements. Certain beams were instrumented with end-slip measuring devices and a continuous slip record during loading was obtained. Also, elec-

---

[a]Letters were chosen to identify the different steel decks, thus, avoiding direct company comparison.

trical strain gages were applied to selected beams, both to the steel deck and concrete.

Review of Literature

The development of composite steel-deck-reinforced concrete slab construction has been greatly influenced and accelerated by the issuance of the various editions of the "Specification for the Design of Cold-formed Steel Structural Members" of the American Iron and Steel Institute (26). This specification pertains only to the design of the steel deck itself and does not apply to composite steel-deck-reinforced systems; nevertheless, it provides basic design information concerning the steel deck itself.

The first significant publication to appear on the subject of composite steel-deck-reinforced floor slabs was authored by Bengt F. Friberg in 1954, (8). His work not only provides an understanding for the design of the particular steel deck profile tested, but also gives the reader an excellent cost evaluation between conventional concrete slabs, and steel deck-reinforced slab construction. S. Bryl (2) reported in 1967 on an investigation of a number of different steel deck profiles acting compositely with the concrete. His discussion regarding the ultimate load carrying capacity of composite steel-deck-reinforced systems gives the reader a thorough understanding of behavior. Based on numerous test results, Bryl outlined the following important behavioral and design characteristics: 1) Sudden failure of the slab occurs without the use of shear devices; 2) Large plastic deformations are accompanied by considerable increase in load-carrying capacity in the slab with shear transfer devices; 3) The slab should be analyzed as an uncracked composite section with the criteria for design of: concrete bending stresses, bond stresses and permissible load on shear transfer devices. Also, he points out that this type of slab construction has many cost-saving advantages and will be exploited in the future, opening up wider markets to the steel constructors. Both Friberg and Bryl employed working stress principles in their respective investigations.

The current state of development of steel-deck-reinforced concrete slabs is the result of a somewhat independent effort by the individual steel deck producers. At this time, a number of composite steel decks are commercially available and are trade-marked such as "Hi-bond"; "Cofar"; "Q-Lock"; "Grip-deck" and others. Each manufacturer has conducted research and prepared unpublished reports concerning the strength and behavior of his particular product. A few such unpublished reports are indicated by references (11), (16), (24), and (29). These proprietory research reports indicate that, based on experimental beam tests, a shear type of failure tends to be more predominate than flexure. Resulting from this research and based on working stress procedures, each steel deck producer has published a catalog pertaining to the design of his product such as given in (9), (10), (18), and (27). In general, these catalogs give permissible superimposed loads, shoring requirements, deflection limitations, amount of shrinkage reinforcement and other design considerations.

The American Iron and Steel Institute is currently sponsoring a research project at Iowa State University relating to the composite action between concrete and steel deck of steel-deck-reinforced concrete slabs. Since the initiation of this research in 1967, several research-progress reports have resulted, namely, references (5), (6), (7), (15), (17), (21), (22) and (23). At its beginning stage, this work entailed extensive testing of composite deck-reinforced pushout tests along with selected companion beam specimens. The intent of the pushout tests was to obtain possible design data and information leading to a better understanding of steel-deck-reinforced concrete systems. It was found that beam specimens failed due to a breakdown at the interface between the steel deck and concrete, and in none of the specimens tested was flexure the primary cause of failure. In other words, shear was the primary mode of failure. The ultimate load carrying capacity was found to vary for each steel-deck-reinforced concrete beam, resulting from the steel deck's unique inherent shear transfer capacity, the shear span, L', and the percentage of steel. However, some difficulty was encountered with certain steel decks in trying to relate pertinent pushout data with respective beam results; therefore, it was concluded that only beam specimens be tested and an ultimate strength approach be employed.

Most recently, two publications by Hugh Robinson (19) and (20) have appeared on the related subject of composite beam design. Here the steel-deck-reinforced concrete slab acts compositely with supporting beams or girders. This composite action is accomplished by the use of standard stud shear connectors or special connectors welded to the supporting members. The work presented in this investigation does not involve this type of composite beam behavior.

Types of Steel Decks

Characteristically, composite steel decks provide certain mechanical horizontal shear transfer devices in order to obtain composite action between the steel deck and concrete under service conditions. Typically, these devices consist of either rolled-in embossments as shown in Figs. 1, 2 and 3, or are smooth with wires or buttons welded to the peaks of the corrugations. See Fig. 4 for an example of smooth deck with wires welded to the top corrugations. In many cases shear transfer devices also provide resistance to vertical separation between the steel deck and concrete, although in some cases the shape of the deck itself provides this function. In addition, shrinkage control may be provided by shear devices such as deformed, wires, etc., placed transversely to the corrugations.

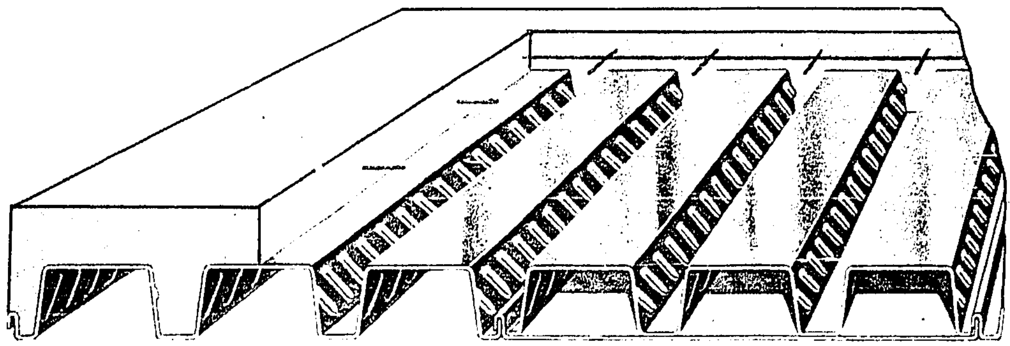

Fig. 1. Example of CATEGORY I - Steel deck utilizing embossments on webs of deck
(Courtesy of the Inland-Ryerson Steel Company)

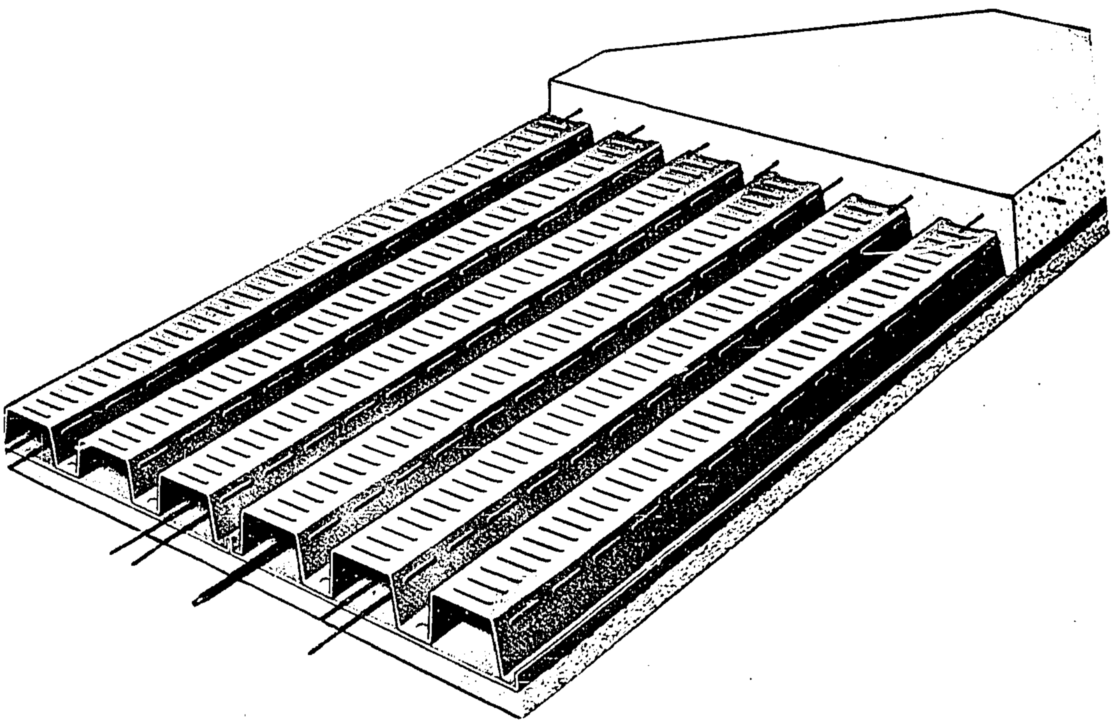

Fig. 2. Example of CATEGORY I - Steel deck utilizing embossments on flanges and webs of deck
(Courtesy of the H. H. Robertson Steel Company)

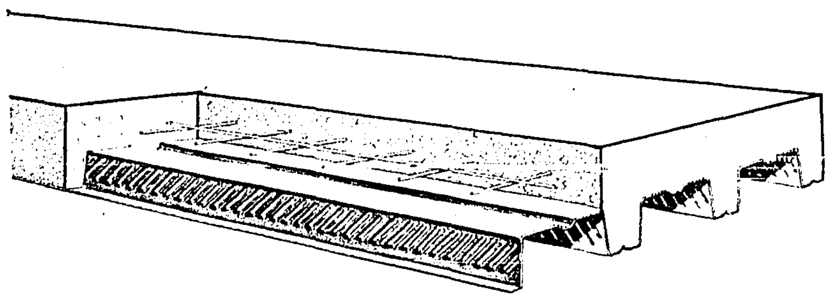

Fig. 3. Example of CATEGORY I - Steel deck utilizing emboss-
ments on webs of deck
(Courtesy of Bowman Building Products)

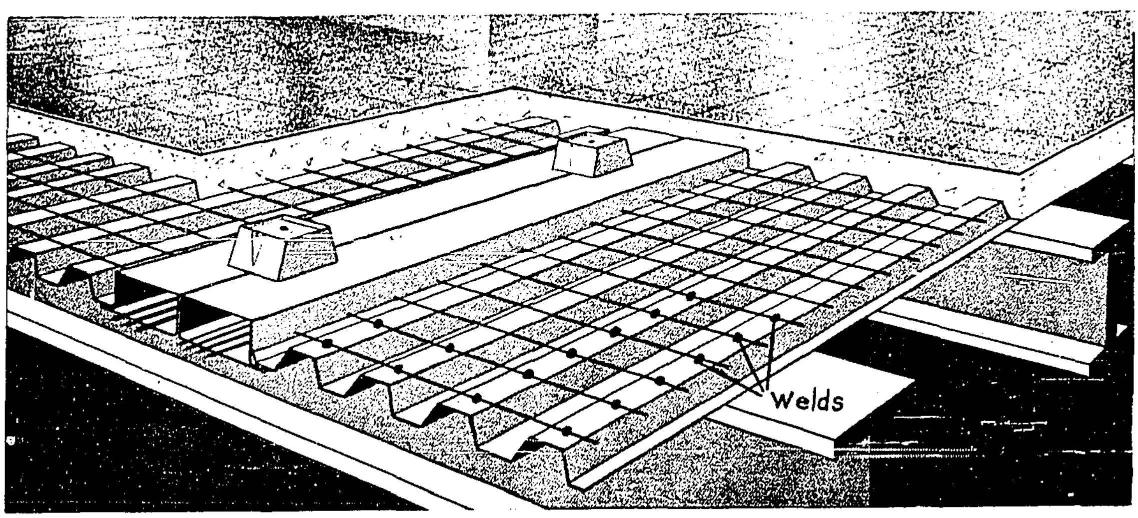

Fig. 4. Example of CATEGORY II - Steel deck utilizing deformed
wires welded to the top of deck
(Courtesy of the Granco Steel Company)

It is most convenient to divide steel deck profiles into three categories based on the pattern of mechanical shear connectors such as embossments, holes, welded wires or buttons. The three categories are stated as follows:

CATEGORY I Steel deck profiles that provide horizontal shear capacity primarily by virtue of a fixed pattern of mechanical shear devices. See Figs. 1, 2, and 3 for examples.

CATEGORY II Steel deck profiles that have a variable spacing of mechanical devices. Fig. 4 shows a typical steel deck of CATEGORY II.

CATEGORY III Steel deck profiles that have no mechanical shear devices, but rely on chemical bond between the deck and concrete.

Review of Present Design Procedures

Design principles for steel-deck-reinforced concrete slab systems are primarily based on conventional reinforced concrete-working stress methods (1). In general, permissible stress values for concrete and steel are obtained from reference (1); however, permissible shear or bond values are based on test results, as conducted by the deck manufacturer. Section properties pertaining to the steel deck alone are calculated in accordance with conventional methods of structural design and the AISI Design Specification (26). Shoring requirements during the construction stage are normally determined by employing conventional elastic flexural and deflection methods.

Flexural stress calculations of steel-deck-reinforced concrete systems are generally based on the following assumptions, accompanied by the usual formulas:

a) Planes remain plane, i.e., the strain of the concrete and steel varies linearly as the vertical distance from the composite neutral axis.

b) Tensile strength of the concrete is neglected below the neutral axis; thus, the steel deck resists all tension due to positive bending.

c) Composite flexural constants are calculated based on a cracked section theory.

$$f_s = \frac{M}{S_b} n \text{ and } f_c = \frac{M}{S_t}$$

where

M = applied bending moment

f_s = stress in the bottom fiber of the steel deck

f_c = stress in the top fiber of the concrete

S_b = composite cracked section modulus transformed to concrete, bottom fiber of steel deck

S_t = composite cracked section modulus transformed to concrete, top fiber of concrete

n = modular ratio

The determination of shear transfer stresses can best be illustrated by considering, separately, steel decks of CATEGO-

RIES I and II. For decks of CATEGORY I, two different approaches are being used, depending on the manufacturers choice. For example, one such approach utilizes the horizontal shear stress expression (11)

$$t = \frac{VQ}{I_T}$$

where

V = the acting external shear force

t = the shear transfer force, per unit length

Q = the statical moment

I_T = moment of inertia of transformed composite section

and the other is based on the following bond relationship (10):

$$u = \frac{V}{\sum_o jd}$$

where

u = the average unit bond stress on contact surface between the steel deck and concrete

$\sum_o$ = the contact surface per unit of length

j = ratio which defines arm of resisting couple

d = distance from top of concrete slab to centroid of steel deck.

In the case of one particular steel deck the horizontal shear stress expression is employed, and is given by:

$$v = \frac{V}{bjd}$$

where

b = the width of slab under consideration.

Modifying this equation, based on an area of slab, (s x g), results in a relationship for the maximum weld shear per-weld, namely

$$w' = \frac{Vsg}{bjd} \quad (9)$$

where

w' = maximum calculated weld shear per-weld

s = spacing of transverse wires

g = transverse width of a repeating section, assuming one weld within each section.

In this case, permissible weld shear values, on a per-weld basis, are given as a measure of the shear capacity.

Naturally, other design considerations such as deflections, shoring requirements, shrinkage reinforcement and others are also taken into account. Minimum factors of safety of 2.0 against shear and 1.67 against flexure seem to be well established figures among composite steel deck manufacturers (10), (18) and (27).

The current state of design criteria, as described above, for steel-deck-reinforced composite slab construction, is the result of a somewhat independent effort by the various steel deck producers. An examination of the separate design criteria by these firms does generally reveal employment of sound engineering principles. In all cases an elastic design procedure has been adopted; however, actual experimental test results are still necessary to determine the shear transfer capacities of the various steel-deck-reinforced systems. Since this is the case, and experimental tests have to be conducted, it would be more advantageous to base the design criteria on an ultimate strength approach. This is further supported by the fact that each steel deck manufacturer wants a standard format for design so that his deck may compete on the same basis with other decks when used for composite slab construction. Also, each composite deck behaves uniquely by virtue of its geometric shape and shear transfer device.

Considering the above mentioned reasons, an ultimate strength procedure, based on laboratory performance tests, is justifiable.

TEST PROGRAM

General Remarks

The purpose of the test program was two-fold, namely, to obtain experimental beam test data for the determination of design expressions, and to provide the steel deck producer with a standard performance test format. Based on experimental testing reported in (6), (7), (17) and (23), beam testing was primarily focused on the nature of shear transfer between the steel deck and concrete. As a result, only shear type failures were encountered; however, the test program described herein also entailed the testing of steel-deck-reinforced slab elements failing in flexure.

The test program described herein was designed in an effort to simulate, as closely as practically possible, beam elements of steel-deck-reinforced concrete slabs as found in common construction practice. Naturally certain assumptions had to be made to reduce the many possible loading parameters, as found in actual field practice, to a minimum. In general, under normal building design procedures, design loads are assumed uniformly distributed over the span. The question of whether or not this is always the case throughout the life of the structure is debatable, since concentrated loads are inevitably experienced in any building structure. However, from the standpoint of design, distributed loads offer simplification and ease of design. In the laboratory, on the other hand, uniformly distributed loads are difficult and time-consuming to simulate. As a conservative approach, all laboratory beam tests were based on a one or two-point concentrated line load system. Thus, an additional factor of safety was realized, since design is based on uniformly distributed loads, yet the shear-bond evaluation is based on concentrated loads.

Materials

All light gage steel decks used in this investigation were supplied by the various manufacturers. Typical cross-sectional profiles of steel decks I, O, and E of CATEGORY I and deck G of CATEGORY II are shown in Figs. 5, 6, 7, and 8, respectively. Pertinent measured and calculated cross-sectional properties of these steel decks are shown in Tables A.1 and A.2. Steel deck yield strengths varied from 40,000 up to as high as 110,000 psi. In the case of decks I and O, the steel conformed to ASTM designation A245-64 or A446-64T having a minimum yield strength of 33,000 psi (0.2% offset method). Decks E and G conformed to ASTM A446-65T for Grade E steel having a minimum yield strength of 80,000 psi (0.1% offset method). Tensile coupon tests, conforming to ASTM designation A370-65, fabricated from actual test steel decks, were performed and the results are tabulated in Table A.3 of Appendix A. Typical stress-strain curves for these samples are shown in Fig. 9.

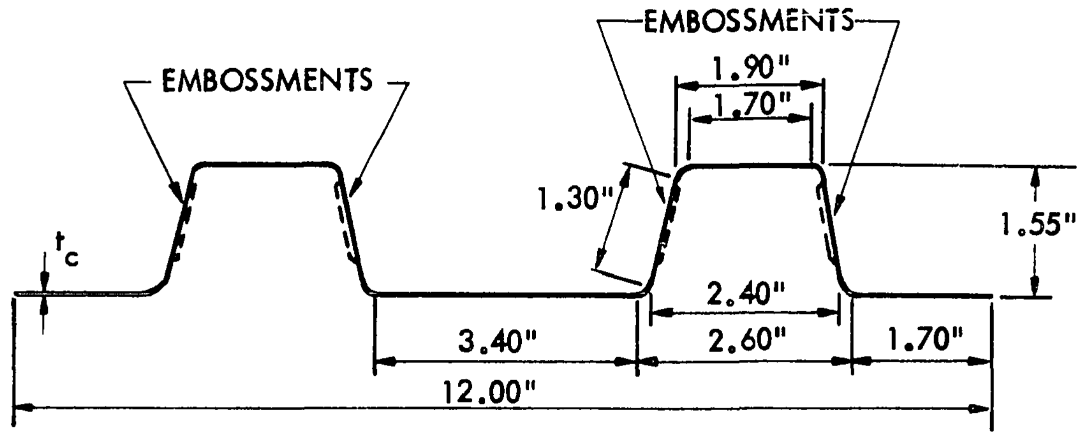

Fig. 5. Typical profile of steel deck I (CATEGORY I)

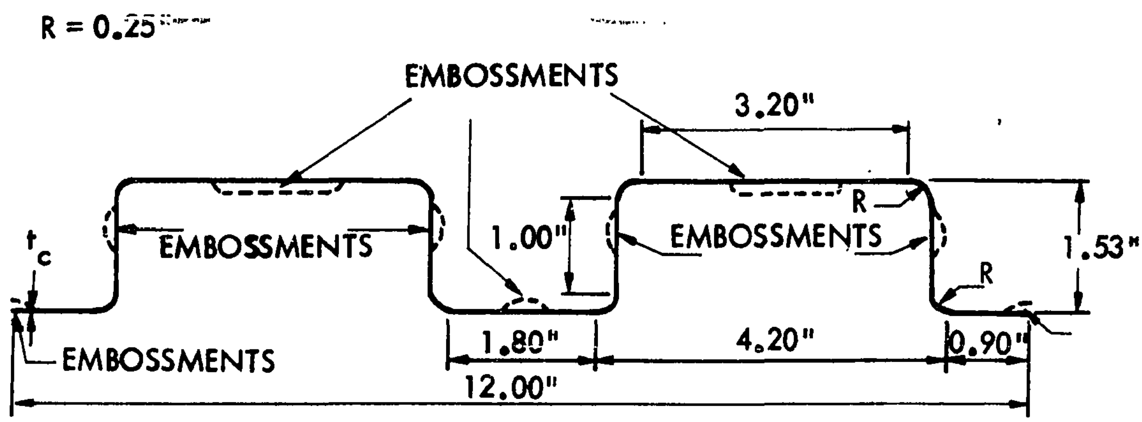

Fig. 6. Typical profile of steel deck O (CATEGORY I)

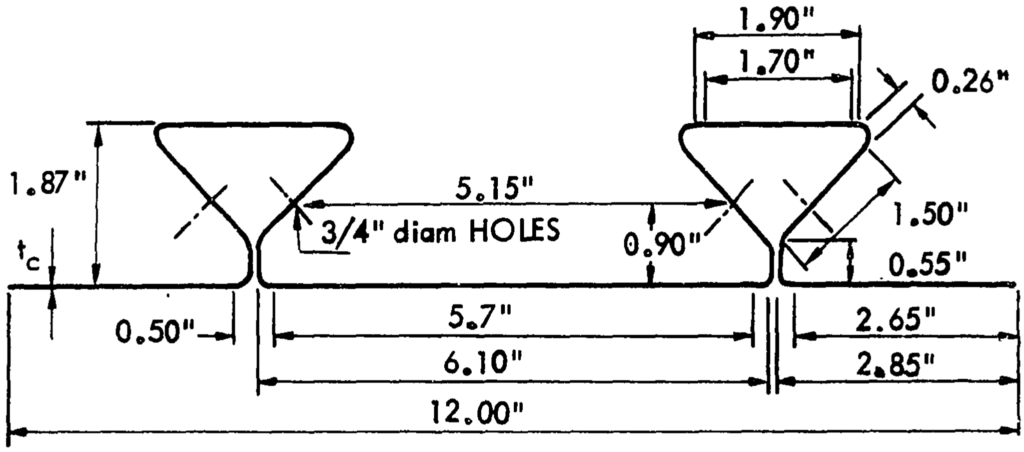

Fig. 7. Typical profile of steel deck E (CATEGORY I)

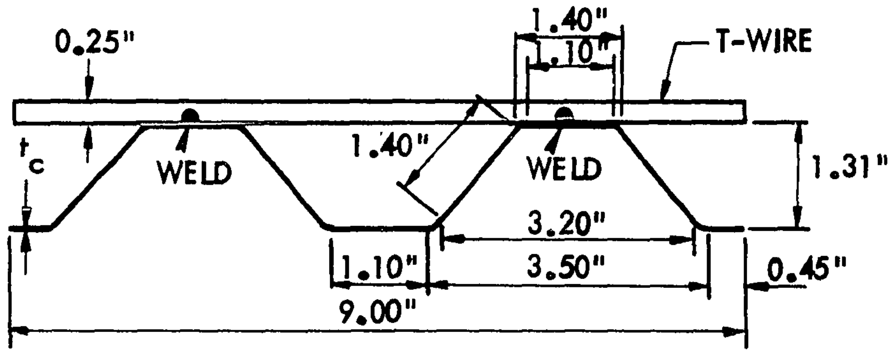

Fig. 8. Typical profile of steel deck G (CATEGORY II)

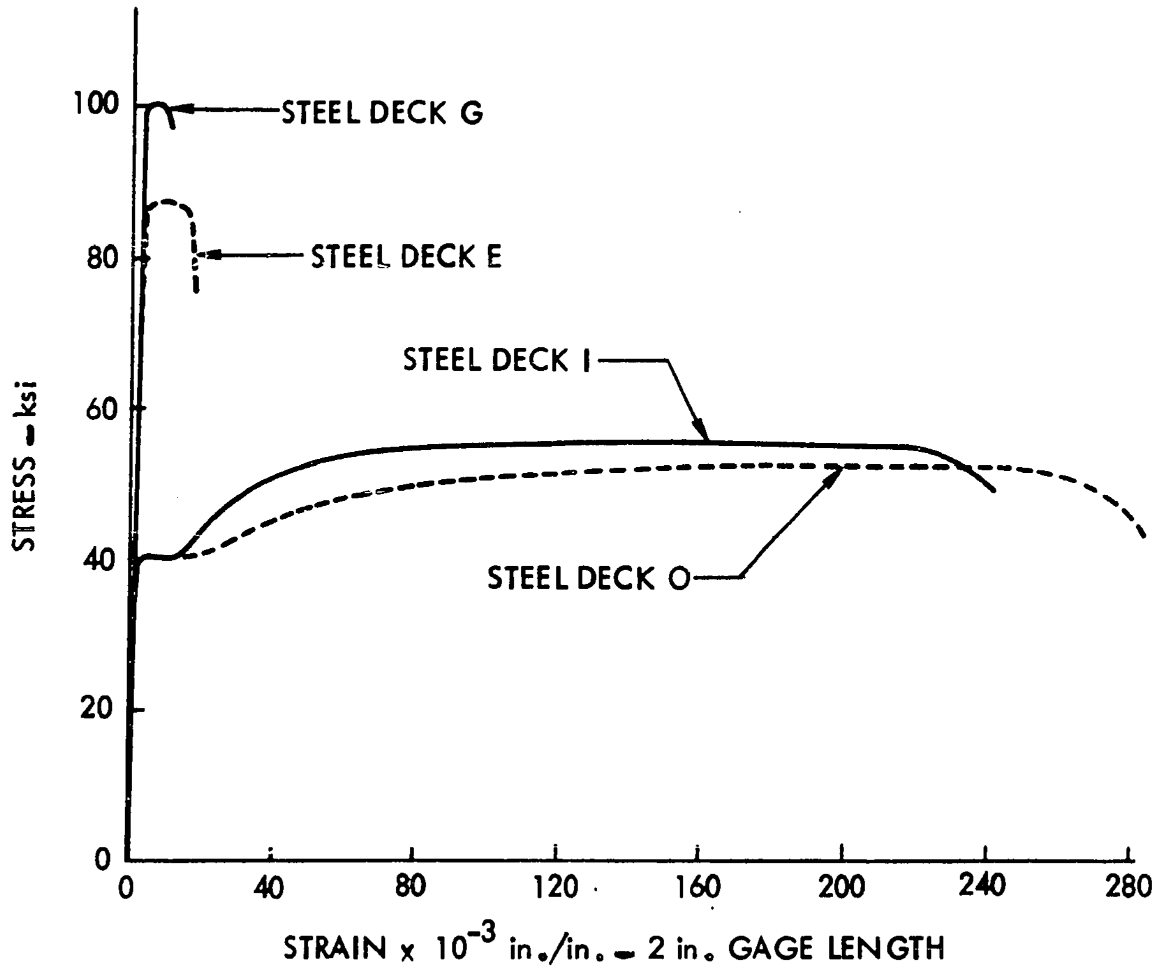

Fig. 9. Typical stress-strain curves for tensile tests of steel coupons consisting of steel decks I, O, G and E

Each particular steel deck had a surface finish such as galvanizing or phosphate treating. The degree of this finish was not considered important and consequently no attempt was made to determine its effectiveness in reference to the ultimate load carrying capacity. Care was taken to insure that steel decks were free of all foreign matter such as grease and oil, so as to create similar field conditions as found in actual construction practice.

The concrete was ordered from a local ready-mix plant to meet the following specfications:

1. 3,000 psi compressive cylinder strength in 7 days.
2. 3/4 in. maximum size crushed rock aggregate except for cast numbers 4, 5 and 6 which was 3/8 in.
3. 3-1/2 to 4 in. slump.
4. No admixtures and no water reducing agents.

See Table A.4 of Appendix A for the listing of all concrete pours, summary of concrete properties and resulting average compressive strengths, f'_c.

Description of Beam Specimens

Steel decks I, O, and E of CATEGORY I and deck G of CATEGORY II were used in constructing the composite steel-deck-reinforcement beam specimens. All steel decks were of out-to-out depth between 1-1/3 and 2 inches, such that the neutral axis of the composite cross-section was located above the top of the steel deck. Beam units were tested in two different lengths, namely, 6 and 12 feet. It was intended, by testing two extreme beam lengths, that in the case of the shorter span a shear-bond failure would be certain to result and in the case of the longer span a flexural failure might be predominant. Beam widths were either 12, 24, 28, or 30 inches, depending on the type of test and standard steel deck panel width as produced by the manufacturer. Steel deck gages were varied, along with the overall concrete depth in an effort to change the percent of steel over a large range.

Tests were conducted on a total of 145 steel-deck-reinfoced concrete beams, including 28 of which were re-tested, and constructed with steel decks I, O, G and E. A detailed description of beam specimens consisting of individual steel decks will be presented and discussed as follows:

Steel deck I (CATEGORY I)

A total of 111 tests were conducted on beams using steel deck I. These involved 87 beams, including 24 which were re-tested. Fifty-one beams were cast 6 feet long, 12 inches wide, 5 inches deep and the shear span, L', was varied symmetrically from a minimum of 12 inches to a maximum of 34 inches. The remaining 36 beams were cast 12 feet long, approximately 24 inches wide, i.e., the standard panel width. The beam depths ranged from 3-1/2 to 5-1/2 inches and the shear spans varied symmetrically from 30 to 70 inches. From these 36 beams, 24 additional test results were obtained by re-testing certain beams. These re-tested beams, being shorter in span length, were tested on relatively short shear spans, namely, ranging from 14 to 40 inches. A table of organization and overall view of the beams tested, consisting of steel deck I, is presented in Table 1.

Table 1. Summary of beams tested utilizing deck I

No. of beams	No. of re-tested beams	Gage of steel	Span length (in.)	Beam depth (in.)	Beam width (in.)
20	none	18	68	5	12
31	none	22	68	5	12
3	3	16	140	3-1/2	24
4	4	16	140	4-1/2	24
3	2	16	140	5-1/2	24
5	3	18	140	3-1/2	24
6	4	18	140	4-1/2	24
4	3	18	140	5-1/2	24
3	1	22	140	3-1/2	24
5	1	22	140	4-1/2	24
3	3	22	140	5-1/2	24
87 +	24 =	111			

Steel deck O (CATEGORY I)

A total of 32 tests were conducted on beams using steel deck O. These tests involved 28 beams, including 4 which were re-tested. Twelve of the beams were cast 6 feet long, 12 inches wide, 5 inches deep and shear spans varied symmetrically from a minimum of 12 inches to a maximum of 34 inches. The remaining 16 specimens were cast 12 feet long, approximately 24 inches wide, with beam depths ranging from 3-1/2 to 5-1/2 inches and the shear span varied symmetrically from 36 to 70 inches. From the 16 beams, 4 additional test results were obtained by re-testing certain beams with shear spans ranging from 24 to 36 inches. Table 2 shows an overall view of the beams tested which were constructed with steel deck O.

Table 2. Summary of beams tested utilizing deck O

No. of beams	No. of re-tested beams	Gage of steel	Span length (in.)	Beam depth (in.)	Beam width (in.)
12	none	20	68	5	12
4	none	22	140	3-1/2	24
2	none	22	140	4-1/2	24
2	none	22	140	5-1/2	24
2	1	16	140	3-1/2	24
3	1	16	140	4-1/2	24
3	2	16	140	5-1/2	24
28 +	4 =	32			

<u>Steel deck G (CATEGORY II)</u>

A total of 18 beam specimens were cast 12 feet in length and tested. Nine of these consisted of 20 gage steel decks, with a width of approximately 28 inches, beam depths ranged from 3-1/2 to 5-1/2 inches, shear spans varying symmetrically from 24 to 70 inches and the shear connector spacing, s, was either 3, 5 or 8 inches. The remaining 9 beams were cast on 24 gage steel decks approximately 30 inches in width and the parameter variations were the same as described above. Table 3, which is similar to Tables 1 and 2, shows data on beams tested which were constructed with deck G.

Table 3. Summary of beams tested utilizing deck G

No. of beams	No. of re-tested beams	Gage of steel	T-wire spacing (in.)	Span length (in.)	Beam depth (in.)	Beam width (in.)
1	none	24	3	140	3-1/2	30
1	none	24	3	140	4-1/2	30
1	none	24	3	140	5-1/2	30
1	none	24	5	140	3-1/2	30
1	none	24	5	140	4-1/2	30
1	none	24	5	140	5-1/2	30
1	none	24	8	140	3-1/2	30
1	none	24	8	140	4-1/2	30
1	none	24	8	140	5-1/2	30
1	none	20	3	140	3-1/2	28
1	none	20	3	140	4-1/2	28
1	none	20	3	140	5-1/2	28
1	none	20	5	140	3-1/2	28
1	none	20	5	140	4-1/2	28
1	none	20	5	140	5-1/2	28
1	none	20	8	140	3-1/2	28
1	none	20	8	140	4-1/2	28
1	none	20	8	140	5-1/2	28
18 +	0 =	18				

Steel deck E (CATEGORY I)

Twelve beam specimens were fabricated with steel deck E and tested. Each beam, consisting of 20 gage steel decking, was 6 feet long, 12 inches wide, 5 inches deep and the shear span was varied symmetrically from 12 to 34 inches.

Fabrication, Casting and Curing of Specimens

All specimens were cast in prefabricated, adjustable steel forms supplied by the Economy Form Company of Des Moines, Iowa.

Prior to inserting the steel decks, the forms were coated with a nonstaining, paraffin form oil to insure easier stripping. In the case of electrically strain gaged specimens, all strain gages applied to the exposed surface of the steel deck were attached prior to casting. The steel decks were then positioned into the assembled forms, parallel to the length of the intended composite beams. Anchors for lifting the beams were placed at about 10 inches from each end.

Casting

Before proceeding with the actual concrete casting of the specimens, a slump test was performed. Generally, two additional slump tests were made at approximately the one-third points as the pour progressed. Vibration of the concrete was accomplished with a small laboratory type, one inch head, vibrator that operated at 10,500 cycles per minute. Periodically during the pour, standard control cylinders were cast in 6 x 12 inch waxed cardboard cylinder molds. These control cylinders were prepared in accordance with Section C39-66 of the ASTM Specification.

Curing

With the control cylinders positioned near the beam specimens, at approximately 4 to 5 hours after concrete placement, the tops of the beams and cylinders were covered with wet burlap and plastic sheets. This was done in an effort to achieve proper and similar curing conditions of the beams and cylinders. After three days, the beams were removed from the economy forms, the test cylinders stripped of their cardboard casings and both beams and cylinders were stored under moist conditions for an additional four days. Specimens and cylinders were then air dried in the laboratory for at least an additional seven days until testing was undertaken.

The above-stated procedure was followed with all test specimens, including those that were cast completely shored or supported throughout. In the case of shored specimens (one shore at midspan), midspan shore supports were removed after the concrete had reached a compressive strength of approximately 2,000 psi. Otherwise the same procedure of curing as described above was followed.

Test Equipment and Instrumentation

Loading apparatus

In obtaining control cylinder concrete compressive strengths, a 300 kip capacity Southwark Emery hydraulic universal testing machine was used. All beam specimens were tested in a Baldwin-Southwark hydraulic 400 kip capacity testing machine, except for a few selected beams which were tested under equivalent gravity dead load conditions in a 50 kip capacity fatigue machine.

Instrumentation

Instrumentation included devices for measuring vertical deflections, electrical strain gages, and deflectometers for detecting end-slip. Only for certain selected beams were strain gages and deflectometers used, whereas vertical deflections were measured in all cases. In the case of beams with electrical strain gages, a Baldwin-Lima-Hamilton Type N SR-4 strain indicator was used to measure strains in the steel and concrete. A Baldwin switching unit was used to improve the efficiency of reading the gages. Some beam specimens were instrumented to measure end-slip between the concrete and steel deck. This was accomplished by attaching a deflectometer assembly to the top of the concrete on each end of the beam. The deflectometers consisted of small aluminum, strain-gaged cantilever beams with the free end attached to the steel deck as shown in Figs. 10 and 11. These deflectometers measuring end-slip, were continuously monitored by a BL-274 Brush amplifier and recorded by an oscillograph throughout the entire test.

Testing Procedures

Control cylinders

Strengths of 6 x 12 inch standard cylinders were determined at the time of beam testing to determine the compressive strength of the concrete.[a] At least three cylinders were used to obtain each average value of f'_c as given in Table A.4. Beam

---

[a]Cylinder tests conducted in accordance with ASTM C39-66.

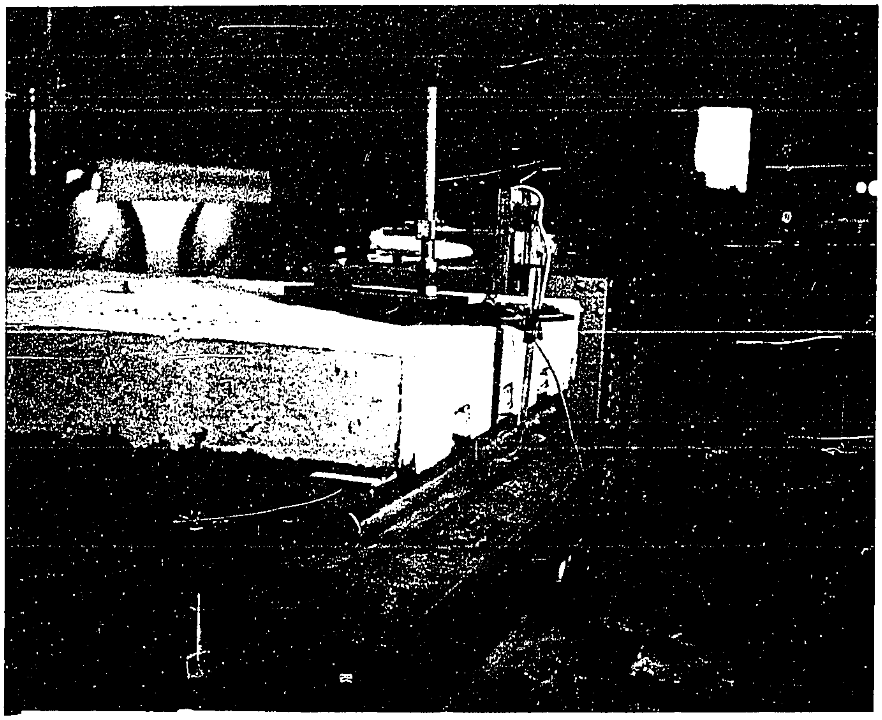

Fig. 10. Overall view of typical end-slip deflectometer instrumentation

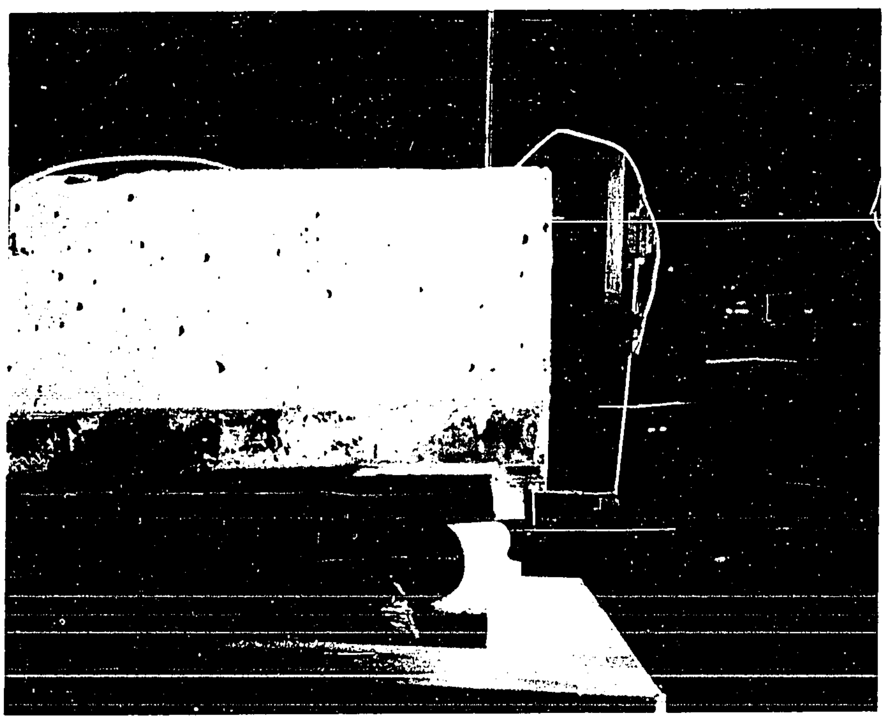

Fig. 11. Elevation view of typical end-slip deflectometer unit

testing was not conducted until the cylinders indicated a minimum concrete strength of 3,000 psi.

Specimen loading scheme

Each composite deck-reinforced beam was tested on simple span supports and subjected to a symmetrical mode of loading, consisting of either a single concentrated line load or two concentrated line loads, as shown in Fig. 12.

All beam specimens were supported on a system of simple support bearing plate arrangements as shown in Detail "A" of Fig. 12. Neoprene bearing pads were first placed on the concrete at points of load application to ensure a more uniform line load distribution. Steel bearing plates were then placed over the neoprene pads before the transverse load beams were positioned. Figure 12 shows a typical overall view of the two point loading scheme along with detailed dimensions. The roller and pin supports and the spherical bearing head of the testing machine eliminated any reasonable amount of longitudinal restraint.

Testing

After the specimen was supported as shown in Fig. 12 the deflection gages were positioned and actual testing was undertaken. However, in the case where electrical strain gages and end-slip instrumentation were employed, testing was not undertaken until all strain gages were adequately wired and end-slip instrumentation was properly attached. All strain gages lo-

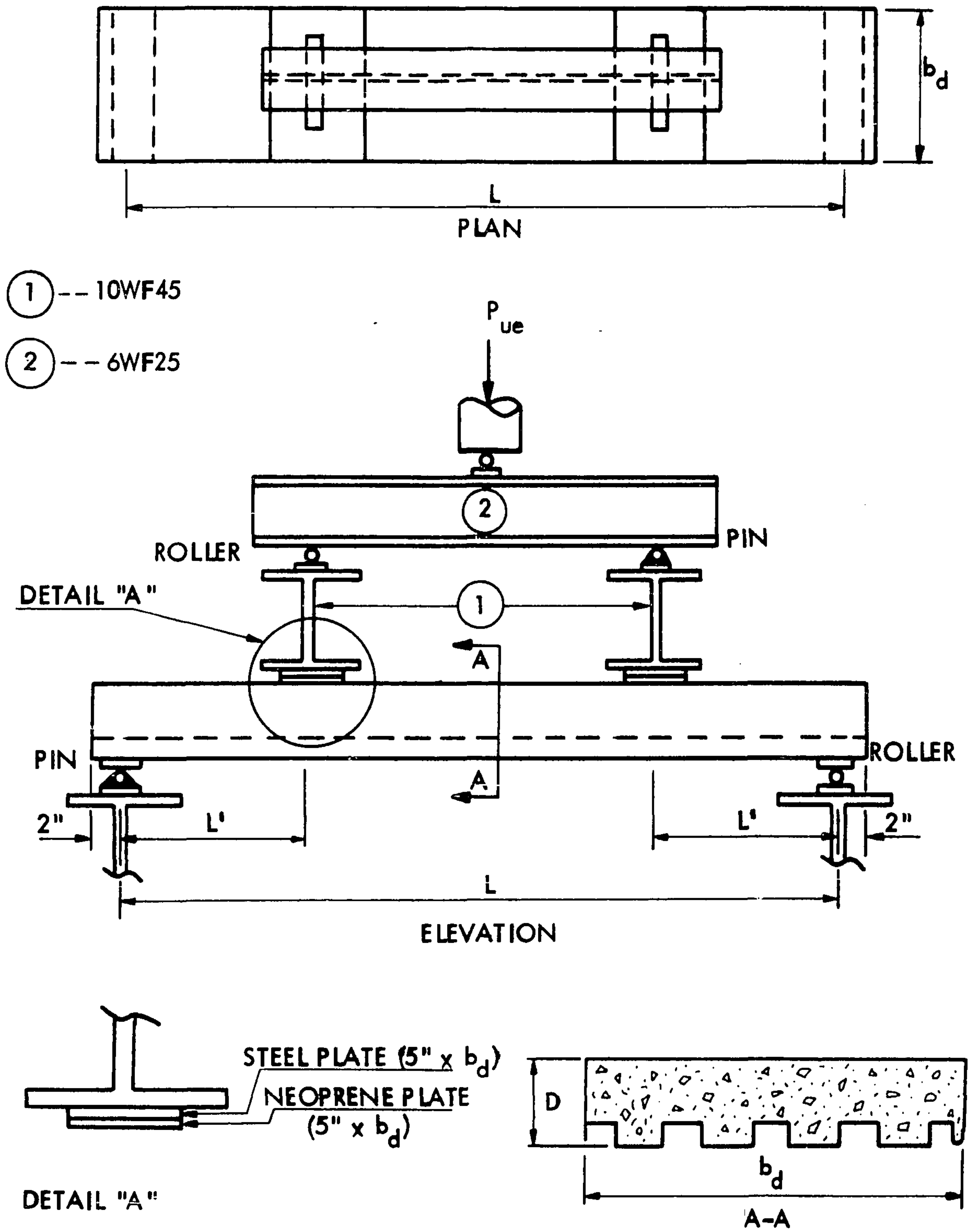

Fig. 12. Typical composite steel-deck-reinforced beam test setup

cated on the surface of the steel deck were applied prior to casting. Strain gages applied to the surface of the concrete were wired after the system was positioned in the testing apparatus.

Loading was then applied and maintained at each 200 lb. increment level only until the necessary deflection and strain gage readings were recorded. Cracking characteristics, mode of failure and end-slip between concrete and steel deck were observed and documented. Since the depth of shored specimens varied slightly along the length of the beam, the depth at the position of the major failure crack was also measured and recorded.

BEHAVIOR RESULTS

General Remarks

In the following sections, failure modes, load-deflection beam behavior, strain gage behavior and end-slip results are discussed and described. Individual attention is given to beams constructed with each steel deck, namely, I, O, G, and E.

The description of failure modes was based on actual laboratory beam test results and characterized into either a shear-bond, flexure-yielding or a flexure-crushing type of failure. In an effort to describe the behavior during testing of all beams, an idealized load-deflection curve was used. Strain gage information of selected beams provided experimental evidence whether or not the steel had reached its yield level and to verify the assumption of strain linearity. End-slip behavior was graphically recorded with certain beam tests and was intended to be used only as a means of identifying a shear-bond failure.

Failure Modes

Characteristically, two major and distinct modes of failure were observed from beam tests, namely, shear-bond and flexure. Shear-bond is the result of a brittle type of failure accompanied by the formation of an approximate diagonal crack, resulting in end-slip and loss of bond between the steel deck and concrete. This simultaneous action of shear and bond is termed shear-bond. Conversely, a flexural failure is a more gradual type which is induced by yielding of the steel or crushing of concrete. A more detailed description of these failure types regarding steel-deck-reinforced systems is given as follows:

Shear-bond

The characterization of this failure was identified by the formation of a major crack (approximate diagonal crack), under or near one of the line loads, resulting in a sudden failure at ultimate load. This failure was accompanied by end-slip between the steel deck and concrete, thus, causing the concrete shear span portion, L', to become disengaged, and loss of bond between steel deck and concrete was experienced. See Figs. 13, 14 and 15 for typical shear-bond failures. Also, selected photographs of typical beam specimens having failed in shear-bond are shown in Figs. B.1 through B.8 of Appendix B. In no case was the ultimate load taken at a value greater than that load at which initial visible end-slip was observed. A shear-bond failure may or may not have been preceded by yielding of the steel, depending on the relative values of the percentage of steel, the shear span, L', and the inherent load transfer capacity of the shear transfer devices. Yielding of the steel deck, whenever in occurrence, initiated at the extreme bottom fibers of the steel deck and in some cases progressed toward the top of the steel deck. In no case, however,

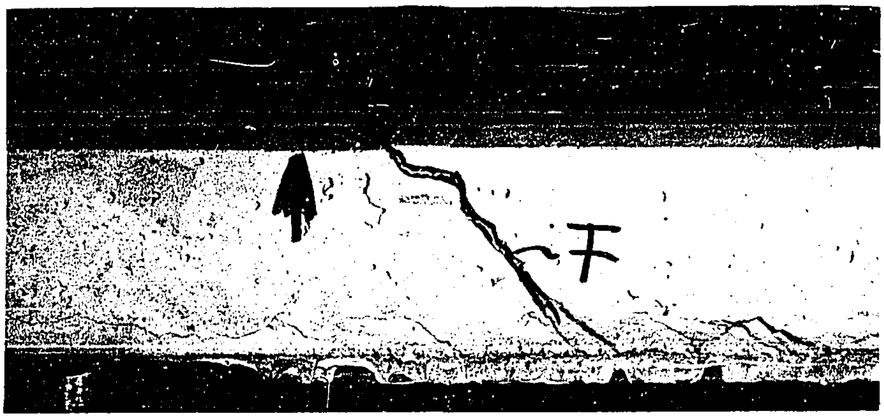

Fig. 13. Typical shear-bond failure crack of beam constructed with steel deck I. Arrow indicates point of load application

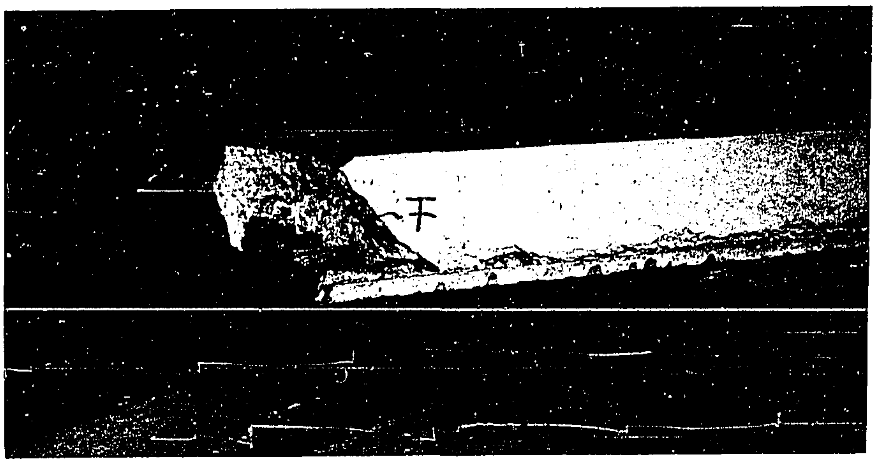

Fig. 14. Cross-section of shear-bond failure crack of beam shown in Fig. 13

Fig. 15. Typical shear-bond failure crack of beam constructed with steel deck G. Also showing end-slip

did the steel deck yield over its entire depth since that would have resulted in a flexure-yielding failure or under-reinforced case.

Flexure

Flexure failure may be divided into two principal categories: 1) yielding of the steel and 2) crushing of the concrete in the compression zone. There was no observable end-slip between the steel deck and concrete with flexural failures.

a) Flexure-yielding resulted when the steel ratio, p, was relatively low (under-reinforced). Complete tearing of the steel deck, accompanied with a sudden collapse of the system was experienced, resulting from a ductile and yielding failure with the steel deck having yielded over its entire depth. See Fig. 16 for a typical fexure-yielding failure.

b) Flexure-crushing on the other hand was experienced when the steel ratio, p, was relatively high (over-reinforced) so that the concrete compression zone reached its ultimate capacity before all fibers of the steel experienced their yield level. As the ultimate load was approached, destruction of the concrete compression zone was observable. Following failure, some residual stiffness of the member was still evident, depending on the steel deck and the extent of failure of the compression zone of the concrete. See Fig. 17, for example, of this type of failure.

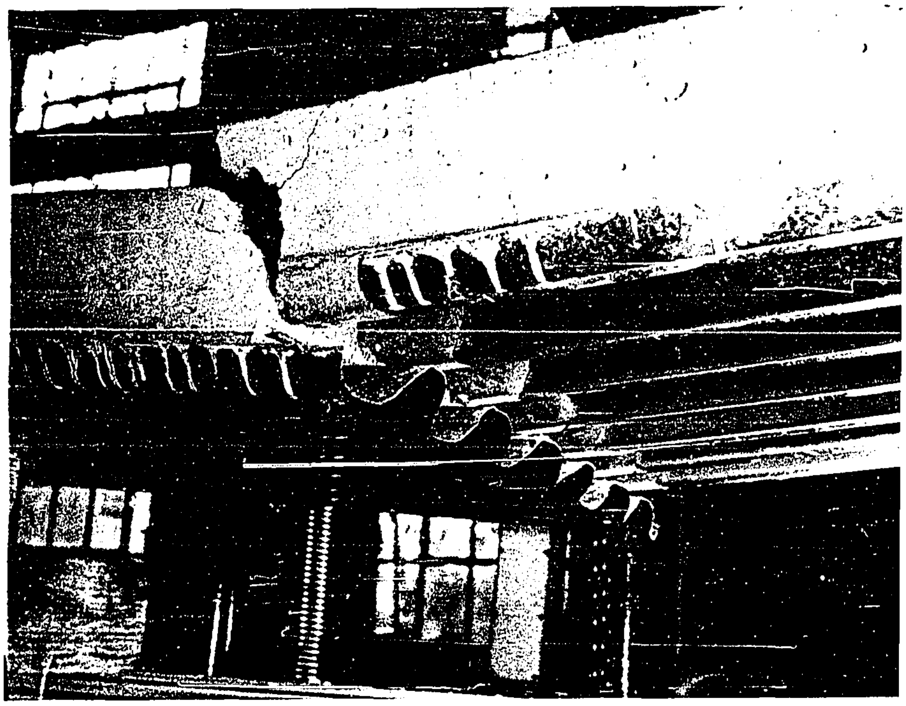

Fig. 16. Typical flexure-yield failure of beam constructed with steel deck G

Fig. 17. Flexure-crushing failure of beam constructed with steel deck G

Explanation of Specimen Notation

Each beam specimen referred to in this investigation, regarding experimental testing conducted by the author, was designated by a beam number followed by a specimen designation. The purpose of the beam number designation was to provide a short and quick method of beam identification which was used in the discussions throughout this presentation. Figure descriptions were identified by using both the beam number and specimen designation. Beam numbers were first sequentially numbered, then identified by the type of steel deck, such as I, O, G or E, and followed by the gage of the steel deck. The specimen designation, on the other hand, was designated by a series of numerals and in some cases letters. The following possible notation format is applicable to beam specimens constructed with steel decks I, O and E, and is illustrated in Example 1 below:

Example 1:

Beam no.	Specimen designation
40I22	46 - 19 - 20SH

where

40 = beam number 40

I = name of steel deck (could also be O or E)

22 = gage of steel deck

46 = length of shear span, L', in inches

19 = cast number (see Table A.4 of Appendix A)

20 = number of days elapsed from casting to testing

SH = beam was shored at midspan (otherwise omitted if completely shored or replaced by SG)

SG = strain gages were placed on beam and beam was shored at midspan.

For beams constructed with steel deck G, the shear transfer device spacing, s, was encorporated in the specimen designation as illustrated in Example 2 below:

Example 2:

Beam no.	Specimen designation
9G24	8 - 28 - 26 - 19SH

where

8 = T-wire spacing, s, in inches.

All other designations remain the same as defined in Example 1. In the case of re-tested beams, the letter R was added following the shear span length, L'. Example 3 shows a typical illustration.

Example 3:

Beam no.	Specimen designation
43I22	30R - 15 - 21

where

R = indicates beam was re-tested.

All other designations remain the same as defined in Example 1.

Load-Deflection Beam Behavior

A general beam behavior discussion during loading, pertaining to all steel decks tested, namely decks I, O, G and E, will be first presented and referenced to the typical idealized load-deflection curve of Fig. 18. Attention should be called to the fact that actual load-deflection curves do not in every case follow this idealized pattern but may deviate to some degree.

When the load was gradually increased from zero to that magnitude that caused the beam to fail, several possible unique stages of behavior were identifiable. Selected actual load-deflection curves, as shown in Figs. 19-22, furnish a consistent view of the mode of action as the loaded beam progressed through the various stages of behavior. Three such stages along with their complimentary transition zones are considered and make up the typical idealized load-deflection curve of Fig. 18. Stage (1) represents the uncracked loading stage. There is no cracking anywhere during this stage; thus, the section is fully composite and the stresses in the concrete and steel are proportional to strains. Horizontal shear stresses are negligible until first cracking occurs. After reaching the load P_1, hair-line cracks begin to develop at the maximum tension interface of concrete and steel deck in the constant moment regions. In the case of two symmetrically placed line loads, the maximum tension region occurs between or at the two load points where the moment is at its maximum and constant,

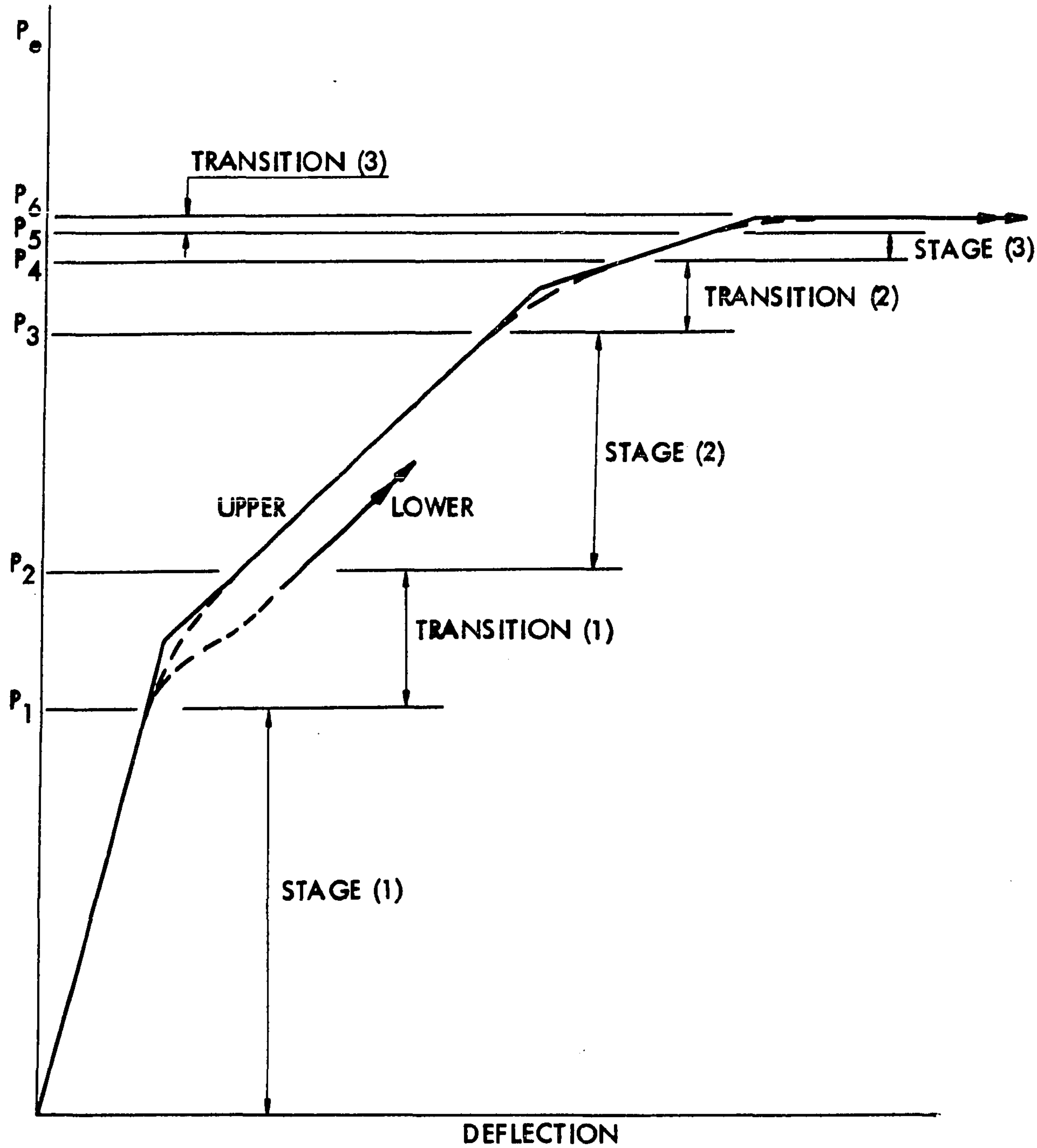

Fig. 18. Typical idealized load-deflection curve for beams constructed with steel decks I, O, G and E

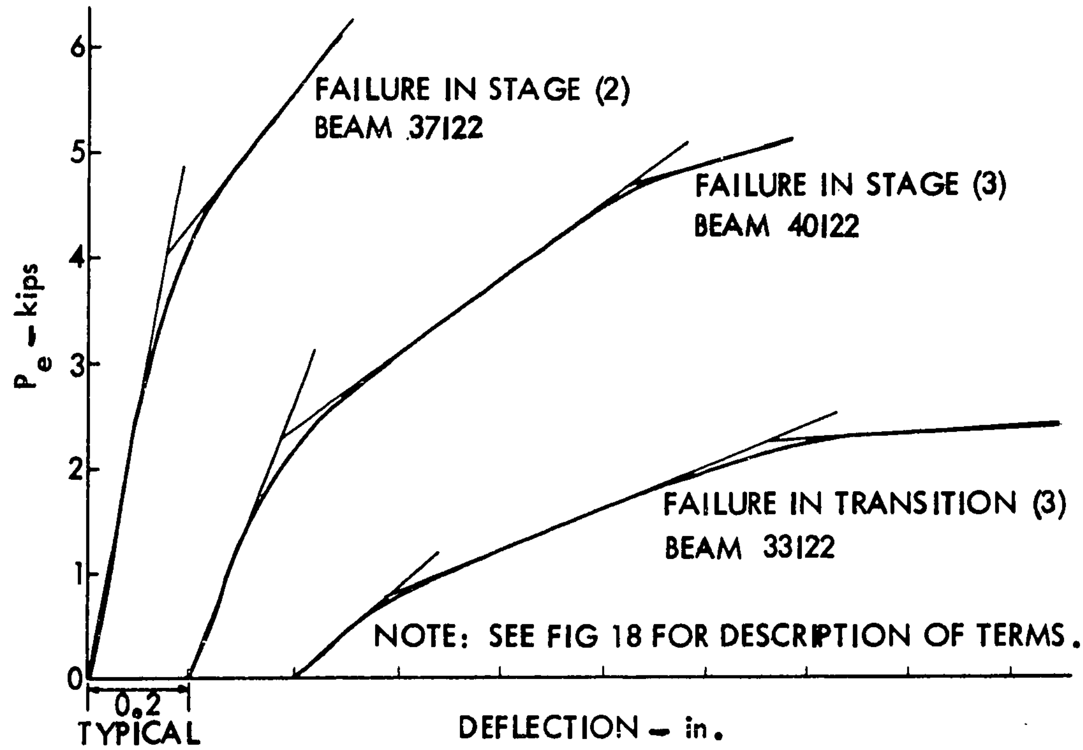

Fig. 19. Applied experimental load, P_e, vs. deflection for typical beams constructed with steel deck I

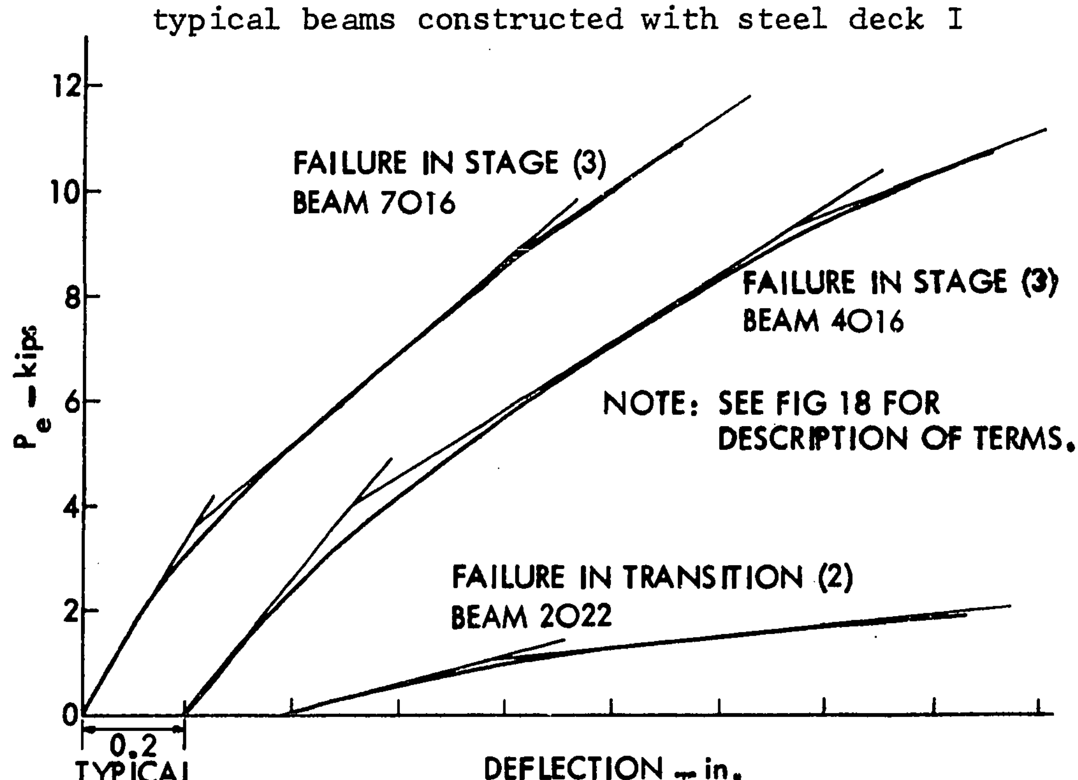

Fig. 20. Applied experimental load, P_e, vs. deflection for typical beams constructed with deck 0

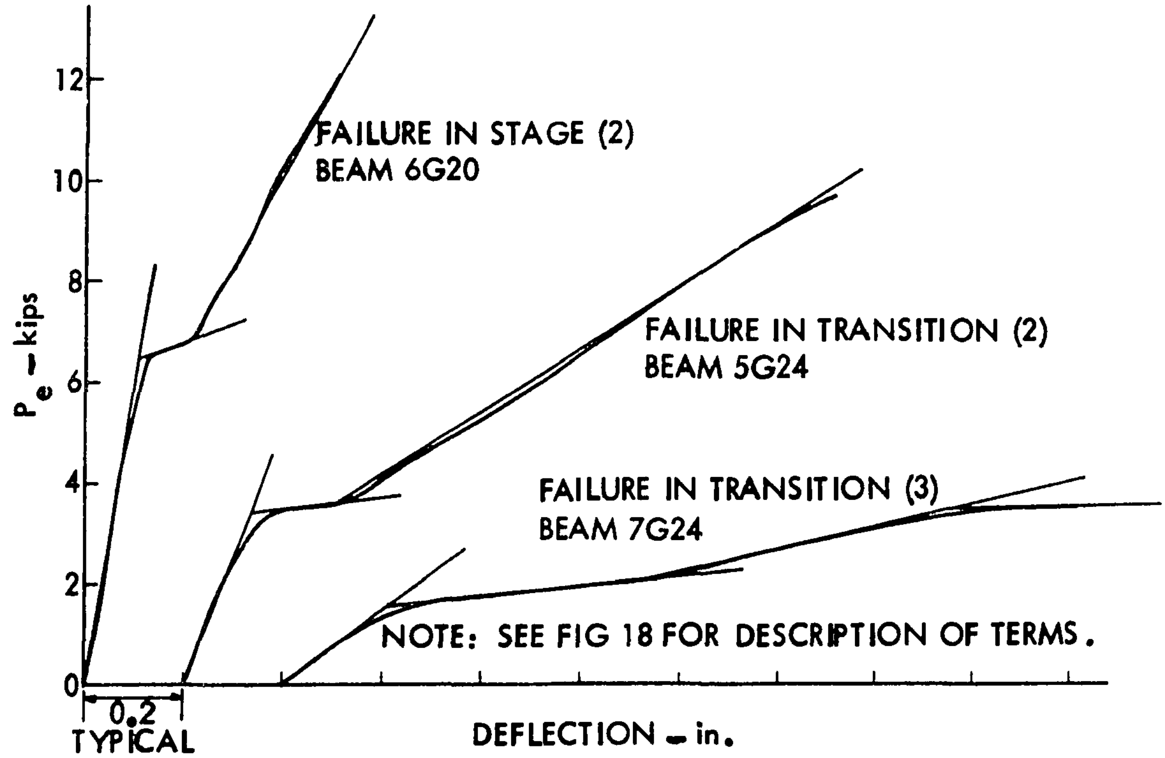

Fig. 21. Applied experimental load, P_e, vs. deflection for typical beams constructed with steel deck G

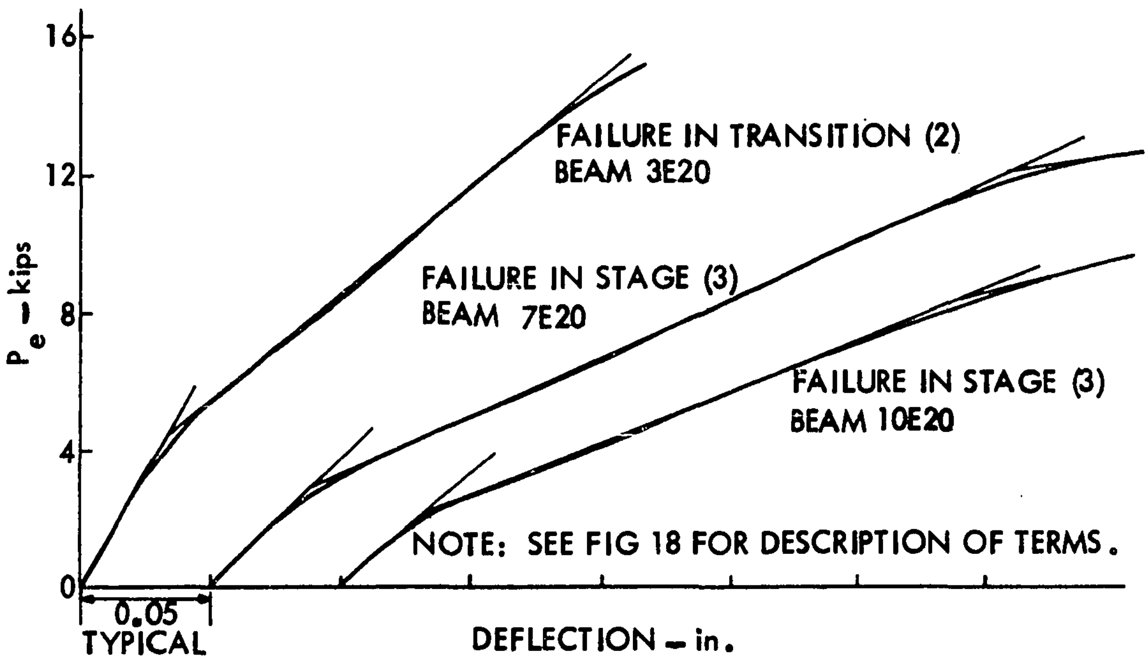

Fig. 22. Applied experimental load, P_e, vs. deflection for typical beams constructed with steel deck E

thus, no shear forces exist. Consequently, the hair-line cracking is caused only by bending forces. However, at the two load point locations, both maximum bending and maximum shear is experienced; thus, two primary potential failure cracks may develop under or near the load points. When the beam is subjected to a single concentrated line load at the center of the span, both maximum bending and maximum shear exists directly under the load. This gives rise to a primary potential failure crack in the immediate region of the point of application of the load. The upper dashed-line transition curve (1), extending from P_1 to P_2, was found to be typical for beams constructed with decks I, O and E, while for beams of deck G, the lower is typical.

With this characteristic readjustment in the load-deflection curve as the load is increased from P_1 to P_2, the mechanical shear transfer devices begin to transfer load in the horizontal direction along the shear span, L'. This action is analogous to bond-type slip in conventional reinforced concrete. Only by means of the shear transfer devices is a load increase beyond P_2 possible. Without shear transfer devices, the additional load above P_1 would depend primarily on the chemical bond between the steel deck and concrete and the shear span length, L'. During stage (2), from P_2 to P_3, shear-bond capacity is provided by the shear transfer devices and an ultimate shear-bond failure may be experienced, depending on the percent of steel and shear span, L'. The shear span, L', being the predominate factor since a relatively short shear span, say the width of the beam, gives rise to large shear-bond stresses, keeping the flexure stresses low. For this reason, the stress in the steel deck is below the yield level and failure would be termed shear-bond without yielding of the steel. The slope of the load-deflection curve in stage (2) is seen to be constant, indicating that the increase in load from P_2 to P_3 is linear and no redistribution of internal stress is experienced. In other words, the primary potential failure crack or cracks, initiated during the transition curve between P_1 and P_2, are progressing into the section undeviated or in a vertical direction. In the immediate region of the potential failure crack, prior to and at failure, localized frictional resistance between the concrete and steel deck is created as the concrete shear span portion, L', tends to become disengaged from the steel deck. Frictional resistance is inherent with all steel-deck-reinforced systems and depends on the type of shear transfer device as well as the nature of composite containment. For example, this friction phenomenon can be observed from Fig. 23. To the right of the major crack, located in the center of the photograph and extending over the entire width of the beam, the inclined embossments show a definite discoloring in reference to the embossments located to the left of the crack. This is believed to be caused by the interactional friction resistance created between the concrete and the steel deck's embossments prior to and to some degree during

Fig. 23. Underside of failed beam constructed with steel deck I with steel deck cut away

the instant of a typical shear-bond failure. At failure, with the ultimate load at or below P_3, a sudden diagonal crack causes end-slip between the steel deck and concrete, hence, deviating the vertical crack at or near the top of the steel deck into an approximate 45^o diagonal crack and resulting in a shear-bond type of failure. Beams 37I22 and 6G20 of Figs. 19 and 21, respectively, failed in stage (2), namely, with the ultimate load at or below P_3, but greater than P_2.

If a shear-bond failure is not encountered when reaching the load P_3, then a diagonal crack is formed under or near the load point as the load is increased up to P_4. This diagonal crack, which in turn is responsible for the readjustment of the load-deflection curve from P_3 to P_4, is clearly visible. Redistribution of stresses is again encountered during this transition curve from P_3 to P_4 as caused by the formation and extension of the diagonal crack. Failure may or may not occur during this action of diagonal crack appearance in transition (2). If failure does impend, with the load between P_3 and P_4, the characterization of this failure is again of the shear-bond type, without yielding of the steel. Failure of beams 2022 and 5G24 of Figs. 20 and 21, respectively, occurred in transition (2), namely, between loads P_3 and P_4.

Stage (3), from P_4 to P_5, marks another linearly varying stage in which a relatively long shear span, L', is being tested, such that enough shear connectors are present to adequately carry the load without failure below P_4. Since the shear span, L', is large, deflections will increase respectively and in turn tend to cause, in addition to shear-bond forces, vertical separation may in some cases be the cause of initiating failure in stage (3). Should a shear-bond failure develop between P_4 and/or at P_5, the steel stress will in most cases still be below yield; however, in some cases yielding might be impending at the bottom of the steel deck. Beam 40I22 of Fig. 19, 4016 and 7016 of Fig. 20 and beams 7E20 and 10E20 of Fig. 22 failed in stage (3).

A further increase in load beyond P_5 is only possible when the shear span, L', is at its largest possible value with the percentage of steel at its minimum. The nonlinear curve between load P_5 and P_6, namely, transition (3), indicates that yielding of the steel has occurred and is extending toward the top of the steel deck. Shear-bond is still the failure mode in transition (3), but the steel deck is experiencing yielding that has almost progressed toward the top of the deck. Beams 33I22 and 7G24 of Figs. 19 and 21, respectively, have failed in transition (3).

The transition curve from P_5 to P_6 becomes asymptotic at the load level of P_6, indicating that no shear-bond failure has occurred and the ultimate properties of the steel and concrete have been exhausted. In other words, flexure is the mode of failure, either by yielding of the steel and possibly resulting in a complete rupture of the deck and/or by crushing of the concrete.

Behavior as Measured by Strain Gages

General remarks

A total of 13 beams of CATEGORY I were strain-gaged with the intent of obtaining experimental behavior results pertaining to the stresses in the steel and concrete. Eight of these were constructed with steel deck I and five of deck O. All strain-gaged beams resulted in shear-bond failures and in no case did a flexural failure occur. Of particular interest was whether or not a shear-bond failure was preceded by yielding of the steel deck. Consequently, strain gages were placed on beams consisting of and being tested under conditions that would result in a possible shear-bond failure with the steel having partially yielded. A number of beams were also strain-gaged and tested under conditions that would assure a shear-bond failure without the steel having yielded. Strain gage results were also used to show strain linearity over the beam cross-section at various load levels.

Experimental steel stress results and strain linearity will be discussed separately in the following sections.

Steel stresses

Experimental steel stress vs. applied load for beams constructed with steel deck I was plotted and shown in Figs. 24 through 29, and for beams constructed with steel deck O in Figs. 30 through 33. Also indicated on these figures are corresponding theoretical stress curves, a beam cross-section showing strain gage locations, and the yield level of the steel.

Experimental steel stresses, f_{es}, below the yield level, were calculated from the following expression:

$$f_{es} = \epsilon_{es} E_s$$

where ϵ_{es} is the experimental strain and E_s the modulus of elasticity of the steel. For strain values greater than the strain at which yielding occurred, steel-stress-strain curves such as shown in Fig. 9 were used to obtain respective steel stress values. Since these stress-strain curves resulted from coupon

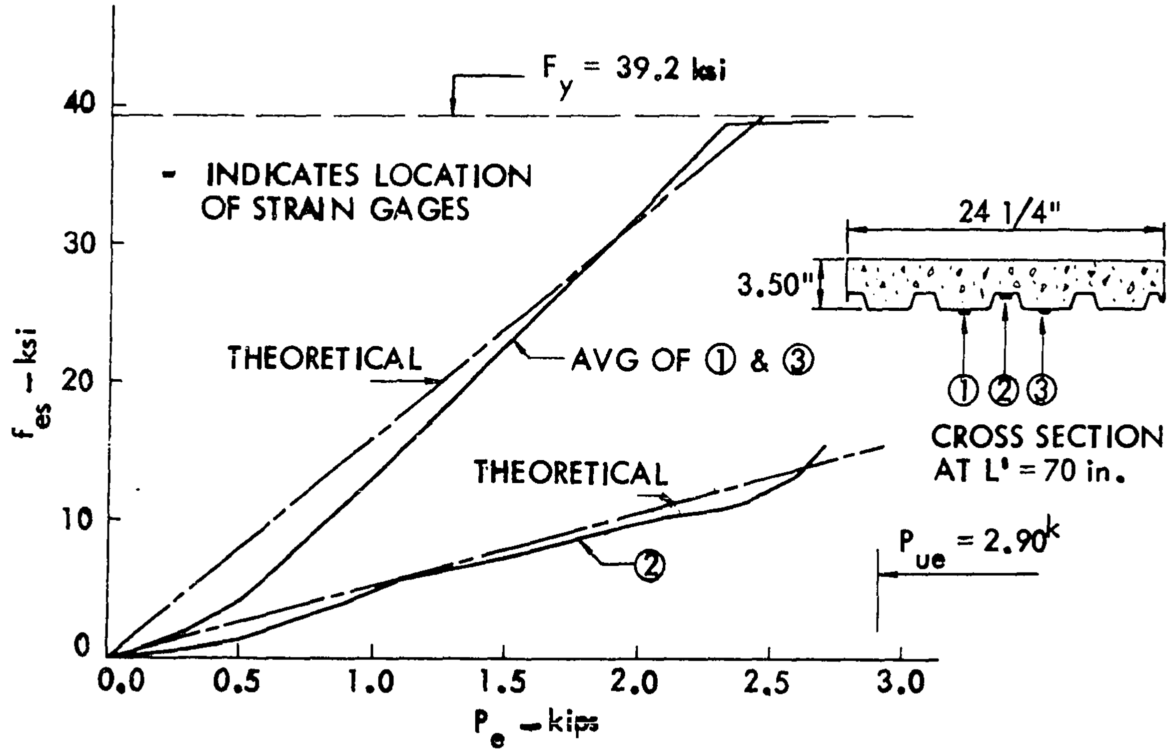

Fig. 24. Experimental steel stress, f_{es}, obtained from strain gage results, vs. experimental applied load, P_e, for beam 41I22-70-19-19SG, constructed with steel deck I

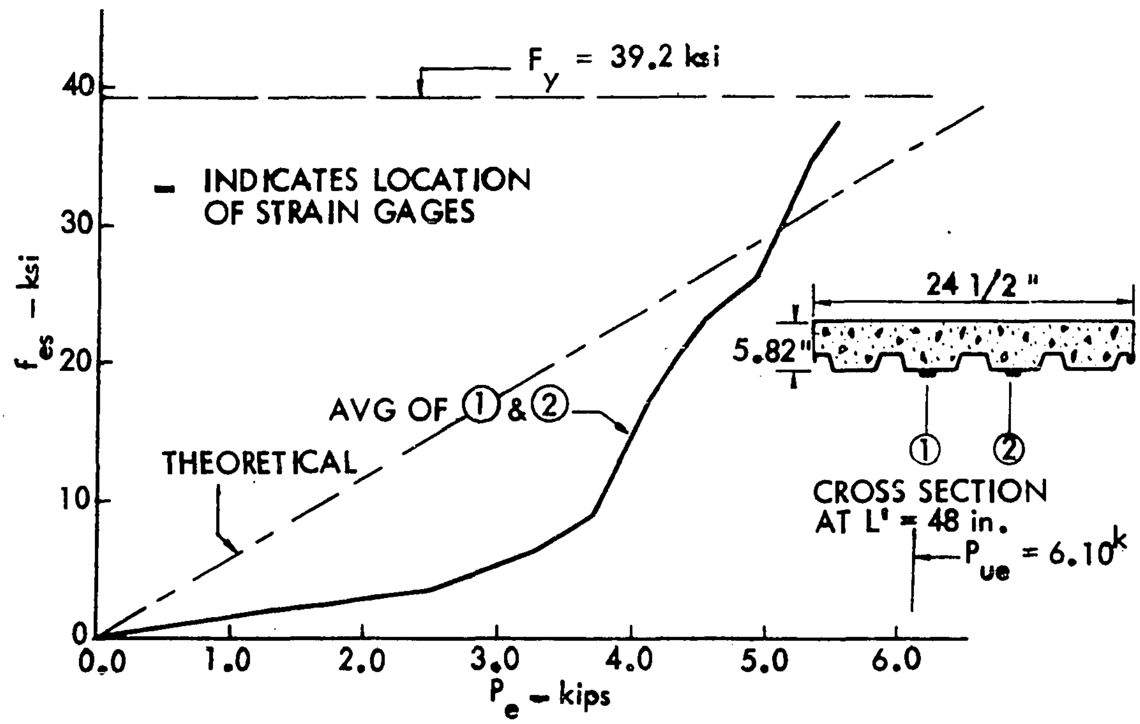

Fig. 25. Experimental steel stress, f_{es}, obtained from strain gage results, vs. experimental applied load, P_e, for beam 42I22-48-20-16SG, constructed with steel deck I

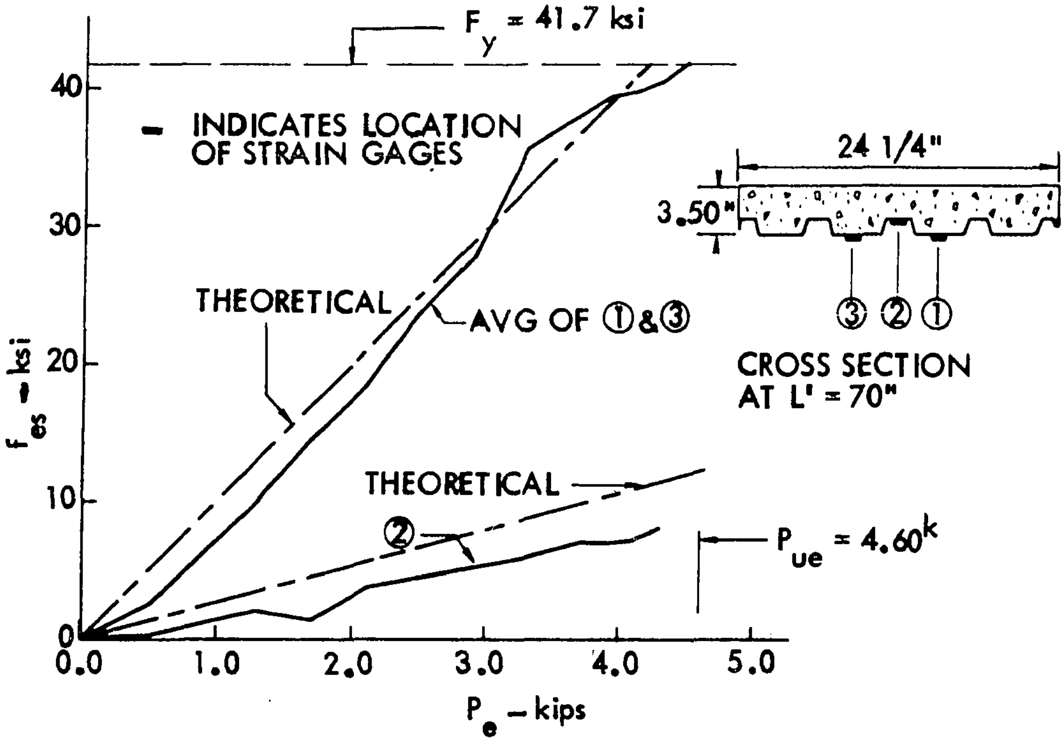

Fig. 26. Experimental steel stress, f_{es}, obtained from strain gage results, vs. experimental applied load, P_e, for beam 33I18-70-19-19SG, constructed with steel deck I

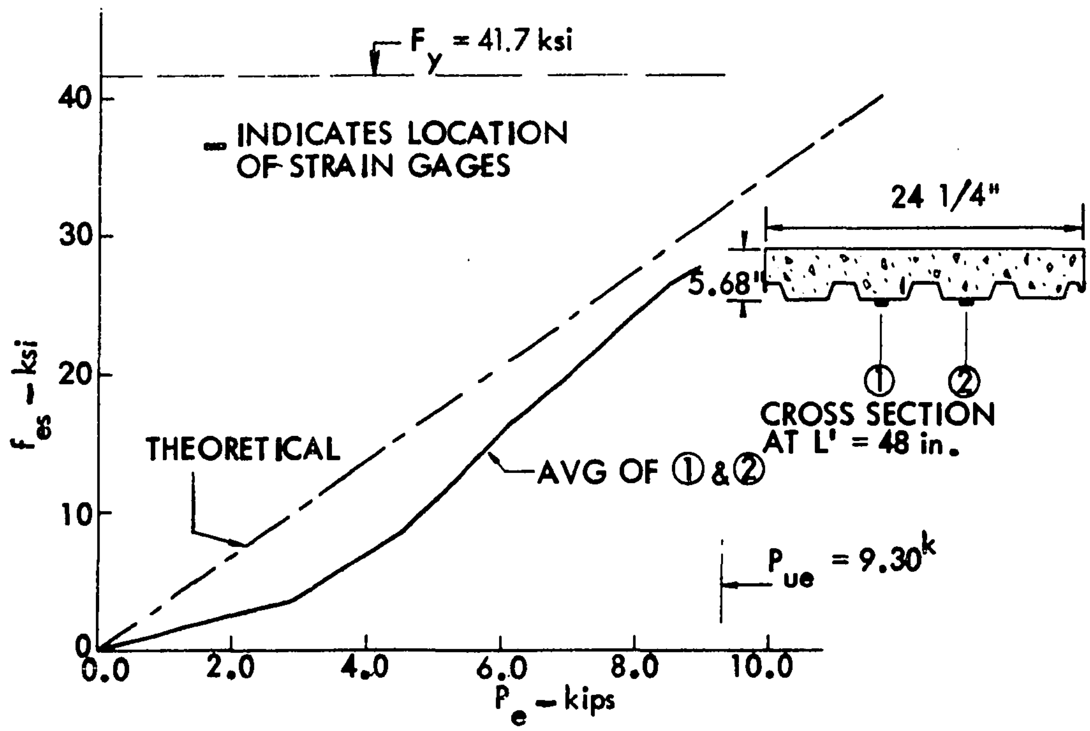

Fig. 27. Experimental steel stress, f_{es}, obtained from strain gage results, vs. experimental applied load, P_e, for beam 35I18-48-20-16SG, constructed with steel deck I

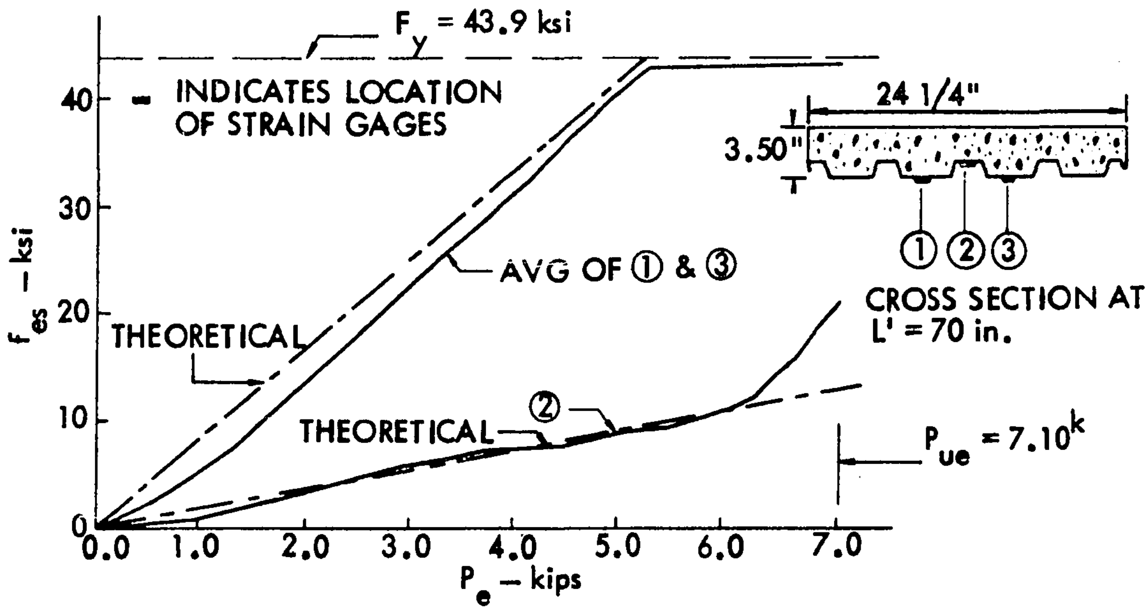

Fig. 28. Experimental steel stress, f_{es}, obtained from strain gage results, vs. experimental applied load, P_e, for beam 8I16-70-19-19SG, constructed with steel deck I

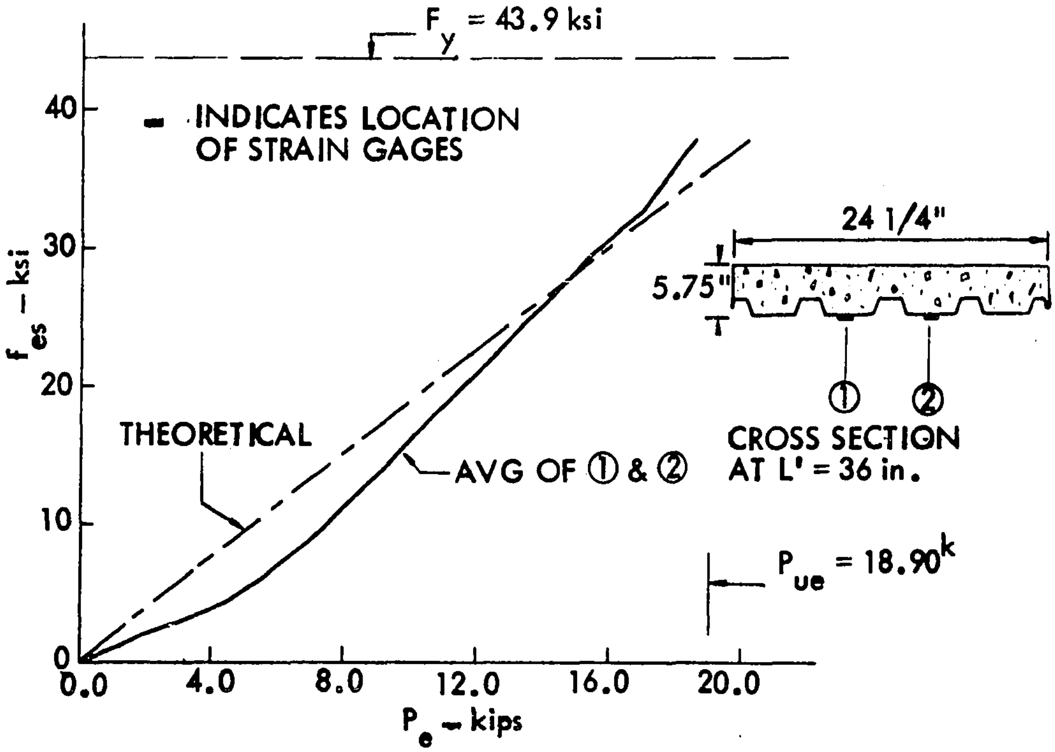

Fig. 29. Experimental steel stress, f_{es}, obtained from strain gage results, vs. experimental applied load, P_e, for beam 10I16-36-20-19SG, constructed with steel deck I

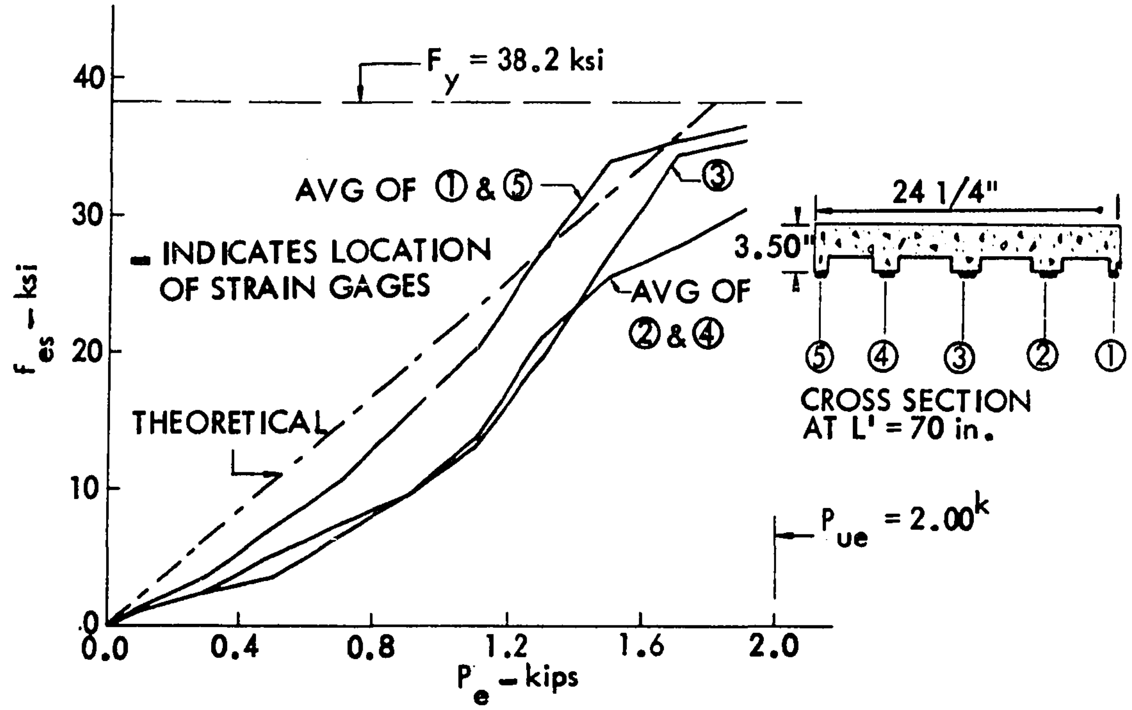

Fig. 30. Experimental steel stress, f_{es}, obtained from strain gage results, vs. experimental applied load, P_e, for beam 7022-70-22-28SG, constructed with steel deck O

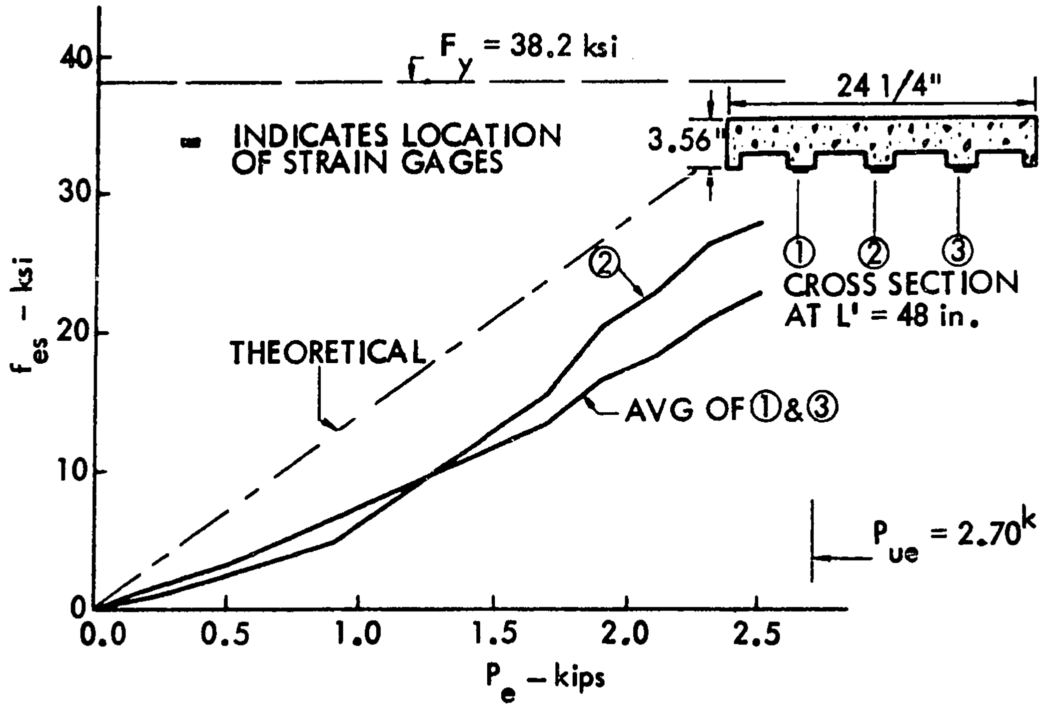

Fig. 31. Experimental steel stress, f_{es}, obtained from strain gage results, vs. experimental applied load, P_e, for beam 8022-48-23-27SG, constructed with steel deck O

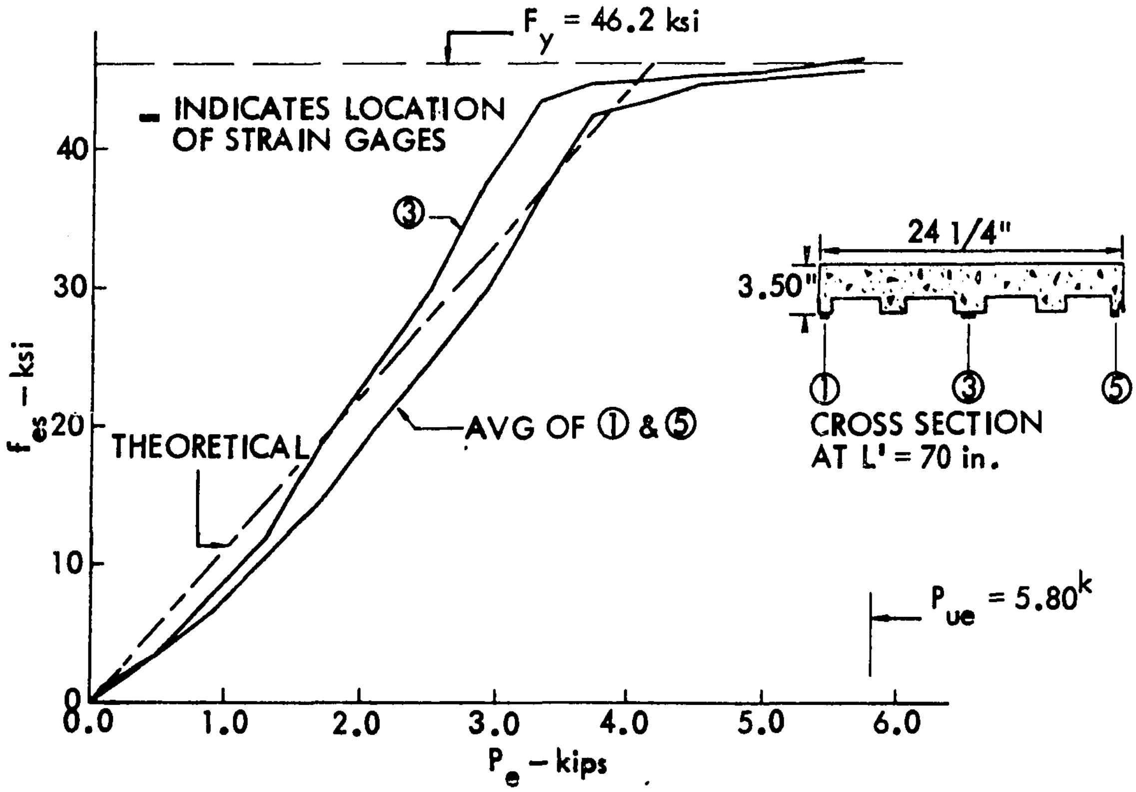

Fig. 32. Experimental steel stress, f_{es}, obtained from strain gage results, vs. experimental applied load, P_e, for beam 6016-70-22-29SG, constructed with steel deck O

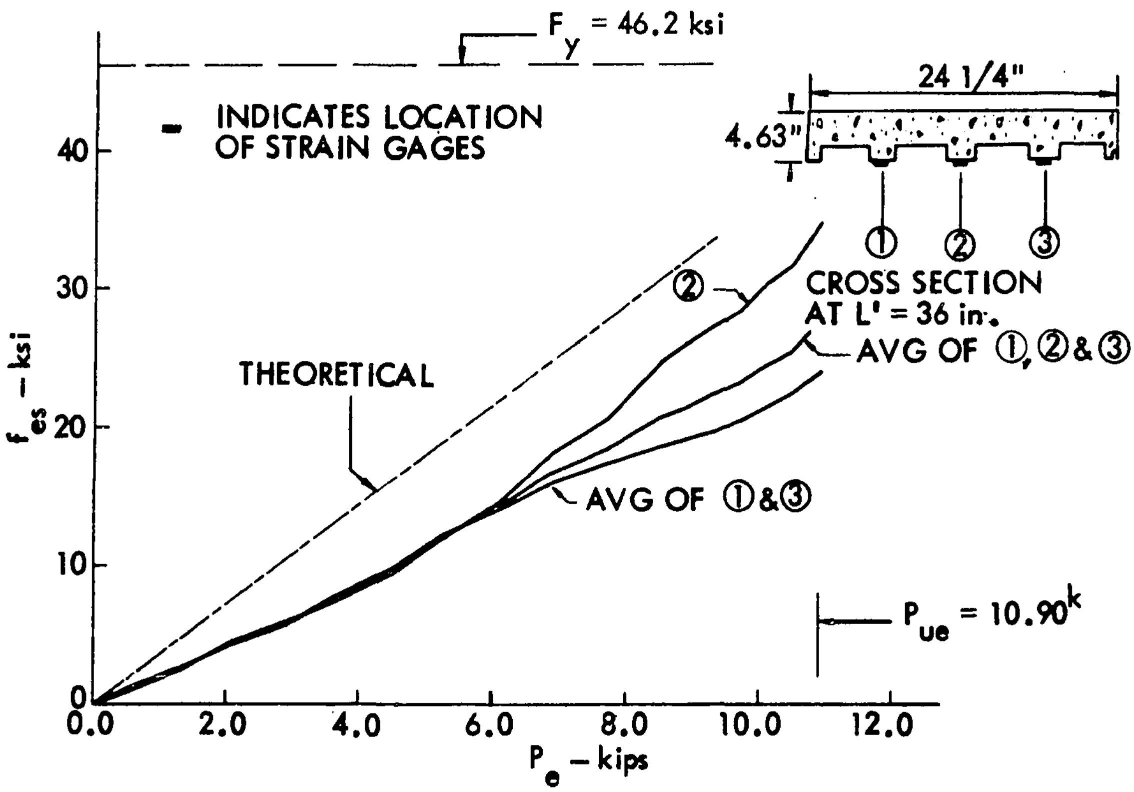

Fig. 33. Experimental steel stress, f_{es}, obtained from strain gage results, vs. experimental applied load, P_e, for beam 7016-36-23-20SG, constructed with steel deck O

tests of typical steel decks and not from respective beams after testing, a slight discrepancy may exist between the calculated yield value and the given yield level.

Theoretical steel stresses were obtained by employing the conventional expression of

$$f_{cs} = \frac{M_{ue}}{I_c}$$

where I_c is the composite moment of inertia transformed to steel, based on a cracked section.

Table 4 shows pertinent information regarding steel deck stresses of strain-gaged specimens. Experimental steel stresses shown in Figs. 24 through 33 are referred to as either yielding or below yield. Yielding in this case indicates that the bottom of the steel deck has reached the yield level. At failure, yielding of the steel deck may have progressed toward the top of the steel deck; however, in no case did the extreme top of the deck experience yielding. The term below yield signifies that the steel deck is below the yield level over the entire depth of the deck. Also shown in Table 4 are shear span, L', reinforcement ratio, p, and balanced reinforcement ratio, p_b. Since all strain-gaged beams resulted in shear-bond failures, it is interesting to note from Table 4 that the reinforcement ratio, p, has no detrimental effect on whether or not the steel deck has reached the yield level. For example, beam 33I18 with a reinforcement ratio of p = 2.640% has experienced yielding of the steel deck, while the steel stress of beam 35I18 with p = 1.500% is below the yield level. This same analogy may also be made by comparing beams 8I16 with 10I16, 7022 with 8022 and 6016 with 7016. Thus, the primary factors influencing the steel stress condition of a shear-bond failure are the shear span, L', and the inherent shear capacity of the shear transfer devices.

Table 4. Condition of steel stress of strain-gaged beams constructed with steel decks I and O, failing in shear-bond

Beam no.	L' (in.)	p (%)	p_b[a] (%)	Steel stress
Deck I				
41I22	70	1.517	3.572	Yielding
42I22	48	0.895	3.735	Yielding
33I18	70	2.640	3.237	Yielding
35I18	48	1.500	3.425	Below yield
8I16	70	3.358	3.034	Yielding
10I16	36	1.976	3.197	Below yield
Deck O				
7022	70	1.568	4.096	Yielding
8022	48	1.533	3.721	Below yield
6016	70	3.357	3.151	Yielding
7016	36	2.341	2.945	Below yield

[a]Calculated in accordance with Equation 24.

Deck I   Figures 24, 25, 26 and 28 represent plots of experimental steel stress, f_{es}, vs. applied load, P_e, for beams 41I22, 42I22, 33I18 and 8I16, respectively, where the bottom of the steel deck has reached the yield level. It can be observed from Fig. 24, for example, that the bottom steel deck fibers have yielded. This is evidenced by the curve consisting of the average of strain gages (1) and (3) becoming asymptotic with the yield level, F_y = 39.20 ksi, at approximately P_e = 2.25 k. The top steel deck fibers, however, as indicated by the curve consisting of strain gage (2), remain well below the yield level even at ultimate load. Thus, beam 41I22, having resulted in a shear-bond failure, was accompanied by partial yielding of the steel deck. Figures 25, 26 and 28 may be similarly interpreted.

Shear-bond failure without yielding of the steel deck is exhibited with beams 35I18 and 10I16 shown in Figs. 27 and 29, respectively. In both cases, the experimental stress in the bottom steel deck fibers is below the yield level, as indicated by the curve consisting of the average of strain gages (1) and (2) in Figs. 27 and 29, respectively.

In all of the experimental steel stress vs. applied load curves shown in Figs. 24 through 29, reasonable correlation exists between theoretical and experimental steel stress results.

Deck O   Figures 30 and 32 reveal that yielding of the bottom steel deck fibers has occurred and Figs. 31 and 33 indicate that steel stresses remain below the yield level at ultimate load. In reference to Fig. 30, yielding of the steel deck of beam 7022 is first initiated at the extreme webs where strain gages (1) and (5) are located. This is evidenced by the curve of the average of strain gages (1) and (5) becoming asymptotic at approximately $P_e = 1.5^k$. The steel at the center of the cross-section, namely, where strain gage (3) is located, begins to yield at about $P_e = 1.9^k$ and remains below the yield level at straining gage locations (2) and (4) even at ultimate load. Beam 6016, shown in Fig. 32, indicates that yielding first occurred at the center of the cross-section, namely, where strain gage (3) is located and was accompanied by yielding of the outside steel webs before reaching the ultimate load.

According to Fig. 31 beam 8022, having failed in shear-bond, was not accompanied by yielding of the steel deck. As can be observed, however, from Fig. 31, the steel stress at the center of the cross-section is greater than that of the average of strain gages (1) and (3) at ultimate load. This same behavior as discussed with beam 8022 of Fig. 31, also applies to beam 7016 of Fig. 33.

Again, reasonable correlation existed between theoretical and experimental steel stress results of Figs. 30 through 33.

Strain linearity

The assumption that strains vary linearly over the beam cross-section is necessary for the derivations of ultimate strength flexural expressions. The integrity of this assumption can only be validated by experimental data such as strain gage results. Figures 34, 35 and 36 show experimental strain distributions at various load levels of beam cross-sections 41I22, 33I18 and 8I16, respectively. The actual load-deflection curve is shown on each figure, indicating the load levels at which strain distribution cross-sections were plotted. A typical beam cross-section showing strain gage locations is also shown on Figs. 34, 35 and 36. In reference to Fig. 34, the first strain distribution was drawn at a load of 0.3^k where the load-deflection curve still maintained its elastic character. At this load level, the distance from the top of the concrete to the experimental composite neutral axis is equal to 1.46 inches. At a load of 0.9 kips the experimental composite neutral axis shifted upward, resulting from initial cracking of the cross-section, and the distance from the neutral axis to the top of the concrete now equals 1.23 inches. This distance remained approximately the same at loads 2.3 and 2.7 kips, as indicated on Fig. 34. Yielding of the bottom fiber steel deck is seen to take place by comparing the unit strain at the time of yielding, ϵ_y, with actual strain readings of Fig. 34. Strain linearity, in reference to the dashed line indicated on each strain distribution curve, is seen to deviate only slightly. According to Fig. 35, the distance from the top of the concrete to the experimental composite neutral axis at load levels 0.9, 3.3, 5.7 and 7.1 kips, equals 1.67, 1.46, 1.57

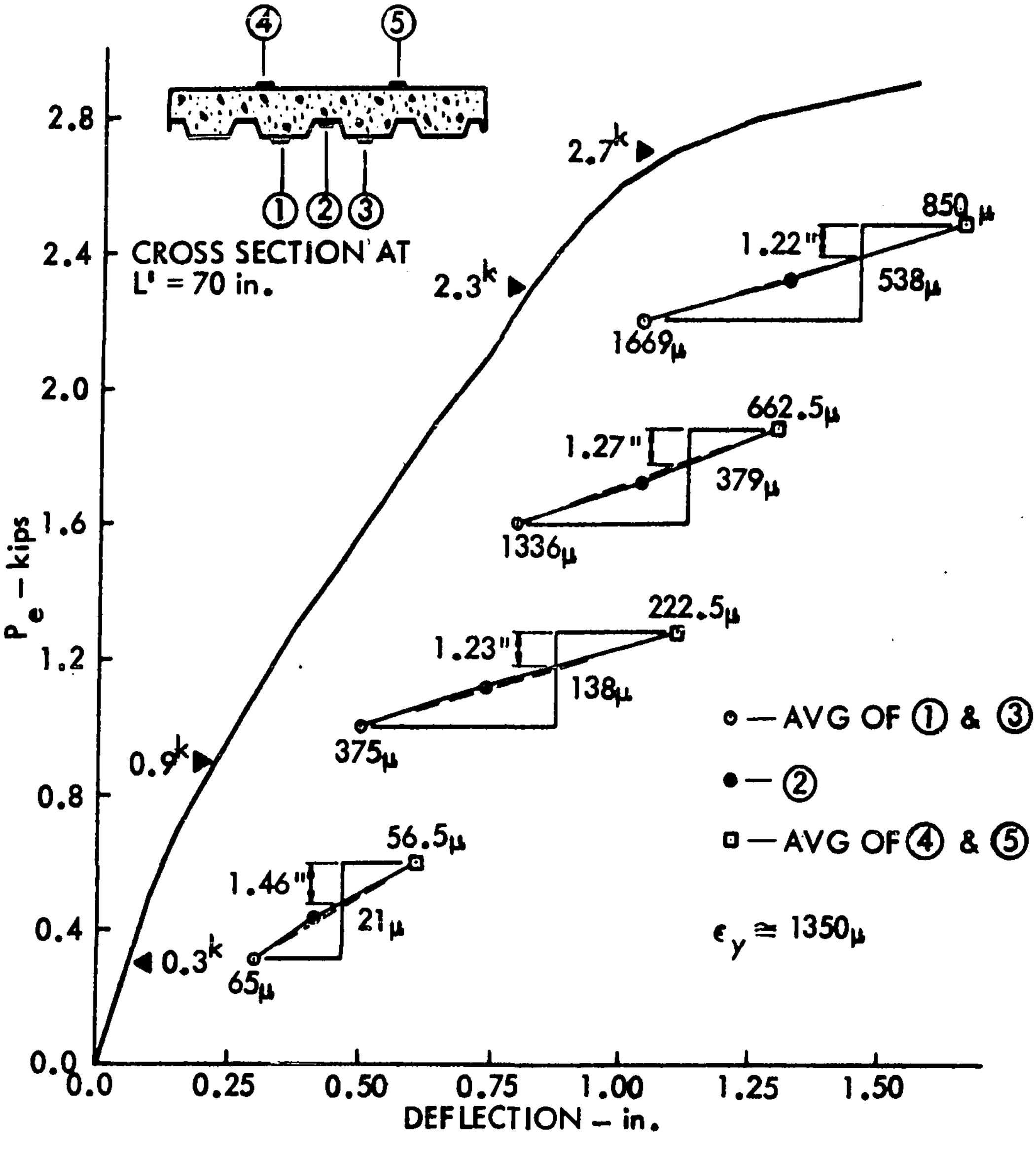

Fig. 34. Experimental strain distribution of selected beam cross-sections plotted on actual load-deflection curve of beam 41I22-70-19-19SG

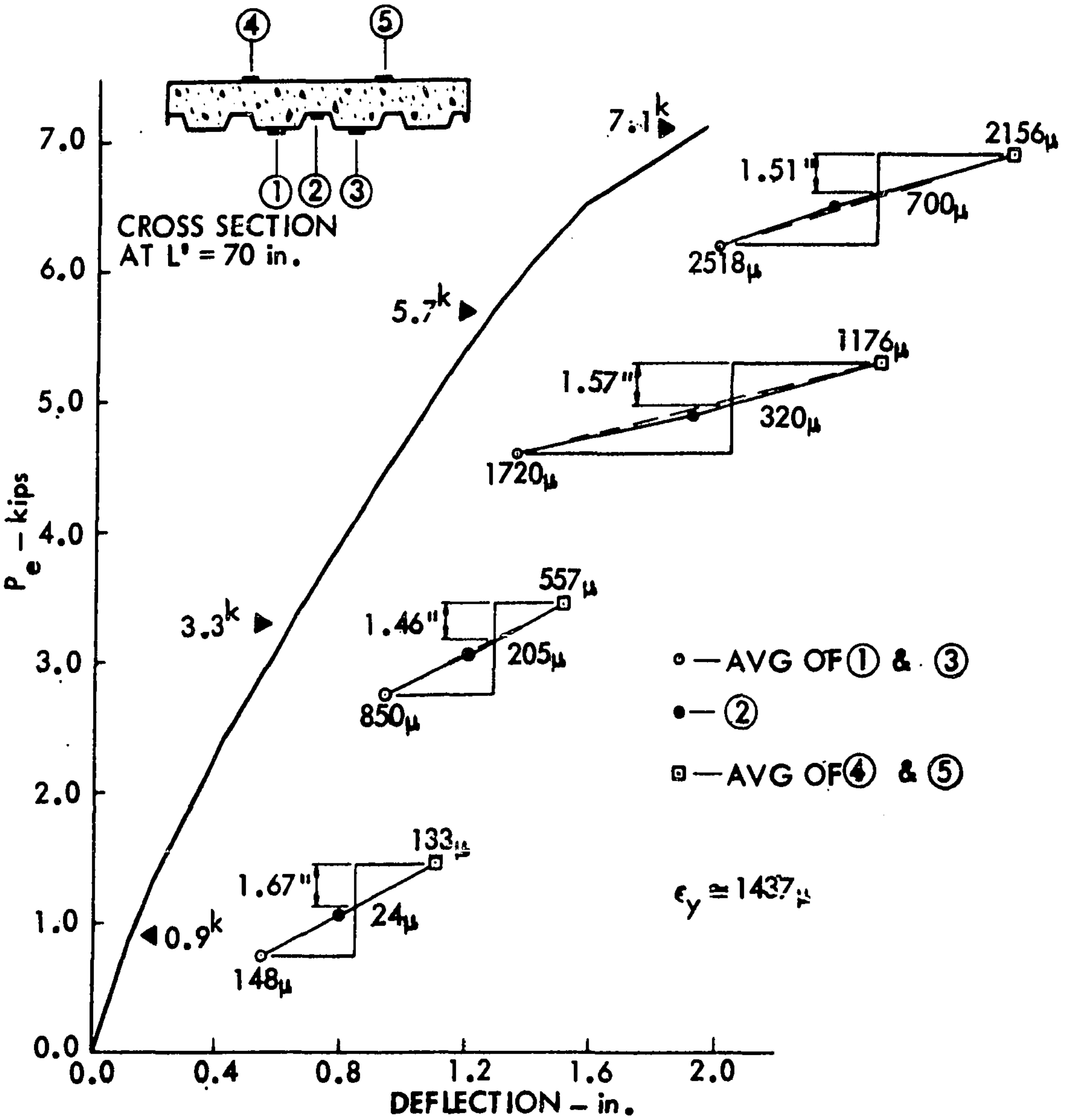

Fig. 35. Experimental strain distribution of selected beam cross-sections plotted on actual load-deflection curve of beam 33I18-70-19-19SG

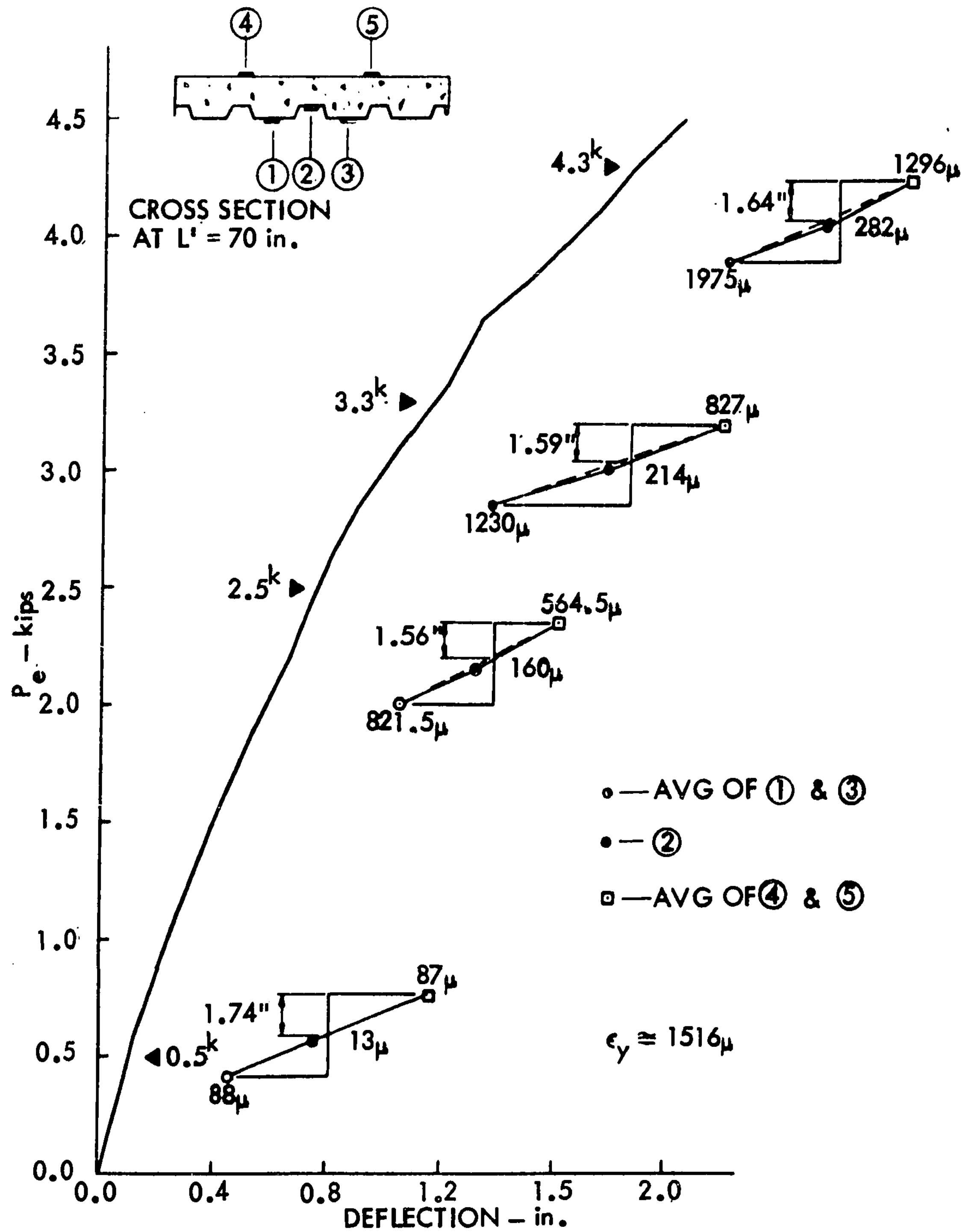

Fig. 36. Experimental strain distribution of selected beam cross-sections plotted on actual load-deflection curve of beam 8I16-70-19-19SG

and 1.51 inches, respectively. Theoretically, neutral axis dimensions reduce in magnitude as the load, P_e, increases from zero to ultimate, since the beam is more severely cracked at ultimate than at initial cracking. However, experimentally this may not always exist because strain gage readings at higher load levels are subject to creep effects inherent in concrete, especially if a considerable amount of time is involved in recording strain values. Figure 36 reveals similar strain distribution characteristics as discussed with Figs. 34 and 35, and indicates that strain linearity is maintained with reasonable accuracy even near ultimate load.

Beam Behavior as Observed by End-Slip Instrumentation

End-slip was recorded graphically of certain beams constructed with steel decks O, I, and E of CATEGORY I and shown in Figs. 37, 38 and 39, respectively. The purpose of instrumenting various beams was to determine whether or not end-slip had occurred prior to ultimate failure and if end-slip is a pertinent criterion for the definitions of the types of failures encountered. This was of particular interest whenever shear-bond was the mode of failure, since the concrete shear span portion, defined by L', became disengaged from the steel deck at the time of ultimate failure. Those beams constructed with steel decks O and I recorded no end-slip until the time of ultimate load, when the ensuing failure forced the concrete shear span section outward with respect to the steel deck.

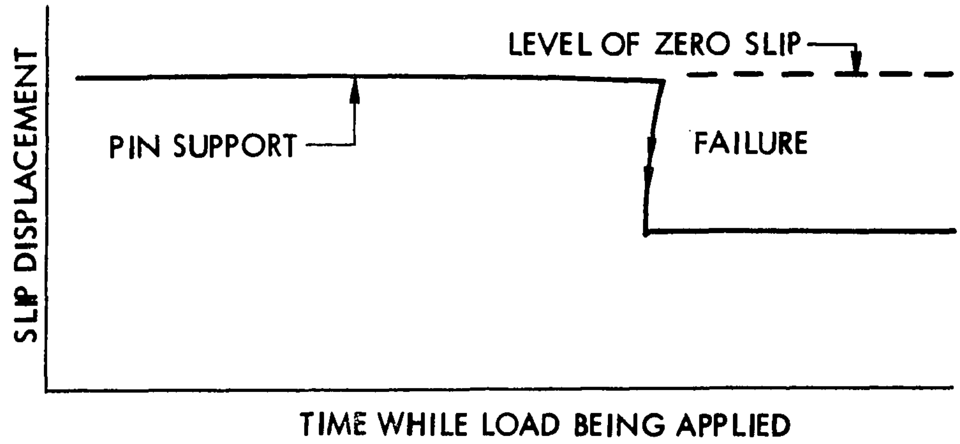

Fig. 37. Typical end-slip deflectometer recording for beams constructed with steel deck O

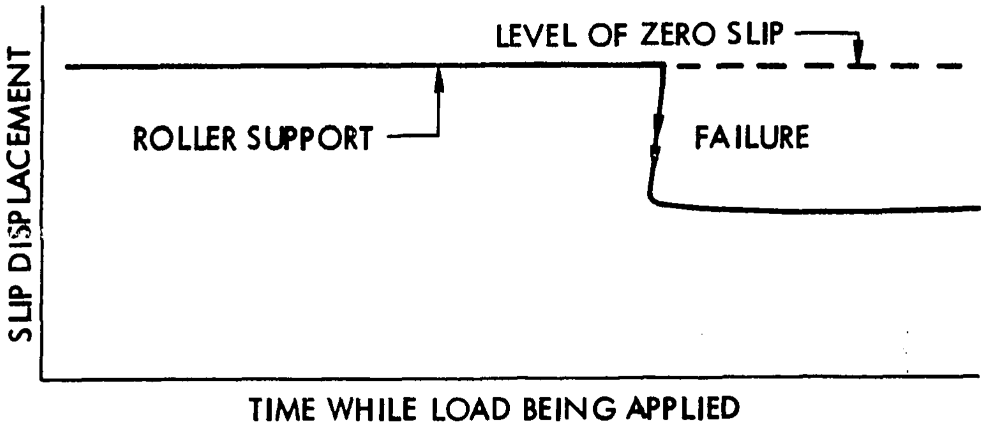

Fig. 38. Typical end-slip deflectometer recording for beams constructed with steel deck I

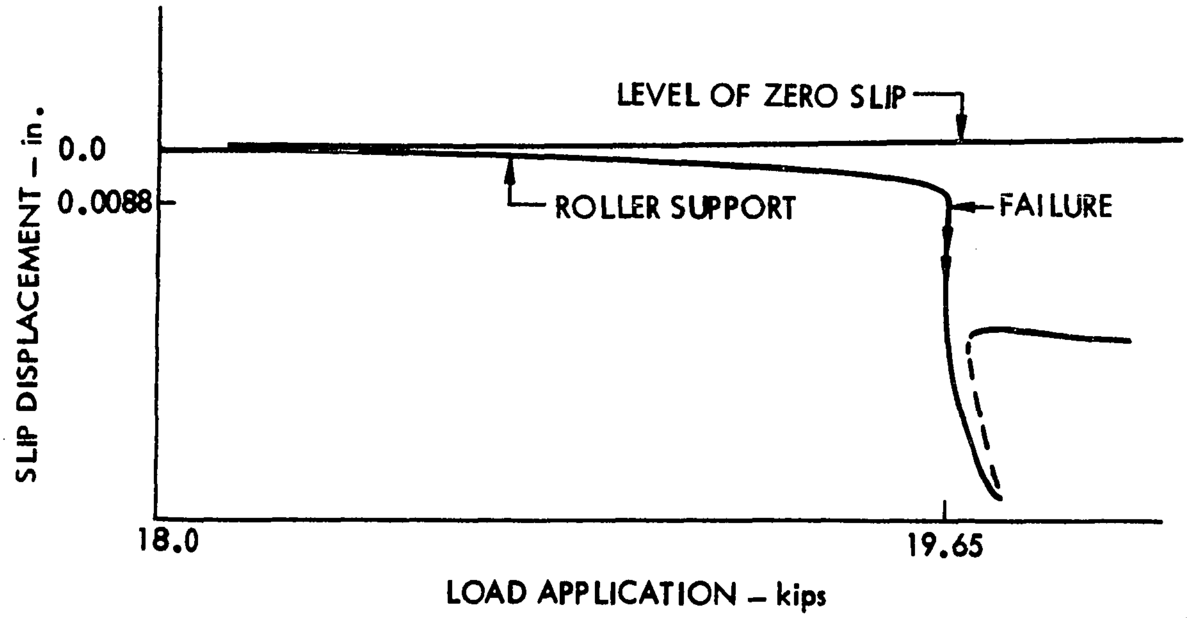

Fig. 39. End-slip deflectometer recording of beam 4E20 constructed with steel deck I

Figures 37 and 38 show typical end-slip deflectometer recordings for beams constructed with steel decks O and I, respectively. In reference to Fig. 37, sudden end-slip was experienced at the instant of failure at the pin-supported end of the beam. This is evidenced by the horizontal line (at pin support) changing direction and becoming vertical as indicated by the two arrows drawn on the curve. Figure 38 demonstrates similar behavior, except end-slip was encountered at the roller supported end of the beam. Based on beam tests cited in reference (17), no measurable end-slip was experienced with beams constructed with steel deck G until the time of ultimate load. However, in the case of certain beams constructed with steel deck E, some end-slip was encountered prior to ultimate failure. According to reference (17), the magnitude of end-slip at failure was influenced by the length of shear span, L'. It was observed that the magnitude of end-slip reduced as the shear span, L', increased. Figure 39 shows the end-slip deflectometer recording of beam 4E20 which has a relatively short shear span, L', namely, 12 inches. This beam showed the most severe magnitude of end-slip of the specimens tested in reference (17). End-slip of beam 4E20 was first encountered at a load of 18.0 kips with the ultimate load reaching 19.65 kips. The amount of measurable end-slip between the 18.0 and 19.65 kip load was 0.0088 inches. Figure 39 reveals that end-slip, occurring at the roller support, was gradual until failure. At failure, the sudden separation between the concrete shear span portion and steel deck caused the line of Fig. 39 to change direction as indicated by the two arrows on the curve. Since end-slip did not occur until almost at ultimate load and with the magnitude of end-slip being negligibly small, beams constructed with steel deck E and failing in shear-bond were assumed to have no end-slip until failure.

In the case of beams constructed with steel decks I, O, G and E, end-slip prior to failure was not used as a criteria for defining the ultimate load of a shear-bond failure. It was concluded that the ultimate load of a beam failing in shear-bond be taken as that load at which a drop of 1/3 to 1/2 of the ultimate load is experienced, resulting in considerable visible end-slip.

ANALYTICAL STRENGTH ANALYSIS

General Remarks

The main concern of this portion of the investigation was to develop a standard ultimate strength procedure that will predict the ultimate load carrying capacity of any steel-deck-reinforced concrete floor slab.

Both, shear-bond and flexural failure phenomena were considered in the expressions developed and given herein. Based on the experimental findings, as presented in the previous chapter, a semi-rational shear-bond concept as adopted, since a truly rational concept is complicated by the nonhomogeniety and nonisotropy of the material. In the case of a flexural failure, the ultimate load-carrying capacity was predictable by employing the well established ultimate moment expressions. Consideration is given to beams constructed with steel decks of CATEGORY I with fixed pattern shear transfer devices and CATEGORY II where spacing of shear devices is a variable.

Shear-Bond

In general, a shear-bond failure regarding steel-deck-reinforced concrete slabs is similar to a shear and diagonal tension failure in conventional reinforced concrete without web reinforcement. The main similarity lies in the formation of an approximate diagonal tension failure crack, resulting from combined shear and bending. This failure crack is not always diagonal in nature but for all practical purposes, a diagonal crack was assumed. Under the combined action of shear and bending, the complexity of the ultimate shear-bond load carrying capacity is greatly increased due to the presence of the numerous variables. Variables influencing a shear and diagonal tension failure in conventional reinforced concrete were found to be of equal importance in a shear bond failure of steel-deck-reinforced system.

Review of variables

Since the derivation of the familiar expression v = V/bjd by Mörsch (14) in 1903, investigations which have been made on reinforced concrete beams failing in shear were generally interpreted by expressing the ultimate nominal unit shear stress, v_u of V_u/bjd, as a function of certain variables. In 1909, Talbot (28) pointed out that the ultimate nominal unit shear stress depends on the following variables: the span-depth ratio, the concrete strength and the percentage of tensile reinforcement. In 1951, A. P. Clark (3) introduced an expression for the depth-span ratio, d/L' involving the effective depth and the shear span, L', of the beam cross-section. Hence, Clark expressed Talbot's notations by a mathematical equation containing the three variables - ratio of depth to shear span, percentage of tensile reinforcement and concrete strength. A slight modification of the general diagonal tension concept led to the development of the M/Vd phenomenon that introduced a semi-rational solution of shear and diagonal tension as a design problem. I. M. Viest (25), based on the work by T. Morrow, derived an expression relating the nominal shear stress, $v = V/bd$, to the three major variables known to influence it: the M/Vd ratio, the percentage of tensile reinforcement, and the strength of the concrete. The work was based on the equation for principal stress at a point and depends on the correlation with test data. This combination of rational theory and test data correlation has been frequently classified as a semi-rational approach to the complex shear and diagonal tension problem. Favorable results have been obtained using this approach and the ACI Building Code 318-63 (1) has adopted a semi-rational expression based on numerous test results.

Concept

Since a typical shear-bond failure resulted in the formation of an approximate diagonal failure crack, it was assumed that this crack was caused by excessive principal tension stresses. However, a failure or breakdown in the mechanical shear transfer devices could have preceded, thus giving rise to the formation of the diagonal failure crack. In the case of beams constructed with decking I and O, namely, deckings that utilize embossments as mechanical shear transfer devices, the diagonal failure crack could have been the result of the concrete shear span portion, L', tending to override the embossments; thus, a breakdown or loss of composite action between the concrete and steel deck along the entire length of the shear span, L', could have preceded the ultimate failure crack. The utilization of holes in the case of deck E, resulting in concrete shear keys, gives rise to the possibility that the failure crack could have been caused by the shearing of the shear keys before excessive principal tension stresses develop at the failure crack. With deck G, the shearing or tearing of the transverse T-wire welds may have been the reason for the formation of the failure crack and not excessive principal tension stresses. In general, it is not known whether the ultimate failure crack was the result of the shear transfer devices failing, or the cause of excessive principal tension stresses. However, consideration was given to the fact that the ultimate failure occurred in the concrete and not in the steel; hence, the assumption that the ultimate failure crack is diagonal in nature and caused by excessive principal tension stresses was used in the forthcoming derivations.

Based on the major variables that have been found to influence shear and diagonal tension in conventional reinforced concrete without web reinforcement, a general expression for the ultimate transverse shear of a shear-bond failure may be written as follows:

$$V_{uc} = f(f'_c, L', d, b, p) \qquad (1)$$

To arrive at an expression containing the variables of Equation 1, it was assumed that the ultimate transverse shear, V_{uc}, is the result of the concrete and steel deck contributing independently. From Fig. 40 it can be observed by applying statics that

$$V_{uc} = V_c + V_d \tag{2}$$

where V_c = the transverse shear carried by the concrete at ultimate load of a shear-bond failure and

V_d = the transverse shear carried by the steel deck at ultimate load of a shear-bond failure.

Development - CATEGORY I

Consideration was first given to the transverse shear carried by the concrete. The following stresses were considered to be acting on an element of concrete below the neutral axis, as shown in Fig. 41:

σ_{ct} concrete tensile bending stress acting between flexure cracks,

σ_{max} maximum concrete tensile stress and

v_c shear stress carried by the concrete.

The exact distribution of these stresses is not known since concrete is not an elastic homogeneous material. It was not the intent of this development to describe the various stress fields, but rather, arrive at an expression that will predict the ultimate shear-bond capacity based on actual test results. Thus, stresses used in the equations to follow were expressed in terms of a nominal value times a constant. This constant

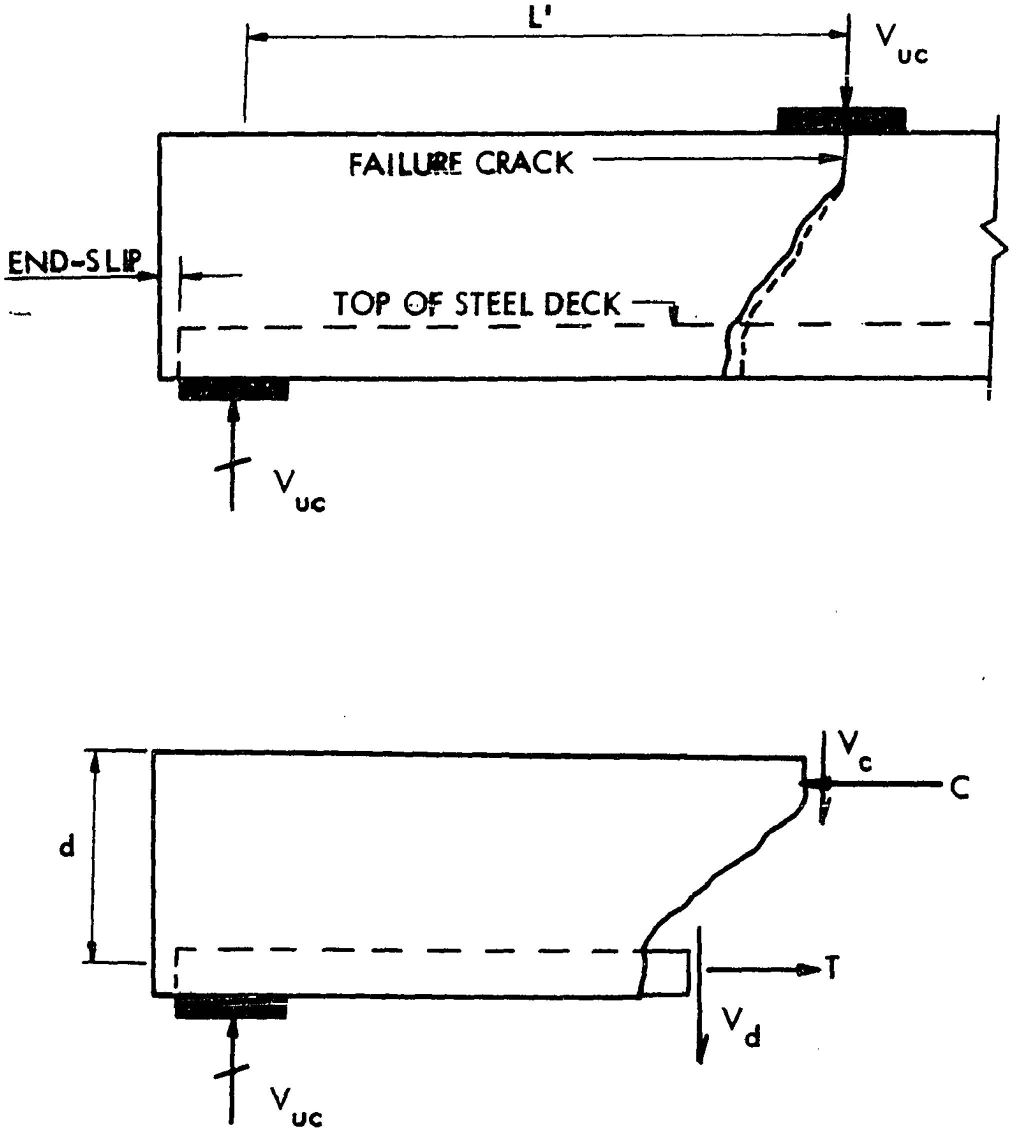

Fig. 40. Forces at ultimate crack of typical shear-bond failure

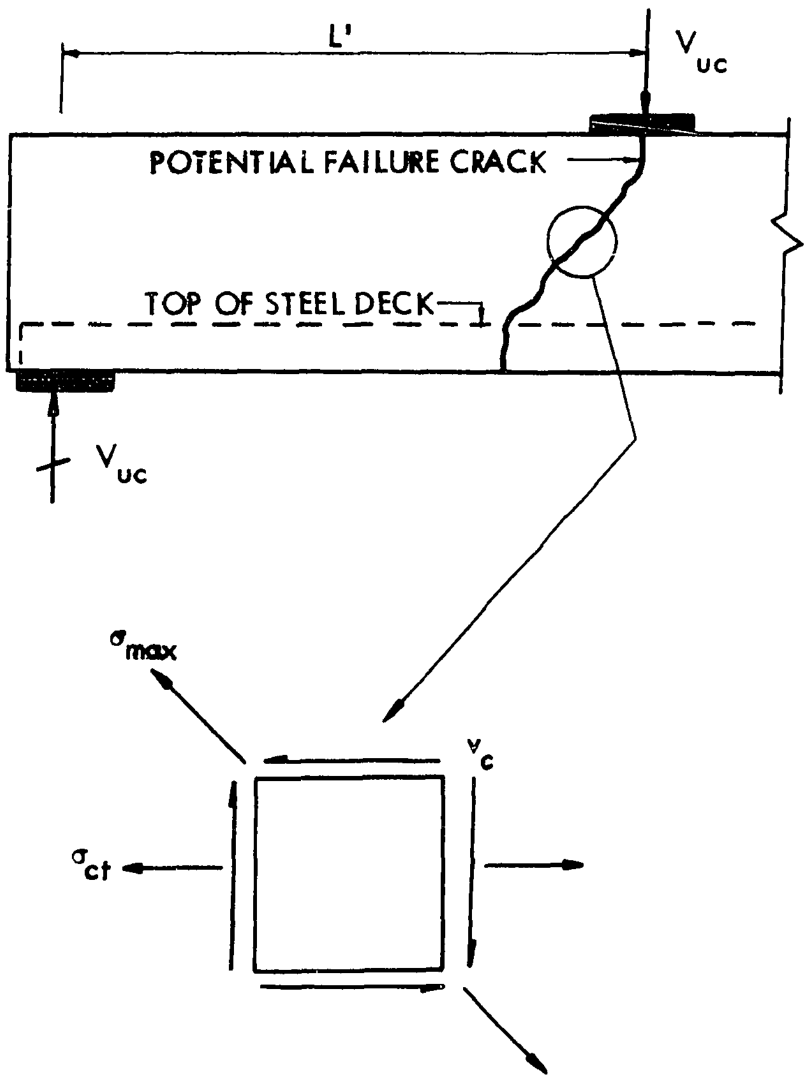

Stresses on concrete element below neutral axis

Fig. 41. Stresses causing diagonal failure crack of a typical shear-bond failure

being a factor of the unknown exact stress distribution.

The maximum concrete tensile stress, σ_{max}, is given by the principal stress equation:

$$\sigma_{max} = \frac{\sigma_{ct}}{2} + \sqrt{[\frac{\sigma_{ct}}{2}]^2 + v_c^2}. \qquad (3)$$

The magnitude of the tensile stress, σ_{ct}, if influenced by the presence of tensile cracks, and consequently cannot be computed directly, with any sufficient accuracy, from an assumed cracked or uncracked section. For this analysis, σ_{ct} was expressed based on the uncracked section theory. The reason for this being that flexural cracks remained virtually unseen, i.e., hairline cracks, at ultimate load.

$$\sigma_{ct} = \text{constant} \cdot \frac{M_c}{bd^2}$$

$$\sigma_{ct} = K_1 \frac{M_c}{bd^2}$$

where M_c = the moment carried by the concrete at ultimate load of a shear-bond failure,

b = the width of the composite beam cross-section,

d = the effective depth from the top of the concrete to the center of gravity of the steel deck.

The shearing stress, v_c, in the concrete was assumed proportional to the average intensity of shear stress on the total cross section.

$$v_c = \text{constant} \cdot \frac{V_c}{bd}$$

$$v_c = K_2 \frac{V_c}{bd}$$

When the maximum principal stress, σ_{max}, exceeds the tensile strength of concrete, f'_t, at the location of the potential diagonal failure crack, shear-bond failure is assumed to impend. The tensile strength of concrete was assumed proportional to the square root of the compressive strength, f'_c, of the concrete. Thus,

$$\sigma_{max} = f'_t = \text{constant} \sqrt{f'_c}$$

$$\sigma_{max} = K_3 \sqrt{f'_c}.$$

Substituting the above stress relationships into Equation 3 results in the following expression:

$$2K_3\sqrt{f'_c} = K_1 \frac{M_c}{bd^2} + \sqrt{[K_1 \frac{M_c}{bd^2}]^2 + [2K_2 \frac{V_c}{bd}]^2} \qquad (4)$$

Rearranging and expressing in terms of V_c/bd, the equation becomes

$$\frac{V_c}{bd} [\frac{1}{2K_3}] = \frac{1}{\frac{K_1}{d\sqrt{f'_c}} \cdot \frac{M_c}{V_c} + \frac{1}{\sqrt{f'_c}}\sqrt{[\frac{K_1}{d} \cdot \frac{M_c}{V_c}]^2 + [2K_2]^2}} \cdot \qquad (5)$$

Now, factoring the term $[K_1/d \cdot M_c/V_c]$ from the square root, the expression reduced to

$$\frac{V_c}{bd}\left[\frac{1}{2K_3}\right] = \frac{1}{\dfrac{K_1M_c}{d\sqrt{f'_c}V_c} + \dfrac{K_1M_c}{d\sqrt{f'_c}V_c}\sqrt{1 + \left[\dfrac{2K_2V_cd}{K_1M_c}\right]^2}}$$

further factoring and letting $2K_2/K_1$ equal a new constant, K_4, gives the following form:

$$\frac{V_c}{bd}\left[\frac{1}{2K_3}\right] = \frac{1}{\dfrac{K_1M_c}{d\sqrt{f'_c}\,V_c}\left[1 + \sqrt{1 + \left(K_4\dfrac{V_cd}{M_c}\right)^2}\,\right]} \qquad (6)$$

The term $[V_cd/M_c]^2$ under the radical sign is relatively small in reference to the number 1 also contained under the sign, and was therefore considered to be zero for all practical purposes. The largest value of V_cd/M_c, as observed in actual testing, was approximately equal to 1/3. Squaring this, gives 1/9, a small enough value in comparison to one. With $[V_cd/M_c]^2$ equal to zero, expression 6 results in

$$\frac{V_c}{bd}\left[\frac{1}{2K_3}\right] = \frac{1}{\dfrac{2K_1M_c}{d\sqrt{f'_c}V_c}}$$

multiplying both sides by $2K_3$ and setting $2K_3/2K_1 = K_5$, the expression for V_c results in the following general form:

$$V_c = \frac{K_5bd^2\sqrt{f'_c}V_c}{M_c}\,. \qquad (7)$$

The transverse shear carried by the steel deck, which in conventional reinforced concrete is commonly referred to as the dowel force, was assumed to be proportional to the cross-sectional area of the steel deck. Thus,

$$V_d = \text{constant} \cdot A_s$$
$$V_d = K_6 A_s. \tag{8}$$

Since the concrete is placed directly over the steel deck, the transverse shear contribution can be quite appreciable, especially when the area of the deck is large and the depth of the concrete is at a minimum. Neglecting this contribution would give conservative results, but was not considered justifiable in this investigation.

Combining expressions 7 and 8 in accordance with Equation 2, yields the following general equation for the ultimate transverse shear:

$$V_{uc} = K_5 \frac{bd^2 \sqrt{f'_c} V_c}{M_c} + K_6 A_s. \tag{9}$$

In terms of unit nominal ultimate shear stress, with v_{uc} = V_{uc}/bd, another general equation may be written:

$$v_{uc} = K_5 \frac{\sqrt{f'_c} d V_c}{M_c} + K_6 p \tag{10}$$

where $p = A_s/bd$.

Equation 10 gives the parameters to be investigated and takes into account the three most important variables that affect the shear-bond strength of flexural members subjected to combined bending and shear; these are the compressive strength of concrete, ratio of reinforcement, and the ratio of external shear to the maximum moment in the shear span. Equation 10 is similar in nature to the expression developed by Clark (3) who is credited as being the first to express the ultimate calculated shear strength in terms of V/M. R. G. Mathey and D. Watstein (12) modified Clark's expression to appear in a similar form as Equation 10; however, their calculated shear expression was based on the shear at which the major diagonal crack first appeared and not on the ultimate shear as Clark did.

Based on actual experimental beam testing as described in the previous chapter, Equation 10 was expressed more specifically for the special case of symmetrical loading. Thus, for simple beams with single or two symmetrically placed line loads, the terms V_c/M_c and $1/L'$, are synonymous since $M_c = V_cL'$ and

$$\frac{V_{uc}}{bd} = K_5 \frac{\sqrt{f'_c}\, d}{L'} + K_6 p. \qquad (11)$$

This relationship indicates the following with regard to the shear-bond load carrying capacity:

Since $v_{uc} = \frac{V_{uc}}{bd}$,

v_{uc} increases with increasing f'_c,

v_{uc} decreases with increasing L',

v_{uc} increases with increasing p, and

v_{uc} increases with increasing d.

The determination of constants K_5 and K_6 will be discussed in the following chapter on strength result evaluation.

Development - CATEGORY II

The same concept was employed in the development of a shear-bond expression for CATEGORY II as was used in CATEGORY I. However, the resulting expression now contains one additional parameter, namely, the spacing of the shear transfer devices, s.

Figure 42 shows a typical steel deck profile of CATEGORY II where the shear transfer device spacing, s, is subject to change. Since all shear transfer devices contained within the length of the shear span, L', are equally subjected to the transverse shear, V_{uc}, the following analysis was pursued:

Summing forces between the horizontal interface of the concrete and top of the steel deck where the shear transfer devices are located, see Fig. 42, an expression that satisfies statics may be written as

$$v_{uc}bs = \frac{b}{g} m_u. \qquad (12)$$

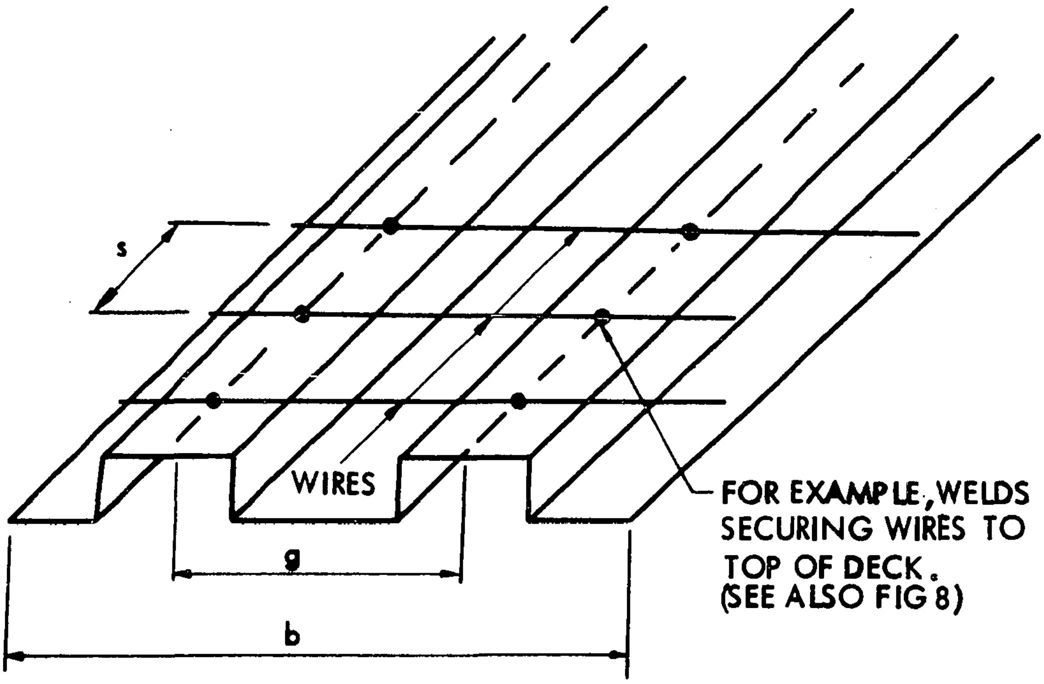

Fig. 42. Typical steel deck profile of CATEGORY II

Here the term b/g indicates the number of shear devices in width b, m_u is the ultimate load in pounds per shear device and v_{uc} is the ultimate shear-bond stress. Reducing this expression further gives

$$v_{uc} = \frac{V_{uc}}{bd} = \frac{1}{sg}[m_u] \tag{13}$$

which indicates that the ultimate shear-bond stress, v_{uc}, is inversely proportional to the shear device spacing, s, and pitch, g, and directly proportional to the ultimate shear device load. Since the dimension, g, of any given deck profile is constant, and with m_u assumed to be directly proportional to the shear-bond capacity, the following expression results from Equation 11 and 13:

$$\frac{V_{uc}}{bd} = \frac{1}{s} [K_7 \frac{\sqrt{f'_c}d}{L'} + K_8 p] \qquad (14)$$

K_7 and K_8 are similar constants as K_5 and K_6 of Equation 11. It can be observed from Equation 14 that when the spacing, s, decreases the ultimate shear-bond capacity increases. All other variables contained in Equation 14 have the same effect as described with Equation 11. The determination of constants K_7 and K_8 will be discussed in the following chapter on strength result evaluation.

Flexure

Ultimate strength relationships pertaining to conventional reinforced concrete beams failing in flexure have been established with more success than semi-rational ultimate strength expressions predicting shear or diagonal tension.

Composite steel-deck reinforced concrete beams failing in flexure are characteristically similar in nature to conventional reinforced concrete beams, and differ only in the steel deck being the positive reinforcement. The type of shear transfer devices and profile of steel deck are no longer important factors when flexure is the mode of failure. The reason for this being that no premature shear-bond failure occurs and either the steel will reach its yield at the top of the deck or the concrete will reach its compressive strength at its outermost fiber. It is also possible for both the steel and concrete to reach their respective ultimate strength levels simultaneously, thus, resulting in a balanced condition. In particular, flexural failures were divided into three parts: flexure-yielding, flexure-crushing and the balanced condition. Asumptions such as specified by Section 1503 of the ACI Building Code were employed in the derivations contained in this section.

Flexure-yielding

In this case the ultimate strength is controlled by yielding of the steel deck and occurs before the concrete has attained its ultimate compressive strength. Yielding begins at the outermost deck fiber, i.e., according to Fig. 43 where $\epsilon_{sb} = \epsilon_y$, and propagates throughout the entire depth of the deck, d_d, until $\epsilon_{st} = \epsilon_y$. When the top fiber of the deck has reached its yield, the ultimate flexure-yielding strength of the cross section will be experienced. Figure 43 shows the strain, actual stress and assumed stress distributions, using the ACI Building Code notation. It was assumed that this notation is well known and needs no further detailed explanation.

From equilibrium of internal forces of the assumed stress diagram in Fig. 43

$$0.85\ f'_c\ ab = A_s F_y, \tag{15}$$

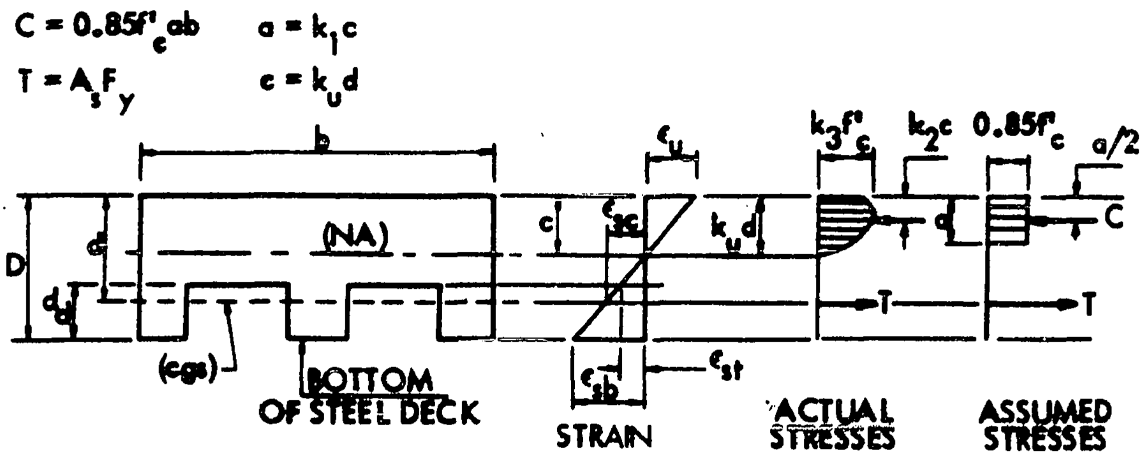

Fig. 43. Conditions at ultimate flexure strength

and from equilibrium of internal and external moments

$$M_{uy} = A_s F_y [d - \frac{a}{2}] \tag{16}$$

where $a = A_s F_y / 0.85\ f'_c b$, as obtained from Equation 15.

Flexure-crushing

In this case it was assumed that crushing of the concrete compression zone takes place while the steel stress, over the entire depth, d_d, is below the yield level. Nevertheless, the possibility does exist that crushing of the concrete occurs while the steel stress has reached the yield at the bottom of the steel deck, and in some cases, yielding might have even progressed toward the top of the steel deck. However, it is believed that in most common proportioned cross-sections this is rare in occurrence; therefore, the following derivation is based on the case where the steel has not reached the yield level.

From equilibrium of internal forces of Fig. 43

$$0.85\ f_c'ab = A_sF_s \tag{17}$$

where, F_s, the stress in the steel considered at the center of gravity of the steel deck is below the yield level. Considering equilibrium of internal and external moments and the actual stress distribution diagram, the following expression may be written:

$$M_{uc} = A_sF_s[d - k_2c]. \tag{18}$$

From the linear strain diagram of Fig. 43 a relationship for k_u results:

$$k_u = \frac{c}{d} = \frac{\epsilon_u}{\epsilon_{sc} + \epsilon_u}\ . \tag{19}$$

Now, solving Equations 17 and 19 for k_u:

$$k_u = \sqrt{pm + (\frac{pm}{2})^2} - \frac{pm}{2} \tag{20}$$

where $m = E_s\epsilon_u/0.85\ k_1f_c'$

and $p = A_s/bd.$

The ultimate moment of resistance may be calculated by substituting the value of k_u obtained from Equation 20 into the following equation:

$$M_{uc} = 0.85\ k_1f_c'bd^2k_u(1 - k_2k_u) \tag{21}$$

where $k_1 = 0.85$ for $f'_c \leq 4000$ psi and decreases by 0.05 for every 1000 psi above 4000.

$k_2 = 0.425$ for $f'_c \leq 4000$ spi and decreases by 0.025 for every 1000 psi above 4000.

Constants k_1 and k_2 were taken from reference (13).

Balanced conditions

In this case simultaneous yielding of the steel at the top of the deck, i.e., according to Fig. 43 where $\epsilon_{st} = \epsilon_y$, and crushing of the concrete takes place. In design, a balanced condition is rarely experienced, thus, it is not the intent to formulate an expression for the ultimate moment capacity of a balanced cross section, but rather, to develop an expression for the reinforcement ratio, p_b, that produces balanced conditions. This balanced reinforcement ratio, p_b, commonly used to determine whether a cross section is under- or over-reinforced, provides information as to the validity of Equations 16 and 21. Equation 16 can only be employed when $p \gtrless p_b$, indicating under- and over-reinforced cross sections, respectively.

Since $a = k_1 c$, a relationship for c may be determined from Equation 15, namely,

$$c = \frac{A_s F_y}{0.85\ f'_c b k_1}$$

and with $p = A_s/bd$

$$c = \frac{pd}{0.85\ k_1} \cdot \frac{F_y}{f'_c} \cdot \tag{22}$$

A second relationship for c can be obtained from the strain geometry of Fig. 43 as follows:

$$c = \frac{\epsilon_u(D - d_d)}{(\epsilon_u + \epsilon_y)}. \tag{23}$$

By equating Equations 22 and 23, the reinforcement ratio, p, now becomes p_b, namely, the ratio that produces balanced conditions. Thus,

$$p_b = \frac{0.85\ k_1 f'_c\ \epsilon_u(D - d_d)E_s}{F_y d\ (\epsilon_u E_s + F_y)}. \tag{24}$$

STRENGTH RESULT EVALUATION

General Remarks

Experimental test data pertaining to 155 beams of CATEGORY I and 18 beams of CATEGORY II are given in Appendix A. The data are contained in tables which give for each test beam, the beam number and designation, pertinent dimensions, the ultimate load, ultimate shear, ultimate moment, mode of failure and strength of concrete. Test beams, or slab elements, were used incorporating four distinct steel decks, namely I, O, G, and E. These data are contained in Tables A.5, A.6, A.7, A.8, and A.9. Other data pertaining to sectional constants for the various steel decks are contained in Tables A.1 and A.2. Tables A.3 and A.4 provide strength properties for the steel decks and concrete, respectively.

The data obtained from the numerous tests which were conducted were assimilated in such a way that the ultimate shear could be related to the various parameters as expressed in Equations 11 and 14. In other words, it was the objective to construct plots from experimental results with values of V_{ue}/bd as ordinates and $\sqrt{f'_c}d/L'p$ as abscissas.

Pertaining to the shear-bond evaluation of beams constructed with steel decks I, O, G and E, Table A.10 gives respective constants resulting from a linear regression analysis. Table A.11 gives similar values, except beam results used in the regression analysis were obtained from companies O and E.

Listed in Tables A.12 through A.16 are ultimate experimental and calculated shear-bond stresses for beams constructed with steel decks I, O, G and E, as well as, ratio-comparisons of these shear-bond stresses. A comparison of ultimate experimental and calculated design shear for beams constructed with decks I, O, G and E is shown in Tables A.17 through A.21. Certain test results, indicated in Tables A.12, A.13 and A.16, were not used in the shear-bond regression analysis because of possible specimen damage prior to testing.

In the following sections, shear-bond regression analysis, beams failing in flexure, and effect of variables, will be discussed and described.

Shear-Bond Regression Analysis

This analysis pertains primarily to the evaluation of regression constants resulting from the ultimate strength shear-bond expressions developed in the previous chapter. Equations 11 and 14, applicable to beams of CATEGORIES I and II, respectively, and failing in shear-bond, provided the necessary dependent and independent variables for the determination of these regression constants. In the case of CATEGORY I, namely, beams constructed with steel decks I, O and E, the following two dependent and independent parameters were used in the statistical linear regression analysis, respectively:

$$\frac{V_{ue}}{bdp}, \frac{\sqrt{f'_c}d}{L'p}.$$

Similarly, for beams of CATEGORY II constructed with steel deck G, the following two terms were used:

$$\frac{V_{ue}s}{bd\ p}\ ,\ \frac{\sqrt{f'_c}\ d}{L'\ p}\ .$$

A computer program was utilized in obtaining regression constants and fitting of respective curves. These constants are shown in Tables A.10 and A.11, and can also be obtained from corresponding plots showing relationships between V_{ue}/bdp and $\sqrt{f'_c}$d/L'p for beams constructed with steel decks I, O, G and E. Curves referred to as regression lines were established by employing the above stated parameters with the necessary experimental data.

A more detailed discussion in reference to the shear-bond-regression results will be presented individually for beams of each steel deck.

<u>Deck I (CATEGORY I)</u>

Figure 44 represents a plot of ultimate strength shear-bond relationships for beams constructed with steel deck I of 22 gage thickness. All beams were shored throughout, except as indicated on Fig. 44. A number of beams were shored at midspan prior to pouring of the concrete and Fig. 44 reveals that no apparent difference exists between beams shored throughout and those shored at midspan only. Also, it may be observed that varying the width of beams between 12 and 24 inches has no effect on the shear-bond relationship shown in Fig. 44. Points

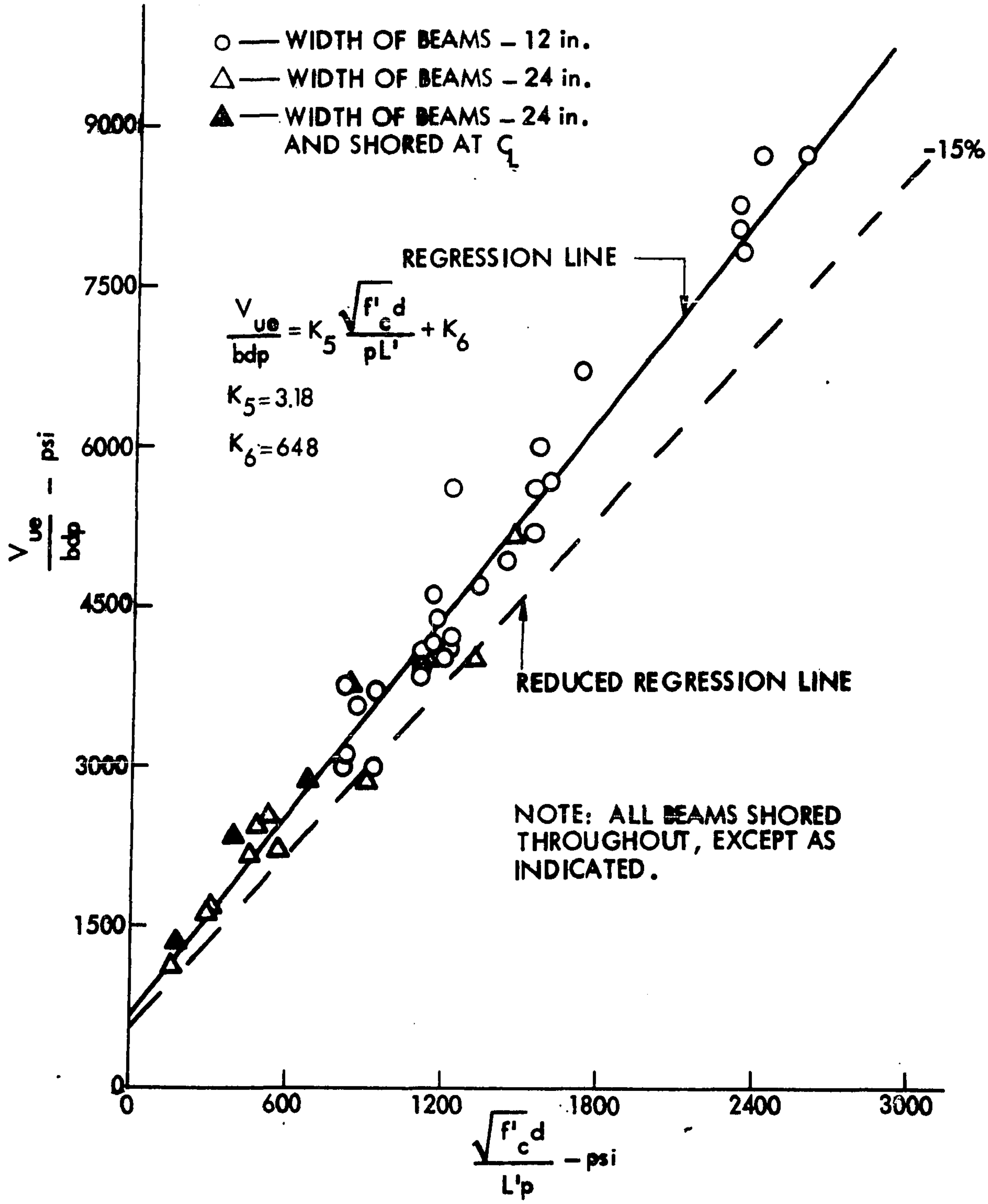

Fig. 44. Relationship between V_{ue}/bdp and $\sqrt{f'_c}d/L'p$ for beams constructed with steel deck I - 22 gage

near the origin resulted from beams having failed in shear-bond with relatively long shear spans and conversely, points at the extreme right resulted from beams subjected to extremely short shear spans. The regression line, resulting from the statistical analysis of best fit, is indicated by the solid curve of Fig. 44. The dashed line (reduced regression line) shown below was ascertained by applying to the equation of the regression line a factor of $\phi = 0.85$ which reduces values by 15%. This factor, ϕ, was adopted from the ACI Building Code (1) and is employed in an effort to take into account the possibility that small adverse variations in material strengths and workmanship may exist. For diagonal tension this factor is taken as, $\phi = 0.85$. By reducing the values from the regression equation by 15%, Fig. 44 reveals that out of the 47 points plotted, only 3 fall on or slightly below the dashed line; thus, making this 15% reduction conservatively justifiable for design. Figure 45 gives a comparison of experimental and calculated ultimate shear-bond stresses for beams having type I steel deck of 22 gage. The calculated shear-bond stresses, v_{uc}, were obtained from Equation 11 with constants K_5 and K_6 resulting from Fig. 44 and given in Table A.10. This same comparison, as shown in Fig. 45, may also be obtained from Table A.12, where a ratio of calculated to experimental shear-bond stress is given for each test result. In reference to Fig. 45, excellent correlation is seen to exist between experimental and calculated values within the $\pm 15\%$ margins outlined by the dashed lines.

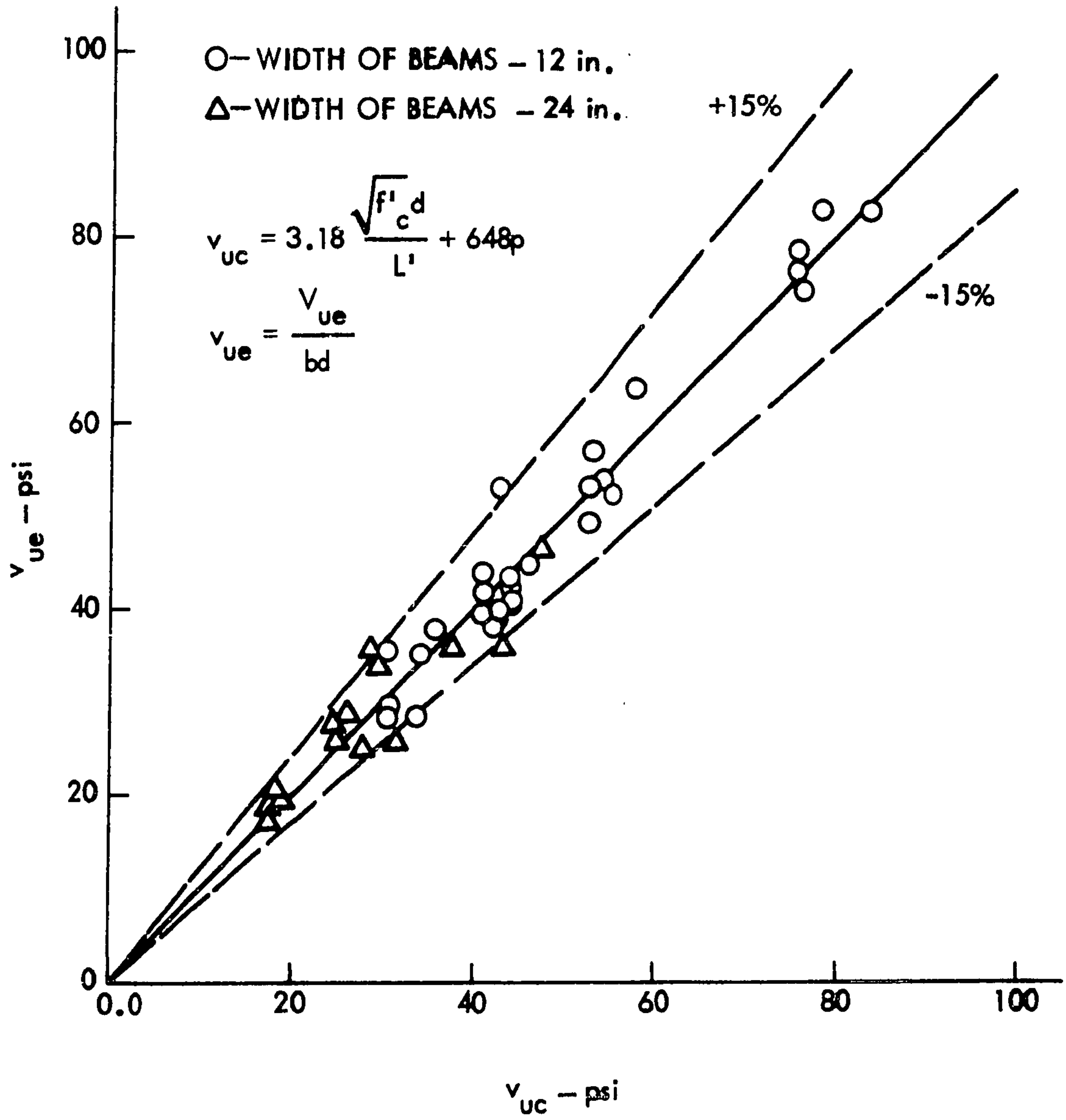

Fig. 45. Comparison of experimental and calculated ultimate shear-bond stresses for beams constructed with steel deck I - 22 gage

Ultimate strength shear-bond relationships for beams consisting of steel deck I-18 gage are shown in Fig. 46. Again, no detrimental difference in shoring, nor effect of beam width can be detected. The same discussion as given with Fig. 44 applies, since the curves of Fig. 46 are similar in nature. Regression constants, K_5 and K_6 resulting from Fig. 46 and given in Table A.10, were used in the comparison of experimental and calculated shear-bond stresses shown in Fig. 47.

Figure 47 should be self explanatory after the discussion of Fig. 45.

In the case of beams constructed with steel deck I-16 gage, only a moderate difference between beams shored throughout and those shored at midspan was detected. Therefore, a separate regression analysis of shored and unshored beams was performed in order to isolate the effect of shoring on the shear-bond strength. Figure 48 represents a plot of ultimate strength shear-bond relationships for beams shored throughout and constructed with steel deck I-16 gage. A comparison of experimental and calculated ultimate shear-bond stresses is represented in Fig. 49. For those beams shored at midspan only, Fig. 50 shows the ultimate shear-bond relationships and Fig. 51 represents a plot comparing experimental and calculated ultimate shear-bond stresses. By comparing regression constants obtained from Figs. 48 and 50, and shown respectively in Figs. 49 and 51, it can be concluded that beams constructed with deck I-16 gage, and shored at midspan only, yield higher shear-bond results than

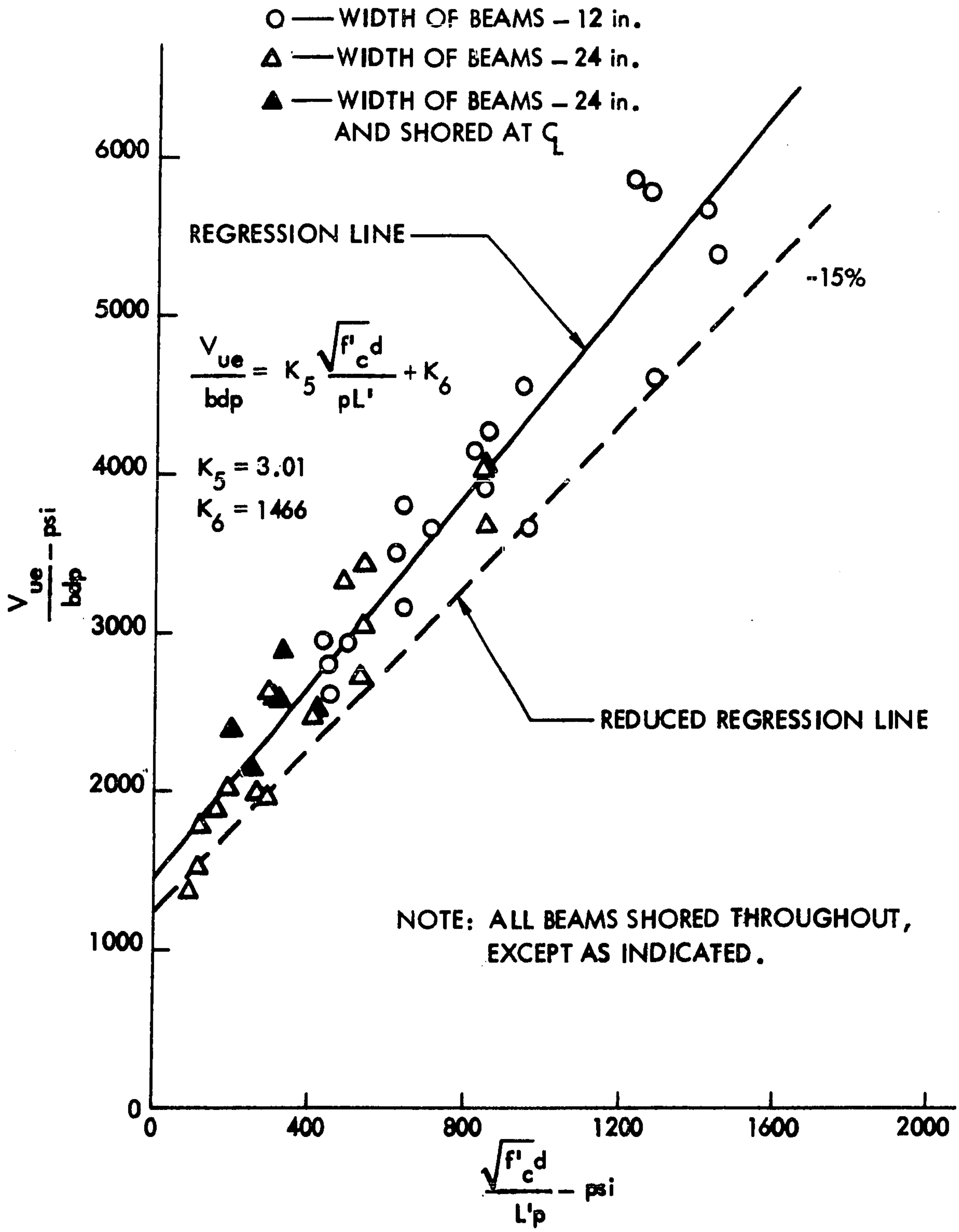

Fig. 46. Relationship between V_{ue}/bdp and $\sqrt{f'_c}d/L'p$ for beams constructed with steel deck I - 18 gage

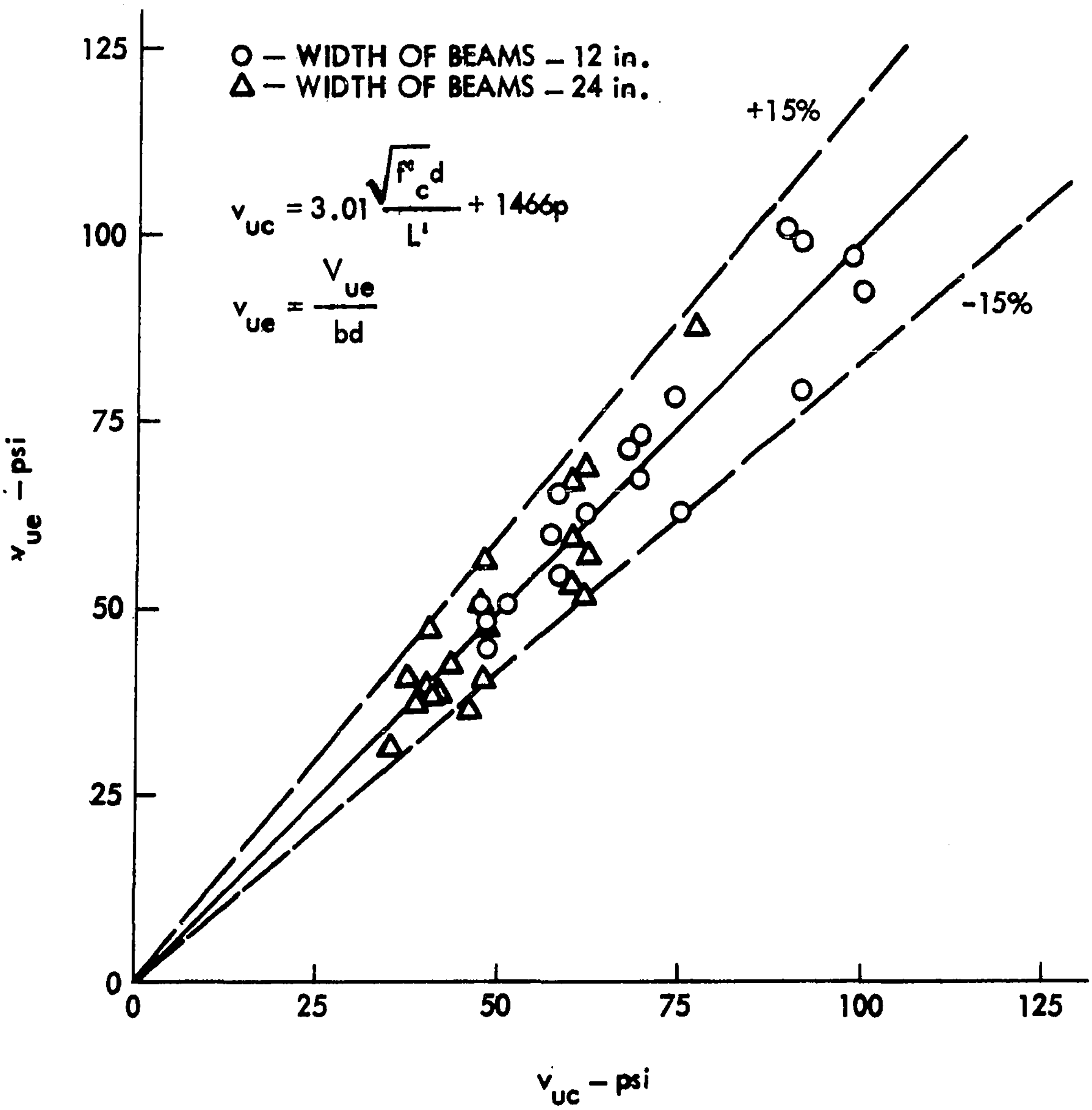

Fig. 47. Comparison of experimental and calculated ultimate shear-bond stresses for beams constructed with steel deck I - 18 gage

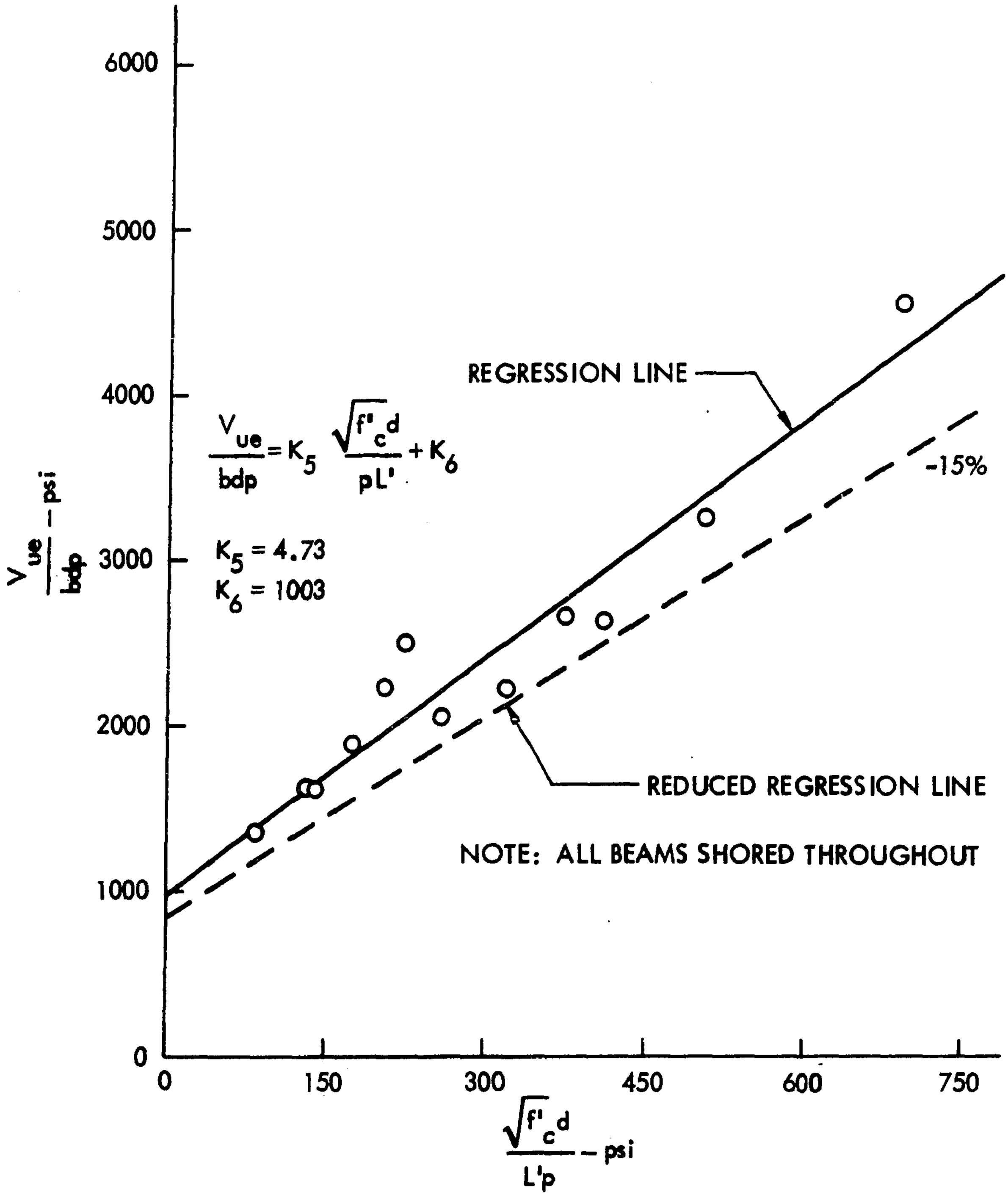

Fig. 48. Relationship between V_{ue}/bdp and $\sqrt{f'_c}d/L'p$ for beams constructed with steel deck I - 16 gage

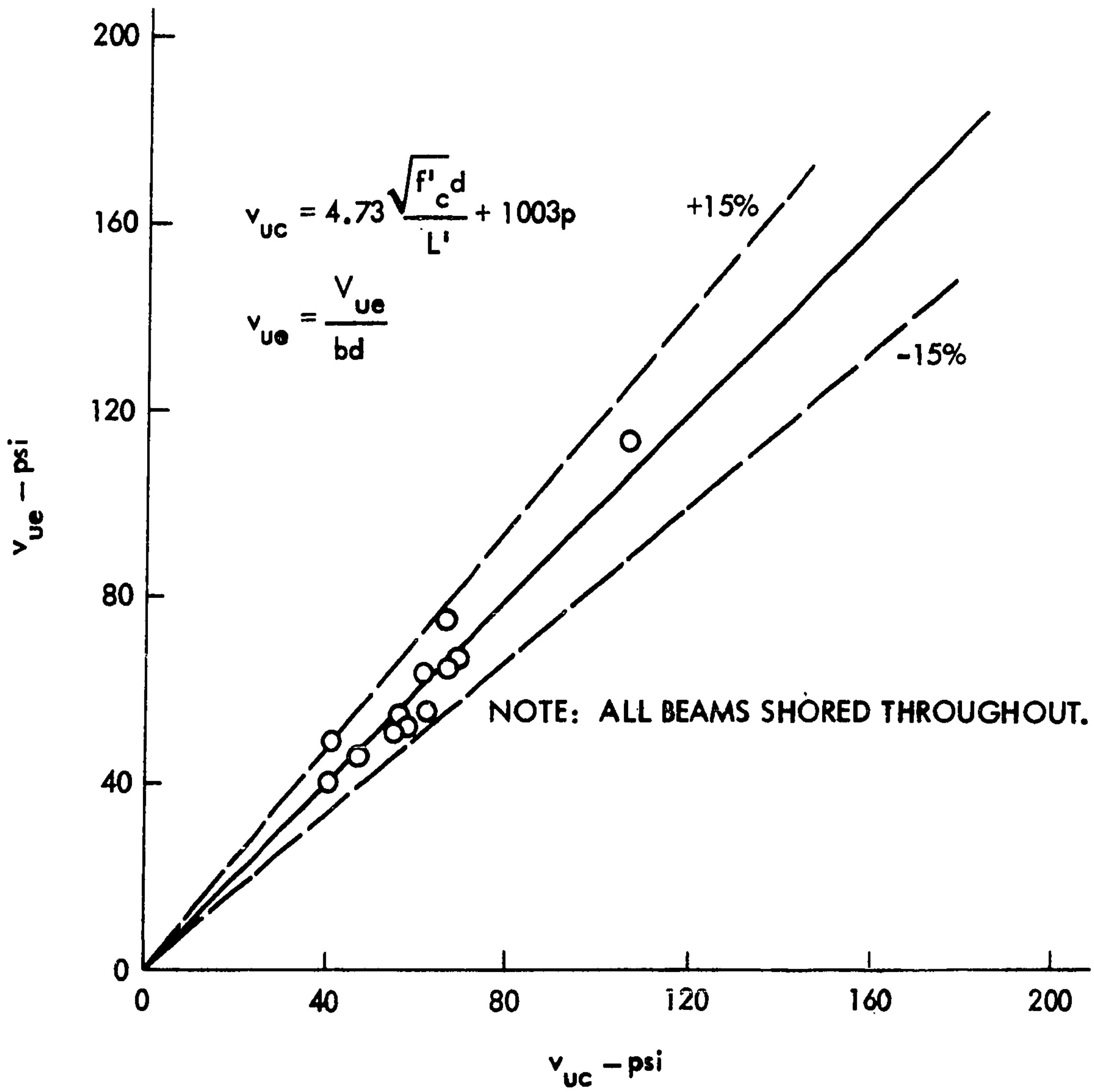

Fig. 49. Comparison of experimental and calculated ultimate shear-bond stresses for beams constructed with steel deck I - 16 gage

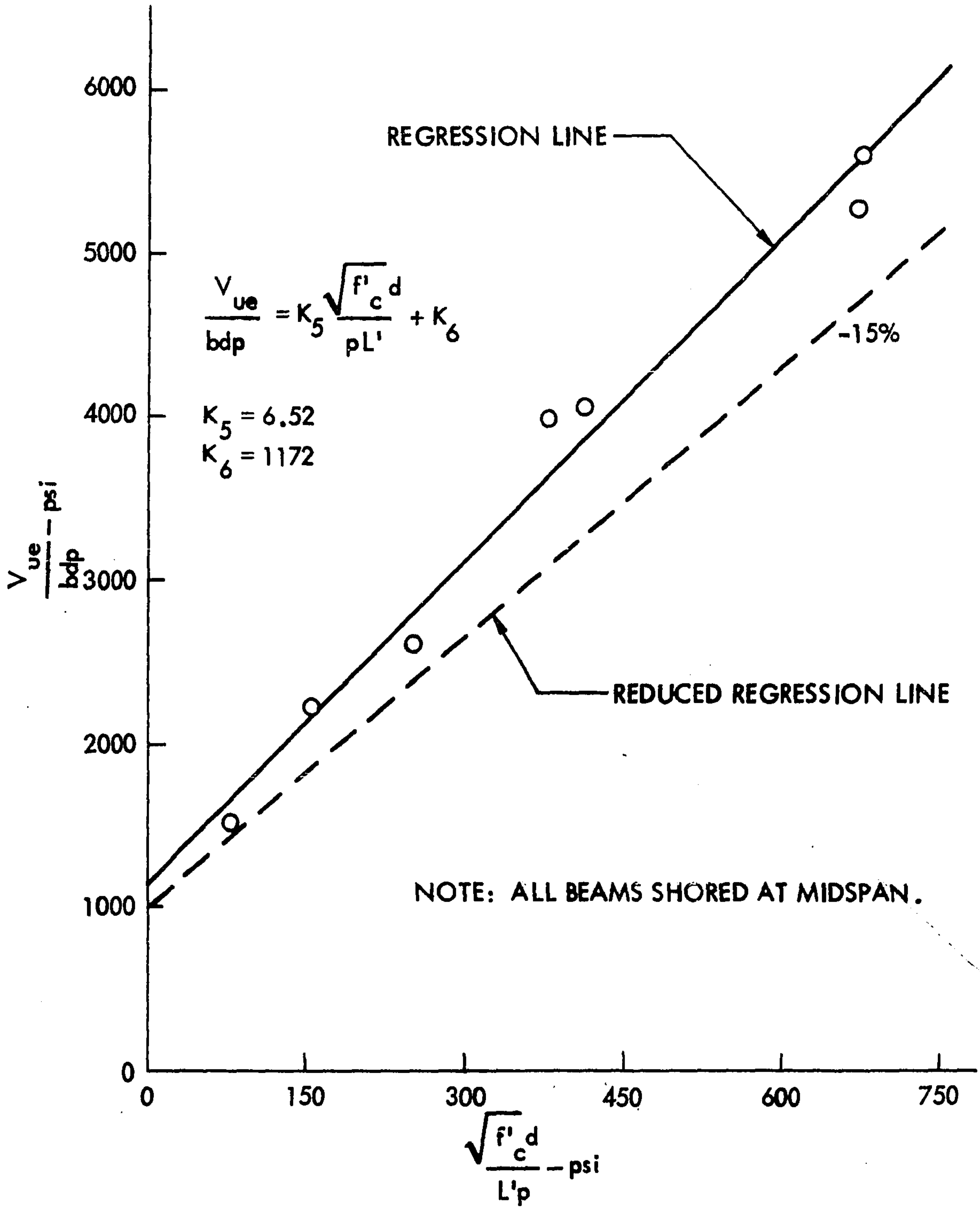

Fig. 50. Relationship between V_{ue}/bdp and $\sqrt{f'_c}d/L'p$ for beams constructed with steel deck I - 16 gage

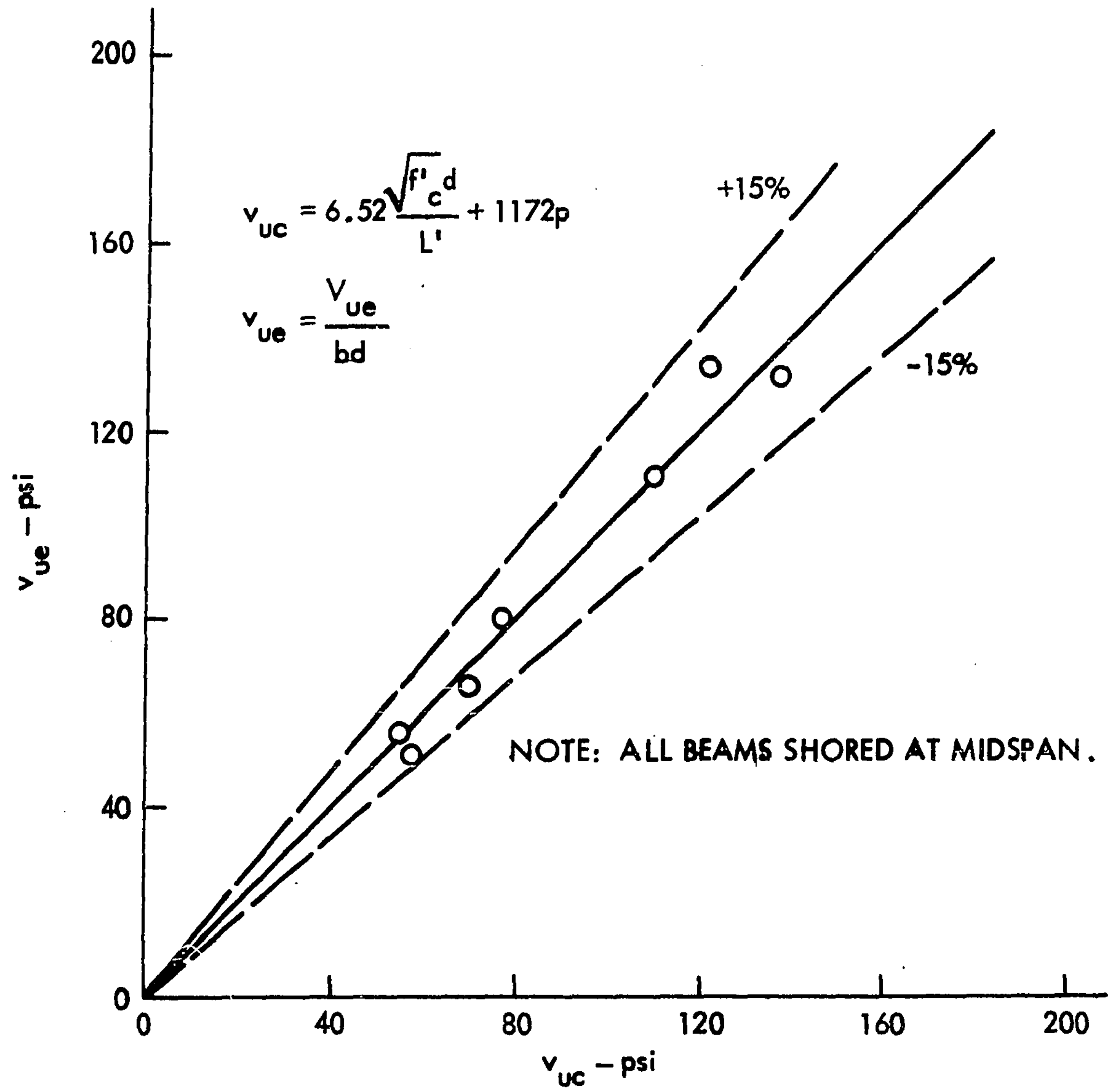

Fig. 51. Comparison of experimental and calculated ultimate shear-bond stresses for beams constructed with steel deck I - 16 gage

those beams shored throughout.

In an attempt to determine the effect of the steel deck thickness on shear-bond failure, Equation 11 was modified by assuming that the dowel shear, V_d, is proportional to the thickness squared. Thus,

$$V_d = K_{10} t^2,$$

and

$$\frac{V_u}{bd} = K_9 \frac{\sqrt{f'_c}\,d}{L'} + K_{10} t^2 \tag{25}$$

where K_9 and K_{10} are constants to be determined from experimental test results. Figure 52 represents a plot of the ultimate strength shear-bond relationship for beams constructed with deck I-16, 18 and 22 gage. As can be observed from Fig. 52, a linear relationship exists for the 99 test results plotted using Equation 25; thus, Equation 25 is also applicable, but only for beams constructed with steel deck I. Figure 53 shows the comparison of experimental and calculated ultimate shear-bond stresses pertaining to values of Fig. 52.

The shear-bond relationships plotted in Figs. 44, 46, 48, and 50 resulting from Equation 11 and Fig. 52 resulting from Equation 25, reveal the linear nature of Equations 11 and 25. In all cases, Figs. 45, 47, 49, 51, and 53 indicate a maximum error of 15 percent between experimental and derived shear-bond stresses. This error is believed to be moderate considering

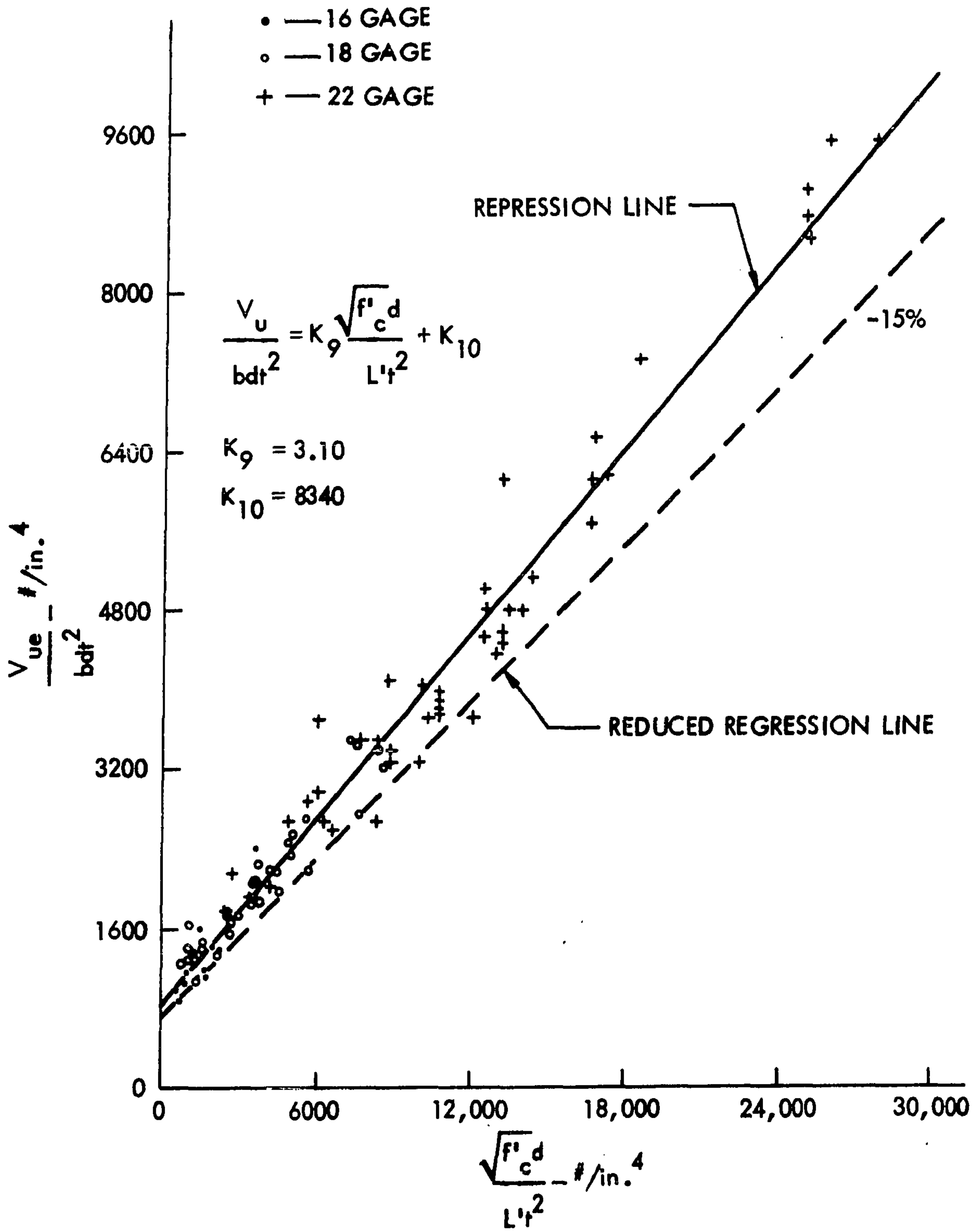

Fig. 52. Relationship between V_{ue}/bdt^2 and $\sqrt{f'_c}d/L't^2$ for beams constructed with steel deck I - 16, 18 and 22 gage

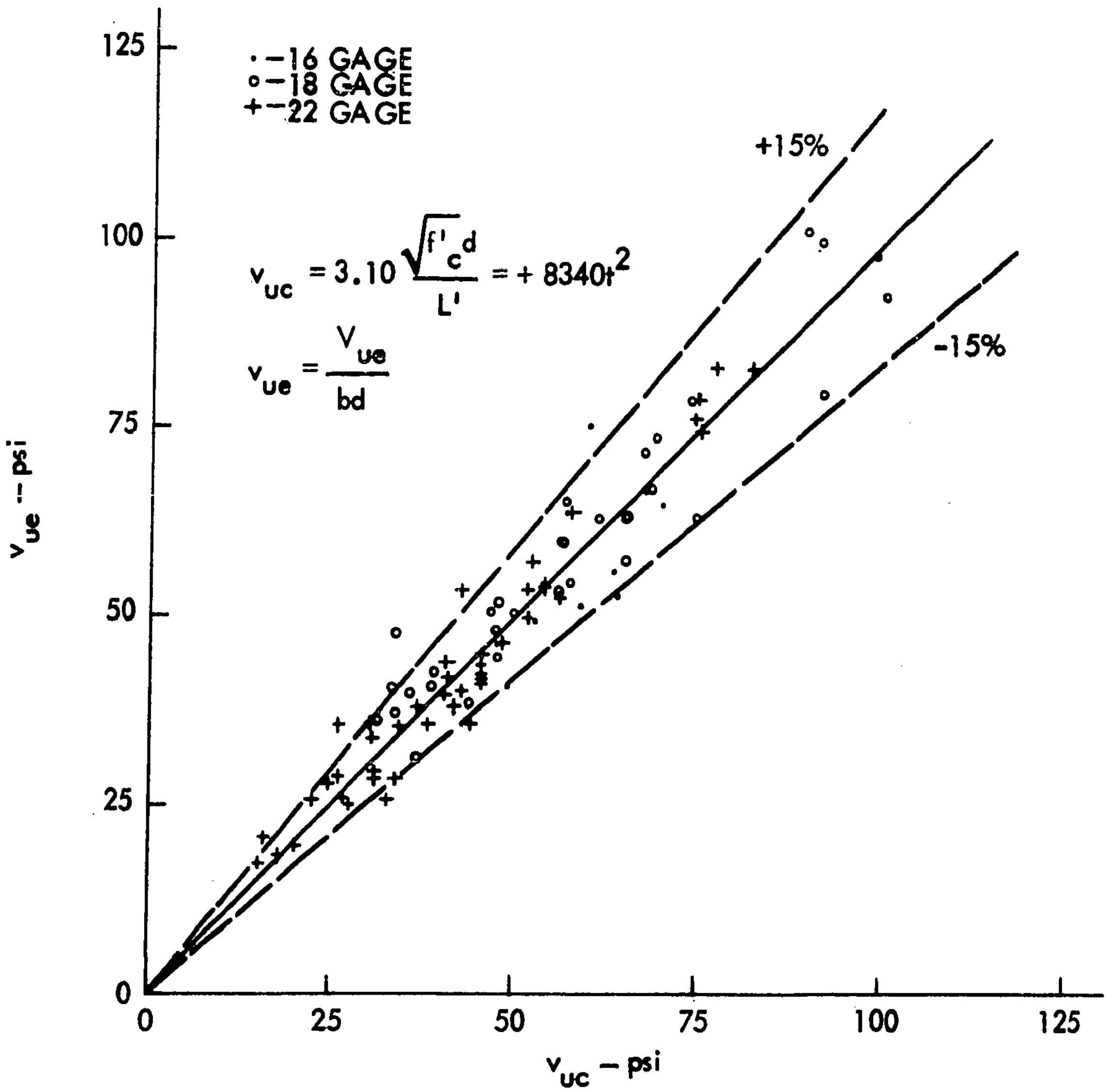

Fig. 53. Comparison of experimental and calculated ultimate shear-bond stresses for beams constructed with steel deck I - 16, 18 and 22 gage

the nonhomogeneity of concrete and the mode of failure, namely shear.

Deck O (CATEGORY I)

Ultimate shear-bond relationships for beams constructed with steel deck O indicate similar strength characteristics as discussed with beams of deck I. For example, Fig. 54 shows the shear-bond relationship for beams with deck of 20 and 22 gage. Beam results of both 20 and 22 gage decking were considered in the regression analysis, since the difference in average steel deck thickness was only 0.0056 inches (see Table A.1 for individual thicknesses). Figure 54 contains the results of 18 beam tests and illustrates the linearity of the shear-bond relationship of Equation 11 as well as showing no observable width of beam effect, nor any detectable difference in strength for beams shored throughout vs. shored at midspan only. Figure 55 shows a comparison of experimental and calculated shear-bond stresses for beams consisting of deck O-20 and 22 gage. In short, the comparison indicates similar correlation as with beams constructed with steel deck I.

Figures 56 and 57 represent, respectively, plots of ultimate strength shear-bond relationships, and comparison of experimental and calculated ultimate shear-bond stresses for beams constructed with deck O-16 gage. Interpretation is similar to that of Figs. 54 and 55.

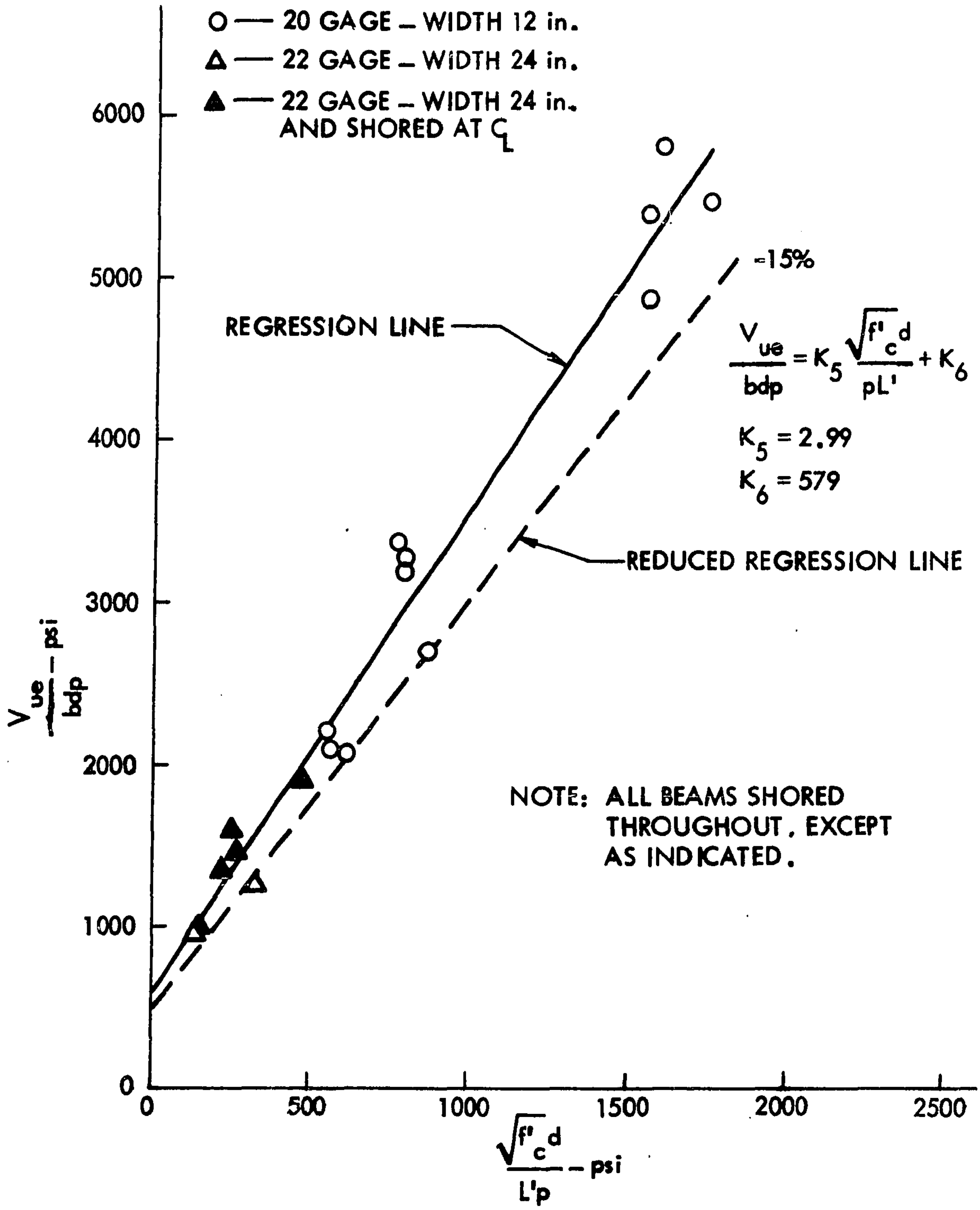

Fig. 54. Relationship between V_{ue}/bdp and $\sqrt{f'_c}d/L'p$ for beams constructed with steel deck O - 20 and 22 gage

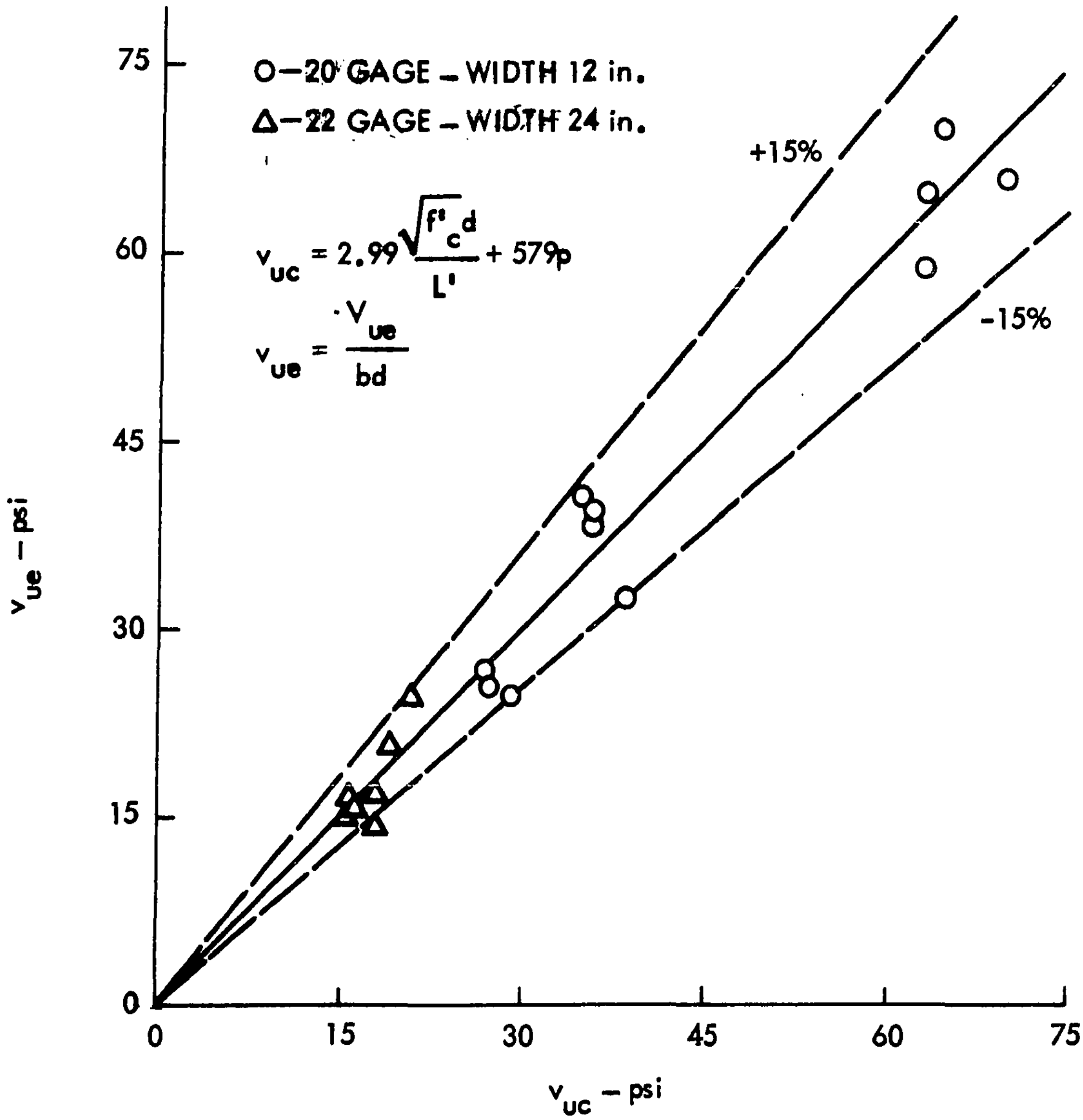

Fig. 55. Comparison of experimental and calculated ultimate shear-bond stresses for beams constructed with steel deck O - 20 and 22 gage

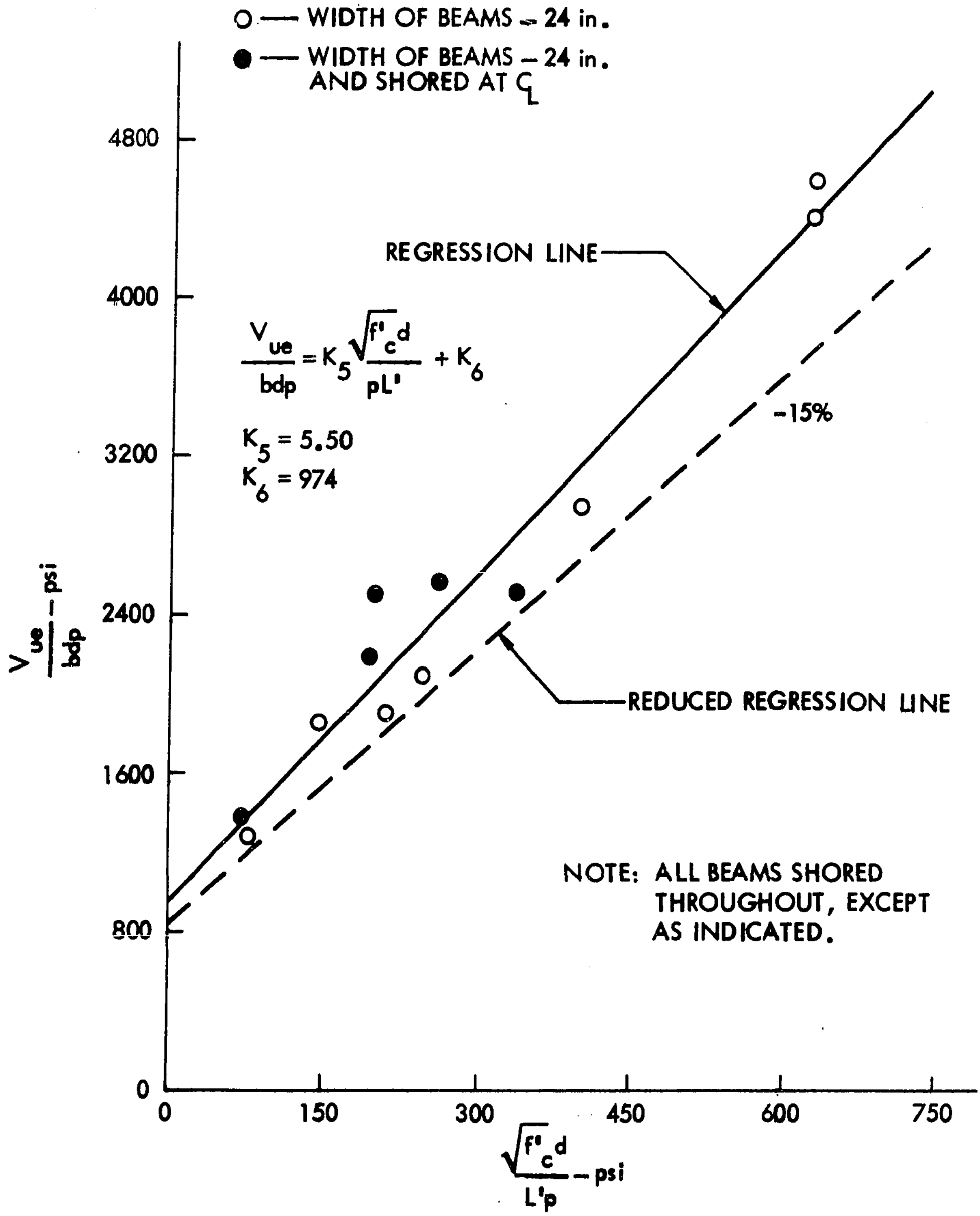

Fig. 56. Relationship between V_{ue}/bdp and $\sqrt{f'_c}d/L'p$ for beams constructed with steel deck 0 - 16 gage

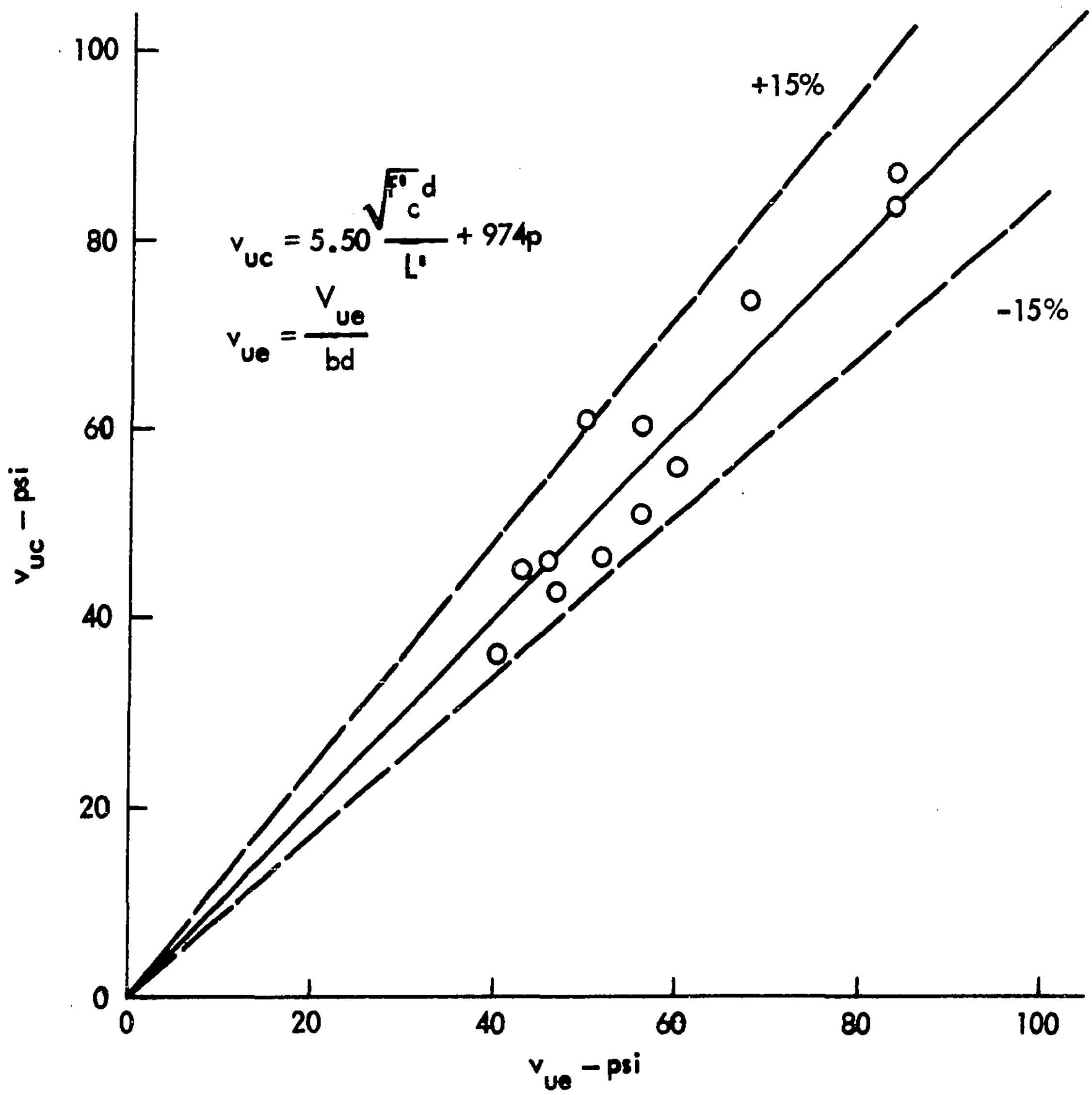

Fig. 57. Comparison of experimental and calculated ultimate shear-bond stresses for beams constructed with steel deck 0 - 16 gage

Figures 58 through 69 pertain only to the shear-bond analysis of beams constructed with steel deck O, conducted by company O. These steel decks have the same general geometric configuration as shown in Fig. 6, but vary in depth from 3.04 to 7.59 inches (see Table A.2 for further information). Test data were limited, but nevertheless, sufficient for establishing regression constants. Also, steel decks of certain groups of beams were greased prior to placing of concrete. Regression constants, resulting from Figs. 58, 60, 62, 64 and 68 are given in Table A.11 and shown on respective figures. Table A.14 gives values plotted in Figs. 59, 61, 63, 65 and 69 as well as ratios of ultimate calculated to experimental shear-bond stresses. Shear-bond relationships of Figs. 58, 60, 62, 64 and 68 indicated a linear behavior of beam specimens, whether greased or nongreased. In general, greased beam specimens resulted in lower ultimate shear-bond values as compared to similar non-greased beams (see Figs. 66 and 67 for direct comparison). This was anticipated, since virtually all chemical bond and frictional contribution is eliminated. Certain beam specimens of Fig. 68 were proportioned such that the composite neutral axis of the cross-section was located within the limits of the steel deck, while the neutral axis of other beams was contained between the top of the concrete and top of steel deck. No appreciable difference in shear-bond strength was detected between these beams of Fig. 68.

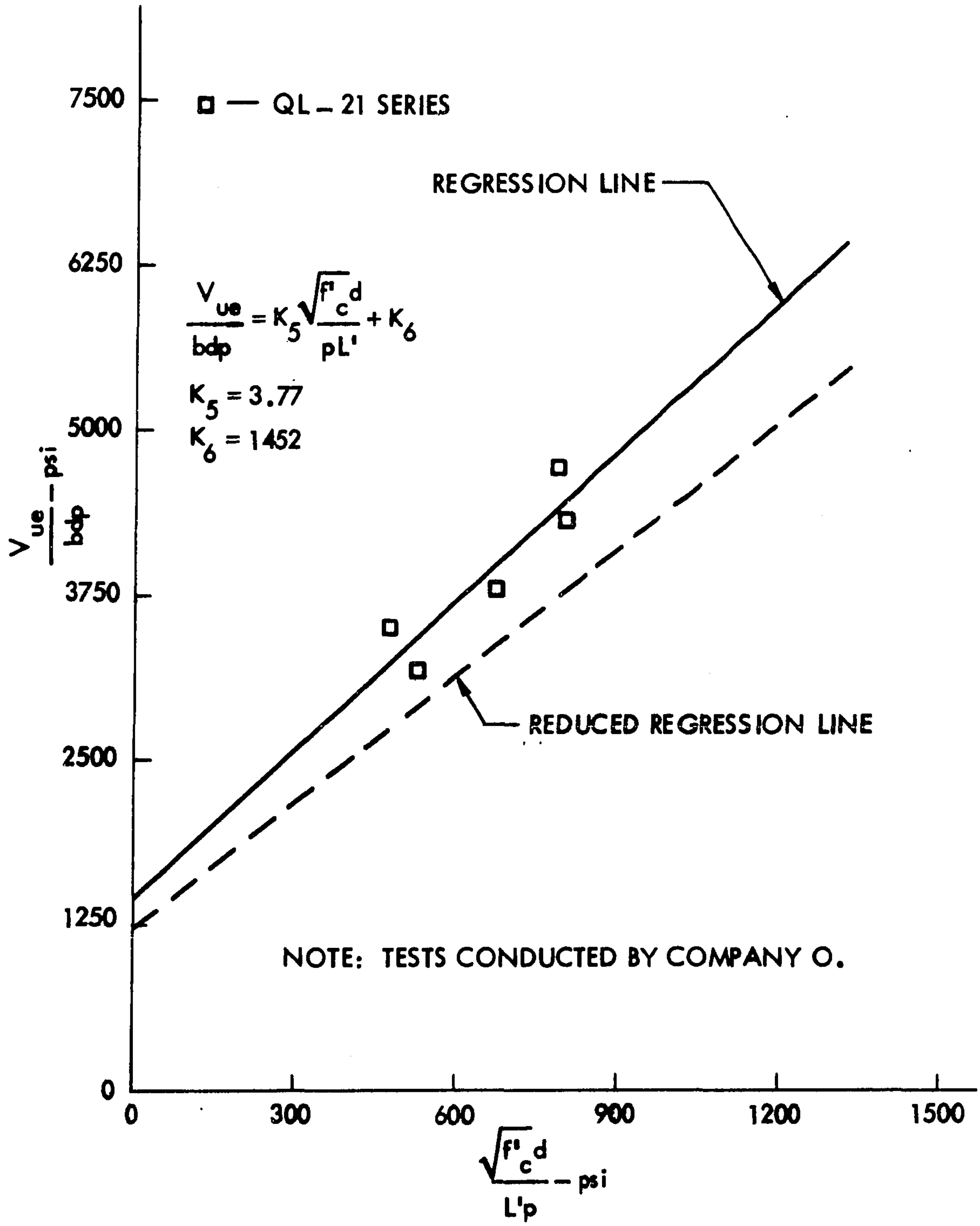

Fig. 58. Relationship between V_{ue}/bdp and $\sqrt{f'_c}$ d/L'p for beams constructed with steel deck O - 20 gage

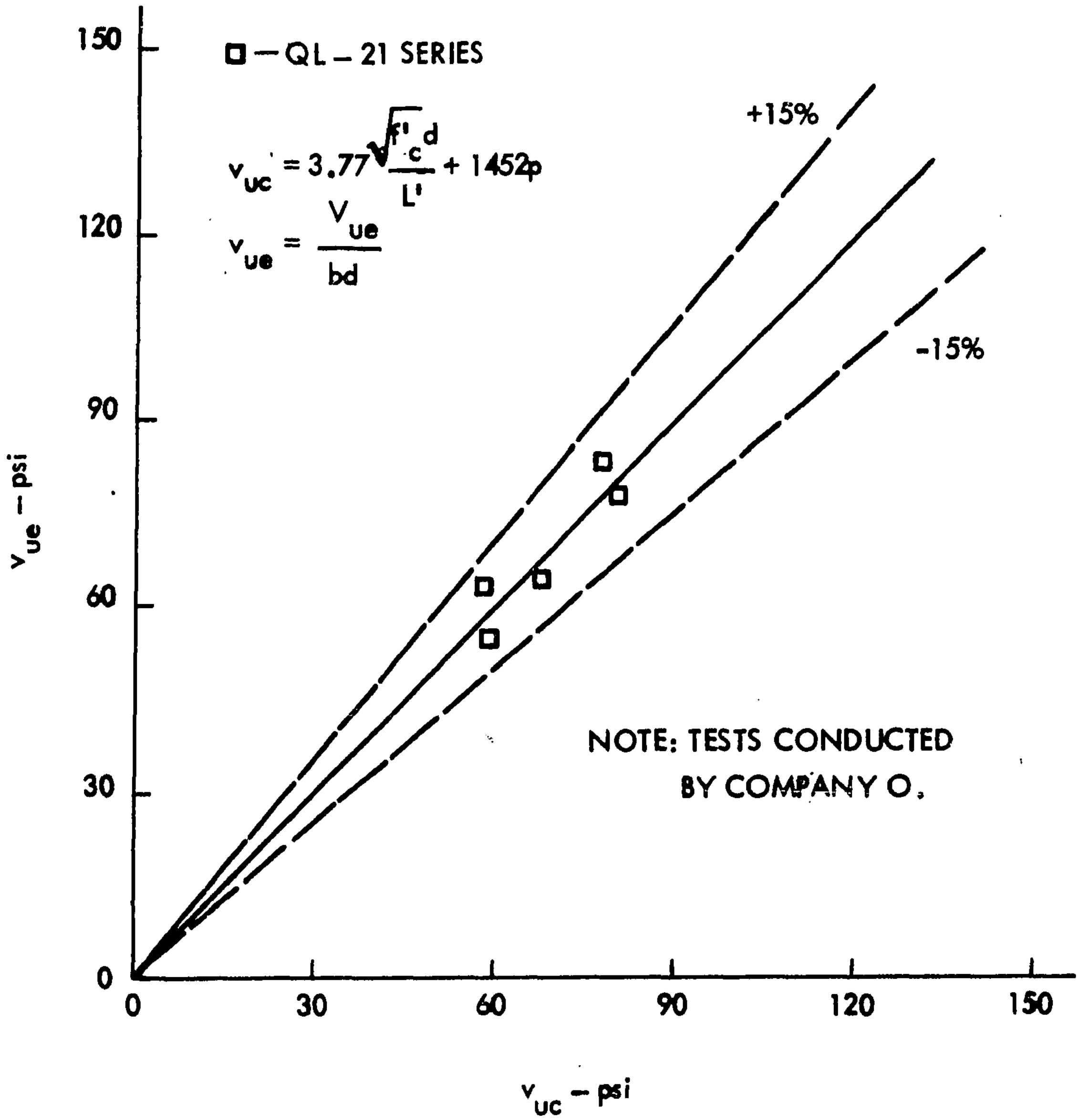

Fig. 59. Comparison of experimental and calculated ultimate shear-bond stresses for beams constructed with steel deck O - 20 gage

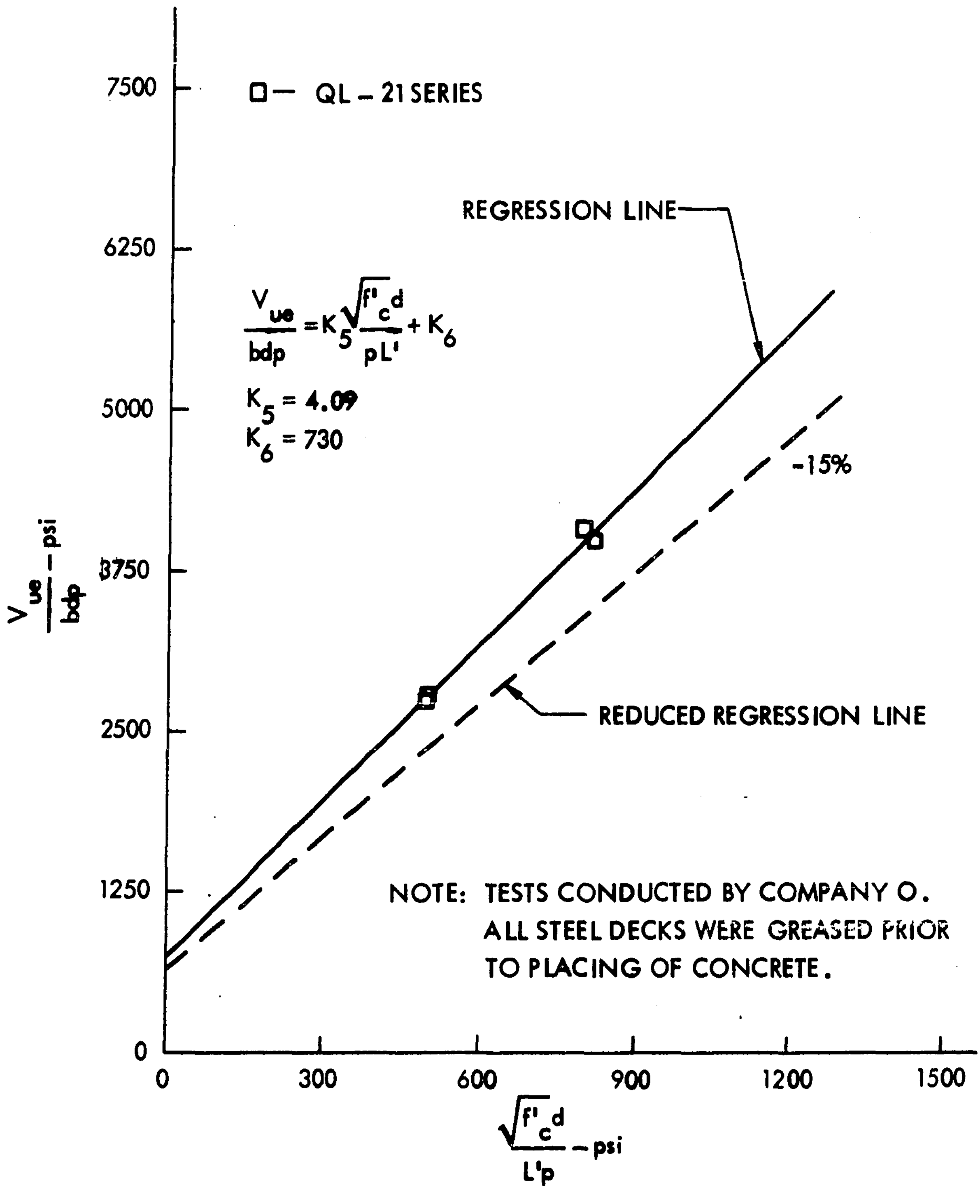

Fig. 60. Relationship between V_{ue}/bdp and $\sqrt{f'_c}$ d/L' p for beams constructed with steel deck O - 20 gage

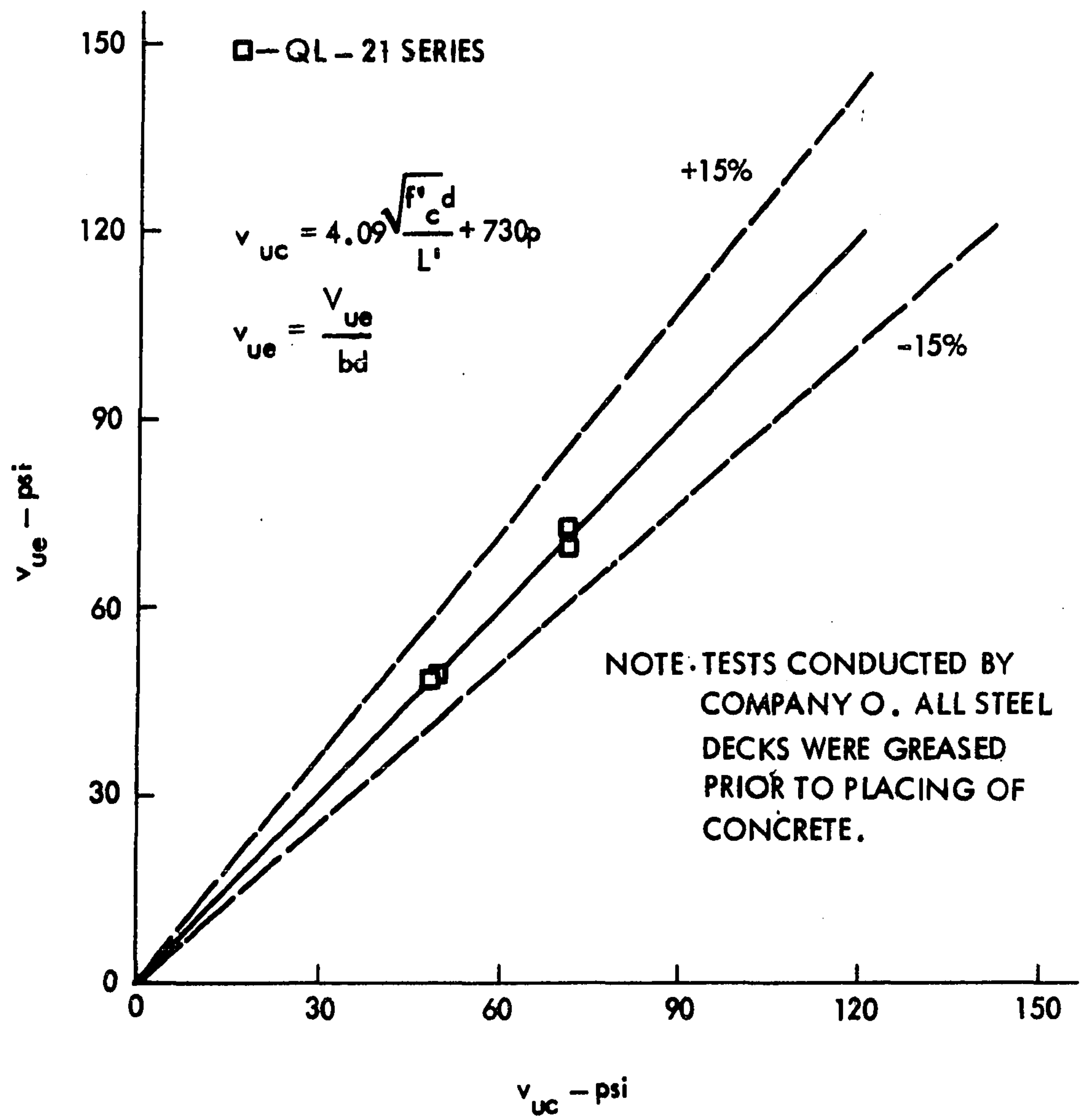

Fig. 61. Comparison of experimental and calculated ultimate shear-bond stresses for beams constructed with steel deck O - 20 gage

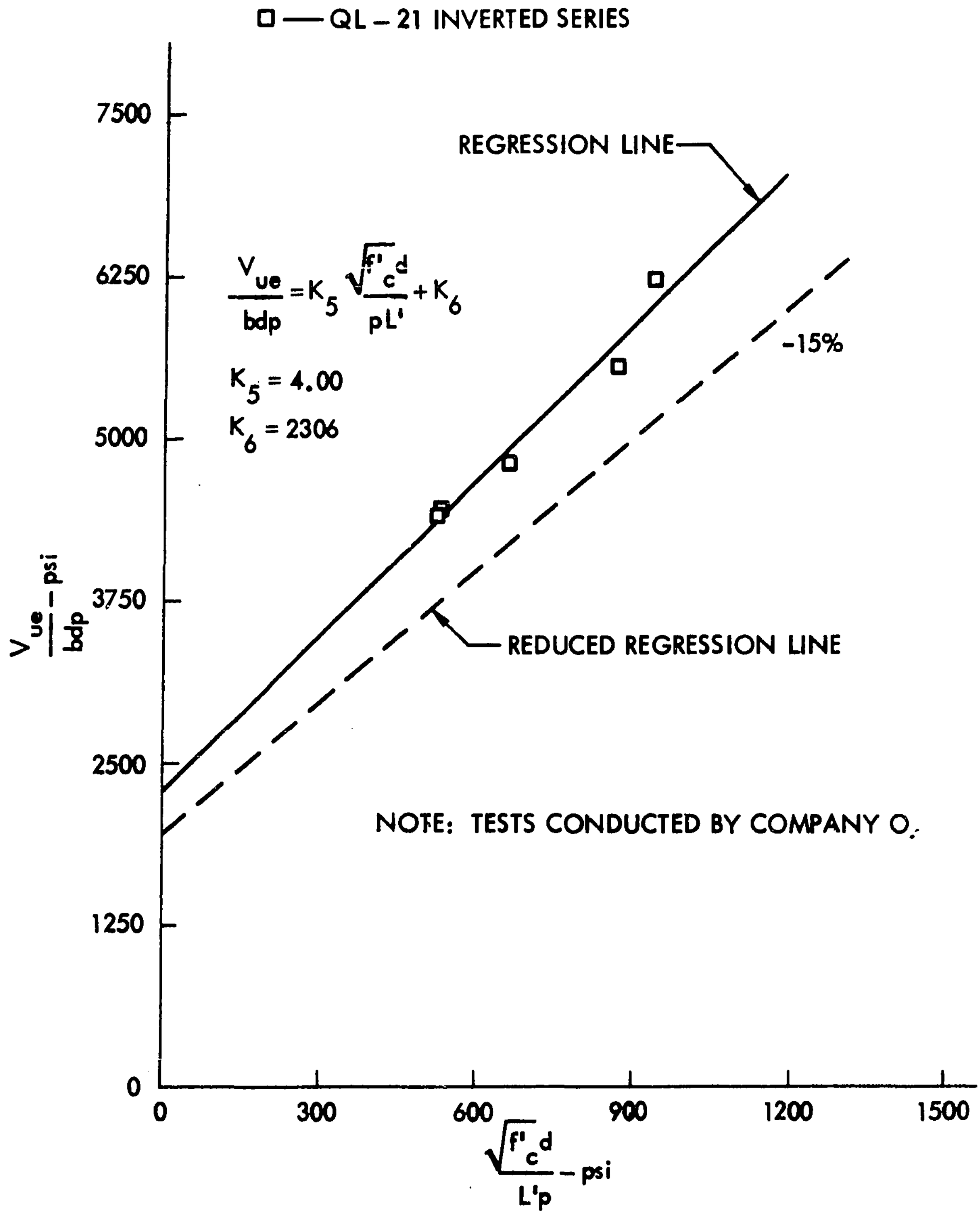

Fig. 62. Relationship between V_{ue}/bdp and $\sqrt{f'_c}$ d/L'p for beams constructed with steel deck O - 20 gage

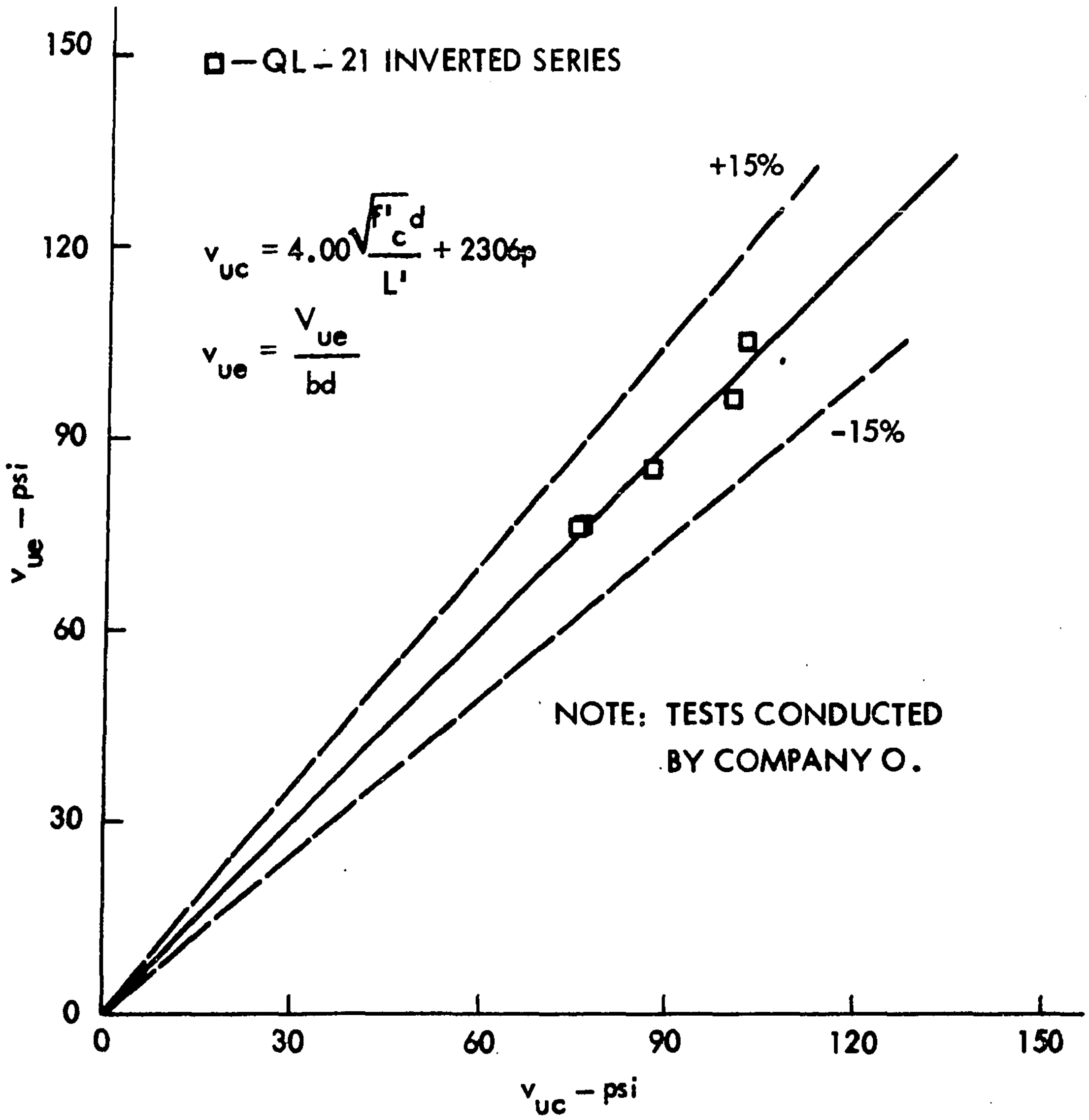

Fig. 63. Comparison of experimental and calculated ultimate shear-bond stresses for beams constructed with steel deck O - 20 gage

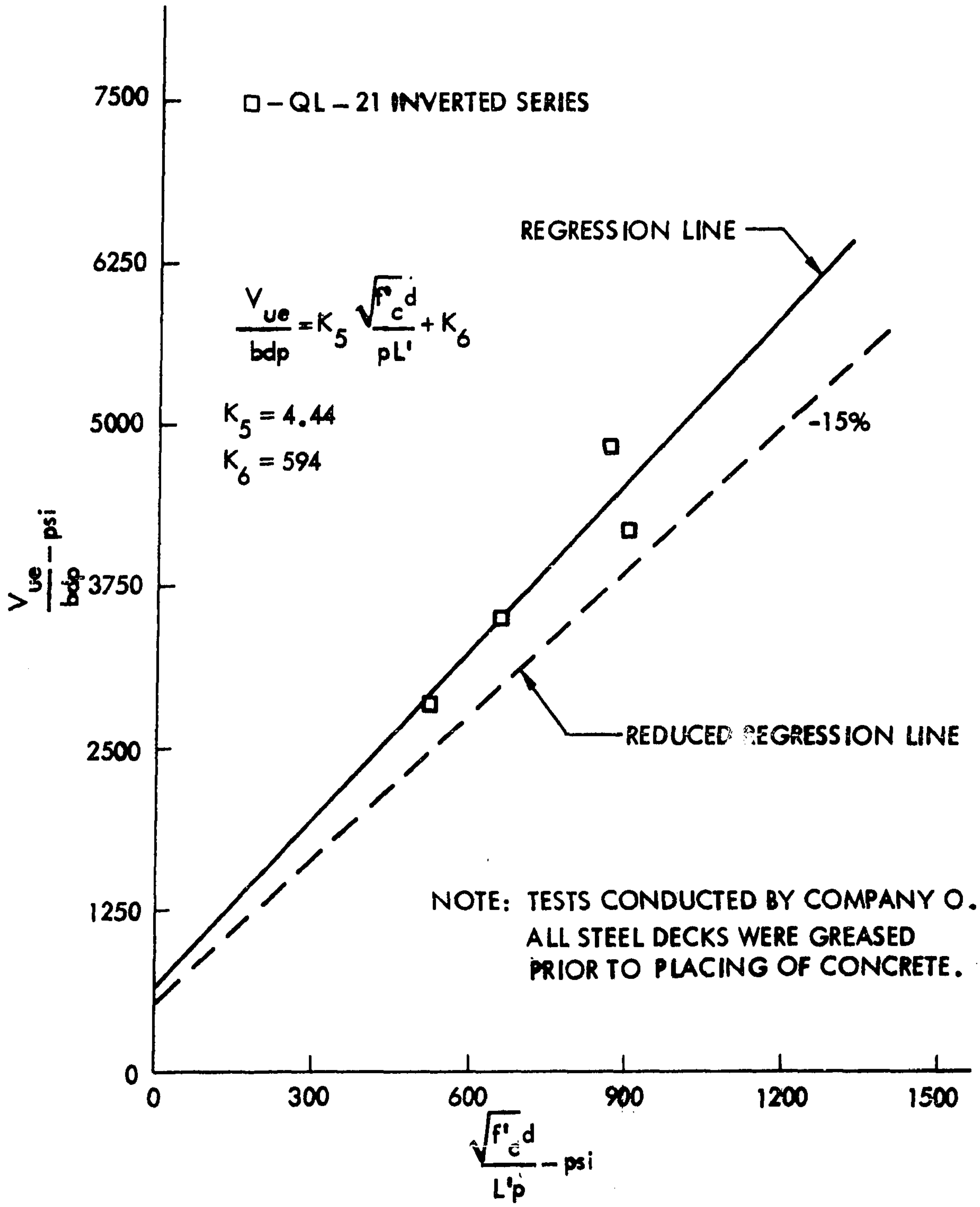

Fig. 64. Relationship between V_{ue}/bdp and $\sqrt{f'_c}$ d/L'p for beams constructed with steel deck O - 20 gage

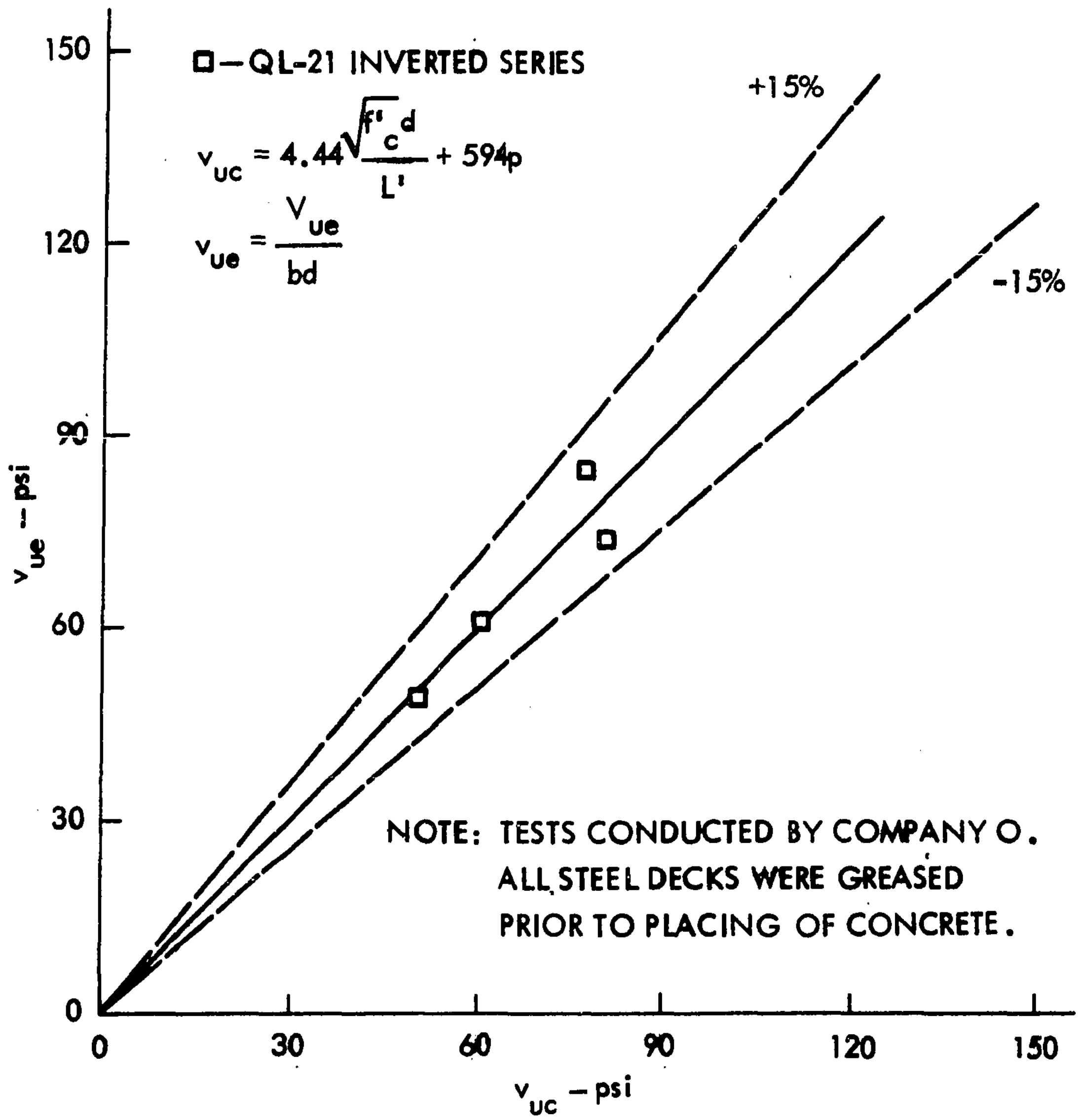

Fig. 65. Comparison of experimental and calculated ultimate shear-bond stresses for beams constructed with steel deck O - 20 gage

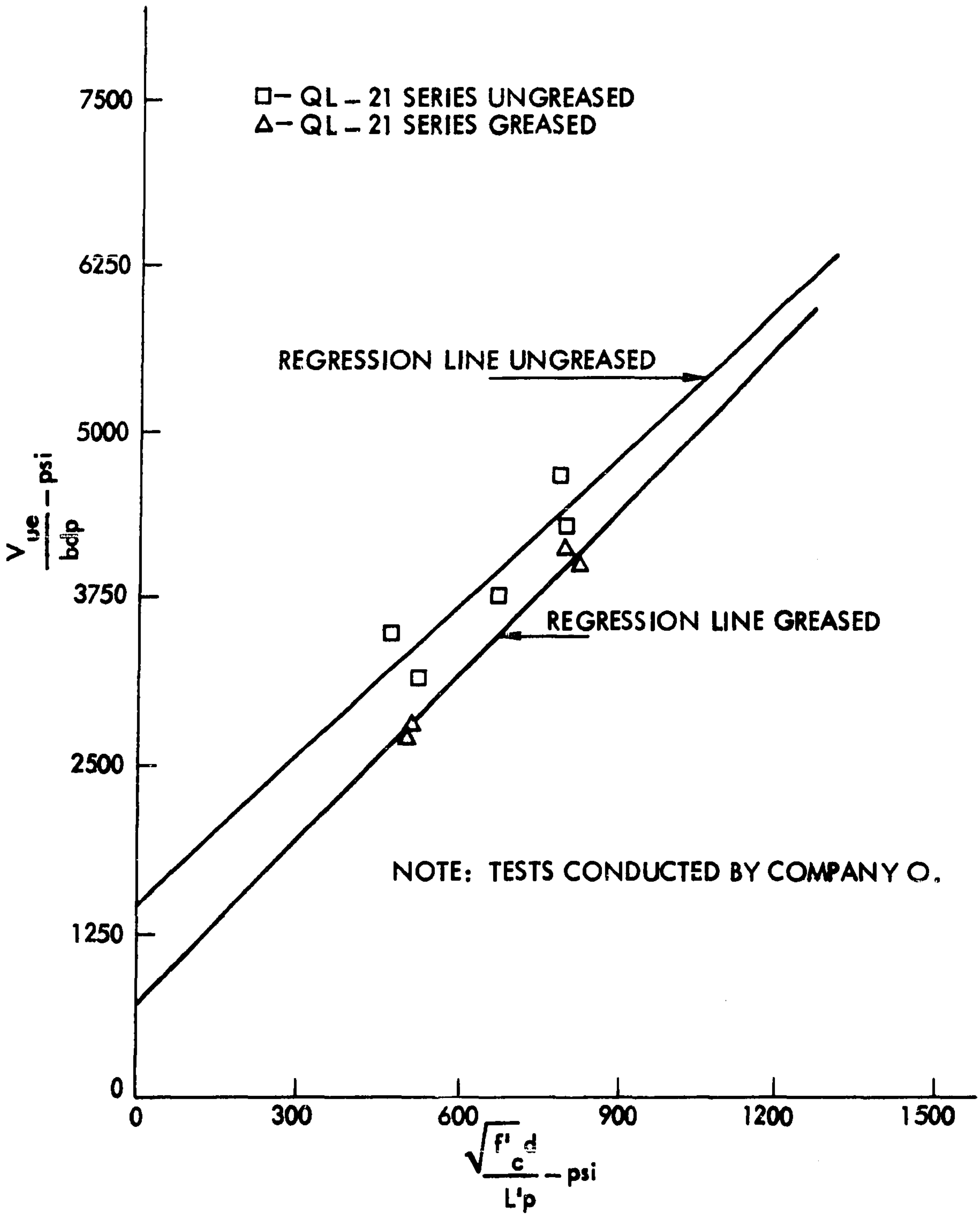

Fig. 66. Relationship between V_{ue}/bdp and $\sqrt{f'_c}\ d/L'p$ for beams constructed with steel deck O - 20 gage

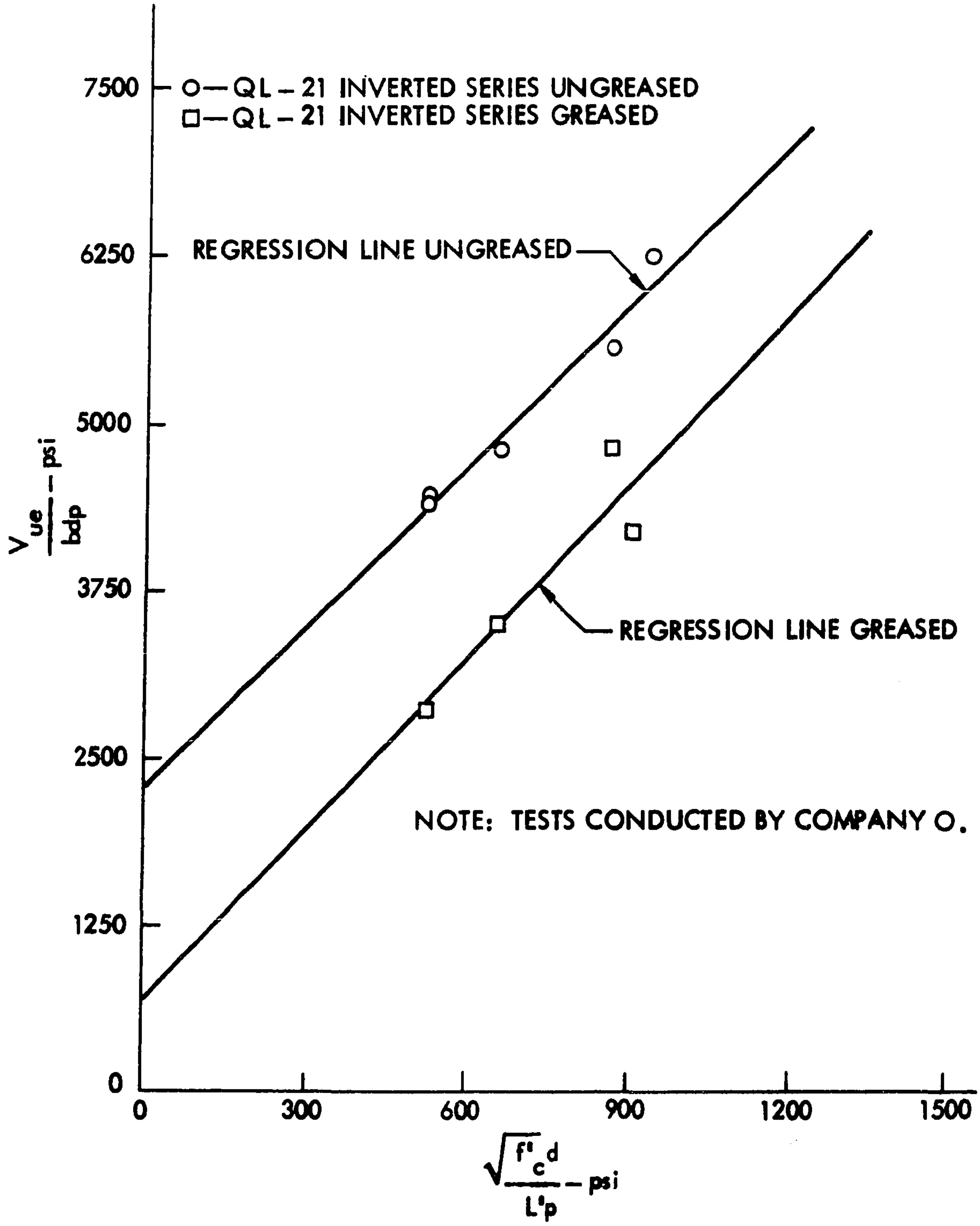

Fig. 67. Relationship between V_{ue}/bdp and $\sqrt{f'_c}$ d/L'p for beams constructed with steel deck O - 20 gage

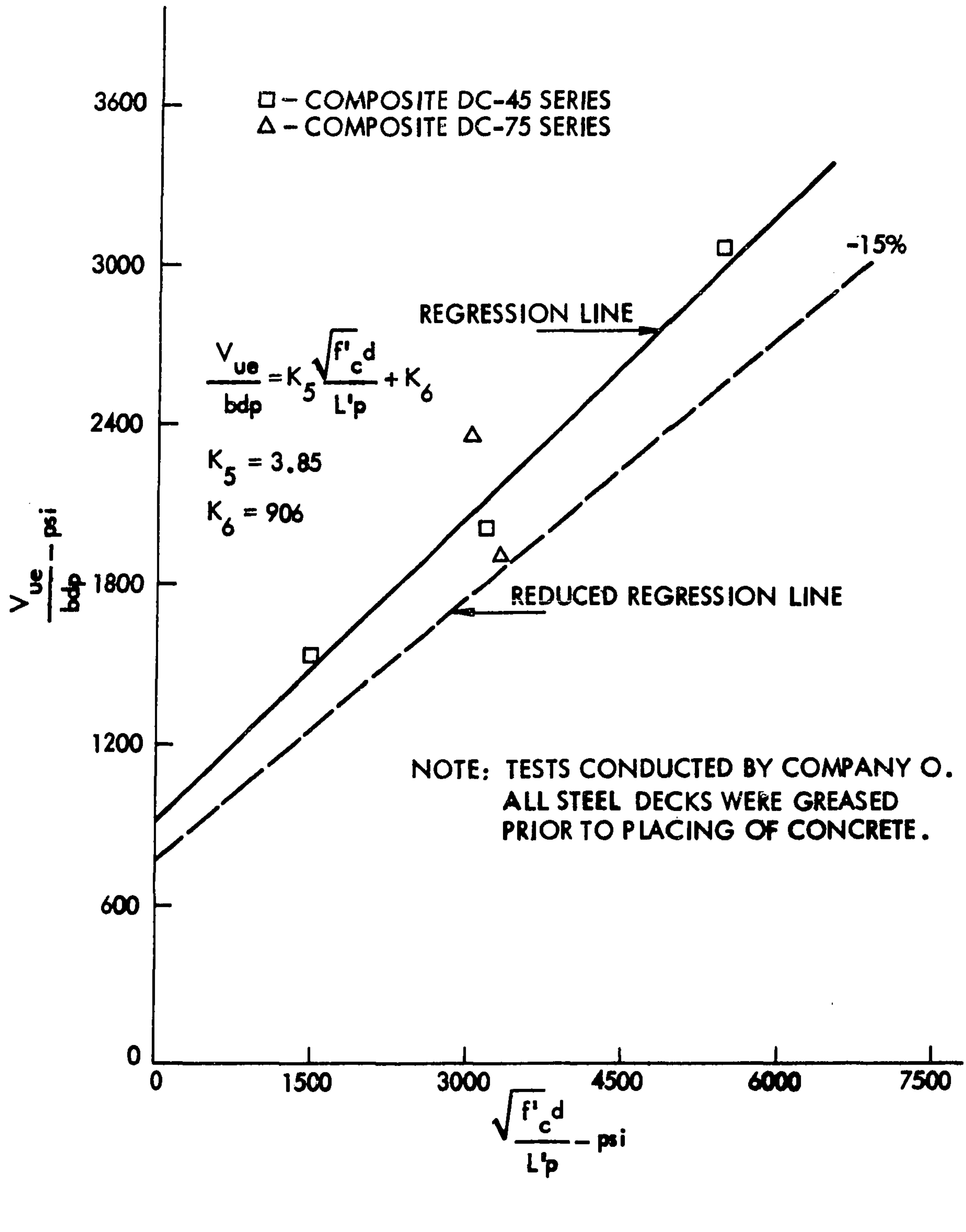

Fig. 68. Relationship between V_{ue}/bdp and $\sqrt{f'_c}$ d/L'p for beams constructed with steel deck O - 18/18 gage

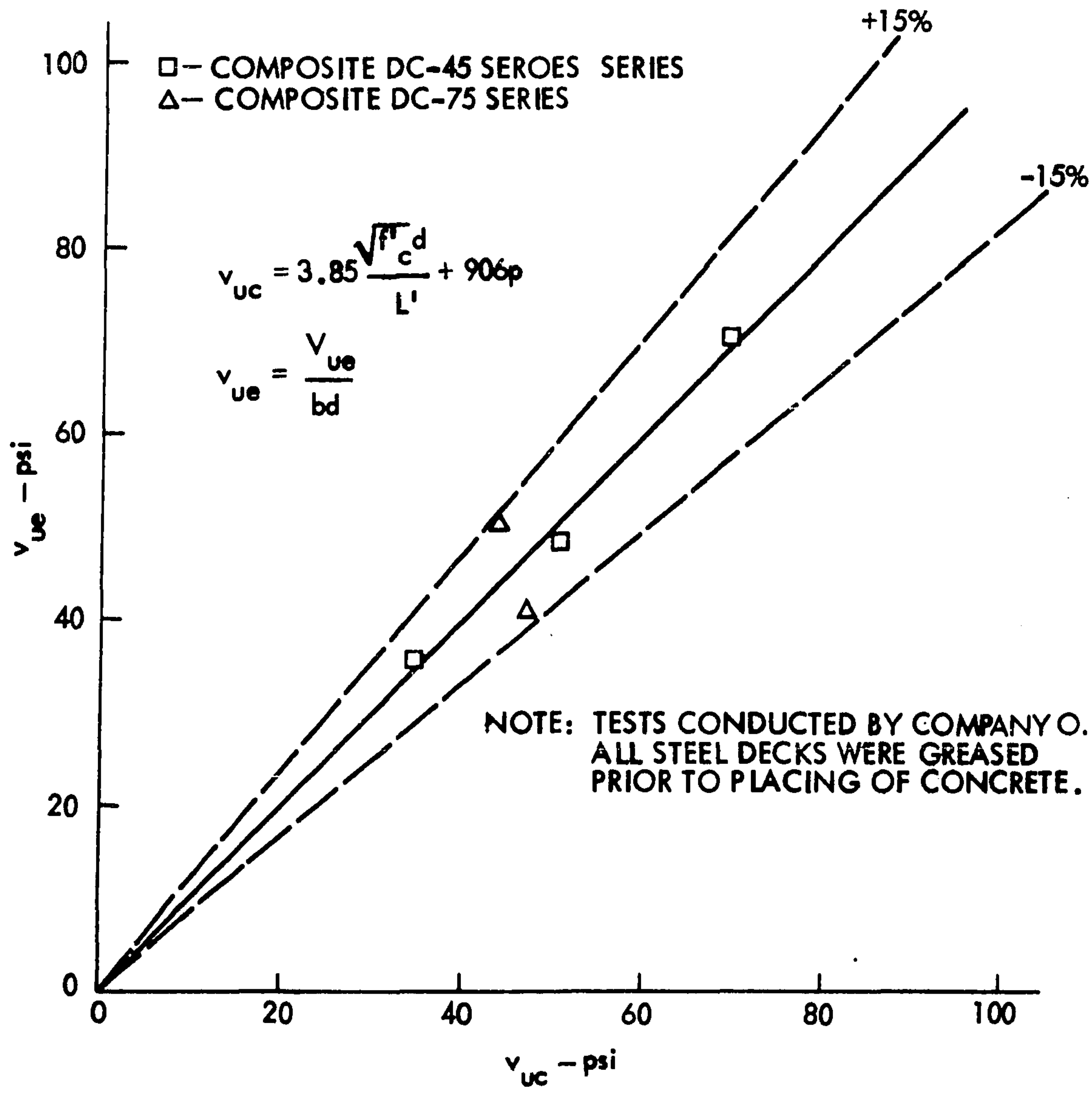

Fig. 69. Comparison of experimental and calculated ultimate shear-bond stresses for beams constructed with steel deck O - 18/18 gage

Deck G (CATEGORY II)

Since beams constructed with steel deck G are categorized in CATEGORY II, Equation 14 applies for the shear-bond regression analysis. Figure 70 represents the ultimate shear-bond relationship for beams constructed with steel deck G-24 gage and Fig. 71 illustrates the comparison of experimental and calculated shear-bond stresses corresponding to Fig. 70. For beams constructed with deck G-20 gage, Figs. 72 and 73 show, characteristically, plots as Figs. 70 and 71, respectively. Table A.10 gives regression constants which are also indicated on Figs. 70 and 72 and Table A.15 gives identical information as plotted in Figs. 71 and 73. Figure 70 reveals that the ultimate shear-bond strength of beams constructed with deck G-24 gage is greater than that of beams constructed with 20 gage decking shown in Fig. 72. This may seem unlikely, since 20 gage decking has an average thickness of 0.0369 inches and 24 gage only 0.0251 inches (see Table A.1 for listing). However, the shear-bond capacity of beams constructed with deck G did not increase with an increase in thickness as was the case with beams of decks I and O, (see Fig. 74 for direct comparison). The reason for this is that in the case of beams constructed with deck G-20 gage, shear-bond failure occurred by shearing of the weld material at points of T-wire locations, while actual tearing of the steel deck was experienced at points of weld locations with beams constructed with deck G-24 gage. It is therefore believed that the shear transfer capac-

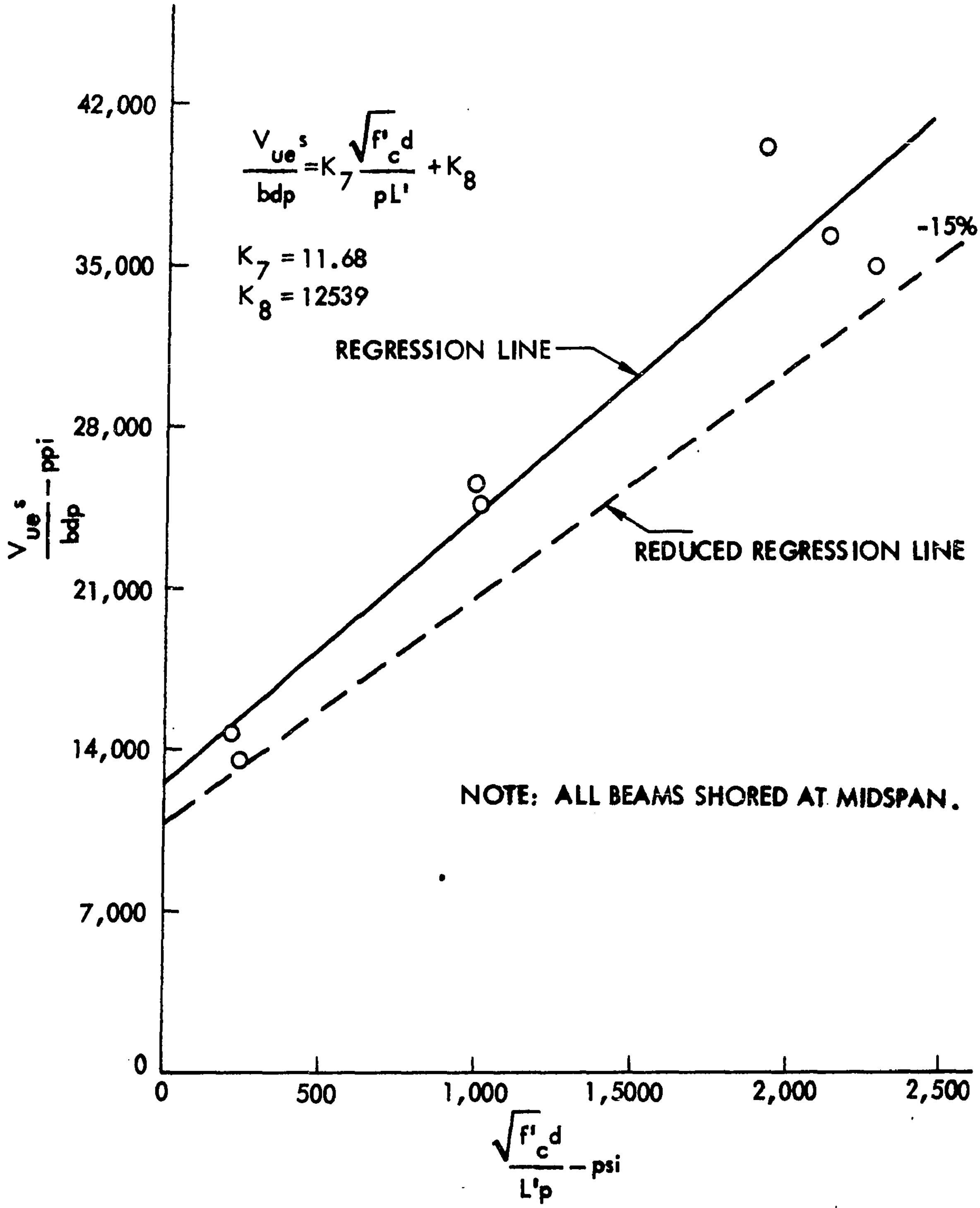

Fig. 70. Relationship between $V_{ue}s/bdp$ and $\sqrt{f'_c}\ d/L'\ p$ for beams constructed with steel deck G - 24 gage

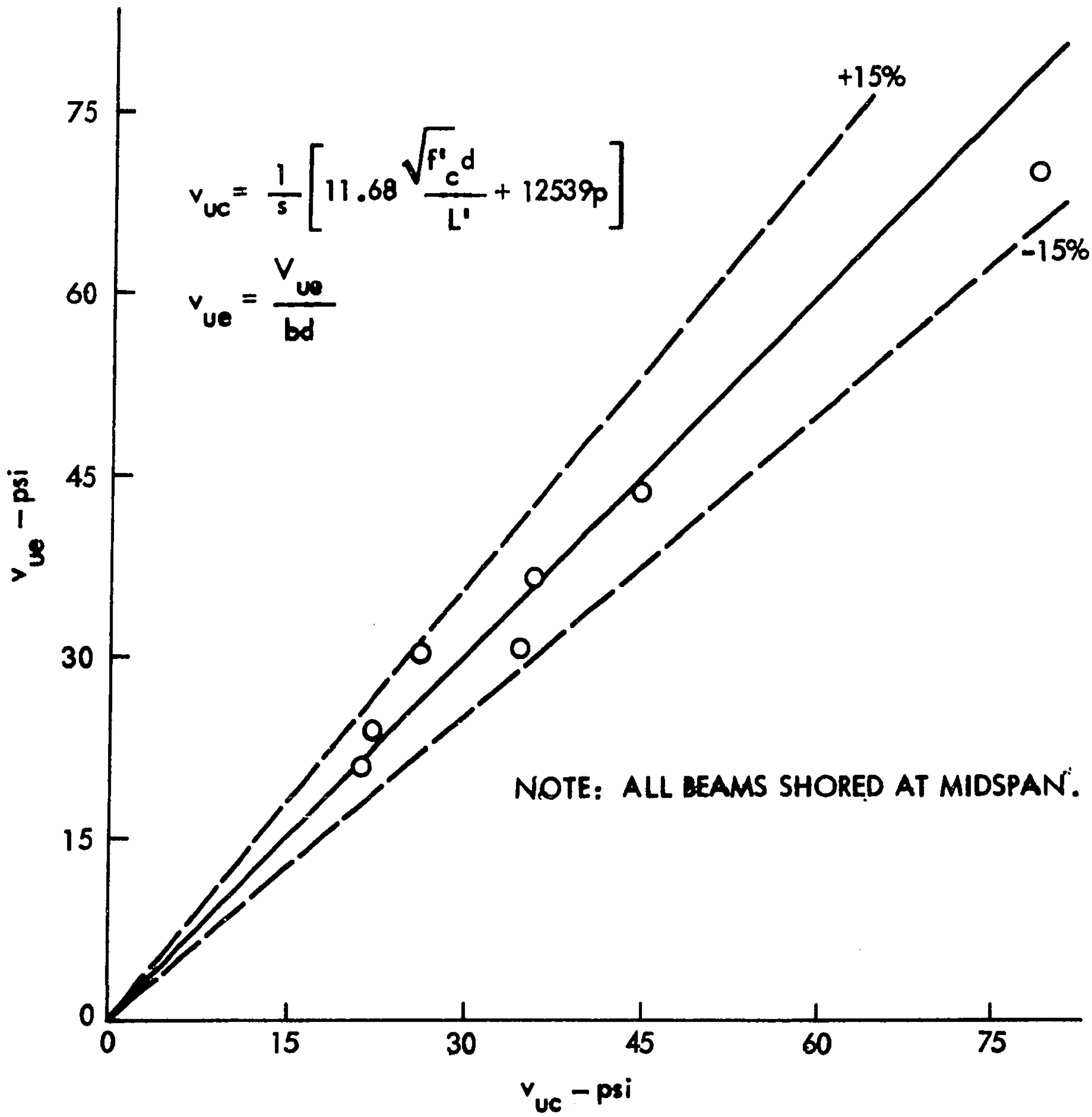

Fig. 71. Comparison of experimental and calculated ultimate shear-bond stresses for beams constructed with steel deck G - 24 gage

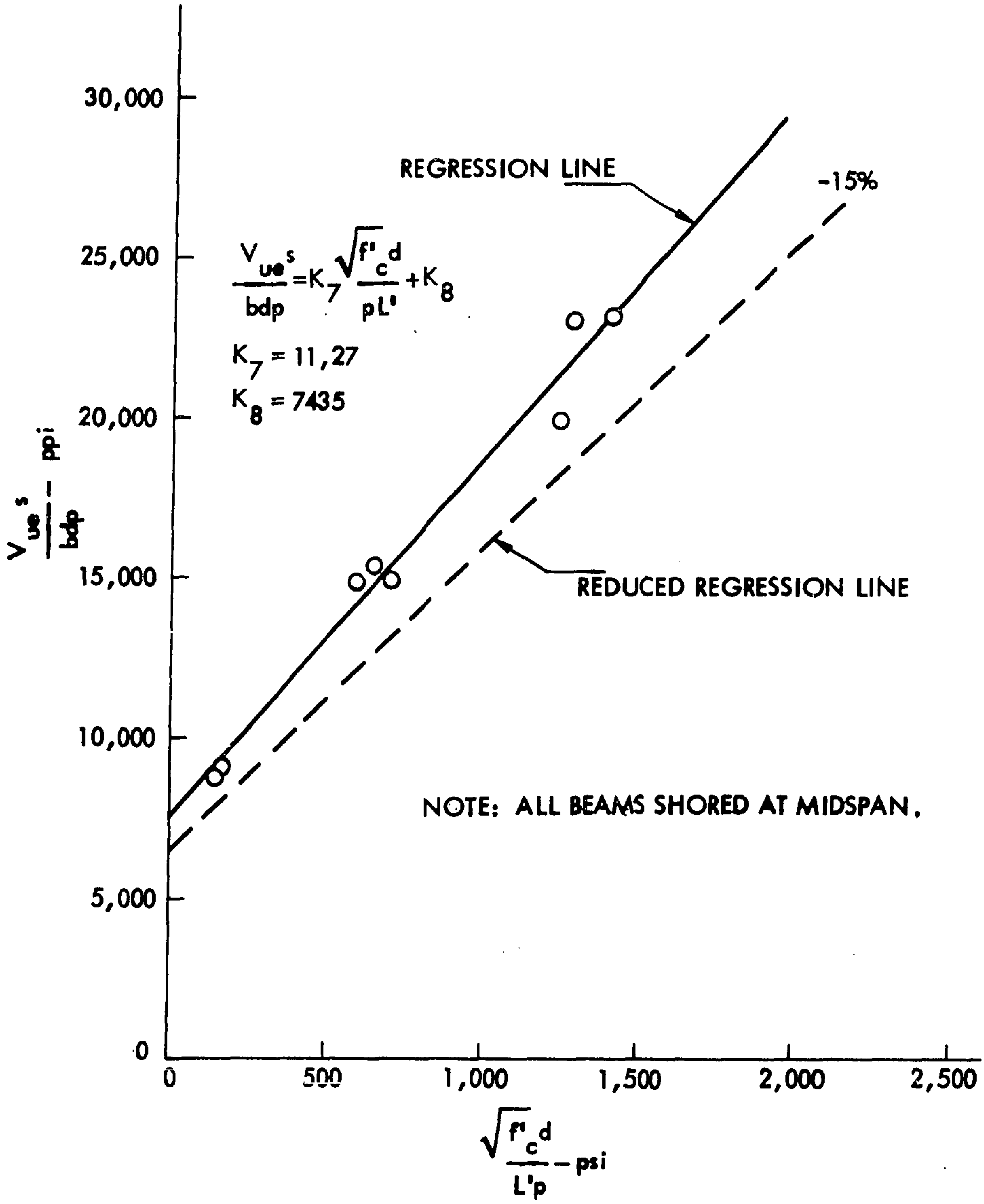

Fig. 72. Relationship between $V_{ue}s/bdp$ and $\sqrt{f'_c}\,d/L'\,p$ for beams constructed with steel deck G - 20 gage

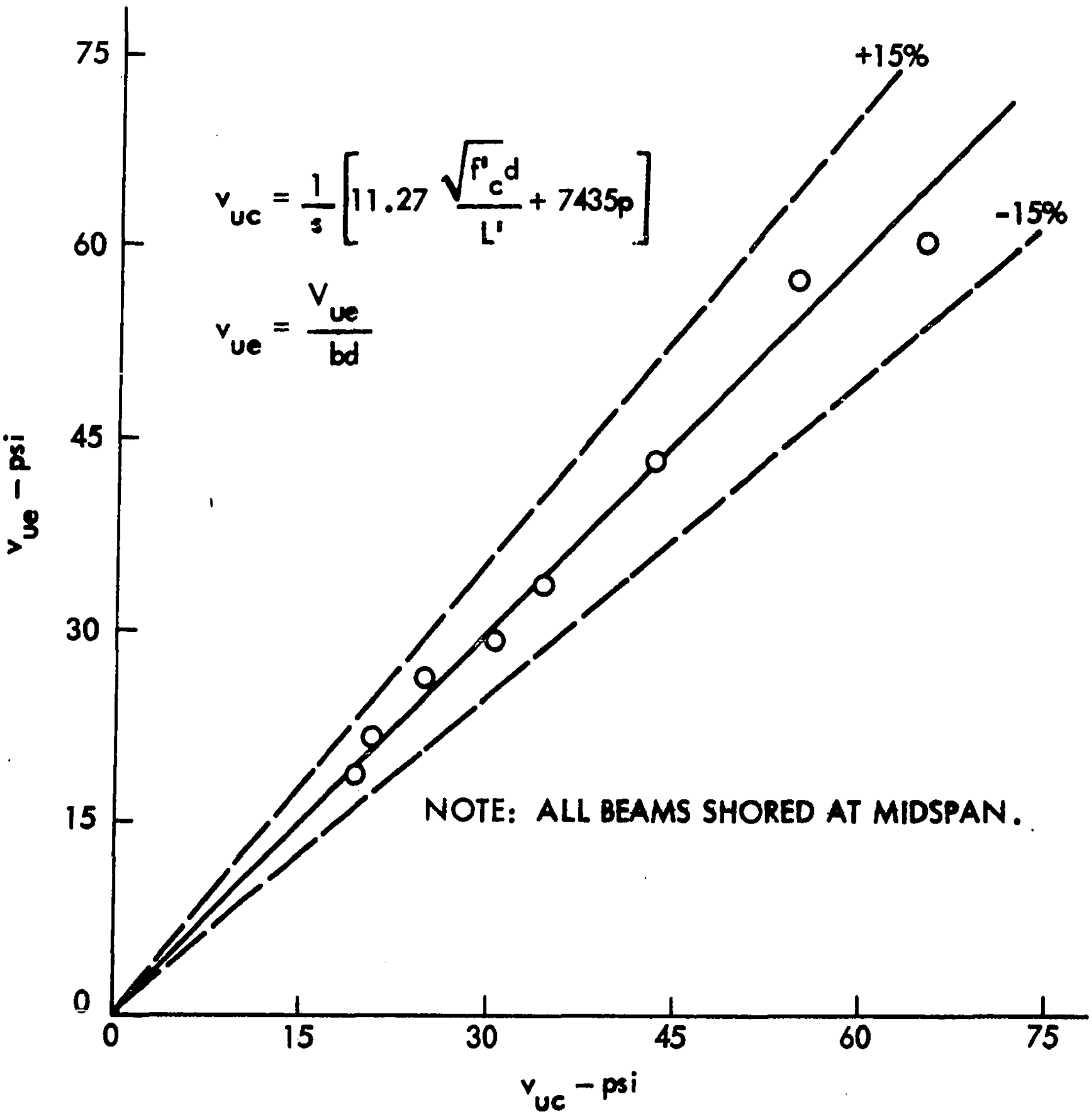

Fig. 73. Comparison of experimental and calculated ultimate shear-bond stresses for beams constructed with steel deck G - 20 gage

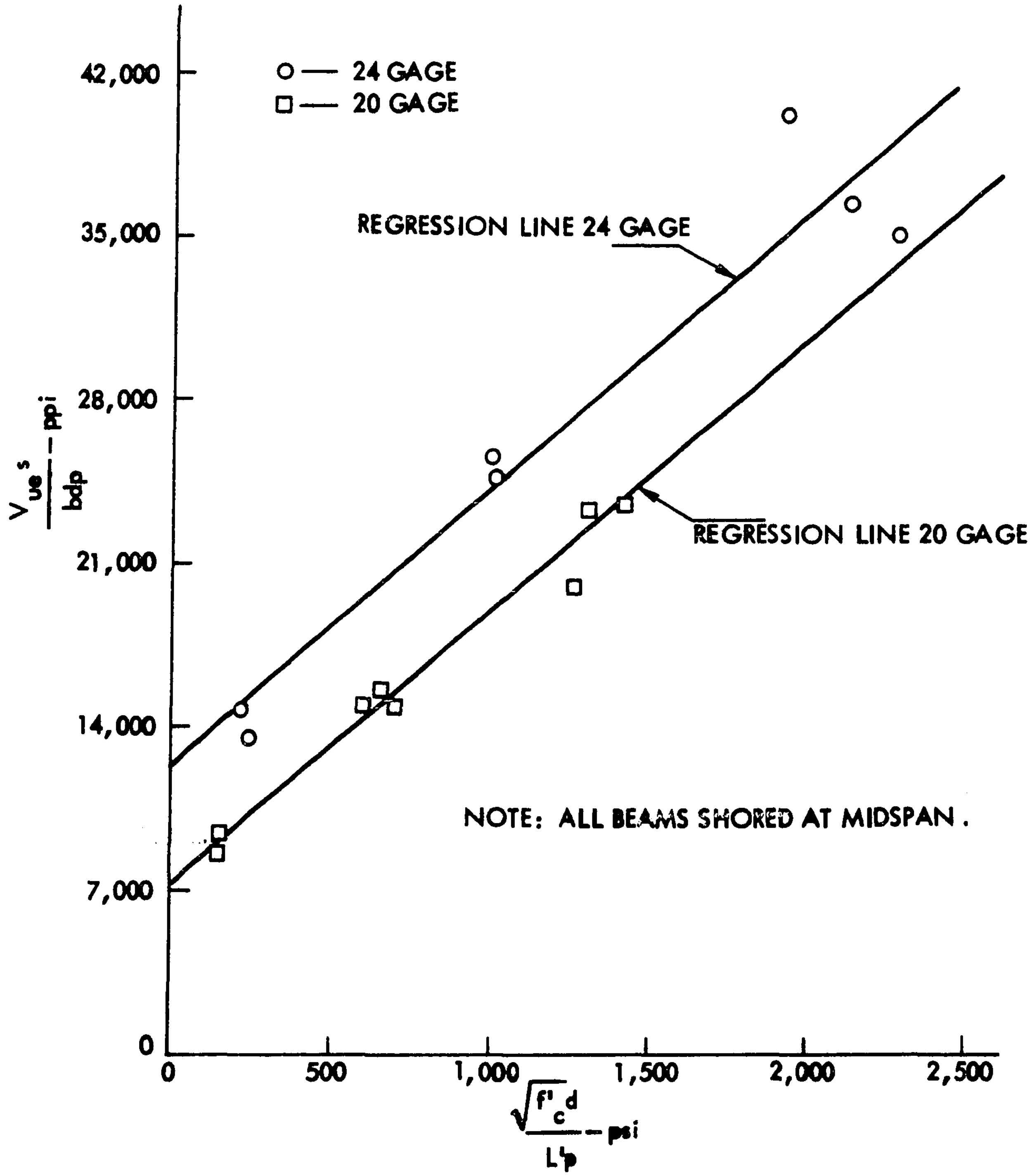

Fig. 74. Relationship between $V_{ue}s/bdp$ and $\sqrt{f'_c}\ d/L'p$ for beams constructed with steel deck G - 20 and 24 gage

ity of beams constructed with deck G is primarily a function of the condition of weld penetration. From this, it may be concluded that more complete penetration of T-wire welds existed with beams of 24 gage steel decks than with those of 20 gage decking. Seemingly, the thickness of steel deck and process of welding are the primary factors in the degree of weld penetration.

Deck E (CATEGORY I)

Ultimate shear-bond relationships, based on Equation 11, were analyzed and plotted separately for both beam test results obtained in this investigation and those obtained from company E. Figure 75 represents a plot of ultimate shear-bond values for beams constructed with steel deck E-20 gage, conducted in this investigation. Regression results of Fig. 75 are also given in Table A.10 and a comparison of corresponding experimental and calculated shear-bond stresses is shown in Fig. 76. Table A.16 shows this same comparison by expressing the shear-bond stresses in terms of a ratio. Points plotted in Fig. 77 were the result of tests conducted by company E on beams constructed with deck E-22 gage. Regression constants resulting from and shown in Fig. 77 are also listed in Table A.11. The comparison of experimental and calculated ultimate shear-bond stresses is shown in Fig. 78 and given numerically in Table A.16. Since the difference in steel deck thickness between the 20 gage and 22 gage decking was only 0.0080 inches

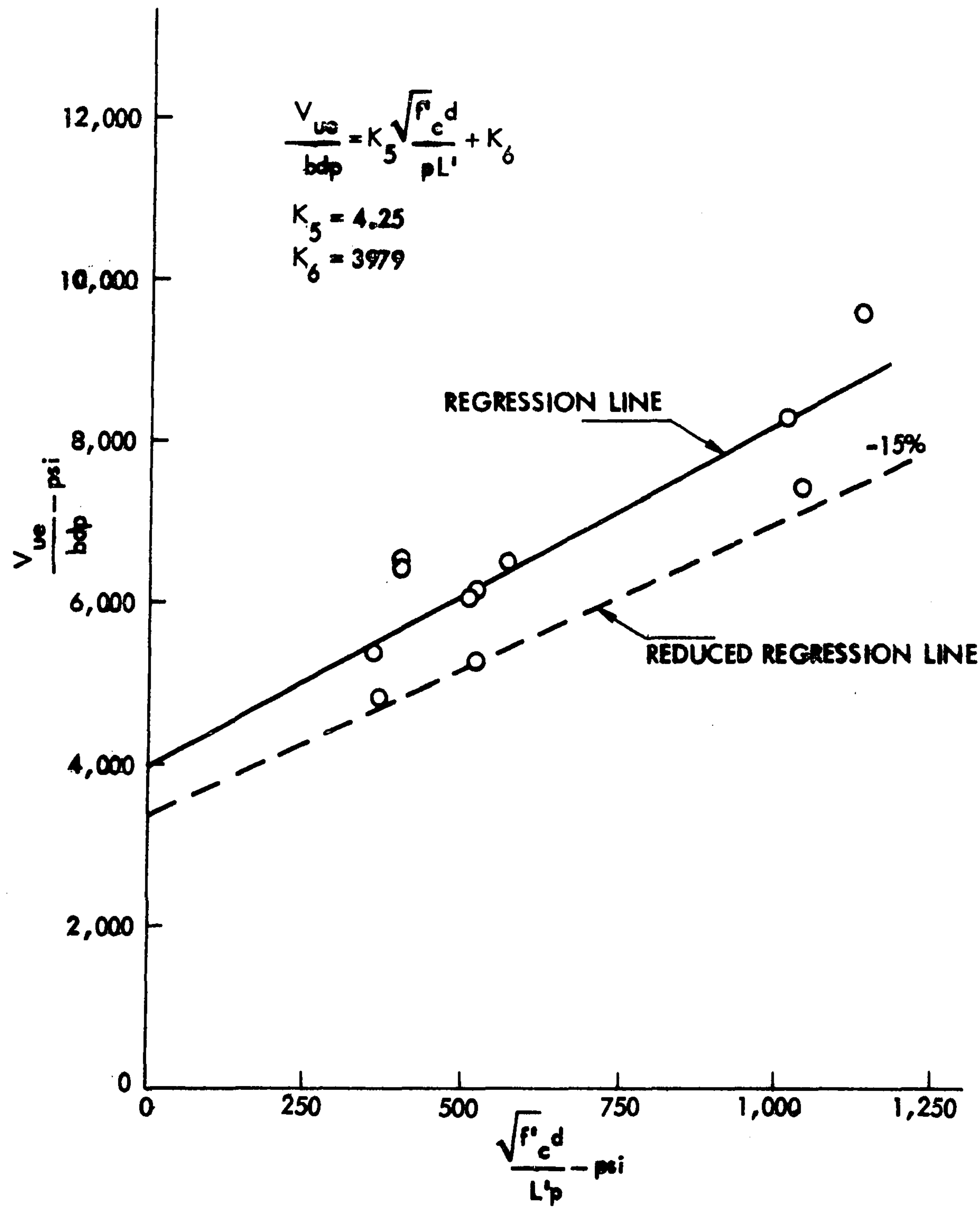

Fig. 75. Relationship between V_{ue}/bdp and $\sqrt{f'_c}\, d/L'\, p$ for beams constructed with steel deck E - 20 gage

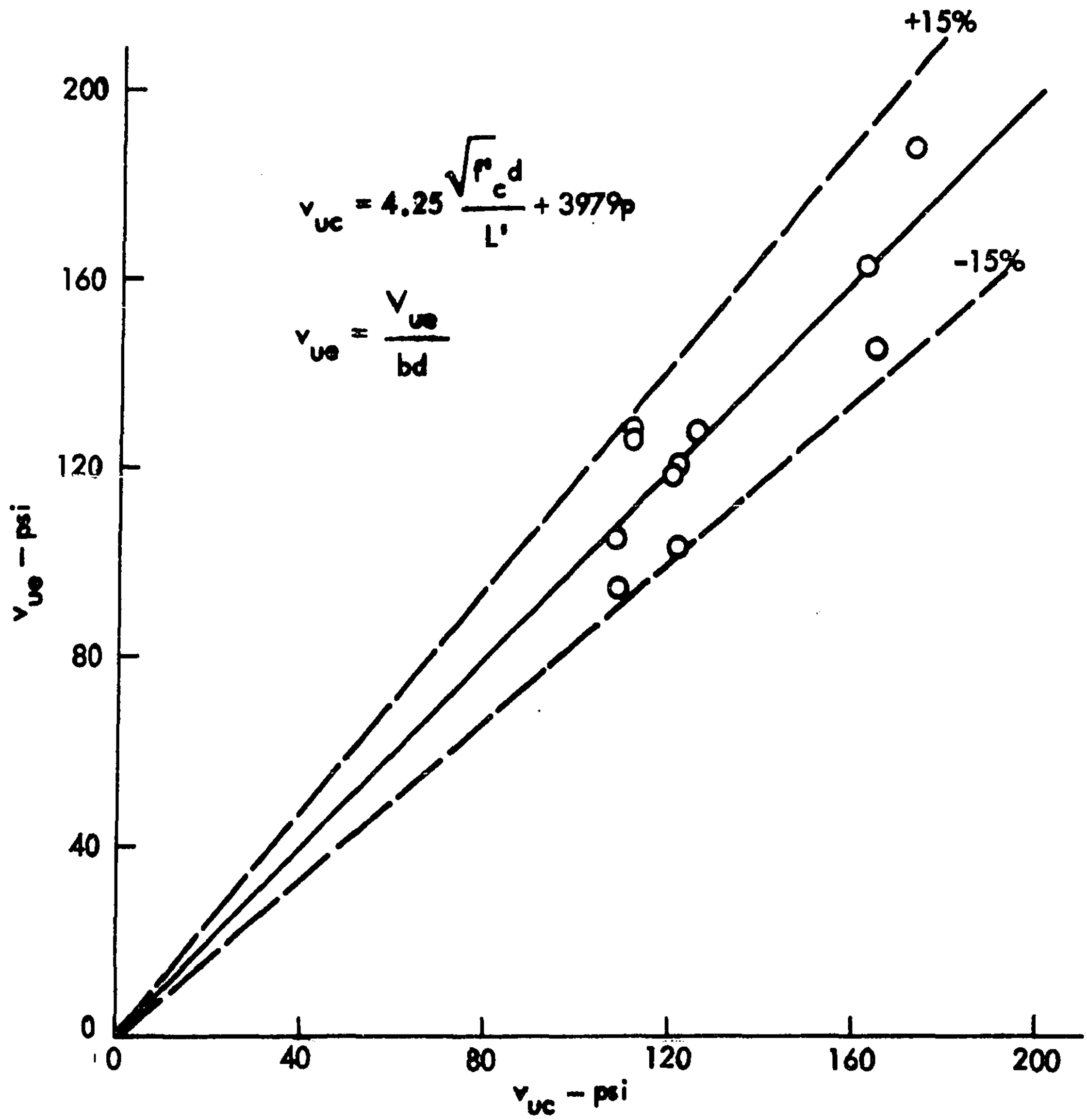

Fig. 76. Comparison of experimental and calculated ultimate shear-bond stresses for beams constructed with steel deck E - 20 gage

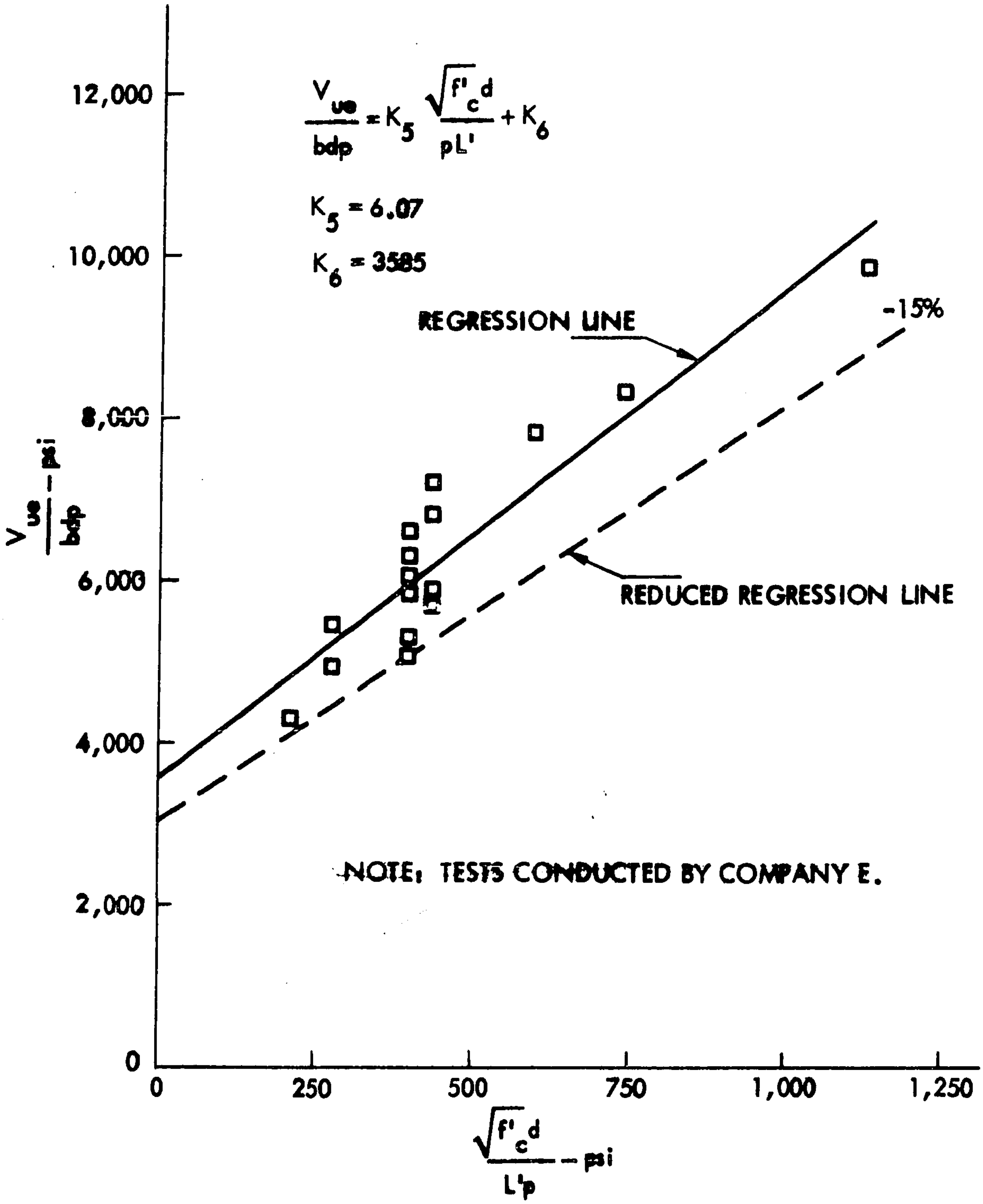

Fig. 77. Relationship between V_{ue}/bdp and $\sqrt{f'_c}\ d/L'\ p$ for beams constructed with steel deck E - 22 gage

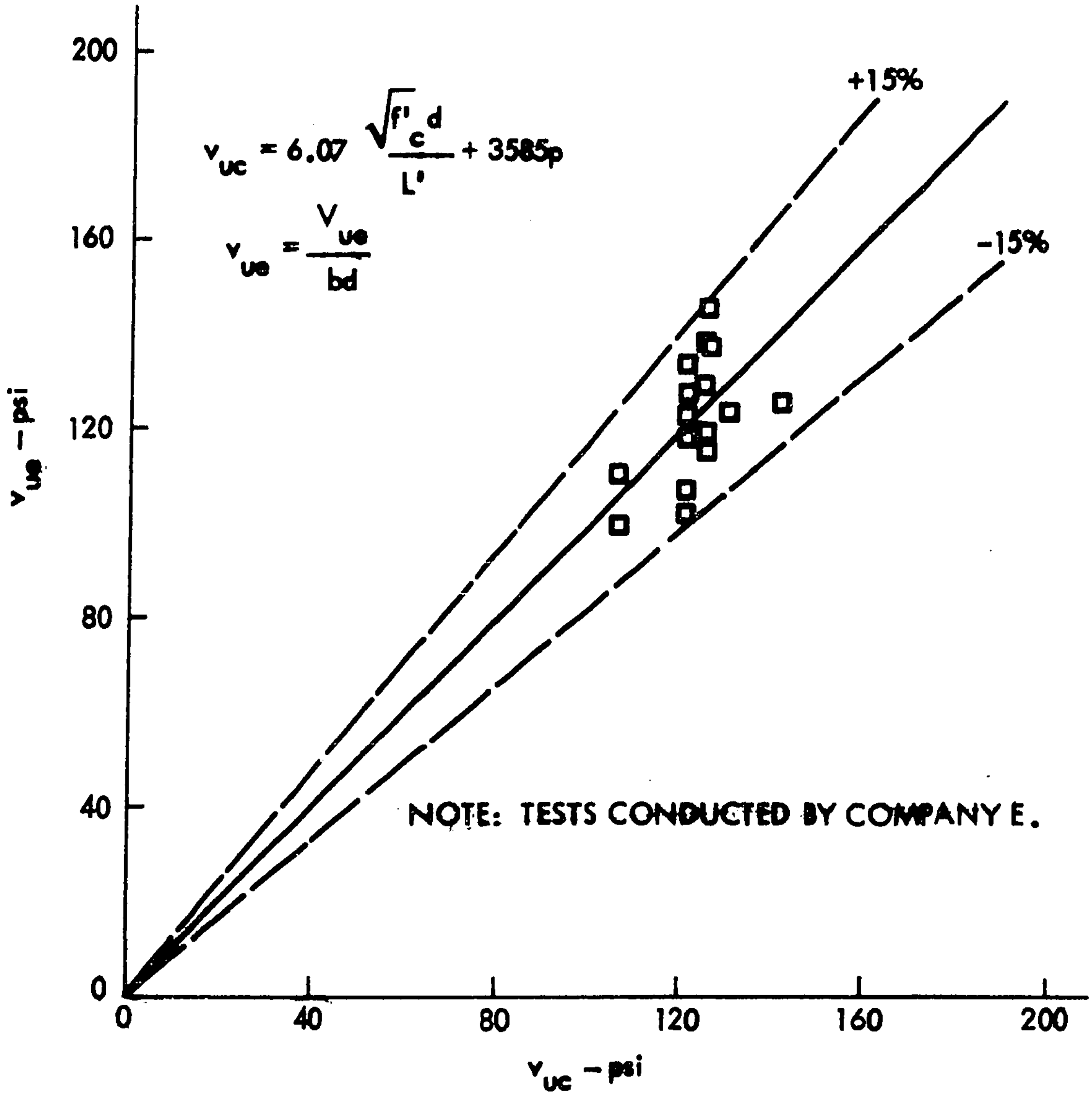

Fig. 78. Comparison of experimental and calculated ultimate shear-bond stresses for beams constructed with steel deck E-22 gage

(see Tables A.1 and A.2 for listing), values of Figs. 75 and 77 were combined in one regression analysis. Figure 79 represents the plot for beams constructed with steel deck E-20 and 22 gage. If the difference in steel deck thickness is relatively small, one may choose to combine two gages if, as shown in Fig. 79, the results are conservative. The comparison of Fig. 80 reveals that values pertaining to Fig. 79, fall within the $\pm 15\%$ acceptable margins; therefore, in an effort to reduce laboratory testing, results of beams consisting of two different steel deck thicknesses may be combined for the determination of regression constants.

Beams Failing in Flexure

The primary intent of the testing program was to obtain information leading to the determination of shear-bond relationships. However, an attempt was also made to obtain flexure failures of selected beams constructed with steel decks I, O and G. Only in the case of beams constructed with steel deck G were flexural failures experienced, namely, beams 1G24, 2G24 and 1G20 as shown in Table A.8. In no case did beams constructed with steel decks I and O result in a flexural mode of failure. Beams 1G24 and 2G24 failed by yielding of the steel, and Equation 16 was used for the determination of respective ultimate calculated moments. In the case of beam 1G20, Equation 21 was employed since the failure was caused by crushing of the concrete. Table 5 gives values of ultimate

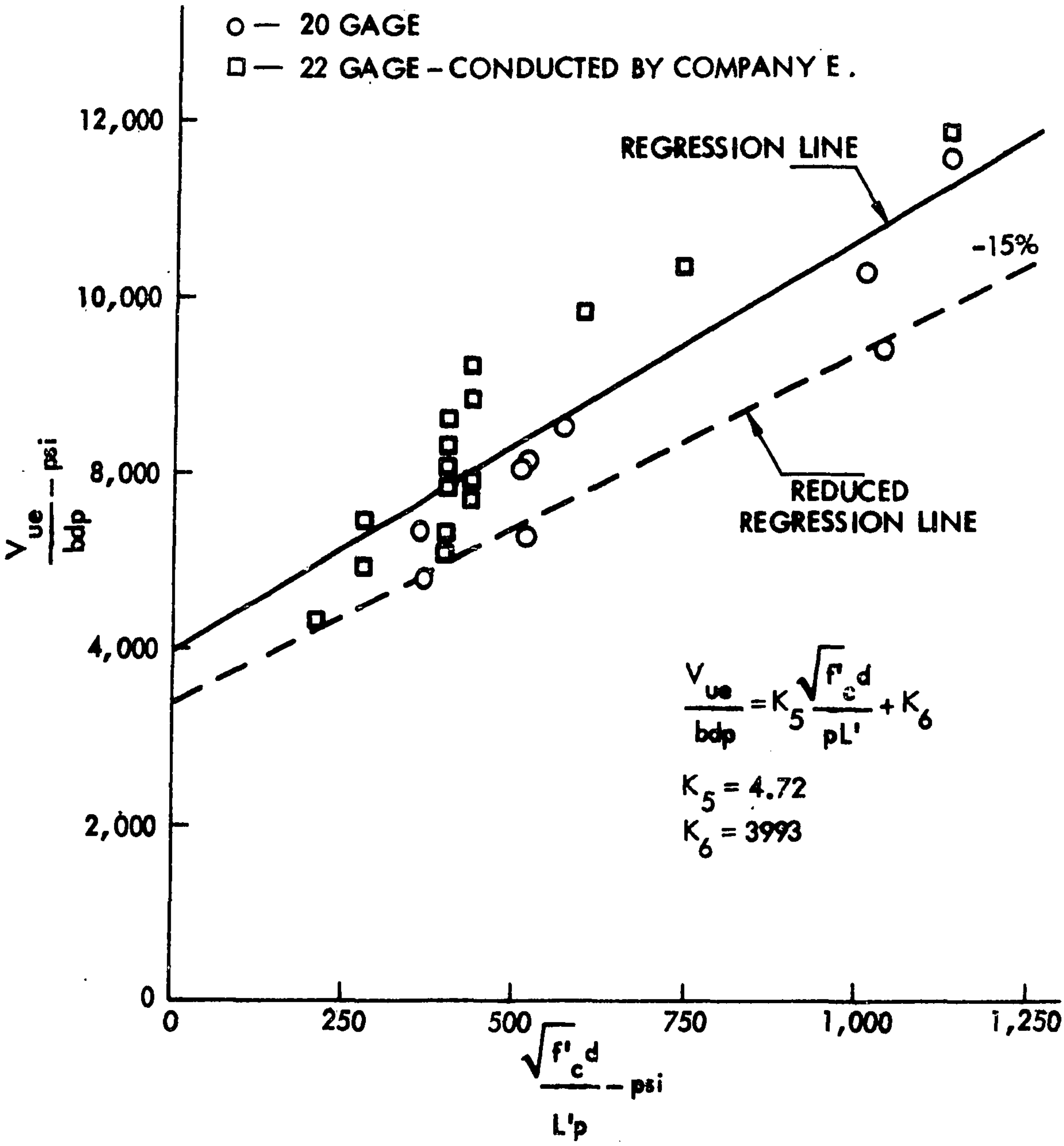

Fig. 79. Relationship between V_{ue}/bdp and $\sqrt{f'_c}\ d/L'\ p$ for beams constructed with steel deck E - 20 and 22 gage

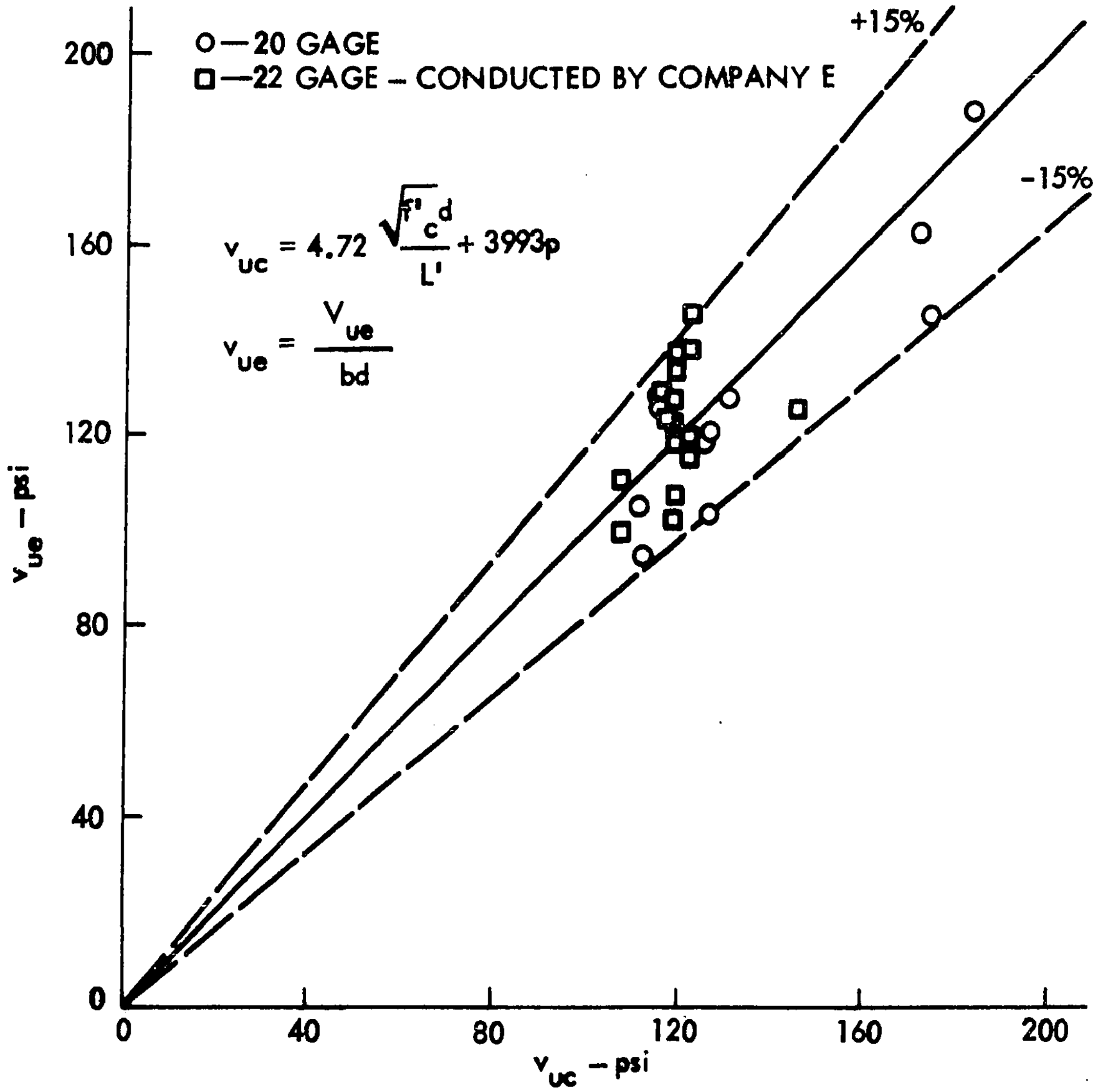

Fig. 80. Comparison of experimental and calculated ultimate shear-bond stresses for beams constructed with steel deck E - 20 and 22 gage

experimental and calculated moments for beams 1G24, 2G24 and 1G20.

Table 5. Ultimate experimental and calculated moment of beams failing in flexure

Beam no.	Ultimate experimental moment (ft-lb/ft)	Ultimate calculated moment (ft-lb/ft)	Experimental / calculated
1G24	7916	8,151	0.97
2G24	9540	12,000	0.80
1G20	9998	10,209	0.98

The comparison ratios shown in Table 5 indicate a conservative correlation between experimental and calculated values.

Effect of Variables

Following the derivation of Equations 11 and 14, a brief discussion regarding the effect of variables on the shear-bond load carrying capacity for beams of CATEGORY I and CATEGORY II was presented. Based on the evaluation of regression constants from experimental data, both Equations 11 and 14 were linear for all cases of beam data. Beams constructed with decks I and O, of the embossment type, inaicated a change in regression constants for the various steel deck thicknesses tested. More specifically, beams of 16 gage decking resulted in higher shear-bond load carrying capacities than similar beams of either 18, 20, or 22 gage decking. This was anticipated, since the inherent shear-bond capacity of an embossment type steel-deck-reinforced system is believed to depend primarily on the transverse and overall stiffness of the embossments. On the other hand, beams constructed with steel deck G exhibited the opposite, namely, higher shear-bond load capacities were experienced with beams of 24 gage decking than with similar beams of 20 gage decking because the shear-bond load carrying capacity is a function of the welds of the T-wires and not the steel deck thickness. In the case of beams constructed with steel deck E, the thickness of steel deck provides no major contribution to the shear-bond load carrying capacity, since the shear-bond capacity is inherent in the concrete shear keys and not in the steel deck thickness. However, in general, even if the thickness of the steel deck does not contribute directly to the shear-bond capacity of the system, the thickness and stiffness of the steel deck undoubtedly influence the dowel action to some degree.

STRENGTH DESIGN CRITERIA

General Remarks

Expressions pertaining to the determination of allowable superimposed design live loads, based on ultimate strength concepts, are presented for both shear-bond and flexure modes of failure. Design live loads were assumed uniformly distributed and are used in derivations presented in this chapter. Since design procedures presented herein are based on ultimate strength methods, load factors and safety provisions were selected to comply with established factors as prescribed by the ACI Building Code. Composite steel-deck-reinforced concrete slab systems are commonly designed on the basis of either a simple or continuous span analysis. Therefore, consideration is given to both, simple and continuous span installations. In the case of continuous span design, an equivalent modified simple span analysis was employed in the development of a shear-bond design expression, using a reduced span length concept. This equivalent simple span analysis is conservative for the shear-bond evaluation of continuous spans, since a simple span system has no continuity over supports while a continuous span system does. In short, simple span tests are easily conducted in the laboratory and the shear-bond expression resulting therefrom can conservatively be also extended to continuous span design.

Load Factors and Safety Provisions

The safety of most structures has been based on a traditional concept of design using dead plus live load with allowable stresses. Thus, working stress design implies a safety factor which is related to the ratio of actual material strength to allowable stress. With accuracy of computation and reasonable control of construction, a safety factor of 2 or more is not exceptional (4).

Ultimate strength methods, on the other hand, base the design of members on conditions just before failure. The ultimate load is obtained by multiplying the actual dead load and anticipated live load by separate overload factors greater than unity. Ultimate design procedures differ, therefore, from working stress design in that dead and live loads are not simply added. It is logical and reasonable to apply a greater safety factor to live loads than to dead loads, since dead loads can be determined with reasonable accuracy whereas live loads are often more uncertain and subject to change during the life of the structure. Hence, ultimate strength design provides a more realistic and flexible design criterion. Load factors may be considered reasonable when approximately the same degree of over-all safety as that which has been inherent in working stress procedures is achieved.

Based on experimental data of steel-deck-reinforced concrete beams, load factors as recommended by the ACI Building Code give reasonable design live load values. In addition to these load factors, the Code also prescribes the use of a strength-capacity-reduction factor, Ø. This capacity-reduction factor gives recognition to the fact that the complete structure, or member, may be understrength because of material strength variations, inaccuracies in workmanship, manufacturing tolerances, variations in the degree of supervision and inherent approximations in the theoretical analysis. Some recognition is also given to the relative importance of the failure mechanism of a structural member and is reflected in the different capacity-reduction factors.

It is recommended that load factors and safety provisions for the design of steel-deck-reinforced concrete slabs be the same as prescribed by the ACI Building Code for conventional reinforced concrete systems. Section 1506(a) of the code states that design loads, based on ultimate strength design, be computed as follows:

$$U = 1.5D + 1.8L. \tag{26}$$

Where U is the ultimate load, D the dead load and L the live load. Rewriting expression 26 in reference to the notation used herein results in:

$$W_u = 1.5(W_1 + W_3) + 1.8W_L. \tag{27}$$

The dead load of expression 27 is divided into two parts, namely, the dead load of the composite slab, W_1, plus the dead load applied to the composite slab, W_3. More specifically, W_1 is the sum of the wet concrete load plus the steel deck load, while W_3 is comprised of any load that is permanently applied to the composite system, such as resulting from partitions, ceiling, floor finish, etc. Safety provisions, or capacity-reduction factors, as given by Section 1504 of the ACI Building Code, were chosen to be applied to the theoretical member strengths calculated based on perfect materials and workmanship.

For shear-bond $\phi = 0.85$.

For flexure $\phi = 0.90$.

Shear-Bond

Ultimate strength shear-bond equations, based on a single or two point symmetrical line load condition, have been established in the previous chapter. Shear-bond regression constants, as obtained from actual test results, are valid for simple and equivalent continuous simple span systems.

Simple span

Simple span analysis or design is normally associated with a system consisting of a series of slabs, simply supported, and placed end-to-end with no provision for negative moment at the interior supports. It is also considered common practice to apply a simple span design to cases where the slab is continuous over interior supports, but has nominal negative reinforcement. Such nominal reinforcement might be in the form of welded wire fabric (mesh), and functions only to control shrinkage cracking.

Considering slabs of CATEGORY I, as well as CATEGORY III, the following ultimate strength equation may be written by employing the shear-bond expression of Equation 11:

$$V_{uc} = bd\ [K_5 \frac{\sqrt{f'_c}\ d}{L'} + K_6 p] + 0.5W_1 L, \qquad (28)$$

where L' is the shear span in inches, L is the span length in feet and the term $0.5W_1L$ takes into account the dead weight of the slab. In general, under normal design procedures, the loads are assumed uniformly distributed over the entire span. Hence, Equation 28 may be expressed in terms of the ultimate uniformly distributed load, W_u. Since $V_{uc} = W_uL/2$ and with b = 12 inches,

$$W_u = \frac{24d}{L}\ [K_5 \frac{\sqrt{f'_c}\ d}{L'} + K_6 p] + W_1. \qquad (29)$$

Equation 29 is dependent upon actual laboratory simple beam tests subjected to concentrated line loading. Since design is based on uniformly distributed loading it is recommended, as a conservative approach and to create an equivalent uniform load condition, that the shear span, L', be equal to one-fourth of the span length, L. This means, that theoretically the shear transfer devices are being subjected to shear over the entire span (see Fig. 81). Actually, with the concentrated loads of the experimental performance tests placed at the quarter points, the shear transfer devices are only being subjected to shear over one-half the span length (see Fig. 82). This should result in a more severe and consequently more con-

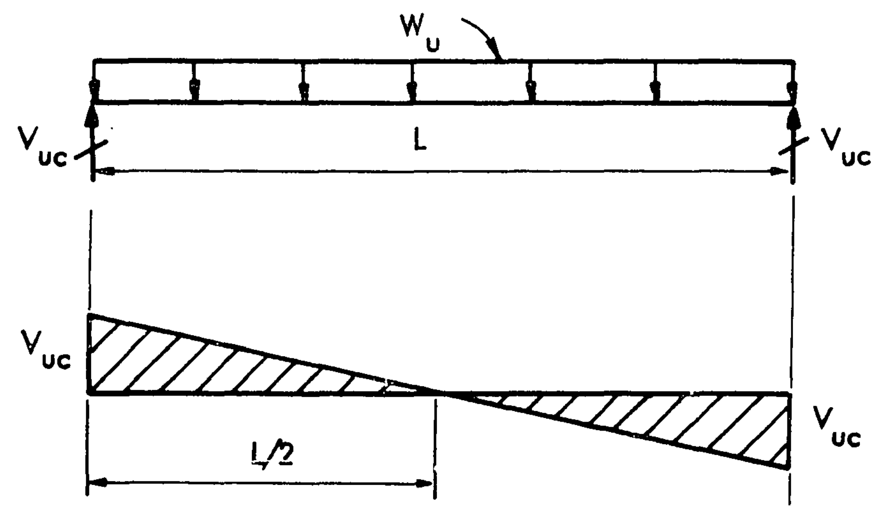

Fig. 81. Assumed live load design condition

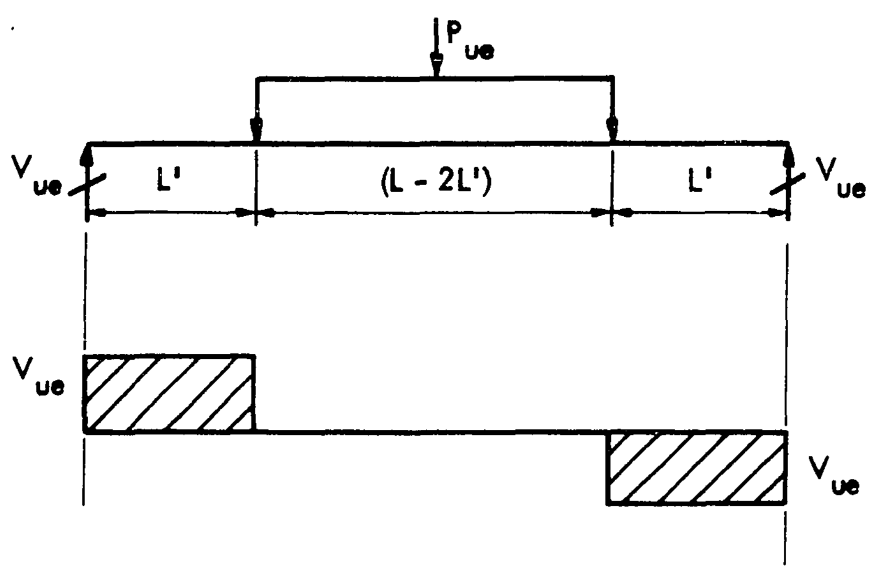

Fig. 82. Experimental performance test condition

servative design loading condition than with a uniform loading. It is observed that with the concentrated loads placed at the quarter points of Fig. 82 the total area under the shear diagram equals the total area under the corresponding shear diagram of Fig. 81. Hence, by shear diagram area, an equivalent uniform design load criterion is obtained from the laboratory performance test condition. Remembering that L is given in feet and substituting L' = 12L/4 into Equation 29, the following expression results:

$$W_u = \frac{8d}{L}\left[K_5 \frac{\sqrt{f'_c}\,d}{L} + 3K_6 p\right] + W_1. \tag{30}$$

Now, equating Equations 27 and 30 results in the expression for the superimposed live load based on a shear-bond type failure.

$$W_L = \frac{\frac{8d}{L}\left[K_5 \frac{\sqrt{f'_c}d}{L} + 3K_6 p\right] - 0.5W_1 - 1.5W_3}{1.8}. \tag{31}$$

Modifying Equation 31 to include the capacity reduction factor, $\phi = 0.85$, yields the final expression for design.

$$W_L = \frac{\frac{6.8d}{L}\left[K_5 \frac{\sqrt{f'_c}d}{L} + 3K_6 p\right] - 0.5W_1 - 1.5W_3}{1.8}. \quad (31)$$

Recognizing that $p = A_s/bd$ and $b = 12$ inches, an ultimate expression is obtained for W_L.

$$W_L = \frac{\frac{1.7}{L}\left[4K_5 \frac{\sqrt{f'_c}d^2}{L} + K_6 A_s\right] - 0.5W_1 - 1.5W_3}{1.8}. \tag{33}$$

Similarly, for slabs of CATEGORY II, the same approach, along with Equation 14, was employed in the determination of a shear-bond-superimposed design live load expression.

$$W_L = \frac{\frac{6.8d}{sL} [K_7 \frac{\sqrt{f'_c} d}{L} + 3K_8 p] - 0.5W_1 - 1.5W_3}{1.8} \quad (34)$$

or

$$W_L = \frac{\frac{1.7}{sL} [4K_7 \frac{\sqrt{f'_c} d^2}{L} + K_8 A_s] - 0.5W_1 - 1.5W_3}{1.8} \quad (35)$$

Continuous spans

Continuous span analysis applies to those slab systems which are continuous over interior supports, and where sufficient steel is provided to satisfactorily develop negative resisting moments over these supports. The negative steel is usually in the form of conventional reinforcing bars and is placed near the top of the slab over interior supports.

In an effort to develop a shear-bond design format for continuous span design, a modified equivalent simple span criterion was employed. A typical shear-bond failure, in association with a simple span system, is the result of the combined action of positive bending and shear. On the other hand, a typical continuous span system, such as shown in Fig. 83, may conservatively be divided into equivalent simple span segments that are also subjected to positive bending and shear. In effect, each of these segments is identical to a simply supported system, but with a reduced span length. This means that the reduced span lengths L''_1, L''_2 ... L''_n, etc. may be substituted for the simple span length, L. It is thus possible to adapt the simple span expressions that have been

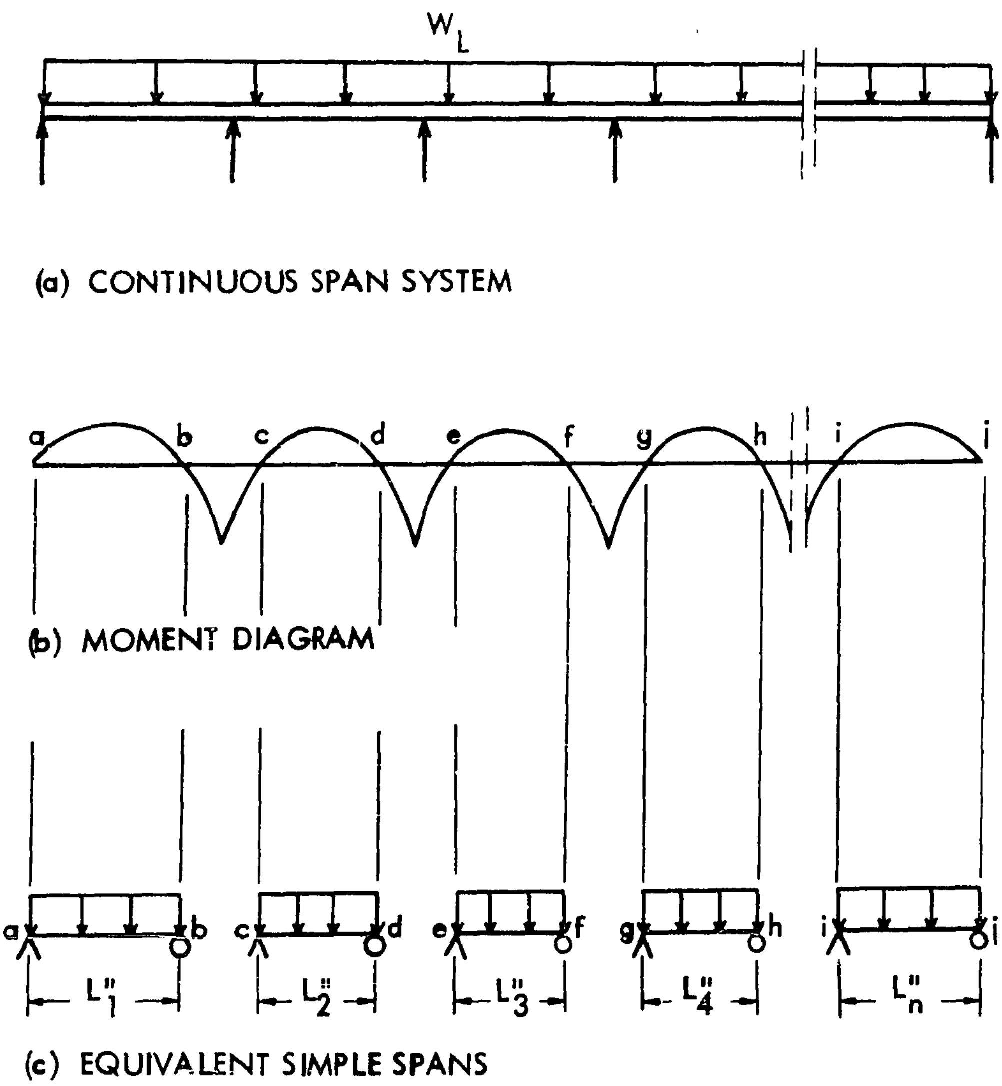

Fig. 83. Typical continuous span system with complimentary moment diagram and equivalent simple spans, L''_n

developed to apply to those segments of a continuous slab subjected to positive bending and shear.

Considering slabs of CATEGORY I, as well as CATEGORY III, Equations 32 and 33 may be respectively revised as follows:

$$W_L = \frac{\frac{6.8d}{L''_n}\left[K_5 \frac{\sqrt{f'_c}\,d}{L''_n} + 3K_6 p\right] - 0.5W_1 - 1.5W_3}{1.8} \tag{36}$$

and

$$W_L = \frac{\frac{1.7}{L''_n}\left[4K_5 \frac{\sqrt{f'_c}\,d^2}{L''_n} + K_6 A_s\right] - 0.5W_1 - 1.5W_3}{1.8} \tag{37}$$

where L''_n is the reduced simple span length of the n^{th}-continuous span, subjected to positive bending and shear.

Similarly, for slabs of CATEGORY II, Equations 34 and 35 were respectively revised as follows:

$$W_L = \frac{\frac{6.8d}{sL''_n}\left[K_7 \frac{\sqrt{f'_c}\,d}{L''_n} + 3K_8 p\right] - 0.5W_1 - 1.5W_3}{1.8} \tag{38}$$

and

$$W_L = \frac{\frac{1.7}{sL''_n}\left[4K_7 \frac{\sqrt{f'_c}\,d}{L''_n} + K_8 A_s\right] - 0.5W_1 - 1.5W_3}{1.8} \tag{39}$$

Validity of load factors

To show the validity of the load factors and capacity-reduction factor, pertaining to a shear-bond type of failure of steel-deck-reinforced concrete systems, the over-all safety factor of each experimental beam test was computed. It is considered reasonable and common practice when approximately the same degree of over-all safety is achieved as that which has been inherent in working stress procedures. Such over-all safety is generally based on a factor of 2.0 or more (4). The over-all safety factor is defined by the ratio of ultimate experimental shear, V_{ue}, to the calculated design shear based on experimental results, V_{de}. Considering CATEGORIES I and III, an expression for the design shear, V_{de}, was obtained by applying the load factors of Equation 27 and capacity-reduction factor to Equation 28. Thus, with W_3 equal to zero,

$$V_{de} = 0.85bd\ [K_5 \frac{\sqrt{f'_c}d}{L'} + K_6 p] - 0.5W_1 L \tag{40}$$

and similarly for CATEGORY II,

$$V_{de} = \frac{0.85bd}{s}\ [K_7 \frac{\sqrt{f'_c}d}{L'} + K_8 p] - 0.5W_1 L. \tag{41}$$

Tables A.17, through A.21 give over-all safety factors for beams constructed with steel decks I, O, G and E, respectively. It can be seen that in general the over-all safety factor is equal to 2 or greater. Thus, load factors, coupled with the capacity-reduction factor, Ø, result in reasonable design expressions.

Flexure

Design expressions governing a flexure-yielding or flexure-crushing type of failure of steel-deck-reinforced concrete systems were established in connection with ultimate strength methods developed in the previous chapter. In cases where the composite neutral axis falls within, on or above the limits of the steel deck, the full cross-sectional steel deck area, A_s, is assumed to be effective. Consideration is given to positive and negative bending moment conditions on the basis of uniformly distributed loading. For negative bending, the area of steel refers to supplementary steel in the form of conventional reinforcing bars. Equations pertaining to flexural design are applicable to steel-deck-reinforced concrete slabs consisting of CATEGORIES I, II and III.

Simple span

Governing a flexure-yielding failure, resulting from an under-reinforced cross-section, Section 1601(a) of the ACI Building Code limits the reinforcement ratio, p, to $0.75p_b$. Or

$$p \leq 0.75p_b$$

where

$$p_b = \frac{0.85k_1 f'_c \epsilon_u E_s \ (D-d_d)}{F_y(\epsilon_u E_s + F_y)d}$$

as given by Equation 24. With $\epsilon_u = 0.003$ and $E_s = 29 \times 10^6$ psi, the following expression for the balanced reinforcement ratio results:

$$p_b = \frac{0.85k_1 f'_c}{F_y} \ \frac{87000(D - d_d)}{(87000 + F_y)d} \ . \tag{42}$$

Equation 42 may be considered in its final form to be used in design. For a uniformly distributed load the external moment $M_{uy} = W_u L^2/8$; therefore, by combining Equations 16 and 27, and with $\emptyset = 0.90$, the permissible superimposed live load results in

$$W_L = \frac{\frac{0.6}{L^2}\,[A_s F_y\ (d - \frac{a}{2})] - 1.5(W_1 + W_3)}{1.8} \qquad (43)$$

where

$$a = \frac{A_s F_y}{0.85 f'_c b}\ .$$

When the reinforcement ratio, p, is greater than the balanced ratio, p_b, the cross-section is termed to be over-reinforced, thus, giving rise to a possible flexure-crushing type of failure. The limitation for this condition may be presented by the following inequality:

$$p > p_b$$

Similarly, Equations 21 and 27 may be combined, along with $\phi = 0.90$, to result in an expression for the permissible superimposed live load. Thus, with b = 12 inches

$$W_L = \frac{\frac{6.12}{L^2}\,[k_1 f'_c d^2 k_u (1-k_2 k_u)] - 1.5(W_1 + W_3)}{1.8} \qquad (44)$$

where $$k_u = \sqrt{pm + (\frac{pm}{2})^2} - \frac{pm}{2}$$

$$m = \frac{E_s \epsilon_u}{0.85 k_1 f'_c}$$

and

k_1 = 0.85 for $f'_c \leq 4000$ psi and decreases by 0.05 for every 1000 psi above 4000.

k_2 = 0.425 for $f'_c \leq 4000$ psi and decreases by 0.025 for every 1000 psi above 4000.

To arrive at a similar expression as given by Equation 44, the ultimate moment can also adequately be approximated for design purposes from Whitney's equation. Thus,

$$M_{uc} = \frac{1}{3} b d^2 f'_c \tag{45}$$

and applying the load factors of Equation 27 with $M_{uc} = W_u L^2/8$ and b = 12 inches, the allowable superimposed live load then results in

$$W_L = \frac{\dfrac{2.67 d^2 f'_c}{L^2} - 1.5(W_1 + W_3)}{1.8} \tag{46}$$

<u>Continuous span</u>

Both positive and negative moment conditions must be investigated. As a conservative approach, it is recommended to determine critical bending moments on the basis of elastic theory. Pertinent moment coefficients for continuous construction have been established by the ACI Building Code and may be found in Section 904. These coefficients provide the designer, in lieu of more exact analysis, with sufficiently accurate design aids in the determination of critical moment values.

Considering positive bending, an expression for the determination of the superimposed live load, pertaining to a flexure-yielding failure, may be written by generalizing Equation

16, namely with $M_{uy} = W_u L^2$,

$$W_L = \frac{\frac{0.90}{12C_m L^2}\,[A_s F_y\,(d - \frac{a}{2})] - 1.5(W_1 + W_3)}{1.8} \tag{47}$$

where C_m is defined as the positive moment coefficient of either the exterior or interior span. C_m is commonly taken as 1/11 for a typical exterior span and 1/16 for a typical interior span (1).

Superimposed live load expressions, regarding a flexure-crushing mode of failure, as given by Equations 44 and 46, were similarly and respectively rewritten as follows:

$$W_L = \frac{\frac{0.765}{L^2 C_m}\,[k_1 f_c' d^2 k_u (1 - k_2 k_u)] - 1.5(W_1 + W_3)}{1.8} \tag{48}$$

and

$$W_L = \frac{\frac{d^2 f_c'}{3L^2 C_m} - 1.5(W_1 + W_3)}{1.8} \tag{49}$$

In the case of negative bending, it is assumed that the resistance to compression of the steel deck is relatively small and therefore considered ineffective and negligible in design. Those portions of the slab which lie in the immediate region of the interior supports, such as segments bc, de, fg, etc. of Fig. 83, are subjected to negative bending and can be treated as any conventionally reinforced concrete cross-section. That is, design and proportioning of the negative reinforcement is to be based on a single reinforced cross-section.

RECOMMENDED PERFORMANCE TEST PROGRAM

General Remarks

It is recommended that each steel deck manufacturer undertake a series of performance tests. The basic objective of these tests is to provide the necessary data for determining ultimate strength and behavior of composite deck-reinforced concrete slabs. The data will permit establishment of ultimate strength values from which design loads may be obtained.

The proposed tests involve full-scale beams, steel coupons, and control concrete cylinders. The full-scale beams embody elements of composite steel-deck-reinforced slabs which have a width equal to the manufacturer's standard steel deck width. A series of beams are to be tested for each steel thickness with variable depths and shear spans. The coupon tests permit determination of the following properties of the steel deck: yield strength, ultimate strength, and percent elongation. The plain concrete control cylinders serve to determine ultimate compressive strength and tensile splitting strength of the concrete during testing.

Testing of Composite Beams

Tests of elements of composite steel-deck-reinforced floor slabs are designed to provide information on slab behavior up to ultimate load. It is proposed to perform tests on identical groups of composite steel-deck-reinforced systems. The loading ordinarily produces either a shear-bond or a flexure mode of failure. In the case of some beams, however, a flexural failure is difficult to obtain even with exceedingly long shear spans. Consequently, a shear-bond failure might be the only obtainable failure mode.

It is recommended to test all beams with simple spans, using two- or one-point line loading, with a gradually increasing load to failure. The two primary parameters to be determined from the tests are:

(a) the ultimate load, and

(b) the mode of failure.

Behaviorial parameters such as crack pattern and load-deflection relationships should also be documented. It is anticipated that after a sufficient number of beam tests, the resulting data might eventually permit a thorough re-evaluation of load factors.

Modes of Failure

Shear-bond

The shear-bond failure mode is characterized by a major crack that forms under or near one of the line loads and a sudden ultimate failure results. This failure is accompanied by sudden end-slip, observable to the naked eye, between the steel deck and concrete. The end-slip is accompanied by a significant reduction in load, assuming that the loading head of the test machine moves at a constant rate. It is evident that the concrete shear span portion, L', has become disengaged after loss of interaction between the steel deck and concrete In no case should the ultimate experimental load, P_{ue}, be greater than that load corresponding to the first observable end-slip.

Flexure

There are two categories of flexural failure: namely, failure by yielding of the steel and failure by crushing of concrete in the compression zone. Flexural failures are characterized by the fact that there is no observable end-slip between the steel deck and concrete.

Flexure-yielding This type of failure results when the steel ratio, p, is relatively low. Near ultimate load a ductile and yielding action results and there is a possibility of complete rupture of the steel deck.

Flexure-crushing This type of failure results when the steel ratio, p, is relatively high so that the concrete compression zone reaches its ultimate capacity before all fibers of the steel deck have reached their yield level. As the ultimate load is approached, destruction of the concrete compression zone may be observed. Following failure, there may still be some residual stiffness of the member, depending on the stiffness of the steel deck and the extent of failure of the compression zone of the concrete.

Specimen Preparation

General remarks

It is recommended that all steel-deck units be in a condition equivalent to that of corresponding units installed at the job site. Care should be taken to insure that the steel decks are free of all foreign matter such as grease and oil.

The composite beam specimens should be prepared and cured in accordance with standard construction requirements stated in applicable sections of the ACI Building Code. Methods of construction of the beams in the laboratory should be simulated as closely as possible to actual practice. Steel decks for composite beams may be completely supported prior to the placement of the concrete, or they may be shored. However, if shoring is used, the steel deck shall not exceed stress and deflection limitations set by the manufacturer for recommended design practice.

Dimensions of composite systems

It is recommended that dimensions of test beams within a particular group be determined as follows:

Length The length of beam test units should be sufficient to properly establish points on Fig. 84.

Width The width of all beam specimens should be at least equal to one steel deck width, b_d.

Depth Slab depths, D, should range from the minimum to the maximum depth established by the manufacturer.

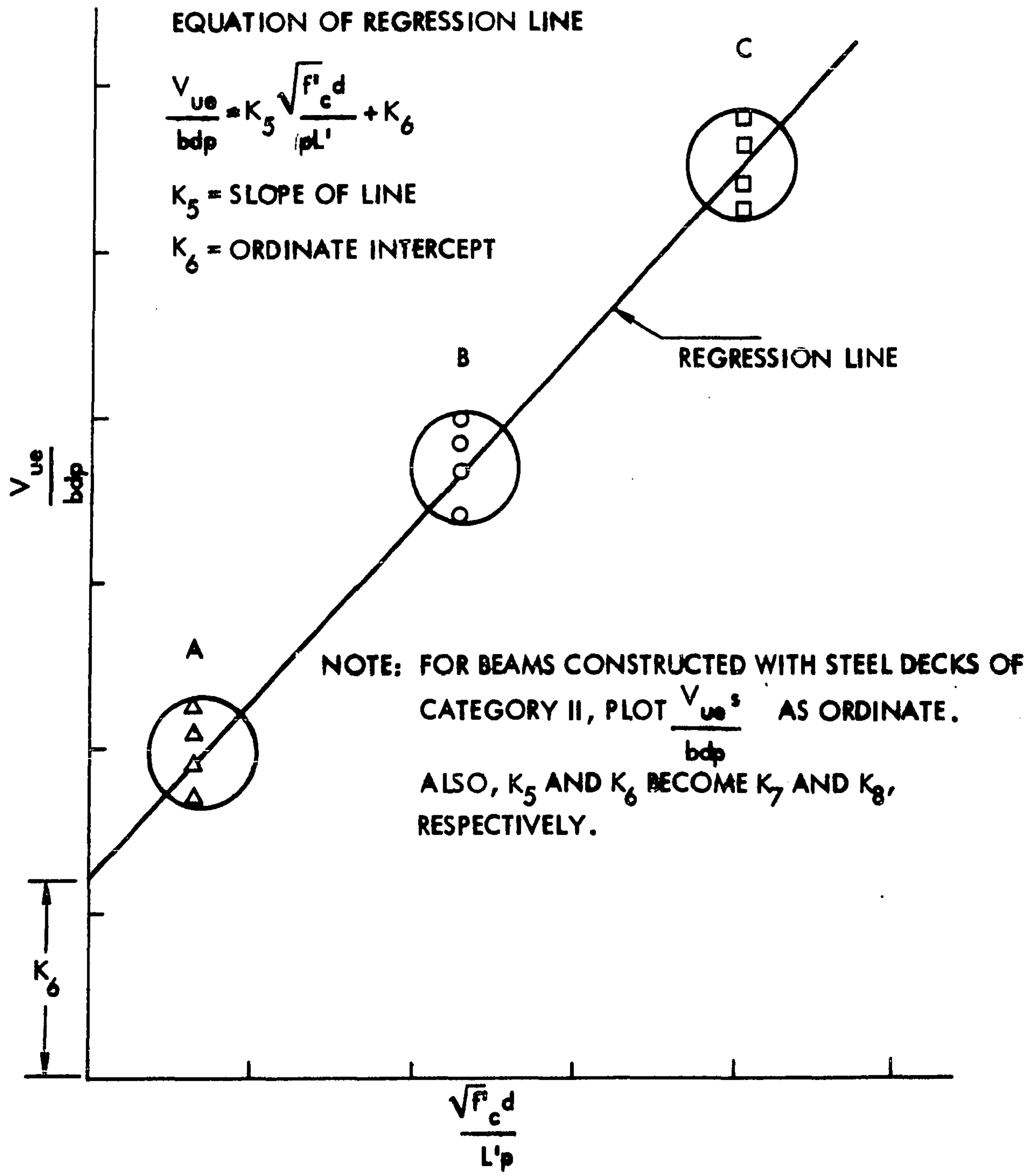

Fig. 84. Typical relationship between V_{ue}/bdp and $\sqrt{f'_c}$ d/L'p for beams of CATEGORY I with one particular gage thickness

Test Procedure

Instrumentation

The only recommended instrumentation beyond load-measuring equipment is a dial gage to measure midspan deflections to the nearest 0.001 inch. Other instrumentation, such as strain gages, may be used at the option of the test engineer.

Loading of specimen

All specimens should be tested on simple supports as indicated in Fig. 12, and subjected to either a single concentrated line load or two symmetrically placed concentrated line loads.

Increments of data

Testing should not be conducted until the specimen has reached a minimum age of 7 days and has obtained a minimum concrete compressive strength of 2500 psi. The following data should be recorded and documented: bd, D, d_d, L, L', s[a], t, f'_c, F_y, W_D and W_w. It is recommended that a brief description of significant events during testing be recorded along with an identification of the final mode of failure. In addition, the following supplementary data is recommended:

(a) Load-deflection relationship to ultimate load,

(b) Information pertaining to cracks:

---

[a]For composite beams made of CATEGORY II steel deck units only.

(i) load at first observable crack,

(ii) width of largest crack at approximately $P_{ue}/2$, and

(iii) number of cracks observable to the naked eye at approximately $P_{ue}/2$.

Recommended Number of Tests

<u>General remarks</u>

The recommended number of beam specimens to be tested by the manufacturer depends on the number of available steel deck thicknesses. A plot, as shown in Fig. 84, must be prepared from test data of beams failing in shear-bond for each steel deck thickness. In cases involving a flexural mode of failure, the plotting of variables as in Fig. 84 is not necessary.

<u>Shear-bond</u>

To establish the most representative linear relationship for the ultimate shear-bond capacity, it is necessary to use the full practical range of values of depth, D, and shear span, L'. Three groups of data are recommended to establish the range as defined by regions A, B and C in Fig. 84. Data for region A are obtained from tests on beams with small depths, D, and relatively large shear spans, L'. Data for region C are obtained from tests with large depths, D, and relatively small shear spans, L'. The intermediate region B is determined from tests on beams with intermediate depths and shear spans. Recommended limiting values of depths and shear spans for the various regions of Fig. 84, to establish ultimate shear-bond capacities, are given in Table 6.

Table 6. Limiting parameters for regions A, B and C of Fig. 84

Region	Depth, D	Shear span, L'
A	Manufacturer's minimum recommended depth, but > 3-1/2 in.	>36 in., but < L/2
C	Manufacturer's maximum recommended depth.	>18 in., and < test section width
B	Average of depths used in regions A and C (May be rounded off to nearest 1/2 in.	Average of shear spans used in regions A and C.

In each of the three regions of Fig. 84 at least four identical composite beam sections should be tested, provided the deviation of any one test result from the mean value of the four tests does not exceed $\pm 20\%$. If the deviation from the mean of any test result exceeds $\pm 20\%$, additional tests of the same kind should be performed. Those values falling within the $\pm 20\%$ range should be considered in the regression analysis described in the chapter on strength result evaluation by Equation 11 or 14.

Flexure

Based on the findings of this investigation, flexural failures may not always occur with each steel-deck-reinforced system. Certain beams, constructed with a particular type of steel deck, and tested as recommended herein, may fail in shear-bond only and not experience flexural failures. On the other hand, flexural failures may be encountered, especially when exceedingly long shear spans are being tested and the full shear-bond capacity has been developed.

In order to establish whether or not a flexural mode of failure is possible, after having determined the shear-bond capacity, it is recommended to calculate the theoretical length of shear span at which shear-bond equals flexure. If this theoretical length of shear span is greater than one-half the longest simple span length recommended by the manufacturer, a flexural mode of failure might not be encountered. This being the case, the manufacturer or testing agency need not try to obtain a flexural mode of failure by testing extremely long span lengths that are not encountered in common construction practice. For beams of CATEGORIES I and III, Equation 11 was set equal to both Equations 16 and 21; thus, by equating Equations 11 and 16, the theoretical shear span length based on flexure-yielding resulted in

$$L'_y = \frac{M_{uy} - K_5 \; bd^2\sqrt{f'_c}}{K_6 A_s}. \tag{50}$$

Similarily, by equating Equations 11 and 21, the theoretical shear span length based on flexure-crushing is given by

$$L_c' = \frac{M_{uc} - K_5\ bd^2\sqrt{f_c'}}{K_6 A_s}. \tag{51}$$

For beams constructed with steel decks of CATEGORY II, Equations 14, 16 and 21 were used for the following relationships:

$$L_y' = \frac{M_{uy}s - K_7\ bd^2\sqrt{f_c'}}{K_8 A_s} \tag{52}$$

and

$$L_c' = \frac{M_{uc}s - K_7\ bd^2\sqrt{f_c'}}{K_8 A_s} \tag{53}$$

For example, the theoretical shear span length, L_c', of beam 1G20 was calculated from Equation 53 to be 60 inches and a flexure-crushing failure was experienced with an actual shear span, L_c', of 70 inches. Similarily, L_c', of beam 1G24, was calculated from Equation 53 at 45 inches, while actual flexure-yielding failure occurred with a shear span of 70 inches.

In cases involving a flexural mode of failure, a minimum of four identical tests should be conducted to establish the validity of the ultimate moments calculated in accordance with either Equation 16 or 21, whichever is applicable. These calculated values should not deviate by more than $\pm 10\%$ from the mean value of the four tests.

Test Result Evaluation

General remarks

Most steel-deck-reinforced concrete beams, having dimensional proportions similar to those found in common construction practice, exhibit a shear-bond type failure. The test result evaluation, therefore, focuses on establishing the ultimate shear-bond load-carrying capacity for any given steel deck thickness. Those cases where a possible flexure failure is experienced are also considered. In evaluating test results, due consideration should be given to any difference that may exist between the yield point of the steel from which the tested sections are formed and the minimum yield point specified for the given steel which the manufacturer intends to use. Consideration should also be given to any variation or difference which may exist between the design thickness and the thickness of the specimens used in the tests.

Shear-bond

Based on the recommended number of tests, a plot of V_{ue}/bdp versus $\sqrt{f'_c}d/L'p$, or $V_{ue}s/bdp$ versus $\sqrt{f'_c}d/L'p$, as shown in Fig. 84, may be developed for each steel deck thickness. A regression line, using all the above required test data, is then established for each plot to determine the slope of the line and the ordinate intercept. It is recommended that the values of slope and ordinate intercepts of Fig. 84 be used in the design expressions given in the chapter on strength design criteria. However, if the deck manufacturer wishes to be more conservative, he may choose to lower the regression line.

Flexure

Evaluating test results of the flexure failure mode should be based on correlation of the experimental and calculated ultimate moment. The ultimate calculated moment may be obtained from one of the two following cases.

(a) Failure by yielding of the steel:

$$M_u = A_s F_y (d - \frac{a}{2}),$$

(b) Failure by crushing of concrete in the compression zone:

$$M_u = \frac{1}{3} bd^2 f_c'.$$

SUMMARY AND CONCLUSIONS

Design criteria based on ultimate strength concepts for composite steel-deck-reinforced concrete floor slabs have been successfully developed. Both shear-bond and flexure were investigated, with shear-bond usually being the predominate design consideration of steel-deck-reinforced concrete slabs. The objective for predicting the shear-bond capacity was accomplished by analysis of numerous test results and development of a semi-rational ultimate strength equation. The prediction of the load carrying capacity of steel-deck-reinforced concrete systems failing in flexure was accomplished by employing known ultimate strength equations of reinforced concrete. Also, a laboratory performance beam test program, necessary for the establishment of ultimate strength shear-bond expressions, has been recommended to be followed by steel deck manufacturers for product evaluation. In addition, tentative recommendations for the design of cold-formed steel decking as reinforcement for concrete slabs, have resulted from the work of this investigation (22). The contents of these recommendations provide the design engineer and steel deck producer with standard design provisions leading to the complete design of steel-deck-reinforced systems. These tentative recommendations pertain to floor slabs in buildings and present uniform provisions applicable to a wide range of composite steel-deck-reinforced systems.

A total of 173 steel-deck-reinforced simply supported composite concrete beams were constructed with steel decks I, O and E of CATEGORY I and deck G of CATEGORY II and tested to failure. In addition, 39 beam test results, conducted by companies O and E, were obtained from the respective companies and used in the shear-bond analysis of this investigation. The following general observations regarding the ultimate shear-bond capacity of beams constructed with steel decks I, O, G and E were noted:

1. Shear-bond is the result of a brittle type of failure accompanied by the formation of an approximate diagonal crack, resulting in end-slip and loss of bond between the steel deck and concrete.
2. End-slip between the concrete and steel deck was only detectable, even with end-slip instrumentation, at the time of ultimate failure; thus, shear-bond failure occurred when visible end-slip was observed.
3. The shear-bond capacity of beams constructed with either steel decks I, O, E of CATEGORY I or G of CATEGORY II increased with an increase in depth of beam, a decrease in shear span, an increase in percent of reinforcement and compressive strength of concrete. Also, beams constructed with deck G indicated an increase in shear-bond capacity with a decrease in shear transfer device spacing.
4. An increase in steel deck thickness gave rise to an increase in shear-bond capacity for beams constructed with

steel decks I and O; while, for beams constructed with deck G, a decrease in steel deck thickness resulted in an increased shear-bond capacity.

5. A $\pm$15% correlation existed between experimental and calculated shear-bond values for all beams used in this investigation.

6. Selected strain gaged beam specimens indicated that a shear-bond failure may be accompanied by partial yielding of the steel deck, but in no case did yielding progress and reach the top of the steel deck.

7. Based on experimental evidence of numerous beam tests, shoring appeared to have no detrimental effect on the ultimate shear-bond capacity.

8. Varying the width of certain beam specimens between 12 and 24 inches had no effect on the ultimate shear-bond capacity.

9. Based on test results obtained from company O, of CATEGORY I beams constructed with steel deck greased prior to concrete placement, gave lower shear-bond capacity results compared to identical nongreased beam specimens.

10. No appreciable difference in shear-bond capacity was experienced between beam specimens where the composite neutral axis was located within the limits and above the top of the steel deck.

Design expressions, governing a shear-bond type of failure, were developed for both simple and continuous span installations.

In the case of continous span design, an equivalent modified simple span analysis was employed in the development of a shear-bond design expression, namely, using a reduced span length concept based on the theoretical location of inflection points. For a typical design example of a continuous span system, see Appendix A of reference (22). Superimposed design live loads, resulting from the ultimate strength shear-bond expressions for beams constructed with steel decks of CATEGORIES I, II and III, were developed in accordance with established load factors and safety provisions of the ACI Building Code (1). Load factors and safety provisions were adopted from Sections 1506(a) and 1504 of the ACI Building Code, respectively. The validity of these load factors and safety provision pertaining to a shear-bond failure, was validated by comparison with the over-all safety factor of each beam specimen. Such over-all safety is generally based on a factor of 2.0 or more, which was substantiated in this investigation.

Only 3 of the 173 beams tested resulted in flexural failures, namely, 3 of the beams constructed with steel deck G. Even with exceedingly long shear spans and highly under-reinforced cross sections, none of the beams constructed with steel decks I and O resulted in flexure failures.

Resulting from the work of this investigation the following future research is proposed:

1. Conduct tests on beam specimens utilizing deep steel decks such that the composite neutral axis falls within the

limits of the steel deck. Check shear-bond relationship.

2. Testing of continuous span steel-deck-reinforced systems to substantiate the proposed equivalent modified simple span analysis.
3. Determine the effect of slump of concrete on the load carrying capacity of steel-deck-reinforced systems.
4. Determine the effect of surface condition (chemical bond) of steel decks on the ultimate shear-bond capacity.
5. Conduct beam tests to determine the effect of shoring on the flexural strength of deck-reinforced systems, describing the locked-in steel stresses and stresses produced by shore removal.

ACKNOWLEDGMENTS

This investigation was sponsored by the American Iron and Steel Institute and was conducted at the Structural Research Laboratory under the auspices of the Engineering Research Institute with Dr. C. E. Ekberg, Jr., as principal investigator.

The author wishes to take this opportunity to express his appreciation to his major professor, Dr. C. E. Ekberg, Jr., for his guidance and advice during the course of this investigation.

Particular acknowledgment is extended to Messrs. Max L. Porter and Lynn A. Boettcher, who worked in the laboratory and on certain assignments in connection with this investigation. Also, thanks are due Messrs. Warren, Arendts, Watanabe, Kao and Wilson who interrupted their graduate studies to assist in casting of concrete specimens.

Special thanks is extended to Mr. A. J. Oudheusden, Chairman of AISI's Task Group Committee on Composite Construction, and the individual members of the Task Group for their useful comments regarding this investigation. Also, thanks is due Economy Form Corporation of Des Moines, Iowa, for the free use of their metal forms in casting the concrete specimens.

Last but not least, I would like to thank my wife, Patricia, for her understanding patience and encouragements during the more trying times of this investigation.

LITERATURE CITED

1. ACI standard building code requirements for reinforced concrete. Detroit, Mich., American Concrete Institute. 1963.

2. Bryl, S. The composite effect of profiled steel plate and concrete in deck slabs. Acier Stahl Steel 10: 448-454. 1967.

3. Clark, A. P. Diagonal tension in reinforced concrete beams. American Concrete Institute Journal 23: 145-156. 1951.

4. Commentary on building code requirements for reinforced concrete. Detroit, Mich., American Concrete Institute. 1965.

5. Ekberg, C. E., Jr. and Schuster, R. M. Floor systems with composite form-reinforced concrete slabs. International Association for Bridge and Structural Engineering Congress Proceedings 8: 385-394. 1968.

6. Ekberg, C. E., Jr., Schuster, R. M. and Porter, M. L. Further investigation of light gage steel forms as reinforcement for concrete slabs. Ames, Iowa, Iowa State Engineering Research Institute Progress Report No. 5: ERI-395. 1969.

7. Ekberg, C. E., Jr., Schuster, R. M. and Porter, M. L. Further testing of light gage steel forms as reinforcement for concrete slabs. Ames, Iowa, Iowa State Engineering Research Institute Progress Report ERI-201. 1968.

8. Friberg, B. F. Combined form and reinforcement for concrete slabs. American Concrete Institute Journal 25: 697-716. 1954.

9. Granco floor/roof construction. Catalog No. 99-1. St. Louis, Mo., Granco Steel Products Company. 1968.

10. Inland-Ryerson floor systems. Catalog 270. Milwaukee, Wis., Inland-Ryerson Construction Products Company. 1969.

11. Jones, T. B. H. H. Robertson Q-lock floor (composite floor). Unpublished research report No. 1388.6. Ambridge, Penn., H. H. Robertson Company. 1965.

12. Mathey, R. G. and Watstein, D. Shear strength of beams without web reinforcement containing deformed bars of different yield strengths. American Concrete Institute Proceedings 60: 183-206. 1963.

13. Mattock, A. H., Kriz, L. B. and Hognestad, E. Rectangular concrete stress distribution in ultimate strength design. American Concrete Institute Proceedings 57: 875-928. 1961.

14. Mörsch, E. Versuche über schubspannungen in betoneisenträgern. Beton und Eisen 2, No. 4: 269-274. 1903.

15. Mouw, K. W. and Ekberg, C. E., Jr. Fatigue testing of light gage metal forms. Ames, Iowa, Iowa State Engineering Research Institute Special Report ERI-348. 1969.

16. Oestreich, M. C. Cofar floor slab tests. Unpublished Report No. 1448 EJS. St. Louis, Mo., Granco Steel Products Company. January 1967.

17. Porter, M. L., Schuster, R. M. and Ekberg, C. E., Jr. Investigation of light gage steel forms as reinforcement for concrete slabs. Ames, Iowa, Iowa State Engineering Research Institute Progress Report ERI-276. 1968.

18. Robertson Q-floor, Q-lock floor, Q-air floor. Pittsburgh, Penn., H. H. Robertson Company. 1968.

19. Robinson, H. Composite beam incorporating cellular steel decking. American Society of Civil Engineers Proceedings 93, No. ST3: 355-380. 1969.

20. Robinson, H. Tests on composite beams with cellular deck. American Society of Civil Engineers Proceedings 93, No. ST4: 139-164. 1967.

21. Schuster, R. M. and Ekberg, C. E., Jr. Tentative recommendations for the design of light gage cold-formed steel forms as reinforcement for concrete slabs. Ames, Iowa, Iowa State Engineering Research Institute Progress Report No. 6. 1969.

22. Schuster, R. M. and Ekberg, C. E., Jr. Tentative recommendations for the design of cold-formed steel decking as reinforcement for concrete slabs. Ames, Iowa, Iowa State Engineering Research Institute Progress Report ERI-64500. 1970.

23. Schuster, R. M., Porter, M. L. and Ekberg, C. E., Jr., Pilot tests of light gage steel forms as reinforcement for concrete slabs. Ames, Iowa, Iowa State Engineering Research Institute Progress Report EPO68-123. 1968.

24. Seaburg, P. A. Composite slabform. Unpublished second progress report. Bethlehem Steel Company Research Department Report No. 62288-2. July 1964.

25. Shear and diagonal tension. Report of ACI-ASCE Committee 326. New York, N. Y., American Society of Civil Engineers. 1962.

26. Specification for the design of cold-formed steel structural members. New York, N. Y., American Iron and Steel Institute. 1968.

27. Steel decks for floors and roofs. Catalog lf/Bo. Pittsburgh, Penn., Bowman Building Products Company. 1970.

28. Talbot, A. N. Tests of reinforced concrete beams: resistance to wet stresses. University of Illinois Engineering Experiment Station Bulletin 29. 1909.

29. Thelen, A. B. Load tests of B-22, B-18, gage galvanized Hi-Bond decks with light weight concrete. Unpublished research report. Milwaukee, Wis., Inland Steel Products Company. 1967.

APPENDIX A: TABLES

Table A.1. Measured and calculated cross-sectional steel deck properties for steel decks I, O, G and E

Deck gage	t_c (in.)	d_d (in.)	y_{sb} (in.)	A_s (in.^{2}/ft)	I_{sf} (in.^{4}/ft)	I_{sp}[a] (in.^{4}/ft)	I_{sn}[a] (in.^{4}/ft)	W_D[b] (psf.)
<u>Deck I</u>								
22	0.0330	1.55	0.623	0.556	0.229	0.208	0.171	2.00
	0.0295	1.55	0.621	0.497	0.204	0.180	0.147	2.00
	0.0311	1.55	0.622	0.524	0.215	0.193	0.158	2.00
18	0.0535	1.57	0.633	0.901	0.371	0.371	0.335	3.20
	0.0539	1.57	0.634	0.908	0.373	0.373	0.338	3.20
16	0.0684	1.59	0.641	1.153	0.474	0.474	0.464	3.90
<u>Deck O</u>								
22	0.0274	1.53	0.880	0.493	0.209	0.141	0.164	1.80
20	0.0330	1.53	0.883	0.594	0.252	0.182	0.210	2.20
16	0.0583	1.56	0.896	1.049	0.445	0.397	0.442	3.80
<u>Deck G</u>								
24	0.0251	1.30	0.648	0.387	0.096	0.083	0.083	1.95
20	0.0369	1.31	0.653	0.569	0.141	0.133	0.133	2.80
<u>Deck E</u>								
20	0.0430	1.87	0.648	1.022	0.587	0.474	0.349	3.70

[a]Calculated in accordance with applicable sections of the AISI design specification.

[b]Obtained from respective company catalogs.

Table A.2. Average steel deck properties obtained from companies O and E

Deck gage	Steel deck designation	t_c (in.)	d_d (in.)	y_{sb} (in.)	A_s (in.^{2}/ft)	F_y (ksi)	E_s (ksi) x 10^3
Deck O							
20	QL - 21	0.0351	3.04	1.82	0.76	38.50	28.0
18/18	DC - 45	0.0441	4.59	1.95	1.48	44.00	28.0
18/18	DC - 75	0.0441	7.59	3.30	1.75	44.00	28.0
Deck E							
22	[a]	0.0350	2.00	0.74	0.79	92.30	29.0

[a] See Table A.9.

Table A.3. Measured mechanical steel tensile properties for steel decks I, O, G, and E (averages of two coupon tests)

Deck gage thickness	Yield strength (ksi)	Ultimate strength (ksi)	Rupture strength (ksi)	Elongation in 2 in. %	Modulus of elasticity (ksi) x 10^3
Deck I					
22					
(0.0330)	40.05[a]	55.30	48.85	34.5	29.1
(0.0295)	39.80[a]	54.20	48.90	31.8	28.7
(0.0311)	39.23[b]	53.00	47.26	48.0	28.4
18					
(0.0535)	40.20[a]	52.30	44.90	36.8	29.3
(0.0539)	41.72[b]	54.60	42.20	21.3	27.5
16					
(0.0684)	43.87[a]	55.96	39.11	29.0	28.5
Deck O					
20					
(0.0330)	40.30[a]	52.40	43.30	44.0	29.8
22					
(0.0274)	38.20[b]	47.30	42.10	25.5	30.8
16					
(0.0274)	46.20[b]	61.40	42.00	30.5	30.5
Deck G[c]					
24					
(0.0251)	110.00	110.00	-	-	29.5

[a]Yield strength determined at 0.1% offset.

[b]Yield strength determined at 0.2% offset.

[c]Values obtained from company G.

Table A.3. Continued

Deck gage thickness	Yield strength (ksi)	Ultimate strength (ksi)	Rupture strength (ksi)	Elongation in 2 in. %	Modulus of elasticity (ksi) x 10^3
20 (0.0369)	103.30	103.30	-	-	29.5
Deck E					
20 (0.043)	84.10[a]	87.20	75.00	5.5	28.1

Table A.4. Summary of concrete mix and strength properties

Pour number	Date of pour	Cement (lb/yd)	Aggregate properties Fine (lb/yd)	Course (lb/yd)	Max. size (in.)
2	03/21/68	470	1466	1868	3/4
3	04/11/68	470	1466	1868	3/4
4	06/21/68	470	1948	1784	3/8
5	06/27/68	460	1645	1790	3/8
6	07/05/68	564	1560	1707	3/8
8	09/28/68	470	1467	1870	3/4
9	10/08/68	470	1466	1868	3/4
10	11/05/68	470	1466	1869	3/4
11	01/14/68	470	1466	1868	3/4
12	11/22/68	470	1486	1868	3/4
14	03/06/69	470	1487	1867	3/4
15	06/10/69	470	1466	1868	3/4
16	06/18/69	470	1466	1868	3/4
17	06/27/69	470	1466	1868	3/4
18	07/08/69	470	1466	1868	3/4
19	07/16/69	470	1466	1868	3/4
20	07/30/69	470	1466	1868	3/4
21	08/14/69	470	1466	1868	3/4
22	08/25/69	470	1466	1868	3/4
23	09/05/69	470	1466	1870	3/4
24	09/20/69	470	1466	1868	3/4
25	09/27/69	470	1466	1870	3/4
26	10/04/69	470	1466	1870	3/4

Slump (in.)	f'_c (psi)	Age of f'_c (days)	w_c (lb/ft^3)	E_c (psi) x 10^6
2-3/4	4126	14	145	3.70
2-3/4	3908	37	145	3.60
3-1/2	2956	12	140	2.97
3-1/2	3103	22	140	3.05
5	3708	22	140	3.33
3-1/2	3849	12	145	3.54
3-1/2	4606	23	145	3.87
3	4432	14	144	3.80
3	4720	20	144	3.92
3-1/2	3350	11	144	3.30
3-1/2	3577	14	144	3.41
3-1/2	3426	11	145	3.37
3-1/2	3634	13	145	3.44
4	3573	11	144	3.41
6	3983	93	144	3.60
3-1/2	3584	14	144	3.41
3-1/2	3518	14	144	3.38
3-1/2	3923	33	144	3.57
2-1/2	4103	15	144	3.65
3-1/2	3458	14	144	3.35
3-1/2	4086	24	144	3.65
3-1/2	4216	34	144	3.70
8	2955	14	143	3.10
3-1/2	3787	15	143	3.51
3-1/2	4139	24	143	3.67
3	4235	20	144	3.71
3	4437	28	144	3.80
3-1/2	3611	16	144	3.42
3-1/2	3654	20	144	3.45
4	3472	19	144	3.36
4	3482	24	144	3.36
4	3527	15	144	3.39
4	4093	29	144	3.65
4	3447	20	144	3.35
4	3671	27	144	3.46
4	3911	34	144	3.57
3-1/2	3765	21	144	3.50
6	4447	20	144	3.80
2-3/4	3630	18	144	3.44

Table A.5. Experimental test results for beams constructed with steel deck I of CATEGORY I

Beam no.	Specimen designation	Ultimate experimental beam load P_{ue} (lb)	Ultimate experimental shear V_{ue} (lb/ft)	Ultimate experimental moment M_{ue} (ft-lb/ft)
22 Gage				
1I22	24-2-13	4450	2225	4450
2I22	24-2-13	4550	2275	4550
3I22	24-2-14	4300	2150	4300
4I22	24-2-14	4350	2175	4350
5I22	18-3-34	5500	2750	4125
6I22	30-3-34	4000	2000	5000
7I22	12-8-12	8700	4350	4350
8I22	12-9-16	8700	4350	4350
9I22	12-10-15	8250	4125	4125
10I22	12-11-13	7800	3900	3900
11I22	12-12-11	8000	4000	4000
12I22	18-8-14	5650	2825	4238
13I22	18-9-16	6700	3350	5025
14I22	18-10-14	5600	2800	4200
15I22	18-11-13	6000	3000	4500
16I22	18-12-11	5200	2600	3900
17I22	24-8-14	4000	2000	4000
18I22	24-9-20	4700	2350	4700
19I22	24-10-14	4150	2075	4150
20I22	24-11-13	4400	2200	4400
21I22	24-12-11	4600	2300	4600
22I22	34-8-23	3000	1500	4250
23I22	34-9-20	3700	1850	5241
24I22	34-10-14	3000	1500	4250
25I22	34-11-14	3100	1550	4391
26I22	34-12-11	3750	1875	5312
27I22	24-14-91	4100	2050	4100
28I22	24-14-91	4200	2100	4200
29I22	24-14-92	4200	2100	4200
30I22	24-14-91	4200	2100	4200
31I22	24-14-91	5600	2800	5600
32I22	36-15-13	3600	891	2673
33I22	70-16-14	2400	594	3465
34I22	36-15-14	4700	1163	3489
35I22	70-16-14	3500	866	5052
36I22	40-18-14	5400	1336	4453
37I22	36-15-13	6100	1509	4527

Beam depth D (in.)	Span length L (in.)	Shear span L' (in.)	Beam width b_d (in.)	Coated steel thickness t_c (in.)	Concrete compressive strength f'_c (psi)	Mode of failure
5.00	68	24	12	0.0330	4126	Shear-bond
5.00	68	24	12	0.0330	4126	Shear-bond
5.00	68	24	12	0.0330	4126	Shear-bond
5.00	68	24	12	0.0330	4126	Shear-bond
5.00	68	18	12	0.0330	3908	Shear-bond
5.00	68	30	12	0.0330	3908	Shear-bond
5.00	68	12	12	0.0295	3849	Shear-bond
5.00	68	12	12	0.0295	4432	Shear-bond
5.00	68	12	12	0.0295	3577	Shear-bond
5.00	68	12	12	0.0295	3634	Shear-bond
5.00	68	12	12	0.0295	3573	Shear-bond
4.00	68	18	12	0.0295	3849	Shear-bond
5.00	68	18	12	0.0295	4432	Shear-bond
5.00	68	18	12	0.0295	3577	Shear-bond
5.00	68	18	12	0.0295	3634	Shear-bond
5.00	68	18	12	0.0295	3573	Shear-bond
5.00	68	24	12	0.0295	3849	Shear-bond
5.00	68	24	12	0.0295	4720	Shear-bond
5.00	68	24	12	0.0295	3577	Shear-bond
5.00	68	24	12	0.0295	3634	Shear-bond
5.00	68	24	12	0.0295	3573	Shear-bond
5.00	68	34	12	0.0295	4606	Shear-bond
5.00	68	34	12	0.0295	4720	Shear-bond
5.00	68	34	12	0.0295	3577	Shear-bond
5.00	68	34	12	0.0295	3634	Shear-bond
5.00	68	34	12	0.0295	3573	Shear-bond
5.00	68	24	12	0.0295	3983	Shear-bond
5.00	68	24	12	0.0295	3983	Shear-bond
5.00	68	24	12	0.0295	3983	Shear-bond
5.00	68	24	12	0.0295	3983	Shear-bond
5.00	68	24	12	0.0295	3983	Shear-bond
3.50	140	36	24-1/4	0.0311	3584	Shear-bond
3.50	140	70	24-1/4	0.0311	3518	Shear-bond
4.50	140	36	24-1/4	0.0311	3584	Shear-bond
4.50	140	70	24-1/4	0.0311	3518	Shear-bond
4.50	140	40	24-1/4	0.0311	3752	Shear-bond
5.50	140	36	24-1/4	0.0311	3584	Shear-bond

Table A.5. Continued

Beam no.	Specimen designation	Ultimate experimental beam load P_{ue} (lb)	Ultimate experimental shear V_{ue} (lb/ft)	Ultimate experimental moment M_{ue} (ft-lb/ft)
38I22	40-18-14	8000	1979	6597
39I22	70-16-15	4600	1138	6638
40I22	46-19-20SH	5200	1287	4933
41I22	70-19-19SG	2900	718	4188
42I22	48-20-16SG	6100	1509	6036
Re-tested				
43I22	30R-15-21	5000	1237	3093
44I22	40R-15-23	5400	1336	4453
45I22	30R-15-21	8500	2103	5258
46I22	26R-16-33	8500	2103	4557
47I22	24R-18-24	11000	2722	5444
<u>18-Gage</u>				
1I18	12-8-23	9700	4850	4850
2I18	12-9-14	10200	5100	5100
3I18	12-10-11	10550	5275	5275
4I18	12-11-13	8300	4150	4150
5I18	12-12-12	10400	5200	5200
6I18	18-8-23	6600	3300	4950
7I18	18-9-14	8200	4100	6150
8I18	18-10-11	7500	3750	5625
9I18	18-11-13	7700	3850	5775
10I18	18-12-12	7050	3525	5288
11I18	24-8-23	4950	2475	4950
12I18	24-9-14	6600	3300	6600
13I18	24-10-11	6300	3150	6300
14I18	24-11-13	5700	2850	5700
15I18	24-12-12	6850	3425	6850
16I18	34-8-23	3150	1575	4462
17I18	34-9-14	5300	2650	7508
18I18	34-10-11	5300	2650	7508
19I18	34-11-13	4700	2350	6658
20I18	34-12-12	5050	2525	7154
21I18	70-17-13	5050	1250	7292
22I18	60-17-24	5600	1386	6930
23I18	48-18-14	6600	1633	6532
24I18	70-17-13	6950	1720	10033
25I18	60-17-14	7450	1843	9215
26I18	48-18-15	7900	1955	7820
27I18	70-17-14	7350	1819	10611

Beam depth D (in.)	Span length L (in.)	Shear span L' (in.)	Beam width b_d (in.)	Coated steel thickness t_c (in.)	Concrete compressive strength f'_c (psi)	Mode of failure
5.50	140	40	24-1/4	0.0311	3752	Shear-bond
4.40	140	70	24-1/4	0.0311	3518	Shear-bond
4.50	140	46	24-1/4	0.0311	4235	Shear-bond
3.50	140	70	24-1/4	0.0311	4235	Shear-bond
5.82	140	48	24-1/4	0.0311	3654	Shear-bond
3.50	92	30	24-1/4	0.0311	3800	Shear-bond
4.50	80	40	24-1/4	0.0311	3800	Shear-bond
5.50	92	30	24-1/4	0.0311	3800	Shear-bond
5.50	52	26	24-1/4	0.0311	3800	Shear-bond
5.50	70	24	24-1/4	0.0311	4139	Shear-bond
5.00	68	12	12	0.0535	4606	Shear-bond
5.00	68	12	12	0.0535	4432	Shear-bond
5.00	68	12	12	0.0535	3350	Shear-bond
5.00	68	12	12	0.0535	3634	Shear-bond
5.00	68	12	12	0.0535	3573	Shear-bond
5.00	68	18	12	0.0535	4606	Shear-bond
5.00	68	18	12	0.0535	4432	Shear-bond
5.00	68	18	12	0.0535	3350	Shear-bond
5.00	68	18	12	0.0535	3634	Shear-bond
5.00	68	18	12	0.0535	3573	Shear-bond
5.00	68	24	12	0.0535	4606	Shear-bond
5.00	68	24	12	0.0535	4432	Shear-bond
5.00	68	24	12	0.0535	3350	Shear-bond
5.00	68	24	12	0.0535	3634	Shear-bond
5.00	68	24	12	0.0535	3573	Shear-bond
5.00	68	34	12	0.0535	4606	Shear-bond
5.00	68	34	12	0.0535	4432	Shear-bond
5.00	68	34	12	0.0535	3350	Shear-bond
5.00	68	34	12	0.0535	3634	Shear-bond
5.00	68	34	12	0.0535	3573	Shear-bond
3.50	140	70	24-1/4	0.0539	3458	Shear-bond
3.50	140	60	24-1/4	0.0539	4086	Shear-bond
3.50	140	48	24-1/4	0.0539	2955	Shear-bond
4.50	140	70	24-1/4	0.0539	3458	Shear-bond
4.50	140	60	24-1/4	0.0539	3458	Shear-bond
4.50	140	48	24-1/4	0.0539	3787	Shear-bond
5.50	140	70	24-1/4	0.0539	3458	Shear-bond

Table A.5. Continued

Beam no.	Specimen designation	Ultimate experimental beam load P_{ue} (lb)	Ultimate experimental shear V_{ue} (lb/ft)	Ultimate experimental moment M_{ue} (ft-lb/ft)
28I18	60-17-14	9550	2363	11815
29I18	47-18-15	9100	2252	8820
30I18	30-20-20SH	11200	2771	6928
31I18	40-19-20SH	9500	2351	7837
32I18	36-22-14SH	12600	3118	9354
33I18	70-19-19SG	4600	1138	6638
34I19	60-20-20SG	8800	2177	10885
35I18	48-20-16SG	9300	2301	9204
Re-tested				
36I18	24R-17-34	14900	3687	7374
37I18	24R-17-34	13500	3340	6680
38I18	24R-18-24	14800	3662	7324
39I18	24R-17-34	11200	2771	5542
40I18	24R-17-34	12600	3118	6236
41I18	24R-18-24	10000	2474	4948
42I18	40R-19-28	10600	2623	8743
43I18	24R-17-34	9600	2375	4750
44I18	24R-18-24	7200	1782	3564
45I18	15R-19-24	12200	3019	3774
16 Gage				
1I16	36-15-14	7500	1856	5568
2I16	60-16-14	6400	1584	7920
3I16	36-15-13	9600	2375	7125
4I16	70-16-14	7600	1880	10967
5I16	36-15-14	12300	3043	9129
6I16	70-16-14	11600	2870	16742
7I16	40-19-20SH	12200	3019	10063
8I16	70-19-19SG	7100	1757	10249
9I16	60-20-19SG	10400	2573	12865
10I16	36-20-19SG	18900	4676	14028
Re-tested				
11I16	30R-15-21	8800	2177	5433
12I16	26R-16-33	10400	2573	5575
13I16	30R-15-21	10400	2573	6433
14I16	26R-16-33	12400	3068	6647
15I16	15R-19-28	21200	5245	6556
16I16	30R-15-22	15200	3761	9403
17I16	14R-20-21	24600	6087	7102
18I16	22R-20-21	26000	6433	11794
19I16	15R-19-28	18600	4602	5753

Beam depth D (in.)	Span length L (in.)	Shear span L' (in.)	Beam width b_d (in.)	Coated steel thickness t_c (in.)	Concrete compressive strength f'_c (psi)	Mode of failure
5.50	140	60	24-1/4	0.0539	3458	Shear-bond
5.50	140	47	24-1/4	0.0539	3787	Shear-bond
3.63	140	30	24-1/4	0.0539	3654	Shear-bond
4.50	140	40	24-1/4	0.0539	4235	Shear-bond
4.68	140	36	24-1/4	0.0539	3527	Shear-bond
3.50	140	70	24-1/4	0.0539	4235	Shear-bond
4.50	140	60	24-1/4	0.0539	3654	Shear-bond
5.68	140	48	24-1/4	0.0539	3654	Shear-bond
5.50	58	24	24-1/4	0.0539	4216	Shear-bond
5.50	48	24	24-1/4	0.0539	4216	Shear-bond
5.50	70	24	24-1/4	0.0539	4139	Shear-bond
4.50	48	24	24-1/4	0.0539	4216	Shear-bond
4.50	48	24	24-1/4	0.0539	4216	Shear-bond
4.50	70	24	24-1/4	0.0539	4139	Shear-bond
4.50	80	40	24-1/4	0.0539	4437	Shear-bond
3.50	48	24	24-1/4	0.0539	4216	Shear-bond
3.50	70	15	24-1/4	0.0539	4139	Shear-bond
3.50	49	15	24-1/4	0.0539	4437	Shear-bond
3.50	140	36	24-1/4	0.0684	3584	Shear-bond
3.50	140	60	24-1/4	0.0684	3518	Shear-bond
4.50	140	36	24-1/4	0.0684	4235	Shear-bond
4.50	140	70	24-1/4	0.0684	3584	Shear-bond
5.50	140	36	24-1/4	0.0684	3518	Shear-bond
5.50	140	70	24-1/4	0.0684	4235	Shear-bond
4.50	140	40	24-1/4	0.0684	3654	Shear-bond
3.50	140	70	24-1/4	0.0684	3584	Shear-bond
4.50	140	60	24-1/4	0.0684	4103	Shear-bond
5.75	140	36	24-1/4	0.0684	3654	Shear-bond
3.50	92	30	24-1/4	0.0684	3800	Shear-bond
3.50	52	26	24-1/4	0.0684	3923	Shear-bond
4.50	92	30	24-1/4	0.0684	3800	Shear-bond
4.50	92	26	24-1/4	0.0684	3923	Shear-bond
4.50	50	15	24-1/4	0.0684	4437	Shear-bond
5.50	92	30	24-1/4	0.0684	3800	Shear-bond
4.50	58	14	24-1/4	0.0684	3654	Shear-bond
5.50	82	22	24-1/4	0.0684	3654	Shear-bond
3.50	50	15	24-1/4	0.0684	4437	Shear-bond

Table A.6. Experimental test results for beams constructed with steel deck 0 of CATEGORY I

Beam no.	Specimen designation	Ultimate experimental beam load P_{ue} (lb)	Ultimate experimental shear V_{ue} (lb/ft)	Ultimate experimental moment M_{ue} (ft-lb/ft)
20 Gage				
1020	12-4-11	5800	2900	2900
2020	12-4-12	6400	3200	3200
3020	12-5-21	6900	3450	3450
4020	12-6-21	6500	3250	3250
5020	24-4-12	4000	2000	4000
6020	24-5-18	3900	1950	3900
7020	24-5-20	3800	1900	3800
8020	24-6-21	3200	1600	3200
9020	34-4-12	2620	1310	3712
10020	34-5-18	2500	1250	3542
11020	34-6-21	1800	900	2550
12020	34-6-21	2450	1225	3471
22 Gage				
1022	70-21-19	1900	470	2742
2022	70-21-19	2900	718	4188
3022	36-21-19	4400	1089	3267
4022	70-22-30SH	3800	940	5483
5022	40-23-20SH	3200	782	2640
6022	60-23-32SH	2500	619	3095
7022	70-22-28SG	2000	495	2887
8022	48-23-27SG	2700	668	2672
16 Gage				
1016	60-21-19	5400	1336	6680
2016	60-21-19	7900	1955	9775
3016	36-21-19	12500	3093	9279
4016	48-22-29SH	10650	2635	10540
5016	70-23-25SH	8100	2004	11690
6016	70-22-29SG	5800	1435	8371
7016	36-23-20SG	10900	2697	8091
8016	48-23-34SG	10650	2635	10540
Re-tested				
9016	24R-21-24	9300	2301	4602
10016	36R-21-24	8900	2202	6606
11016	24R-23-53	19450	4812	9624
12016	24R-23-55	18650	4615	9230

Beam depth D (in.)	Span length L (in.)	Shear span L' (in.)	Beam width b_d (in.)	Coated steel thickness t_c (in.)	Concrete compressive strength f'_c (psi)	Mode of failure
5.00	68	12	12	0.0330	2956	Shear-bond
5.00	68	12	12	0.0330	3103	Shear-bond
5.00	68	12	12	0.0330	2956	Shear-bond
5.00	68	12	12	0.0330	3103	Shear-bond
5.00	68	24	12	0.0330	2956	Shear-bond
5.00	68	24	12	0.0330	2956	Shear-bond
5.00	68	24	12	0.0330	3103	Shear-bond
5.00	68	24	12	0.0330	3708	Shear-bond
5.00	68	34	12	0.0330	2956	Shear-bond
5.00	68	34	12	0.0330	3103	Shear-bond
5.00	68	34	12	0.0330	3103	Shear-bond
5.00	68	34	12	0.0330	3708	Shear-bond
3.50	140	70	24-1/4	0.0274	3472	Shear-bond
4.50	140	70	24-1/4	0.0274	3472	Shear-bond
5.50	140	36	24-1/4	0.0274	3472	Shear-bond
5.50	140	70	24-1/4	0.0274	4093	Shear-bond
3.56	140	40	24-1/4	0.0274	3447	Shear-bond
4.50	140	60	24-1/4	0.0274	3911	Shear-bond
3.50	140	70	24-1/4	0.0274	4093	Shear-bond
3.56	140	48	24-1/4	0.0274	3671	Shear-bond
3.50	140	60	24-1/4	0.0583	3472	Shear-bond
4.50	140	60	24-1/4	0.0583	3472	Shear-bond
5.50	140	36	24-1/4	0.0583	3472	Shear-bond
4.50	140	48	24-1/4	0.0583	4093	Shear-bond
5.50	140	70	24-1/4	0.0583	3671	Shear-bond
3.50	140	70	24-1/4	0.0583	4093	Shear-bond
4.63	140	36	24-1/4	0.0583	3447	Shear-bond
5.63	140	48	24-1/4	0.0583	3911	Shear-bond
3.50	[illegible]		24-1/4	0.0583	3482	Shear-bond
4.50	[illegible]	[illegible]	24-1/4	0.0583	3482	Shear-bond
5.50	60	24	24-1/4	0.0583	3813	Shear-bond
5.50	58	24	24-1/4	0.0583	3813	Shear-bond

Table A.7. Experimental test results for beams constructed with steel deck O. All tests conducted by company O

Beam no.	Specimen designation	Ultimate experimental beam load P_{ue} (lb)	Ultimate experimental shear V_{ue} (lb/ft)	Ultimate experimental moment M_{ue} (ft-lb/ft)
20 Gage				
13020	QL-21	23072	2884	4807
14020	QL-21	19344	2418	5037
15020	QL-21	28720	3590	4488
16020	QL-21	21312	2664	5550
17020	QL-21	26272	3284	4105
18020	QL-21[a]	24272	3034	3793
19020	QL-21[a]	24832	3104	3880
20020	QL-21[a]	16672	2084	4342
21020	QL-21[a]	16992	2124	4425
22020	QL-21 INV.	37952	4744	5930
23020	QL-21 INV.	27152	3394	7071
24020	QL-21 INV.	26912	3364	7008
25020	QL-21 INV.	33872	4234	5293
26020	QL-21 INV.	29352	3669	6115
27020	QL-21 INV.[a]	25472	3184	3980
28020	QL-21 INV.[a]	21352	2669	4448
29020	QL-21 INV.[a]	29392	3674	4593
30020	QL-21 INV.[a]	17312	2164	4508
18/18 Gage				
1018/18	DC-45[a]	11808	2952	11808
2018/18	DC-45[a]	8956	2239	15673
3018/18	DC-45[a]	17916	4497	8994
4018/18	DC-75[a]	16488	4133	21641
5018/18	DC-75[a]	13284	3321	17435

[a]Indicates steel decks were greased prior to placing of concrete.

Beam depth D (in.)	Span length L (in.)	Shear span L' (in.)	Beam width b_d (in.)	Coated steel thickness t_2 (in.)	Concrete compressive strength f'_c (psi)	Mode of failure
5.56	102	20	48	0.0351	3680	Shear-bond
5.52	102	25	48	0.0351	3700	Shear-bond
5.42	102	15	48	0.0351	3310	Shear-bond
5.35	102	25	48	0.0351	3600	Shear-bond
5.34	102	15	48	0.0351	3760	Shear-bond
5.46	102	15	48	0.0351	3450	Shear-bond
5.38	102	15	48	0.0351	3570	Shear-bond
5.36	102	25	28	0.0351	3930	Shear-bond
5.49	102	25	48	0.0351	3480	Shear-bond
5.58	102	15	48	0.0351	3930	Shear-bond
5.53	102	25	48	0.0351	3630	Shear-bond
5.48	102	25	48	0.0351	3720	Shear-bond
5.49	102	15	48	0.0351	3700	Shear-bond
5.41	102	20	48	0.0351	4150	Shear-bond
5.42	102	15	48	0.0351	4320	Shear-bond
5.48	102	20	48	0.0351	3800	Shear-bond
5.44	102	15	48	0.0351	3880	Shear-bond
5.50	102	25	48	0.0351	3690	Shear-bond
7.10	192	48	24	0.0441	4980	Shear-bond
7.18	252	84	24	0.0441	3300	Shear-bond
7.25	96	24	24	0.0441	3280	Shear-bond
10.16	252	63	24	0.0441	3440	Shear-bond
10.04	252	63	24	0.0441	4380	Shear-bond

Table A.8. Experimental test results for beams constructed with steel deck G of CATEGORY II

Beam no.	Specimen designation	Ultimate experimental beam load P_{ue} (lb)	Ultimate experimental shear V_{ue} (lb/ft)	Ultimate experimental moment M_{ue} (ft-lb/ft)
<u>24 Gage</u>				
1G24	3-70-24-19SH	6900	1357	7916
2G24	3-36-25-21SH	15900	3180	9540
3G24	3-24-24-21SH	22700	4502	9004
4G24	5-70-25-21SH	5300	1051	6130
5G24	5-36-24-19SH	9700	1908	5724
6G24	5-28-25-21SH	14100	2808	6552
7G24	8-70-26-19SH	3600	714	4165
8G24	8-36-26-19SH	6200	1235	3705
9G24	8-28-26-19SH	9700	1940	4527
<u>20 Gage</u>				
1G20	3-70-24-24SH	8000	1714	9998
2G20	3-36-26-17SH	13100	2820	8460
3G20	3-28-26-19SH	17500	3784	8829
4G20	5-70-26-17SH	4600	995	5804
5G20	5-36-25-19SH	7900	1693	5079
6G20	5-24-24-24SH	12300	2636	5272
7G20	8-70-25-19SH	3000	643	3751
8G20	8-36-24-24SH	5100	1093	3279
9G20	8-30-25-19SH	7600	1636	4090

Beam depth D (in.)	Span length L (in.)	Shear span L' (in.)	Beam width b_d (in.)	Coated steel thickness t_c (in.)	Concrete compressive strength f'_c (psi)	Mode of failure
3.50	140	70	30-1/2	0.0251	3765	Flex.-Yield.
4.50	140	36	30	0.0251	4447	Flex.-Yield.
6.00	140	24	30-1/4	0.0251	3765	Shear-bond
3.50	140	70	30-1/4	0.0251	4447	Shear-bond
5.00	140	36	30-1/2	0.0251	3765	Shear-bond
6.00	140	28	30-1/8	0.0251	4447	Shear-bond
3.50	140	70	30-1/4	0.0251	3630	Shear-bond
5.00	140	36	30-1/8	0.0251	3630	Shear-bond
6.00	140	28	30	0.0251	3630	Shear-bond
3.50	140	70	28	0.0369	3778	Flex.-Crush.
4.75	140	36	27-7/8	0.0369	3630	Shear-bond
5.88	140	28	27-3/4	0.0369	3630	Shear-bond
3.50	140	70	27-3/4	0.0369	3630	Shear-bond
4.88	140	36	28	0.0369	4447	Shear-bond
5.75	140	24	28	0.0369	3778	Shear-bond
3.50	140	70	27-7/8	0.0369	4447	Shear-bond
4.88	140	36	28	0.0369	3778	Shear-bond
5.88	140	30	28	0.0369	4447	Shear-bond

Table A.9. Experimental test results for beams constructed with steel deck E of CATEGORY I

Beam no.	Specimen designation	Ultimate experimental beam load P_{ue} (lb)	Ultimate experimental shear V_{ue} (lb/ft)	Ultimate experimental moment M_{ue} (ft-lb/ft)
<u>20 Gage</u>				
1E20	12-4-11	11700	5850	5850
2E20	12-4-12	17000	8500	8500
3E20	12-5-21	15200	7600	7600
4E20	12-6-20	19650	9825	9825
5E20	24-4-12	12400	6200	12400
6E20	24-5-18	10800	5400	10800
7E20	24-5-20	12600	6300	12600
8E20	24-6-20	13350	6675	13350
9E20	34-4-12	11000	5500	15583
10E20	34-5-18	9900	4950	14025
11E20	34-6-19	13150	6575	18629
12E20	34-6-20	13350	6675	18912
<u>22 Gage</u>[a]				
1E22	10-11	5684	3410	6820
2E22	10-2	7201	4320	12420
3E22	10-3	7685	4610	9220
4E22	10-4	8318	4990	9980
5E22	10-5	8718	5230	10460
6E22	10-7	9002	5400	10800
7E22	14-2	6501	3900	11212
8E22	14-3	6985	4190	8380
9E22	14-4	8002	4800	9600
10E22	14-7	7502	4500	9000
11E22	14-10	6685	4010	8020
12E22	18-1	7768	4660	9320
13E22	19-1	9502	5700	11400
14E22	10-12	11002	6600	13200
15E22	10-13	13003	7800	15600
16E22	4-1/2"x69"x12"	12400	6200	12400

[a]All tests from 1E22 to 16E22 conducted by company E

Beam depth D (in.)	Span length L (in.)	Shear span L' (in.)	Beam width b_d (in.)	Coated steel thickness t_c (in.)	Concrete compressive strength f'_c (psi)	Mode of failure
5.00	68	12.0	12	0.0430	2956	Shear-bond
5.00	68	12.0	12	0.0430	2956	Shear-bond
5.00	68	12.0	12	0.0430	3103	Shear-bond
5.00	68	12.0	12	0.0430	3708	Shear-bond
5.00	68	24.0	12	0.0430	2956	Shear-bond
5.00	68	24.0	12	0.0430	3103	Shear-bond
5.00	68	24.0	12	0.0430	3103	Shear-bond
5.00	68	24.0	12	0.0430	3708	Shear-bond
5.00	68	34.0	12	0.0430	2956	Shear-bond
5.00	68	34.0	12	0.0430	3103	Shear-bond
5.00	68	34.0	12	0.0430	3708	Shear-bond
5.00	68	34.0	12	0.0430	3708	Shear-bond
3.00	69	24.0	10	0.0350	4100	Shear-bond
4.00	69	34.5	10	0.0350	3450	Shear-bond
4.00	69	24.0	10	0.0350	3450	Shear-bond
4.00	69	24.0	10	0.0350	3450	Shear-bond
4.00	69	24.0	10	0.0350	3450	Shear-bond
4.00	69	24.0	10	0.0350	4100	Shear-bond
4.00	69	34.5	10	0.0350	3450	Shear-bond
4.00	69	24.0	10	0.0350	3450	Shear-bond
4.00	69	24.0	10	0.0350	3450	Shear-bond
4.00	69	24.0	10	0.0350	4100	Shear-bond
4.00	69	24.0	10	0.0350	3430	Shear-bond
4.00	69	24.0	10	0.0350	4100	Shear-bond
4.00	69	24.0	10	0.0350	4100	Shear-bond
5.00	69	24.0	10	0.0350	4100	Shear-bond
6.00	69	24.0	10	0.0350	4100	Shear-bond
4.50	69	24.0	24	0.0310	4400	Shear-bond

Table A.10. Shear-bond regression constants for beams constructed with steel decks I, O, G, and E

Deck gage	Number of specimens used in regression	K_5	K_6 (psi)	Average t_c (in.)	Fig. no. of plotted data
Deck I					
22	47	3.18	648	0.0312	44
18	40	3.01	1466	0.0537	46
16	12	4.73	1003	0.0684	48
16	7	6.52	1172	0.0684	50
Deck O					
22 20	18	2.99	580	0.0302	54
16	12	5.50	974	0.0583	56
Deck G					
24[a]	7	11.68	12539[b]	0.0251	70
20[a]	8	11.27	7435[b]	0.0369	72
Deck E					
20	11	4.25	3979	0.0430	75

[a]Constants K_5 and K_6 become K_7 and K_8, respectively.

[b]Units change to pounds per inch.

Table A.11. Shear-bond regression constants for beams constructed with steel decks O and E. Tests conducted by respective companies

Deck gage	Specimen designation	Number of specimens used in regression	K_5	K_6 (psi)	Average t_c (in.)	Fig. no. of plotted data
Deck O						
20	QL-21	5	3.77	1452	0.0351	58
20	QL-21[a]	4	4.09	730	0.0351	60
20	QL-21INV.	5	4.00	2306	0.0351	62
20	QL-21INV.[a]	4	4.44	594	0.0351	64
18/18 } 18/18	DC-45[a] DC-75[a]	5	3.85	906	0.0441	68
Deck E						
22	b	16	6.07	3585	0.0350	74
22 } 20[c]	b b	27	4.72	3993	0.0390	77

[a]Steel decks were greased prior to placing of concrete.

[b]See Table A.9.

[c]Tests conducted in this investigation.

Table A.12. Comparison of experimental and calculated ultimate shear-bond stresses for beams constructed with deck I

Beam no.	Specimen designation	Ultimate shear-bond stresses: Experimental $v_{ue}=\frac{V_{ue}}{bd}$ (psi)	Calculated $v_{uc}=\frac{K_5\sqrt{f'_c}\,d}{L'}+K_6 p$ (psi)			$\frac{v_{uc}}{v_{ue}}$
<u>22 Gage</u>						
1I22	24-2-13	42.4	44.1	37.2	6.9	1.04
2I22	24-2-13	43.3	44.1	37.2	6.9	1.02
3I22	24-2-14	40.9	44.1	37.2	6.9	1.08
4I22	24-2-14	41.4	44.1	37.2	6.9	1.06
5I22	18-3-34	52.4	55.2	48.3	6.9	1.05
6I22	30-3-34	38.1	35.8	29.0	6.9	0.94
7I22	12-8-12	82.8	78.1	71.9	6.1	0.94
8I22	12-8-12	82.8	83.3	77.2	6.1	1.01
9I22	12-10-15	78.5	75.5	69.3	6.1	0.96
10I22	12-11-13	74.2	76.0	69.9	6.1	1.02
11I22	12-12-11	76.1	75.4	69.3	6.1	0.99
12I22	18-8-14	53.8	54.1	48.0	6.1	1.01
13I22	18-9-16	63.9	57.6	51.5	6.1	0.90
14I22	18-10-14	53.3	52.4	46.2	6.1	0.98
15I22	18-11-13	57.1	52.7	46.6	6.1	0.92
16I22	18-12-11	49.5	52.3	46.2	6.1	1.06
17I22	24-8-14	38.1	42.1	36.0	6.1	1.11
18I22	24-9-20	44.7	46.0	39.8	6.1	1.03
19I22	24-10-14	39.5	40.8	34.7	6.1	1.03
20I22	24-11-13	41.9	41.1	34.9	6.1	0.98
21I22	24-12-11	43.8	40.8	34.7	6.1	0.93
22I22	34-8-23	28.5	33.9	27.8	6.1	1.19
23I22	34-9-20	35.2	34.2	28.1	6.1	0.97
24I22	34-10-14	28.5	30.6	24.5	6.1	1.07
25I22	34-11-14	29.5	30.8	24.7	6.1	1.04
26I22	34-12-11	35.7	30.6	24.5	6.1	0.86
27I22	24-14-91	39.0	42.7	36.6	6.1	1.10
28I22	24-14-91	40.0	42.7	36.6	6.1	1.07
29I22	24-14-92	40.0	42.7	36.6	6.1	1.07
30I22	24-14-91	40.0	42.7	36.6	6.1	1.07
31I22	24-14-91	53.0	42.7	36.6	6.1	0.80
32I22	36-15-13	25.8	25.0	15.2	9.8	0.97
33I22	70-16-14	17.2	17.6	7.7	9.8	1.02
34I22	36-15-14	25.0	27.8	20.5	7.3	1.11
35I22	70-16-14	18.6	17.8	10.4	7.3	0.95
36I22	40-18-14	28.7	26.2	18.9	7.3	0.91
37I22	36-15-13	25.8	31.6	25.8	5.8	1.23

Table A.12. Continued

Beam no.	Specimen designation	Ultimate shear-bond stresses: Experimental $v_{ue}=\frac{V_{ue}}{bd}$ (psi)	Calculated $v_{uc}=\frac{K_5\sqrt{f'_c}\,d}{L'}+K_6p$ (psi)			$\frac{v_{uc}}{v_{ue}}$
38I22	40-18-14	33.8	29.5	23.7	5.8	0.87
39I22	70-16-15	19.4	18.9	13.1	5.8	0.97
40I22	46-19-20SH	27.7	24.7	17.4	7.3	0.89
41I22	70-19-19SG	20.8	18.3	8.5	9.8	0.88
42I22	48-20-16SG	25.8	25.3	19.5	5.8	0.98
Re-tested						
43I22	30R-15-21	35.8	28.6	18.8	9.8	0.80
44I22	40R-15-23	28.7	26.3	19.0	7.3	0.92
45I22	30R-15-21	35.9	37.6	31.8	5.8	1.05
46I22	26R-16-33	45.9	43.1	37.3	5.8	1.20
47I22	24R-18-24	46.5	47.3	41.5	5.8	1.02
<u>18 Gage</u>						
1I18	12-8-23	92.6	98.9	72.1	26.9	1.08
2I18	12-9-23	97.3	97.6	70.7	26.9	1.01
3I18	12-10-11	100.7	88.3	61.5	26.9	0.88
4I18	12-11-13	79.2	90.9	64.0	76.9	1.15
5I18	12-12-12	99.2	90.3	63.5	26.9	0.91
6I18	18-8-23	63.0	74.9	48.1	26.9	1.19
7I18	18-9-14	78.2	74.0	47.1	26.9	0.94
8I18	18-10-11	71.6	67.8	41.0	26.9	0.94
9I18	18-11-13	73.5	69.5	42.7	26.9	0.94
10I18	18-12-12	67.3	69.2	42.3	26.9	1.02
11I18[a]	24-8-23	—	—	—	—	—
12I18	24-9-14	63.0	62.2	35.4	26.9	0.98
13I18	24-10-11	60.1	57.6	30.7	26.9	0.95
14I18	24-11-13	54.4	58.9	32.0	26.9	1.07
15I18	24-12-12	65.4	58.6	31.7	26.9	0.89
16I18[a]	34-8-23	—	—	—	—	—
17I18	34-9-14	50.6	51.8	25.0	26.9	1.01
18I18	34-10-11	50.6	48.6	21.7	26.9	0.94
19I18	34-11-13	44.8	49.5	22.6	26.9	1.08
20I18	34-12-12	48.2	49.3	26.9	26.9	1.00
21I18	70-17-13	36.3	46.0	7.3	38.7	1.26
22I18	60-17-24	40.3	47.9	9.2	38.7	1.19
23I18	48-18-14	47.5	48.5	9.8	38.7	1.02
24I18	70-17-13	37.1	38.5	9.8	28.7	1.04
25I18	60-17-14	39.7	40.1	11.4	28.7	1.01

[a]Not included in regression analysis.

Table A.12. Continued

Beam no.	Specimen designation	Ultimate shear-bond stresses: Experimental $v_{ue} = \frac{V_{ue}}{bd}$ (psi)	Calculated $v_{uc} = \frac{K_5\sqrt{f'_c}\, d}{L'} + K_6 p$ (psi)			$\frac{v_{uc}}{v_{ue}}$
26I18	48-18-15	42.1	43.6	14.9	28.7	1.04
27I18	70-17-14	31.2	35.1	12.3	22.8	1.13
28I18	60-17-14	40.5	37.2	14.4	22.8	0.92
29I18	47-18-15	38.6	42.0	19.2	22.8	1.09
30I18[a]	30-20-20SH	—	—	—	—	—
31I18	40-19-20SH	50.7	47.6	18.4	28.7	0.94
32I18[a]	36-22-14SH	—	—	—	—	—
33I18[a]	70-19-19SG	—	—	—	—	—
34I18	60-20-20SG	46.9	40.4	11.7	28.7	0.86
35I18	48-20-16SG	38.0	41.1	19.1	22.0	1.08
Re-tested						
36I18	24R-17-34	63.1	62.5	39.7	22.8	0.99
37I18	24R-17-34	57.2	62.5	39.7	22.8	1.09
38I18	24R-18-24	62.7	62.1	39.3	22.8	0.99
39I18	24R-17-34	59.7	60.2	31.5	28.7	1.01
40I18	24R-17-34	67.2	60.2	31.5	28.7	0.90
41I18	24R-18-24	53.3	59.9	31.2	28.7	1.12
42I18	40R-19-28	56.5	48.1	19.4	28.7	0.85
43I18	24R-17-34	69.1	62.1	23.4	38.7	0.90
44I18	24R-18-24	51.8	61.8	23.1	38.7	1.19
45I18	15R-19-24	87.8	77.0	38.3	38.7	0.88
<u>16 Gage</u>						
1I16	36-15-14	54.1	56.1	22.5	33.7	1.04
2I16	60-16-14	46.2	47.0	13.4	33.7	1.02
3I16	36-15-13	51.3	55.3	30.3	24.9	1.08
4I16	70-16-14	40.6	40.4	15.5	24.9	1.00
5I16	36-15-14	52.5	58.0	38.2	19.8	1.11
6I16	70-16-14	49.2	40.8	21.0	19.8	0.83
7I16	40-19-20SH	65.2	70.1	40.9	29.2	1.08
8I16	70-19-19SG	51.2	56.7	17.3	39.4	1.11
9I16	60-20-19SG	55.6	54.5	25.3	29.2	0.98
10I16	36-20-19SG	80.2	76.3	53.2	23.2	0.95
Re-tested						
11I16	30R-15-21	63.5	61.4	27.8	33.7	0.97
12I16	26R-16-33	75.0	66.2	32.5	33.7	0.88
13I16	30R-15-21	55.6	62.4	37.5	24.9	1.12
14I16	26R-16-33	66.3	68.9	43.9	24.9	1.04
15I16	15R-19-28	113.3	105.9	81.0	24.9	0.94
16I16	30R-15-22	64.5	67.0	47.2	19.8	1.04
17I16	14R-20-21	131.4	137.7	108.5	29.2	1.05
18I16	22R-20-21	110.3	110.1	87.0	23.2	1.00
19I16	15R-19-28	134.1	122.1	82.7	39.4	0.91

Table A.13. Comparison of experimental and calculated ultimate shear-bond stresses for beams constructed with deck O

Beam no.	Specimen designation	Ultimate shear-bond stresses: Experimental $v_{ue} = \frac{V_{ue}}{bd}$ (psi)	Calculated $v_{uc} = \frac{K_5\sqrt{f'_c}\,d}{L'} + K_6 p$ (psi)	$\frac{K_5\sqrt{f'_c}\,d}{L'}$	$K_6 p$	$\frac{v_{uc}}{v_{ue}}$
20 Gage						
1020	12-4-11	58.7	62.8	55.8	7.0	1.07
2020	12-4-12	64.8	62.8	55.8	7.0	0.97
3020	12-5-21	69.8	64.2	57.2	7.0	0.92
4020	12-6-21	65.8	69.5	62.5	7.0	1.06
5020	24-4-12	40.5	34.9	27.9	7.0	0.86
6020	24-5-18	39.5	35.6	28.6	7.0	0.90
7020	24-5-20	38.5	35.6	28.6	7.0	0.92
8020	24-6-21	32.4	38.2	31.2	7.0	1.18
9020	34-4-12	26.5	26.7	19.7	7.0	1.01
10020	34-5-18	25.3	27.2	20.2	7.0	1.07
11020[a]	34-6-21	—	—	—	—	—
12020	34-6-21	24.8	29.1	22.1	7.0	1.17
22 Gage						
1022	70-21-19	14.9	15.7	6.6	9.1	1.05
2022	70-21-19	16.5	15.7	9.1	6.6	0.95
3022[a]	36-21-19	—	—	—	—	—
4022	70-22-30SH	17.0	17.7	12.6	5.1	1.05
5022	40-23-20SH	24.6	20.6	11.8	8.9	0.84
6022	60-23-32SH	14.2	17.9	11.3	6.6	1.25
7022	70-22-28SG	15.7	16.2	7.2	9.1	1.03
8022	48-23-27SG	20.8	19.0	10.1	8.9	0.91
16 Gage						
1016	60-21-19	42.8	46.8	14.1	32.7	1.09
2016	60-21-19	45.2	43.1	19.5	26.6	0.95
3016	36-21-19	56.0	59.9	41.1	18.5	1.07
4016	48-22-29SH	60.9	50.0	26.4	23.6	0.82
5016	70-23-25SH	36.3	40.4	21.9	18.5	1.11
6016	70-22-29SG	45.9	45.8	13.1	32.7	1.00
7016	36-23-20SG	60.2	56.3	33.5	22.8	0.94
8016	48-23-34SG	46.4	51.9	33.9	18.0	1.12
Re-tested						
9016	24R-21-24	73.6	67.9	35.2	32.7	0.92
10016	36R-21-24	50.9	56.1	32.5	23.6	1.10
11016	24R-23-53	87.1	83.6	65.1	18.5	0.96
12016	24R-23-53	83.5	83.6	65.1	18.5	1.00

[a]Not included in regression analysis.

Table A.14. Comparison of experimental and calculated ultimate shear-bond stresses for beams constructed with deck O. All tests conducted by company O

Beam no.	Specimen designation	Ultimate shear-bond stresses: Experimental $v_{ue} = \frac{V_{ue}}{bd}$ (psi)	Calculated $v_{uc} = \frac{K_5\sqrt{f'_c}\, d}{L'} + K_6 p$ (psi)			$\frac{v_{uc}}{v_{ue}}$
20 Gage						
13020	QL-21	64.3	67.4	42.7	24.7	1.05
14020	QL-21	54.5	58.8	33.9	24.9	1.08
15020	QL-21	83.1	77.6	52.0	25.6	0.93
16020	QL-21	62.9	58.0	31.9	26.1	0.92
17020	QL-21	77.7	80.4	54.2	26.2	1.03
18020	QL-21[a]	69.5	71.0	58.3	12.7	1.02
19020	QL-21[a]	72.7	71.0	58.0	13.0	0.98
20020	QL-21[a]	49.1	49.4	36.3	13.1	1.01
21020	QL-21[a]	48.2	48.0	35.4	12.6	1.00
22020	QL-21 INV.	105.1	101.8	62.9	38.9	0.97
23020	QL-21 INV.	76.2	75.3	35.8	39.5	0.99
24020	QL-21 INV.	76.6	75.7	35.7	40.0	0.99
25020	QL-21 INV.	96.1	99.5	59.6	39.9	1.04
26020	QL-21 INV.	85.2	87.1	46.3	40.8	1.02
27020	QL-21 INV.[a]	73.7	80.5	70.1	10.5	1.09
28020	QL-21 INV.[a]	60.8	60.4	50.1	10.3	0.99
29020	QL-21 INV.[a]	84.6	77.2	66.8	10.4	0.91
30020	QL-21 INV.[a]	49.0	50.0	39.7	10.2	1.02
18/18 Gage						
1018/18	DC-45[a]	47.9	50.6	29.1	21.6	1.06
2018/18	DC-45[a]	35.7	35.0	13.7	21.3	0.98
3018/18	DC-45[a]	70.8	69.5	48.6	21.0	0.98
4018/18	DC-75[a]	50.1	43.8	24.6	19.3	0.88
5018/18	DC-75[a]	41.1	46.8	27.2	19.6	1.14

[a]Indicates steel decks were greased prior to placing of concrete.

Table A.15. Comparison of experimental and calculated ultimate shear-bond stresses for beams constructed with deck G

		Ultimate shear-bond stresses				
		Experimental	Calculated			
Beam no.	Specimen designation	$v_{ue} = \frac{V_{ue}}{bd}$ (psi)	$v_{uc} = \frac{K_7 \sqrt{f'_c}\, d}{L'} + K_8 p$ (psi)			$\frac{v_{uc}}{v_{ue}}$
<u>24 Gage</u>						
1G24[a]	3-70-24-19SH	——	——	——	——	——
2G24[a]	3-36-24-21SH	——	——	——	——	——
3G24	3-24-24-21SH	70.1	78.5	53.3	25.2	1.12
4G24	5-70-25-21SH	30.7	34.7	6.3	28.4	1.13
5G24	5-36-24-19SH	36.5	35.9	17.3	18.6	0.98
6G24	5-28-25-21SH	43.7	44.9	29.8	15.1	1.03
7G24	8-70-26-19SH	20.9	21.3	3.6	17.7	1.02
8G24	8-36-26-19SH	23.6	22.2	10.6	11.6	0.94
9G24	8-28-26-19SH	30.2	26.2	16.8	9.4	0.87
<u>20 Gage</u>						
1G20[a]	3-70-24-24SH	——	——	——	——	——
2G20	3-36-26-17SH	57.4	54.5	25.8	28.7	0.95
3G20	3-28-26-19SH	60.3	64.7	42.3	22.5	1.07
4G20	5-70-26-17SH	29.1	30.3	5.5	24.8	1.04
5G20	5-36-25-19SH	33.4	34.3	17.7	16.7	1.03
6G20	5-24-24-24SH	43.1	43.3	29.4	13.8	1.00
7G20	8-70-25-19SH	18.8	19.3	3.8	15.5	1.03
8G20	8-36-24-24SH	21.5	20.6	10.2	10.4	0.96
9G20	8-30-25-19SH	26.1	24.8	16.4	8.4	0.95

[a]Flexure failures.

Table A.16. Comparison of experimental and calculated ultimate shear-bond stresses for beams constructed with deck E

Beam no.	Specimen designation	Ultimate shear-bond stresses: Experimental $v_{ue} = \frac{V_{ue}}{bd}$ (psi)	Calculated $v_{uc} = \frac{K_5\sqrt{f'_c}\ d}{L'} + K_6 p$ (psi)			$\frac{v_{uc}}{v_{ue}}$
20 Gage						
1E20[a]	12-4-11	———	———	———	———	———
2E20	12-4-12	162.8	161.7	83.8	77.9	0.99
3E20	12-5-21	145.5	163.7	85.8	77.9	1.13
4E20	12-6-20	188.1	171.7	93.8	77.9	0.91
5E20	24-4-12	118.7	119.8	41.9	77.9	1.01
6E20	24-5-12	103.4	120.8	42.9	77.9	1.17
7E20	24-5-20	120.6	120.8	42.9	77.9	1.00
8E20	24-6-20	127.8	124.8	46.9	77.9	0.98
9E20	34-4-12	105.3	107.4	29.6	77.9	1.02
10E20	34-5-18	94.8	108.2	30.3	77.9	1.14
11E20	34-6-19	125.9	111.0	33.1	77.9	0.88
12E20	34-6-20	127.8	111.0	33.1	77.9	0.87
22 Gage[b]						
1E22	10-11	125.7	141.0	36.6	104.4	1.12
2E22	10-2	110.4	106.1	33.7	72.4	0.96
3E22	10-3	117.8	120.8	48.4	72.4	1.03
4E22	10-4	127.6	120.8	48.4	72.4	0.95
5E22	10-5	133.7	120.8	48.4	72.4	0.90
6E22	10-7	138.0	125.7	52.8	72.4	0.91
7E22	14-2	99.7	106.1	33.7	72.4	1.06
8E22	14-3	107.1	120.8	48.4	72.4	1.13
9E22	14-4	122.7	120.8	48.4	72.4	0.99
10E22	14-7	115.0	125.2	52.8	72.4	1.09
11E22	14-10	102.5	120.7	48.3	72.4	1.18
12E22	18-1	119.1	125.2	52.8	72.4	1.05
13E22	19-1	145.7	125.2	52.8	72.4	0.86
14E22	10-12	129.1	124.4	69.0	55.4	0.96
15E22	10-13	123.6	130.1	85.2	44.9	1.05
16E22	4-1/2"x69"x12"	137.4	125.9	63.1	62.8	0.92

[a]Not included in regression analysis.

[b]Tests conducted by company E.

Table A.17. Comparison of experimental and calculated design shear for beams constructed with deck I, failing in shear-bond

Beam no.	Specimen designation	Ultimate experimental shear V_{ue} (lb/ft)	Calculated design shear V_{de} [a] (lb/ft)	$\frac{V_{ue}}{V_{de}}$
22 Gage				
1I22	24-2-13	2225	995	2.236
2I22	24-2-13	2275	995	2.286
3I22	24-2-14	2150	995	2.161
4I22	24-2-14	2175	995	2.186
5I22	18-3-34	2750	1270	2.166
6I22	30-3-34	2000	791	2.530
7I22	12-8-12	4350	1839	2.365
8I22	12-8-12	4350	1970	2.208
9I22	12-8-12	4125	1775	2.324
10I22	12-10-15	3900	1789	2.180
11I22	12-11-13	4000	1774	2.254
12I22	12-12-11	2825	1244	2.270
13I22	18-8-14	3350	1331	2.516
14I22	18-10-14	2800	1202	2.330
15I22	18-11-13	3000	1211	2.478
16I22	18-12-11	2600	1201	2.165
17I22	24-8-14	2000	947	2.112
18I22	24-9-20	2350	1043	2.254
19I22	24-10-14	2075	915	2.268
20I22	24-11-13	2200	922	2.387
21I22	24-12-11	2300	914	2.515
22I22	34-8-23	1500	744	2.017
23I22	34-9-20	1850	752	2.460
24I22	34-10-14	1500	662	2.267
25I22	34-11-14	1550	667	2.325
26I22	34-12-11	1875	661	2.825
27I22	24-14-91	2050	962	2.130
28I22	24-14-91	2100	962	2.182
29I22	24-14-92	2100	962	2.182
30I22	24-14-91	2100	962	2.182
31I22	24-14-91	2800	962	2.920
32I22	36-15-13	891	266	3.354
33I22	70-16-14	594	144	4.124
34I22	36-15-14	1163	429	2.710

[a]Values for V_{de} were calculated from Equation 40.

Table A.17. Continued

Beam no.	Specimen designation	Ultimate experimental shear V_{ue} (lb/ft)	Calculated design shear V_{de} (lb/ft)	$\frac{V_{ue}}{V_{de}}$
35I22	70-16-14	866	208	4.159
36I22	40-18-14	1336	393	3.396
37I22	36-15-13	1509	652	2.313
38I22	40-18-14	1979	596	3.321
39I22	70-16-15	1138	303	3.757
40I22	46-19-20SH	1287	362	3.557
41I22	70-19-19SG	718	156	4.594
42I22	48-20-16SG	1509	479	3.147
Re-tested				
43I22	30R-15-21	1237	373	3.316
44I22	40R-15-23	1336	474	2.819
45I22	30R-15-21	2103	896	2.348
46I22	26R-16-33	2103	1111	1.984
47I22	24R-18-24	2722	1199	2.271
<u>18 Gage</u>				
1I18	12-8-23	4850	2349	2.065
2I18	12-9-23	5100	2315	2.203
3I18	12-10-11	5275	2086	2.528
4I18	12-11-13	4150	2150	1.931
5I18	12-12-12	5200	2136	2.434
6I18	18-3-23	3300	1754	1.881
7I18	18-9-14	4100	1732	2.368
8I18	18-10-11	3750	1579	2.374
9I18	18-11-13	3850	1622	2.374
10I18	18-12-12	3525	1613	2.186
11I18[b]	24-8-23	2475	———	———
12I18	24-9-14	3300	1440	2.291
13I18	24-10-11	3150	1326	2.376
14I18	24-11-13	2850	1357	2.099
15I18	24-12-12	3425	1351	2.536
16I18[b]	34-8-23	1575	———	———
17I18	34-9-14	2650	1102	2.404
18I18	34-10-11	2650	1102	2.404
19I18	34-11-13	2350	1125	2.090
20I18	34-12-12	2525	1120	2.255
21I18	70-17-13	1250	638	1.960
22I18	60-17-24	1386	668	2.074
23I18	48-18-14	1633	677	2.411

[b]Not included in regression analysis.

Table A.17. Continued

Beam no.	Specimen designation	Ultimate experimental shear V_{ue} (lb/ft)	Calculated design shear V_{de} (lb/ft)	$\frac{V_{ue}}{V_{de}}$
25I18	60-17-14	1843	727	2.536
26I18	48-18-15	1955	801	2.439
27I18	70-17-14	1819	775	2.348
28I18	60-17-14	2363	829	2.849
29I18	47-18-15	2252	958	2.350
30I18	30-20-20SH	2771	818	3.389
31I18	40-19-20SH	2351	887	2.651
32I18	36-22-14SH	3118	892	3.494
33I18[b]	70-19-19SG	1138	——	——
34I18	60-20-20SG	2177	750	2.901
35I18	48-20-16SG	2301	981	2.345
Re-tested				
36I18	24R-17-34	3687	1636	2.253
37I18	24R-17-34	3340	1652	2.021
38I18	24R-18-24	3662	1607	2.278
39I18	24R-17-34	2771	1275	2.173
40I18	24R-17-34	3118	1275	2.445
41I18	24R-18-24	2474	1240	1.995
42I18	40R-19-28	2623	976	2.688
43I18	24R-17-34	2375	987	2.406
44I18	24R-18-24	1782	961	1.855
45I18	15R-19-24	3019	1222	2.471
16 Gage				
1I16	36-15-14	1856	803	2.310
2I16	60-16-14	1584	616	2.572
3I16	36-15-13	2375	1144	2.076
4I16	70-16-14	1880	731	2.571
5I16	36-15-14	3043	1598	1.904
6I16	70-16-14	2870	998	2.876
7I16	40-19-20SH	3019	1126	2.681
8I16	70-19-19SG	1757	600	2.930
9I16	60-20-19SG	2573	812	3.167
10I16	36-20-19SG	4676	1611	2.902
Re-tested				
11I16	30R-15-21	2177	963	2.260
12I16	26R-16-33	2573	1104	2.330
13I16	30R-15-21	2573	1407	1.829
14I16	26R-16-33	3068	1586	1.934
15I16	15R-19-28	4602	1671	2.745
16I16	30R-15-22	3761	1990	1.890
17I16	14R-20-21	6087	2589	2.343
18I16	22R-20-21	6433	2563	2.510
19I16	15R-19-28	5245	2671	1.964

Table A.18. Comparison of experimental and calculated design shear for beams constructed with deck O, failing in shear-bond

Beam no.	Specimen designation	Ultimate experimental shear V_{ue} (lb/ft)	Calculated design shear V_{de}[a] (lb/ft)	$\frac{V_{ue}}{V_{de}}$
20 Gage				
1020	12-4-11	2900	1369	2.119
2020	12-4-12	3200	1369	2.338
3020	12-5-21	3450	1401	2.463
4020	12-6-21	3250	1525	2.131
5020	24-4-12	2000	718	2.786
6020	25-5-18	1950	734	2.657
7020	24-5-20	1900	734	2.589
8020	24-6-21	1600	796	2.010
9020	34-4-12	1310	527	2.488
10020	34-5-18	1250	538	2.324
11020[b]	34-6-21	900	——	——
12020	34-6-21	1225	582	2.106
22 Gage				
1022	70-21-19	470	91	5.178
2022	70-21-19	718	141	5.095
3022[b]	36-21-19	1089	——	——
4022	70-22-30SH	940	246	3.826
5022	40-23-20SH	792	169	4.681
6022	60-23-32SH	619	185	3.338
7022	70-22-28SG	495	99	4.992
8022	48-23-27SG	668	144	4.634
16 Gage				
1016	60-21-19	1336	541	2.467
2016	60-21-19	1955	693	2.823
3016	36-21-19	3093	1337	2.313
4016	48-22-29SH	2635	835	3.158
5016	70-23-25SH	2004	828	2.421
6016	70-23-29SG	1435	527	2.723
7016	36-23-20SG	2697	999	2.701
8016	48-23-34SG	2635	1161	2.270
Re-tested				
9016	24R-21-24	2301	951	2.420
10016	36R-21-24	2202	1049	2.098
11016	24R-23-53	4812	2085	2.308
12016	24R-23-55	4615	2088	2.210

[a]Values for V_{de} were calculated from Equation 40.

[b]Not included in regression analysis.

Table A.19. Comparison of experimental and calculated design shear for beams constructed with deck O, failing in shear-bond. All tests conducted by company O

Beam no.	Specimen designation	Ultimate experimental shear V_{ue} (lb/ft)	Calculated design shear V_{de}[b] (lb/ft)	$\frac{V_{ue}}{V_{de}}$
20 Gage				
13020	QL-21	2884	1261	2.29
14020	QL-21	2418	1067	2.27
15020	QL-21	3590	1420	2.53
16020	QL-21	1664	999	2.67
17020	QL-21	3284	1442	2.28
18020	QL-21[a]	3034	1300	2.33
19020	QL-21[a]	3104	1270	2.44
20020	QL-21[a]	2084	829	2.51
21020	QL-21[a]	2124	834	2.55
22020	QL-21 INV.	4744	2002	2.37
23020	QL-21 INV.	3394	1416	2.40
24020	QL-21 INV.	3364	1406	2.39
25020	QL-21 INV.	4234	1904	2.22
26020	QL-21 INV.		1609	2.28
27020	QL-21 INV.[a]	3184	1480	2.15
28020	QL-21 INV.[a]	2669	1088	2.45
29020	QL-21 INV.[a]	3674	1420	2.59
30020	QL-21 INV.[a]	2164	876	2.47
18/18 Gage				
1018/18	DC-45[a]	2952	1078	2.74
2018/18	DC-45[a]	2239	508	4.41
3018/18	DC-45[a]	4497	1881	2.39
4018/18	DC-75[a]	4122	966	4.27
5018/18	DC-75[a]	3321	1231	2.70

[a]Indicates steel decks were greased prior to placing of concrete.

[b]Values for V_{de} were calculated from Equation 40.

Table A.20. Comparison of experimental and calculated design shear for beams constructed with deck G, failing in shear-bond

Beam no.	Specimen designation	Ultimate experimental shear V_{ue} (lb/ft)	Calculated design shear[b] V_{de} (lb/ft)	$\frac{V_{ue}}{V_{de}}$
24 Gage				
1G24[a]	3-70-24-19SH	1357	——	——
2G24[a]	3-36-25-21SH	3180	——	——
3G24	3-24-24-21SH	4502	2139	2.104
4G24	5-70-25-21SH	1051	418	2.512
5G24	5-36-24-19SH	1908	685	2.787
6G24	5-28-25-21SH	2808	1121	2.504
7G24	8-70-26-19SH	714	202	3.536
8G24	8-36-26-19SH	1235	348	3.551
9G24	8-28-26-19SHS	1940	557	3.486
20 Gage				
1G20[a]	3-70-24-24SH	1714	——	——
2G20	3-36-26-17SH	2820	1070	2.635
3G20	3-28-26-19SH	3784	1680	2.252
4G20	5-70-26-17SH	995	343	2.897
5G20	5-36-25-19SH	1693	624	2.715
6G20	5-24-24-24SH	2636	1017	2.592
7G20	8-70-25-19SH	643	166	3.869
8G20	8-36-24-24SH	1093	294	3.712
9G20	8-30-25-19SH	1636	497	3.292

[a]Flexural failures.

[b]Values for V_{de} were calculated from Equation 41.

Table A.21. Comparison of experimental and calculated design shear for beams constructed with deck E, failing in shear-bond

Beam no.	Specimen designation	Ultimate experimental shear V_{ue} (lb/ft)	Calculated design shear V_{de}[b] (lb/ft)	$\frac{V_{ue}}{V_{de}}$
<u>20 Gage</u>				
1E20	12-4-11	5850	—	—
2E20	12-4-12	8500	3889	2.186
3E20	12-5-21	7600	3940	1.929
4E20	12-6-20	9825	4137	2.375
5E20	24-4-12	6200	2856	2.171
6E20	24-5-18	5400	2881	1.874
7E20	24-5-20	6300	2881	2.187
8E20	24-6-20	6675	2980	2.240
9E20	34-4-12	5500	2552	2.155
10E20	34-5-18	4950	2570	1.926
11E20	34-6-19	6575	2639	2.491
12E20	34-6-20	6675	2639	2.529
<u>22 Gage</u>[a]				
1E22	10-11	3410	1743	1.956
2E22	10-2	4320	1877	2.301
3E22	10-3	4610	2150	2.144
4E22	10-4	4990	2150	2.321
5E22	10-5	5230	2150	2.433
6E22	10-7	5400	2230	2.421
7E22	14-2	3900	1877	2.077
8E22	14-3	4190	2150	1.949
9E22	14-4	4800	2150	2.233
10E22	14-7	4500	2230	2.017
11E22	14-10	4010	2147	1.868
12E22	18-1	4660	2230	2.089
13E22	19-1	5700	2230	2.555
14E22	10-12	6600	2901	2.275
15E22	10-13	7800	3756	2.077
16E22	4-1/2"x69"x12"	6200	2590	2.394

[a]Tests conducted by company E.

[b]Values for V_{de} were calculated from Equation 40.

APPENDIX B: PHOTOGRAPHS OF TYPICAL FAILED BEAMS

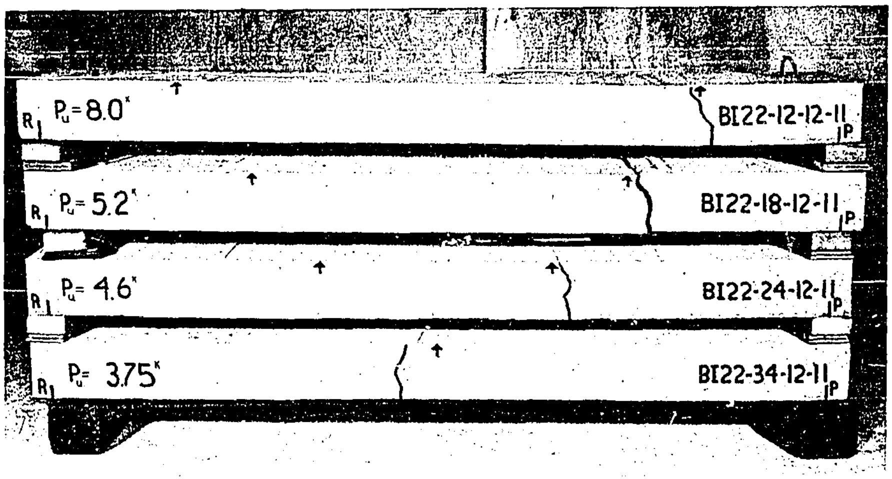

Fig. B.1. Typical shear-bond failures of beams constructed with deck I-22 gage. Each beam was 12 inches wide and 6 feet in length

Fig. B.2. Typical shear-bond failures of beams constructed with deck I-18 gage. Each beam was 12 inches wide and 6 feet in length

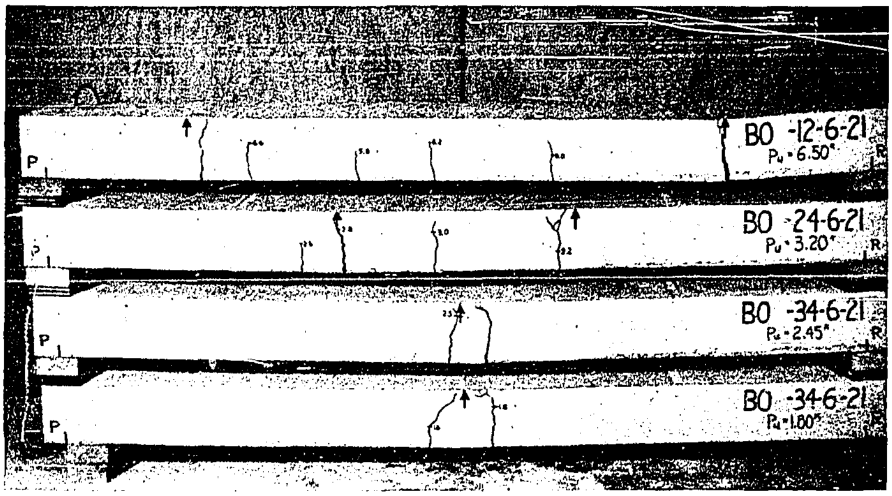

Fig. B.3. Typical shear-bond failures of beams constructed with deck O-20 gage. Each beam was 12 inches wide and 6 feet in length

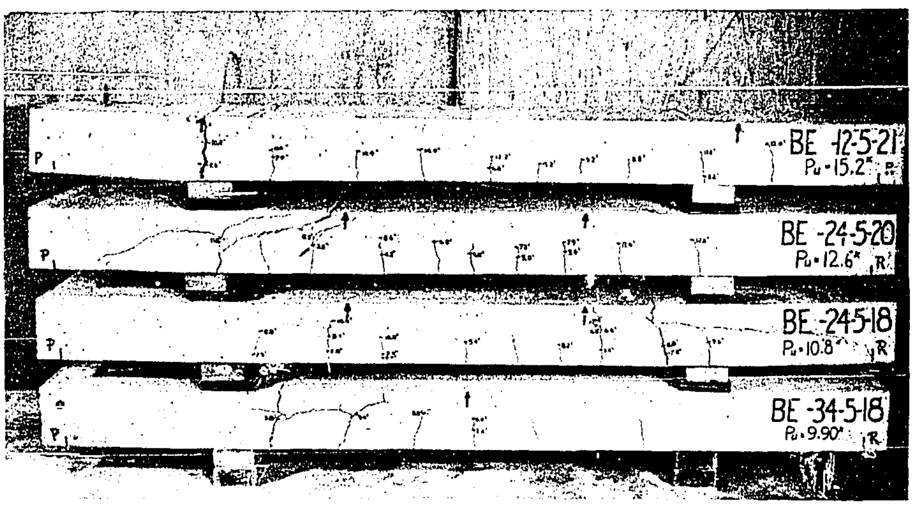

Fig. B.4. Typical shear-bond failures of beams constructed with deck E-20 gage. Each beam was 12 inches wide and 6 feet in length

Fig. B.5. Typical shear-bond failures of beams constructed with deck I-18 gage. Each beam was 24 inches wide and 12 feet in length with variable depths

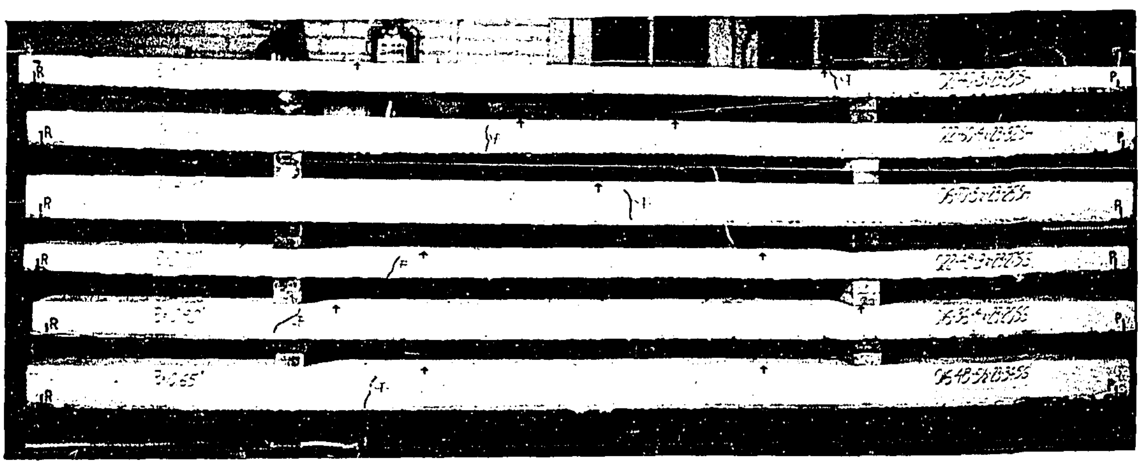

Fig. B.6. Typical shear-bond failures of beams constructed with deck O-22 and 16 gage. Each beam was 24 inches wide and 12 feet in length with variable depths

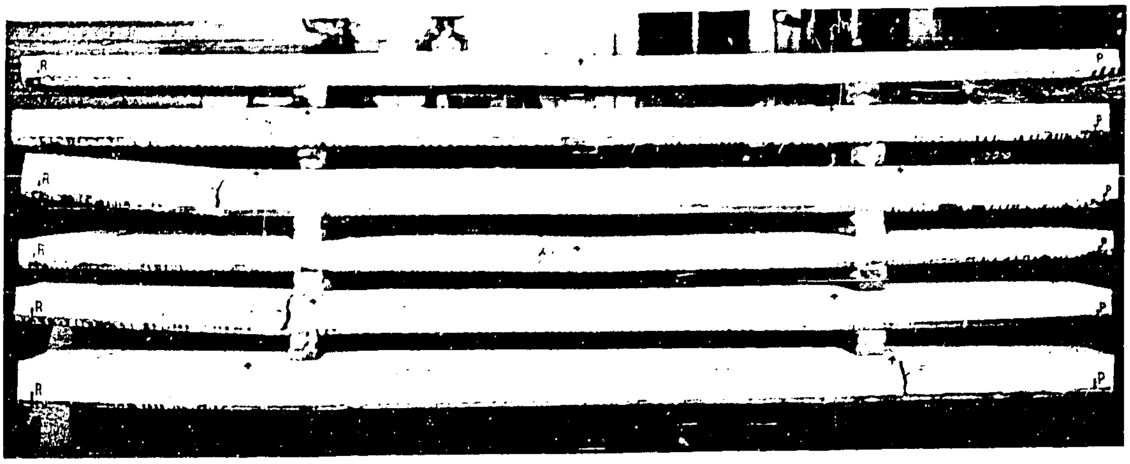

Fig. B.7. Typical shear-bond failures of beams constructed with deck G-20 and 24 gage. Each beam was approximately 28 inches wide and 12 feet in length with variable depths

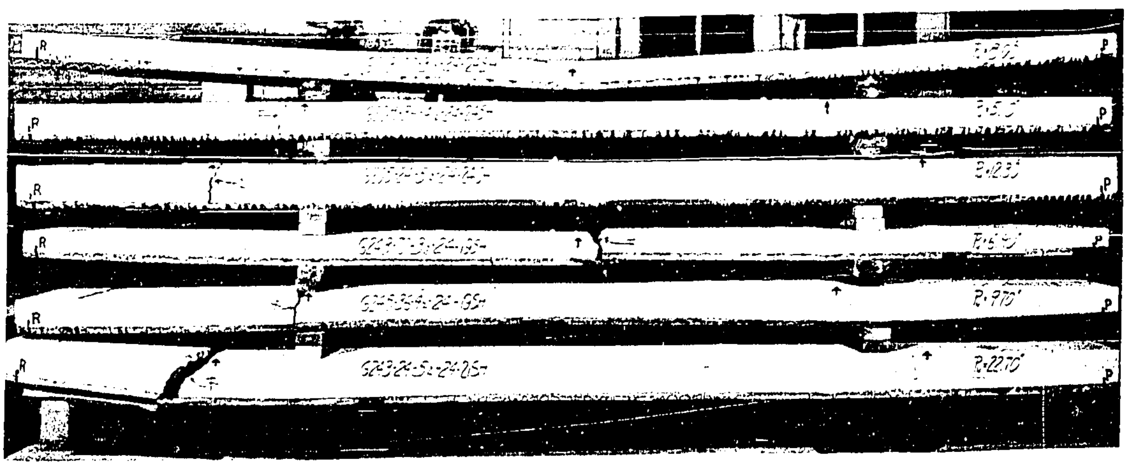

Fig. B.8. Typical shear-bond and flexure failures of beams constructed with deck G-20 and 24 gage. Each beam was approximately 28 inches wide and 12 feet in length with variable depths